UNIVERSITY OF OKLAHOMA

GRADUATE COLLEGE

PETROLOGY OF THE MOUNT SCOTT GRANITE

A Dissertation

SUBMITTED TO THE GRADUATE FACULTY

in Partial fulfillment of the requirements for the

degree of

DOCTOR OF PHILOSOPHY

By

JONATHAN DARREL PRICE

Norman, Oklahoma

1998

UMI Number: 9911870

UMI
300 North Zeeb Road
Ann Arbor, MI 48103

Petrology of the Mount Scott Granite

A dissertation APPROVED FOR THE
SCHOOL OF GEOLOGY & GEOPHYSICS

BY

ACKNOWLEDGMENTS

I thank the following sources for their financial support of the research within this dissertation. Funding for this study was provided by the U.S. Geological Survey National Cooperative Mapping Program, grants #1434-HQ-AG-01547 and #1434-HQ-97-AG-01727 to J. D. Price and M.C. Gilbert; by Eberly Chair Funds available to M. C. Gilbert; and by NSF grant #EAR-9316144 to J. P. Hogan and M. C. Gilbert. Funding for the experimental investigation within Chapter 3 was furnished by NSF grants #EAR-9625517 and #EAR-9618867 to D. London. Additional funds were provided by the Lance Ruffel Field Studies Fund, the Hugh Hunter Petrology Fund, and the School of Geology and Geophysics, University of Oklahoma.

Presentation and interaction with other researchers at professional meetings greatly improved the research in this dissertation. I thank those contributors that made travel to meetings possible. Funding for travel was provided by the Geological Society of America South Central Section, the American Geophysical Union, the University of Oklahoma Graduate Student Senate, Eberly Chair Funds, and the School of Geology and Geophysics, University of Oklahoma.

I thank Sam Waldstein and his staff at the Wichita Mountains Wildlife Refuge, for their cooperation. I am also grateful to Glenn Wampler and E. J. Ardon and their staff at the Fort Sill Wildlife Office for their cooperation, assistance, and information. I also thank the landowners within the Wichita Mountains for land access particularly, Jim Snell for the generous access to his property in the Hale Spring Area.

I wish to thank Jud Ahern, Benjamin Powell, and Tim Denison for their reviews of Chapter 5. Thanks also go to George Morgan for his review of Chapter 3, and also for his assistance with experimental petrology, his skilled operation of the electron microprobe, and his voluminous knowledge of igneous systems. I extend my gratitude to Karen Hogan and Liu Huaibo for thin section preparation.

I thank Hans Huckenholz for his help in the field and lab. I thank Kevin Smart for his insights into the structural styles in my field area. I also thank James Payne, Joe Dischinger, and Jon Mollison for their assistance in the lab.

I thank David London, Thomas Dewers, Kenneth Taylor, and Lawford Anderson for serving on the dissertation committee. Their reviews, comments, and questions greatly strengthened this work. Additional thanks go to David London for the use of his laboratory, and all of his the assistance with experiments. I also thank Barry Weaver for his comments and questions during the development of this work.

Thanks go to John P. Hogan for serving on my committee as deputy advisor, and for his, direction, enthusiasm, insight, encouragement, advice, and friendship during the last five years. I also thank my advisor and committee chair, M. Charles Gilbert for his support, guidance, instruction, counsel and for giving me the opportunity to engage in numerous avenues of investigation.

I thank my many friends at the School of Geology and Geophysics, particularly fellow igneous students Aditya Kar and Joey Evensen for their assistance and friendship. I also extend my gratitude to all my friends for their continued support throughout the years. I thank my parents, Darrel and Genevieve Price, for the many sacrifices they made for my education. Finally, I thank my wife Cindy, partly for her proofing the final version of this dissertation, but chiefly for her continuing support, patience, and understanding throughout my endeavors.

Table of Contents

List of Tables

LIST OF ILLUSTRATIONS

Chapter 1. Overview

The Wichita Mountains of southern Oklahoma are unique in many ways. Rising up from the prairie, they provide the only topographic relief for miles. The variety of igneous rocks exposed within these rocky hills and promontories is unmatched anywhere else in the southern plains. The Wichita Mountains provide a window into the past of the southern midcontinent, revealing a story of magmatism and tectonism associated with the breakup of a supercontinent.

The granites of these mountains provide insight into felsic magmatism within continental rifts. The largest of these, the Mount Scott Granite, is well exposed, and therefore provides a natural laboratory for investigating magmatic characteristics, crystal development, emplacement phenomena, and subsolidus alteration of granites in a rift environment.

Location

The study area encompasses the near-continuous block of the Mount Scott Granite exposed within the eastern Wichita Mountains, Comanche County, Oklahoma, west of I-44 and east of Oklahoma 54, and adjacent to Oklahoma, 49, 34° 38' to 53' N Latitude, 98° 13' to 99° 0' W Longitude, Zone 14S, 5000000 to 555500 Easting, 3833000 to 3860000 Northing UTM, and Township 2 to 4 N, Range 12 to 17 W, Oklahoma Coordinates (Figure 1-1). Much of the area is within the Wichita Mountains Wildlife Refuge (U.S. Fish and Wildlife Service). The southern portion of the area is within the

U.S. Army Fort Sill Military Reservation. The land adjacent to Lake Lawtonka is owned and managed by the City of Lawton. The land adjacent to Tom Steed Reservoir is state park land. All remaining land in the area is held by private landowners.

Previous Work

Work on the geology of this region begins with Shumard's (1853) observations on the Marcy expedition. Hill (1891) observed the landforms of the region and correlated them to those seen in the Ouachita Mountains, pointing out the antiquity of both ranges. Comstock and Cummins (1889) compared the region with the igneous geology of the Llano Uplift, Texas. Spencer in Vaughan (1899) was first to document the diversity of the igneous rocks in the region. Bain (1900) recorded further details of the igneous geology, particularly with respect to economic deposits. Taff (1904), with C. N. Gould, produced one of the earliest geologic maps of the Wichita Mountains and described in detail the nature of the rock types. Taff (1904) also included an appendix by H. F. Bain on analyses of purported ore deposits in the area. Greater detail on the granites and the geology of the eastern Wichita Mountains (roughly the same area as this study) came with studies by Taylor (1915) and by Hoffman (1930), both defining the nature, relative age, and extent of many of the units discussed in this study. Schoonover (1948) investigated the geology of the Fort Sill Military Reservation, and compiled a detailed geologic map of that area. Chase of the Oklahoma Geological Survey assembled a manuscript geologic map of the eastern Wichita Mountains, and although unpublished, it greatly influenced subsequent investigations of this area. Additionally, Chase mapped the Permian Post Oak Formation (Chase, 1954) and recent alluvium deposits within the mountains, including a detailed geologic map immediately adjacent to Mount Scott (Chase, 1952).

Recent studies on the Wichita Mountains are numerous, and for the sake of brevity, only those that have great impact on this dissertation are mentioned here. Fundamental to the current understanding of the Wichita Mountains is the work of Ham *et al.* (1964) on the basement rocks of southern Oklahoma, which provided the overall framework for the Wichita Igneous Province, including the unconformable relationship between the older mafic and younger felsic rocks. Shatski (1946), and later Hoffman *et al.* (1974), popularized the idea that the rocks of this area were associated with continental rifting, part of aulacogen formation in the Cambrian. Merritt (1965) provided the "modern" description of the Mount Scott Granite, as did Merritt (1966) for the feldspars of the Quanah Granite. Most of the nomenclature for individual units within the eastern Wichita Mountains stems from Merritt (1967), Powell *et al.* (1980 a, b), and Myers *et al.* (1981). Merritt (1967) separated several of the felsic units and defined age relationships through compositional differentiation. Powell *et al.*, (1980 a, b) framed the group-level igneous stratigraphy. Myers *et al.* (1981) defined the members of the granite group using their composition as a key indicator. Gilbert (1983) showed the relationships between the igneous rocks and continental rifting. Gilbert and Denison (1993) summarized the nature of the Southern Oklahoma Aulacogen magmatism, incorporating the conclusions of recent investigations. Hogan and Gilbert (1997) described the emplacement characteristics and sheet geometry of the granites. Hogan and Gilbert (1995) and Hogan *et al.* (1998) quantified the physical processes of emplacement for the sheet granites and the other igneous rocks of the province.

Numerous field guides cover this area. Prominent works include Johnson and Denison (1973), Powell and Fisher (1976), Gilbert and Donovan (1982), Gilbert (1986), Gilbert and Powell (1988), Gilbert *et al.* (1990), Hogan and Gilbert (1995), and Price *et al.* (1998). Both Gilbert and Donovan (1982) and Gilbert (1986) contain a large number of stop descriptions for localities within this area and have numerous papers covering specific aspects of the region.

Dissertation Research on the Petrology of the Mount Scott Granite

The following dissertation is a collection of studies, arranged as chapters, on the Mount Scott Granite and associated lithologies. Each chapter contains its own appropriate background and focuses on the topic at hand more or less independently of the other chapters. This first chapter outlines the contributions of the other five chapters to the current understanding of the Mount Scott Granite and of the Wichita Igneous Province.

Feldspar crystallization

Merritt (1965) listed the common gray, ovoid feldspar phenocrysts as a defining characteristic of the Mount Scott Granite. Detailed petrographic and phase composition data from the Mount Scott Granite reveal five distinct populations of feldspar within the rock. The ovoid phenocrysts are compositionally bimodal: one population is Na-rich anorthoclase crystals (Or_{15-33}), the second population is more K-rich (Or_{54-64}). Many of these ovoid phenocrysts are mantled with thin rims of plagioclase (An_{12-31}) (*i.e.*, rapakivi texture). Although plagioclase rims resulting from exsolution (rim albite) are found mantling some alkali feldspars within the Quanah Granite (Merritt, 1966), they differ in appearance and composition from the rims seen on Mount Scott Granite ovoid phenocrysts. Rims appear distinct from exsolution features, thus are likely to have precipitated from a magma. Other primary plagioclase (An_{6-14}) is found as small grains within the matrix. The matrix is otherwise largely comprised of quartz and relatively K-rich alkali feldspar (Or_{58-75}).

Hornblende geobarometry indicates the magma that gave rise to the Mount Scott Granite began crystallization at a depth of 7-8 km (≈200 MPa), prior to ascent and emplacement at ≈1.5 km (≈50 MPa) (Hogan and Gilbert, 1995). Depressurization related to magma ascent has been previously linked to rapakivi formation (Nekvasil, 1991). Thermodynamic modeling in the Qz-Ab-Or-An-H_2O system using EQUIPATH.FOR (Nekvasil, 1990) indicates that alkali feldspar resorption and subsequent plagioclase rim growth is likely for the Mount Scott Granite magma during its ascent from the pondng depth to the emplacement depth.

Some samples of the Mount Scott Granite contain abundant ovoid phenocrysts that are not mantled with plagioclase. Furthermore, the abundance of plagioclase rims correlates negatively with granophyric content each sample. Gilbert *et al.* (1990) noted that granophyre-rich samples typically contain higher concentrations of fluorite relative to titanite, similar to observations regarding F in metamorphic rocks (*e.g.*, Bohlen and Essene, 1978), suggesting that titanite-poor samples resulted from higher fluorine activity. Likewise, feldspars would also be affected by higher F in melt, which would reduce plagioclase solubility by placing calcium into fluorite (as suggested by Price *et al.*, 1996) and sodium into cryolite component. Also, because fluorine might also inhibit the nucleation rate and increase the growth rate, in much the same way that water does, the magma may develop a lag in crystallization during cooling. Such a lag might mean that portions of the mama relatively enriched in F forgo plagioclase rim growth. The crystallization following the lag might be quite rapid, producing granophyric intergrowth.

Therefore, it is likely that portions of the magma represented by samples containing abundant granophyre and phenocrystic alkali feldspars largely lacking in rimming plagioclase contained higher levels of F during crystallization.

The following scenario is proposed for feldspar crystallization within the magma that gave rise to the Mount Scott Granite. Early crystallization at a depth of 7-8 km produced Na-rich feldspar followed by K-rich feldspar as a solvus pair crystallizing near 750 °C. Both phases were partially resorbed during magma ascent to the emplacement level Fluorine-poorer portions of the magma produced abundant rims on the resorbed phenocrysts. Final crystallization at the emplacement level resulted in granophyre growth of alkali feldspar and quartz in portions of the magma relatively enriched in F, and seriate growth in those portions relatively depleted in F.

Fluorine in the Mount Scott Granite

The feldspar work suggests the significance of fluorine in the crystallization history of the Mount Scott Granite, first noted by Gilbert *et al.* (1990). Although the granophyre-rich samples contain relatively higher concentrations of fluorite and biotite, and lower concentrations of plagioclase, titanite, and hornblende, together indicating that granophyre-rich Mount Scott Granite crystallized from a relatively F-enriched magma, the concentration of F in granophyre-rich samples (whole-rock analysis) is not greater than that of their granophyre-poor counterparts. Therefore, the magmatic F variation implicated by the change in phase assemblage and the change in texture is not preserved in the Mount Scott Granite. It is also like that the whole-rock F value misrepresents that of the magma.

Through the addition of "lost" melt components, fluorine and water, an experimental investigation conducted near the initial crystallization conditions of the Mount Scott Granite magma (850 °C, 200 MPa, $fO_2 \approx$ Ni - NiO buffer) places initial F concentration $\approx$ 1 wt.% for portions of the magma producing both titanite and fluorite. This value is five times that of the whole-rock fluorine concentration of the Mount Scott Granite.

Experiments also reveal that without added components the Mount Scott Granite undergoes dehydration melting through the breakdown of biotite at these conditions. Runs with 10 wt.% additional water indicate the Mount Scott Granite achieves water-saturation at these conditions when H_2O in melt = 7.5 wt.%. Water saturated runs with F > 1.05 wt.% in melt produced the highest degree of melting (>95%) and contained highly refractory zircon and an assemblage of biotite + fluorite + magnetite ± apatite. Runs with lower F concentrations produced an assemblage of zircon + titanite + amphibole + magnetite ± apatite.

Mount Scott Granite intrusion as a CCC granite

The Medicine Park Granite and the previously undefined Rush Lake granite crop out adjacent to the Mount Scott Granite within the eastern Wichita Mountains. Contacts between the three units reveal that the Rush Lake and Mount Scott Granites are nearly simultaneous. Mount Scott Granite contacts with the Medicine Park Granite indicate a somewhat older age for the Medicine Park Granite, although the similarity of texture indicates that these two granites are separated by little time. Chemical and mineralogical similarities suggest a genetic relationship between all three granite plutons. Major-element least squares and trace-element Rayleigh fractionation modeling indicates that the Rush Lake granite and Medicine Park Granite can be developed from small amounts of hornblende (6-7%) and plagioclase (6-10%) fractionation from a parental magma of nearly Mount Scott Granite composition. These three granite plutons were dubbed *CCC granites*, defined as *contiguous* (adjacent to one another), *consanguineous* (compositionally related), and *coeval* (intruded roughly at the same time). These felsic intrusive plutons were derived from a single magma and intruded a single horizon in the crust. Intrusion of these magmas produced similar granitoid bodies that interacted during intrusion.

Triple C granites might arise from numerous processes. This example seems to have originated through segmented crystallization of a parental magma, as suggested previously by the two-stage feldspar crystallization history seen in the Mount Scott Granite. These granite bodies originated from a single parental magma, perhaps during ponding at 7-8 km during ascent. Small amounts of fractional crystallization of hornblende + plagioclase, followed by separation of the liquid fraction, produced a small volume of fractionated magma which then ascended to the shallow crust and intruded as the small tabular Medicine Park Granite pluton. Subsequent fractionation within the remaining parental magma produced a fractionated magma that ascended to the same level as the Medicine Park Granite eventually became the Rush Lake granite. The intrusion of the Rush Lake granite was closely followed by much of the remaining magma which formed the Mount Scott Granite. Because of the prior ascent of the Rush Lake granite, the pathway for the larger volume, later granite was preheated, allowing for nearly adiabatic ascent, resulting in the rapakivi-texture development. Although not far separated in time, the Medicine Park Granite body had cooled sufficiently enough to chill these other two granites, and behave as rigid part of the crust.

Post-intrusion processes within the Hale Spring Area

Magmatism continued following the intrusion of the Mount Scott Granite. Although activity was previously considered dominantly felsic, evidence now points to intrusion of some Roosevelt Gabbro plutons subsequent to that of the granite. The results of a surface and shallow-subsurface investigation suggest such a relationship by defining the shape of the Sandy Creek Gabbro (a Roosevelt Gabbro), and constrained the nature of weathering within the Wichita Mountains igneous units. Investigation of this area was initiated with a drilling investigation by M. C. Gilbert and J. P. Hogan, producing one 88 m deep core into the granite, and a short core into the gabbro. Although the granite core provided new insight into the nature of the shallow subsurface under the granite highlands, it did not resolve the nature of the contact between the Mount Scott Granite and the Sandy Creek Gabbro. Because of the relatively elevated magnetic susceptibility of the gabbro, it was possible to image the geometry of the gabbro in the subsurface through modeling of magnetic anomaly data.

Magnetic surveying, scientific drilling, and the exposed geology of the Hale Spring area suggest that the Sandy Creek Gabbro intruded Mount Scott Granite. Surface geology indicates that exposures of the Sandy Creek Gabbro are near the roof of that pluton. Two dimensional forward modeling of magnetic survey data reveals a complicated geometry for the granite/gabbro contact with depth. The Sandy Creek Gabbro pluton is largely steep walled, with at least one thin ledge protruding to the south near the upper margin of the pluton. Such a geometry is consistent with gabbro intruding the granite, rather than *vice-versa* as previously advocated (*e.g.*, Powell *et al.*, 1982).

Uplift of these shallow intrusives in the late Paleozoic and in the Phanerozoic exposed these rocks to weathering processes. Detailed magnetic susceptibility work and petrographical observations revealed that the igneous oxide assemblage of the upper 27 m of the granite core has been altered through oxidation and hydration. Below 27 m, fractures are largely not seen, and the oxide phases are largely unaltered. The intensity of fracturing also increases above 27 m, indicating that this alteration is fracture-controlled, occurring through localized fluid-rock interactions. With decreasing fracture intensity, the degree of alteration substantially lessened.

In contrast, the oxide minerals of the gabbro core are relatively unaltered. Drilling retrieved only 1.3 m of core, all within 10.3 m of the surface, where weathering should be most pervasive. Although the gabbro core was fractured, microfractures, common to the granite, were very rare. Alteration, where present, was limited to the immediate surface of the fracture with very little penetration into the rock. Thus, rock competency may control the weathering characteristics of the igneous units of the Wichita Mountains.

Field studies in the eastern Wichita Mountains

To better understand the nature of the Mount Scott Granite and adjacent lithologies, this study constructed detailed (1:12,000 scale) maps for the easternmost Wichita Mountains (Plate I, II, III). This area provides the greatest amount of exposure of lithologic contacts. The maps provide new insight into the processes involved in magma emplacement, the relationships between units, and the character of the units.

Mapping results defined one new unit, the Rush Lake granite. Previous reports included this unit as a facies of the Mount Scott Granite (*e.g.*, Myers *et al.*, 1981). The Rush Lake granite contains subtle differences in composition and character that make it separable from the Mount Scott Granite. Mapping documented the interfingering and graded contacts of these two units. These are interpreted to result from liquid/liquid interaction, indicating the two granites were intruded at the same horizon simultaneously.

Mapping data refine the igneous stratigraphy and relative age relations between previously defined units. An example is the Medicine Park Granite. Cross sections of the Medicine Park indicate the Medicine Park Granite rests as a flat sheet on top of the Rush Lake and Mount Scott Granites, while further east at Welsh Hill, the Medicine Park Granite and the Mount Scott Granite share a near-vertical contact. The Rush Lake and Mount Scott Granites fine towards their contacts with the Medicine Park Granite, indicating that they are relatively younger than the Medicine Park Granite.

Mapping data identify a likely floor for the Mount Scott Granite Pluton. Petrographic analysis of banded and unbanded outcrops of buff-colored fine-grained felsic rock suggested both are metarhyolite, leading to redesignation of these two facies into one unit, the Davidson metarhyolite. Despite differences in color, the Davidson metarhyolite has a granoblastic texture similar to porphyritic Carlton rhyolite and is commonly adjacent to the Carlton rhyolite. Thus, it is a likely member of the Carlton Rhyolite Group, a voluminous body of volcanics exposed and preserved in the subsurface of southern Oklahoma. Metamorphism to hornfels conditions, although poorly constrained, probably results from intrusion of the Mount Scott Granite. Exposures of the Davidson metarhyolite are limited to a NW-SE trending swath across the eastern Wichita Mountains. This swath is aligned with the an anticline exposed within the central Wichita Mountains, and thus it may outline the core of that anticline within the eastern Wichita Mountains. Exposures stratigraphically underlie adjacent exposures of Mount Scott

Granite, and thus represent the local floor for intrusion of the Mount Scott Granite within the Carlton Group.

Mapping results define a zone of rhyolite with pink-colored spherulitic bands within the hills underlain by Carlton rhyolite on Fort Sill. These bands are suggestive of eutaxitic structures, however they bear little resemblance to such textures seen in rhyolite exposures north of the Meers Fault. They differ from other typical examples of fiammi-bearing rock as the bands are largely linear features and contain phenocrysts. However, the spherulitic texture in the bands are likely devitrification textures, implying a volcanic origin for these bands that may be useful in resolving the emplacement of these Carlton outcrops.

Mapping is unable to document demonstrable faults within the eastern Wichita Mountains. Kinematic indicators, such as offsets of quartz veins and dikes are typically small, and the fractures or zones of fracturing associated with these offsets are difficult to trace for any great extent. Highly brecciated exposures are found, but these are typically isolated. Most importantly, lithologic contacts within the Cambrian units show little evidence for juxtapositioning through faulting, and many strongly suggest intrusive relationships.

Conclusion

Combined, these studies provide new data on the Mount Scott Granite and associated lithologies of the eastern Wichita Mountains, which yield new conclusions on the emplacement, crystallization, and behavior of these rocks. These studies build on an existing body of knowledge for this region and provide new insight into the geologic processes involved. Specifically, these studies provide an understanding of the crystallization, the effect of fluorine on phase stability, and the evolution of the magmatic system for the Mount Scott Granite magma. They provide information on the relationship between gabbroic magmatism and the granite and on post-emplacement alteration. They constrain the spatial distribution of these units to a higher level of detail than previously undertaken.

Works Cited

Bain, H. F., 1900, Geology of the Wichita Mountains. Bulletin of the Geological Society of America, 11, p. 127-144.

Bohlen, S. R., & Essene, E. J., 1978, The significance of metamorphic fluorite in the Adirondacks. *Geochimica et Cosmochimica Acta*, 42, p. 1669-1678.

Chase, G. W., 1952, Ilmenite in alluvial sands of the Wichita Mountain System, Oklahoma. Oklahoma Geological Survey, Circular 30, 44 p.

Chase, G. W., 1954, Permian conglomerate around Wichita Mountains, Oklahoma. Bulletin of the American Association of Petroleum Geologists, v. 38, p. 2028-2035.

Christiansen, E. H., and Lee, D. E., 1986, Fluorine and chlorine in granitoids from the Basin and Range Province, western United States. Economic Geology, 81. p. 1484-1494.

Comstock, T. B., and Cummins, W. F., 1889, A preliminary report on the geology of the central mineral region of Texas. First Annual report of the Texas Geological Survey, p. 319-328.

Gilbert, M. C., 1983, Timing and chemistry of igneous events associated with the Southern Oklahoma Aulacogen. Tectonophysics, 94, p. 439-435.

Gilbert, M. C., ed., 1986, Petrology of the Cambrian Wichita Mountains Igneous Suite, Oklahoma Geological Survey. Guidebook 23, p. 172-178.

Gilbert, M. C., and Denison, R. E., 1993, Late Proterozoic to early Cambrian basement of Oklahoma, *in* Van Schmus, W. R., and Bickford, M. E., eds., Transcontinental Proterozoic Provinces, in Read, J. C., Bickford, M. E., Houston, R. S., Link, P. K., Ransking, D. W., Sims, P. K., and Van Schmus, W. R., Precambrian, Conterminous U.S. Geological Society of America, The Geology of North America, volume C-2, p. 303-314.

Gilbert, M. C., and Donovan, R. N., eds., 1982, Geology of the Eastern Wichita Mountains Southwestern Oklahoma. Oklahoma Geological Survey, Guidebook 21, p.118-123.

Gilbert, M. C., and Powell, B. N., 1988, Igneous geology of the Wichita Mountains, southwestern Oklahoma, *in* Hayward, O. T., ed., Geological Society of America Centennial Field Guide - South-Central Section. Geological Society of America, p. 109-126.

Gilbert, M. C., Hogan, J. P., and Myers, J. D., 1990, Geology, geochemistry, and structure of low-pressure sheet granites, Wichita Mountains, Oklahoma: Guidebook of Filed Trip no. 5, Geological Society of America Annual Meeting, Dallas Geological Society, 65 p.

Ham, W. E., Denison, R. E., and Merritt, C. A., 1964, Basement Rocks and structural evolution of southern Oklahoma. Oklahoma Geological Survey, Bulletin 95, 302 p.

Hill, R. T., 1891, Notes on a reconnaissance of the Ouachita mountain system in Indian Territory: American Journal of Science, 3rd series, vol. 42, p. 122-123.

Hoffman, M. G., 1930, Geology and petrology of the Wichita Mountains: Oklahoma Geological Survey, Bulletin 52, 83 p.

Hoffman, P., Dewey, J. F., and Burke, K., 1974, Aulacogens and their genetic relation to geosynclines, with a Proterozoic example from Great Slave Lake, Canada. Society of Economic Paleontologists and Mineralogists, Special Publication, 19, p. 38-55.

Hogan, J. P., and Gilbert, M. C., 1995, The A-type Mount Scott Granite Sheet: Importance of Crustal Magma Traps: Journal of Geophysical Research, 100, B8, p. 15779-15792.

Hogan, J. P., and Gilbert, M. C., 1997, The intrusive style of A-type sheet granites from the Southern Oklahoma Aulacogen, *in* R. W. Ojakangas, A. B. Dickas, and J. C. Green, eds., Middle Proterozoic to Cambrian Rifting: Mid-North America, Geological Society of America Special Paper, 312, p. 299-311.

Hogan, J. P., Price, J. D., and Gilbert, M. C., 1998, Crustal magma traps and magma driving pressure: consequences for pluton shape and level of emplacement. Journal of Structural Geology, in press.

Icenhower, J. P., and London, D., 1997, Partitioning of fluorine and chlorine between biotite and granitic melt: experimental calibration at 200 MPa H_2O; Contributions to Mineralogy and Petrology, 127, p. 17-29.

Johnson, K., and Denison, R. E., 1973, Igneous geology of the Wichita Mountains and economic geology of Permian rocks in southwest Oklahoma: Oklahoma Geological Survey Special Publication 73-2, Guidebook for field trip 6, Geological Society of America annual meeting, Dallas, 33p.

Merritt, C. A., 1965, Mt. Scott Granite, Wichita Mountains, Oklahoma: Oklahoma Geology Notes, v. 25, p. 263-272.

Merritt, C. A., 1966, Rim albite in coarse-grained Quanah Granite, Wichita Mountains, Oklahoma. Oklahoma Geology Notes, 26, p. 211-213.

Merritt, C. A., 1967, Names and relative ages of granites and rhyolites in the Wichita Mountains, Oklahoma. Oklahoma Geology Notes, 27, p. 45-53.

Myers, J. D., Gilbert, M. C., and Loiselle, M. C., 1981, Geochemistry of the Cambrian Wichita Granite Group and revisions of its lithostratigraphy. Oklahoma Geology Notes, 41, p. 172-195.

Nekvasil, H., 1990, EQUIPATH.FOR, program for calculating equilibrium crystallization paths based on thermodynamic constraints. FORTRAN 77 program.

Nekvasil, H., 1991, Ascent of felsic magmas and formation of rapakivi. *American Mineralogist*, 76, p. 1279-1290.

Powell, B. N., and Fischer, J. F., 1976, Plutonic igneous geology of the Wichita Magmatic Province, Oklahoma. Oklahoma Geological Survey Special Publicaiton, 76-1, 35 p.

Powell, B. N., Gilbert, M. C., and Fischer, J. F., 1980a, Lithostratigraphic classification of basement rocks of the Wichita province, Oklahoma. Geological Society of America Bulletin Part I, 91, p. 509-514.

Powell, B. N., Gilbert, M. C., and Fischer, J. F., 1980b, Lithostratigraphic classification of basement rocks of the Wichita province , Oklahoma: Geological Society of America Bulletin Part II, 91, p. 1875-1994.

Powell, B. N., Stockton, M. L., Giddens, J. D., III., and Gilbert, M. C., 1982, Stop 3 - Hale Spring Locality, *in* Gilbert, M. C.; and Donovan, R. N., eds., Geology of the Eastern Wichita Mountains Southwestern Oklahoma. Oklahoma Geological Survey, Guidebook 21, p. 102-117.

Price, J. D., Hogan, J. P., Gilbert, M. C., and Denison, R. E., 1998, Field guide to the basement rocks of the Southern Oklahoma Aulacogen. South Central Meeting of the Geological Society of America, 76 p.

Schoonover, F. E., 1948, The igneous rocks of the Fort Sill Reservation, Oklahoma. University of Oklahoma, Unpublished M.S. Thesis, 123 p.

Shatski, N. S., 1946, The Great Donets Basin and the Wichita System. Comparative tectonics of ancient platforms. Bulletin de l'Académie des Sciences de l'URSS, Sérié Geologique, 6, p. 57-90.

Shumard, G. G., 1853, Remarks on the General Geology of the country passed over by the exploring expedition to the sources of the Red River. Senate Ex. Doc. No.54, 32nd Congress, Washington, p. 179- 195.

Taff, J. A., 1904, Preliminary report on the geology of the Arbuckle and Wichita Mountains in Indian Territory and Oklahoma. U.S. Geological Survey, Professional Paper 31, 97 p.

Taylor, C. H., 1915, Granites of Oklahoma. Oklahoma Geological Survey Bulletin, 20, 108 p.

Vaughan, T. W., 1899, Geologic notes on the Wichita Mountains, Oklahoma, and the Arbuckle Hills, Indian Territory, with a report on the igneous rocks by Dr. A. C. Spencer. American Geologist, 24, p. 44-45.

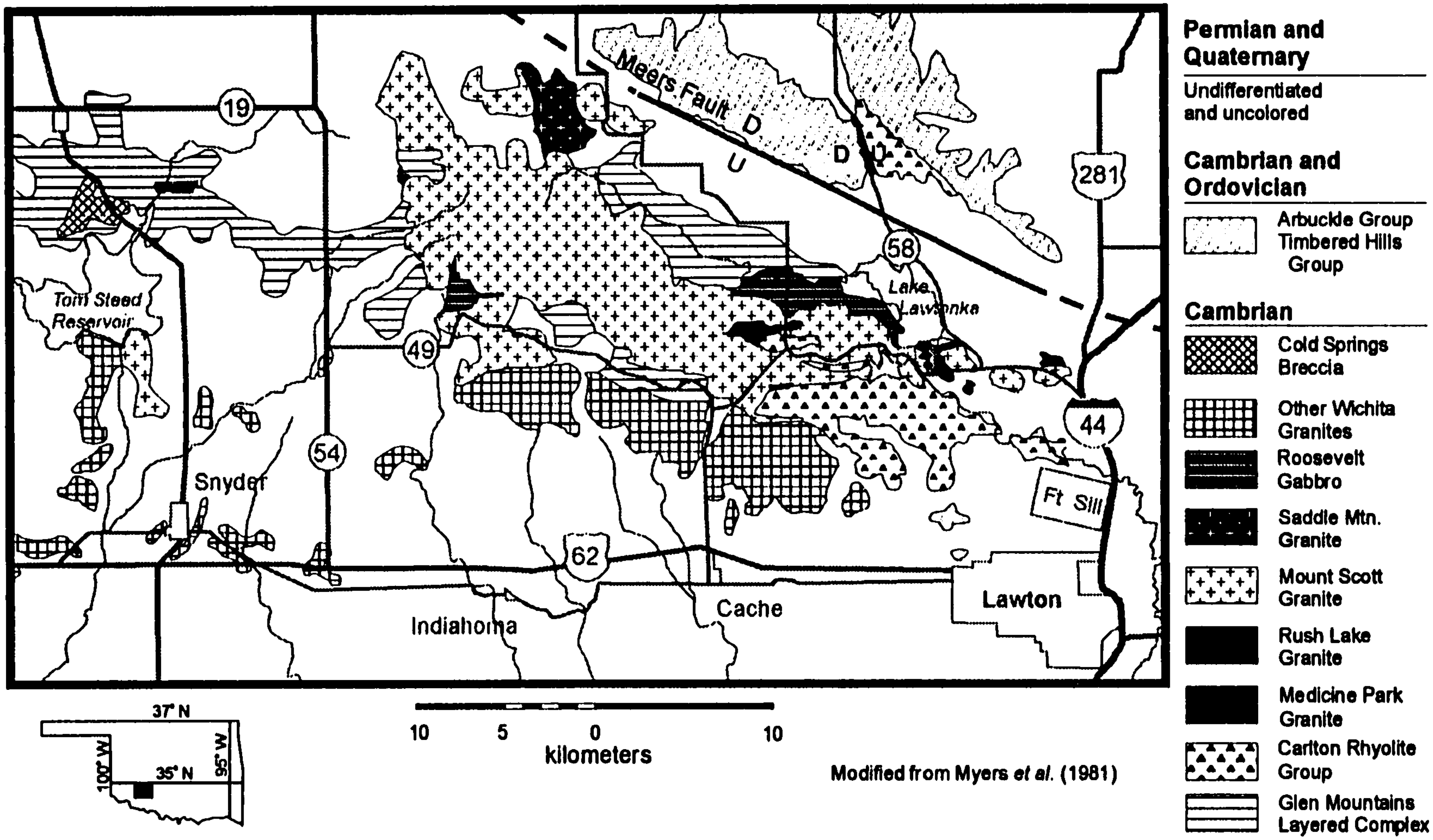

Figure 1-1. Geologic map of the study area, the eastern Wichita Mountains, Oklahoma, showing the outcrop exposure of the Mount Scott Granite and adjacent units.

Chapter 2. Rapakivi Texture in the Mount Scott Granite, Wichita Mountains, Oklahoma

Introduction

The petrogenetic significance of rapakivi texture, rounded alkali feldspar phenocrysts mantled by sodic plagioclase (Bates and Jackson, 1987), has attracted the regard of numerous investigators since the work of Sederholm (1891) called attention to this striking texture. A plethora of explanations, including replacement (*e.g.*, Blacklund, 1938), overgrowth due to decompression (*e.g.*, Tuttle and Bowen, 1958), exsolution (*e.g.*, Gates, 1953), synneusis (Stull, 1979), magma-mixing (*e.g.*, Hibbard, 1981), and accretion of hydrosilicates and thixotropic liquefaction (Elliston, 1985), have been proposed for the origin of this texture. Recently, renewed attention has been focused on the importance of magma mixing (Bussy, 1990; Stimac and Wark, 1992; Wark and Stimac, 1992), exsolution (Dempster *et al.*, 1991), and changes in feldspar phase relationships as a result of decompression during magma ascent (Nekvasil, 1991). This study reports a previously unrecognized occurrence of rapakivi-texture feldspar in an A-type sheet granite with somewhat peculiar and complicated textural relations among the associated feldspars.

The A-type Mount Scott Granite of southwestern Oklahoma (Figure 2-1) is recognized by the presence of distinctive gray to greenish-gray, rounded to ellipsoidal anorthoclase phenocrysts rimmed by sodic plagioclase and then mantled by salmon-red orthoclase and quartz. Although the "zoned" nature of these phenocrysts was noted by Merritt (1965), emphasis was placed on color variation between phenocryst and matrix feldspar and the less obvious rapakivi texture was not discussed. Detailed petrographic and electron microprobe analysis characterized textural and compositional relations among two types of alkali feldspar phenocrysts, their plagioclase rims, matrix alkali feldspar, and sparse, but widely distributed, plagioclase grains. The petrogenetic significance of rapakivi feldspar in the A-type Mount Scott Granite is discussed in light of recent models for rapakivi formation.

Geologic setting

Mount Scott Granite is part of the epizonal bimodal igneous activity associated with the Cambrian Southern Oklahoma Aulacogen (Ham *et al.*, 1964; Powell *et al.*, 1980). Igneous activity associated with the early stages of rifting is dominantly mafic and represented by intrusion of the Raggedy Mountains Gabbro Group, whereas igneous activity associated with the waning stages of extension is dominantly felsic and represented by extrusion of the voluminous Carlton Rhyolite Group, intrusion of sheet-granites of the A-type Wichita Granite Group, and intrusion of volumetrically minor diabase of the Late Diabase Dike suite (Gilbert, 1983; McConnell and Gilbert, 1990; Hogan and Gilbert, 1997). Evidence for contemporaneous mafic and felsic magmatism is scarce and observed only locally (Vidrine and Fernandez, 1986). A hiatus in igneous activity, accompanied by extensive erosion, is postulated to separate the two episodes of magmatism (Ham *et al.*, 1964; Powell and Phelps, 1977). Erosion is thought to have been accentuated by normal faulting and block rotation associated with uplift and extension of the brittle upper crust during rifting (McConnell and Gilbert, 1990).

Mount Scott Granite is comprised predominantly of medium- to fine-grained, hypidomorphic to allotriomorphic, inequigranular, alkali-feldspar leucogranite. It is readily distinguished from other Wichita Granites by the presence of gray to greenish-gray rounded or elliptical anorthoclase phenocrysts (1-4 mm) set in a red to orange-red fine-grained, variably granophyric (0 - >70 vol.%) groundmass that gives it a distinctive porphyritic appearance. The porphyritic nature of Mount Scott Granite indicates an earlier period of crystallization prior to final emplacement beneath Carlton Rhyolite. Geobarometric studies plumb this early episode of crystallization at a depth of approximately 7-8 km in a temporary *crustal magma trap* (Hogan and Gilbert, 1995). Ascent of the magma from this depth was arrested at a shallower crustal magma trap created by the unconformity between overlying penecontemporaneous Carlton Rhyolite and underlying older Raggedy Mountains Gabbro Group. Here Mount Scott magma spread out to form a laterally extensive (55x17 km) but thin (<0.5 km) A-type sheet-granite (Hogan and Gilbert, 1997). Final crystallization conditions are interpreted to be <50 MPa at depths > 1.4 km based on stratigraphic constraints (Ham *et al.*, 1964). Evidence for mechanical and chemical interaction between Mount Scott magma and underlying gabbroic substrate is abundant within the vicinity of the contact. Formation of hybrid rock types along this contact is thought to be the result of assimilation of partial melts derived from hydrated weathered gabbro saprolite (developed along the unconformity) during intrusion of the high-temperature A-type granite magmas (Gilbert and Myers, 1986).

Cambrian igneous rocks of the Southern Oklahoma Aulacogen were later buried by 4 to 5 km of Paleozoic sediments. Subsequently, the Wichita Mountains were uplifted as a horst and eroded during the Pennsylvanian Ouachita Orogeny, reburied in the Permian and Cretaceous, and regionally uplifted and uncovered in the later Cenozoic (Gilbert, 1983).

Methods

Feldspars were investigated using microscopy and electron microprobe analysis of individual grains, including x-ray element mapping and back-scattered electron imaging. Samples selected for microprobe analysis were from two localities: a porphyritic granite with a very fine-grained granophyre-rich (~70%) matrix from the easternmost exposure of the Mount Scott granite sheet (JH1-94, W738), and a porphyritic fine-grained granite with little granophyre from the inactive Ira Smith Quarry (SQ series) in the approximate center of the sheet. Although these sample localities are 25 km apart, they have identical chemistry (Table 2-1). The Ira Smith Quarry, a type locality for Mount Scott Granite (Merritt, 1965), was the site of an exploratory drill hole (Hogan *et al.*, 1994) and samples used in this study were from depths of 5.8, 31, 86 m below the surface.

Feldspar analyses were performed at the University of Oklahoma using a fully automated Cameca SX-50 electron microprobe equipped with a five spectrometer wavelength dispersive system. Operating conditions were maintained at an accelerating voltage of 20 kV. A combination of well characterized natural and synthetic mineral standards was used in the calibration of the analytical scheme, with PAP corrections using on-board analytical software. Analyses with oxide totals outside of the range of (101.50 - 98.50), with less than 13 cations p.f.u., or Si + Al « 4 were rejected. Original compositions of exsolved feldspars were estimated by integrating analyzed cryptoperthitic domains along orthogonal line traverses using a beam size of 3 or 15μ, and averaging the results. Plagioclase analyses used a 3μ spot size.

Petrography

General description

The following description of Mount Scott Granite is summarized from Merritt (1967), Powell *et al.* (1980), Gilbert *et al.* (1990), Hogan *et al.* (1994), and Hogan and Gilbert (1995, 1997) with new descriptions pertinent to feldspar relationships. Mount Scott Granite is typically salmon-pink, weathering to a darker red, porphyritic alkali-feldspar leucogranite. Gray ± pink ovoid-shaped feldspars phenocrysts are set in a matrix that varies from medium to fine-grained, seriate (Figure 2-2A) to granophyric (Figure 2-2B), with granophyric varieties being more common. These two textural end members (granophyre-poor and granophyre-rich) have subtle but significant differences. Ovoid feldspar phenocrysts in granophyre-poor granite are commonly rimmed by a thin layer of plagioclase (*e.g.*, wiborgite; Haapala & Rämö, 1992), not previously noted in the literature, but distinct with hand lens. In contrast plagioclase rims on feldspar phenocrysts are less common in samples with abundant granophyre; plagioclase rims are absent or incomplete on many phenocrysts (*e.g.*, pyterlite; Haapala & Rämö, 1992). Ferro-edenitic hornblende, ± sodic amphibole, annite-rich biotite, titanomagnetite, ilmenite, titanite, zircon, apatite, fluorite, and allanite nominally make up a small percentage of the rock (<5%). These minerals typically occur in clots, enhancing the porphyritic appearance of the rock. Despite a low color index, the dark gray ovoid feldspars darken the rock to a more mafic appearance. Secondary minerals include chlorite, titanite, carbonate, hematite, zoisite, albite, quartz, and white mica. The amount of hematite varies greatly reflecting various oxidation processes subsequent to emplacement.

Feldspar populations

Mount Scott Granite has previously been treated as a hypersolvus (*i.e.*, one feldspar) granite. However, more recent detailed petrographic studies reveal the presence of at least five optically distinct feldspar populations at least two of which appear to have coexisted as early magmatic phases. Averages of compositions from electron microprobe analysis (data presented in Table 2-2 and Appendix 2) demonstrates these optically distinct populations are also compositionally distinct and define unique fields in the ternary feldspar system (Figure 2-3). The textural and geochemical characteristics of these distinct feldspar populations are discussed below with special emphasis on rapakivi textures.

Anorthoclase-N Phenocrysts

Gray ovoid feldspar phenocrysts (Figure 2-4A and B) are a defining characteristic of Mount Scott Granite (Merritt, 1965). They comprise 4-13% of the mode. Ovoid forms (long axis 1-4 mm, aspect ratios typically = 2.5:1) are typical although more blocky forms are present . They have exsolved to patch micro-antiperthite, with lessor ribbon micro-antiperthite (Ab_{25}, Or_{65}, An_{10} lamella in a Ab_{85}, Or_{5}, An_{10} host) and are commonly rimmed by 50 to 250μ of plagioclase (Ab_{80-88}, Or_{1-2}, An_{12-18}) (Figure 2-5A). Reintegration of exsolved components yields an average composition of approximately Ab_{63-76}, Or_{15-33}, An_{4-12}. Large anorthoclase-N phenocrysts may contain perthite subdomains similar in composition to anorthoclase-K ovoid phenocrysts discussed below. Amphibole inclusions are common in some grains. In granophyric samples (*e.g.* W738) these phenocrysts commonly contain numerous tiny (1-3 μ) inclusions of fluorite.

Anorthoclase-K Phenocrysts

Pink and gray ovoid feldspar phenocrysts are less common, and smaller in size (0.5 - 1 mm diameter) than the anorthoclase-N ovoid feldspars (Figure 2-6A and B). On average, these phenocrysts are less elongate and exhibit a rounder cross-section than most anorthoclase-N ovoid feldspars. Anorthoclase-K ovoid feldspars have exsolved to patch microperthite (Ab_{65}, Or_{30}, An_5 lamellae in a Ab_{36}, Or_{62}, An_2 host) and are also commonly rimmed by plagioclase (50-250μ) (Figure 2-5B), except in granophyre-rich samples, where plagioclase rims may be either incomplete or absent. Reintegration of exsolved components yields average compositions that are more potassic (Ab_{35-53}, Or_{44-64}, An_{1-3}) than anorthoclase-N phenocrysts. Only one anorthoclase-K grain from the granophyre-rich JH1-94 (738) samples has been reintegrated, and it is more sodic than SQ anorthoclase-K grains (Figure 2-3). Additional individual analysis points on other JH1-94 anorthoclase-K grains indicate that these phenocrysts are largely more sodic than SQ anorthoclase-K phenocrysts.

Plagioclase Rims

Plagioclase rims are readily recognizable in thin section and can commonly be observed in hand sample with a hand lens. Albite twinning is observed, especially where rim thickness exceeds 200μ. Plagioclase rims are mantled by matrix alkali feldspar with numerous quartz inclusions. Contacts between rims and phenocrysts and between rims and matrix grains are sinuous to irregular. The rim composition averages Ab_{80-88}, Or_{1-2}, An_{12-18} (Table 2-2). Plagioclase rims are optically (Figure 2-7) zoned, with extinction converging near the central portion of the rim, and compositionally zoned (from Ab_{90}, Or_0, An_{10} at the edges to Ab_{83}, Or_0, An_{17} in the center) (Figure 2-5A). For anorthoclase-K phenocrysts the internal compositional boundary between phenocryst and rim is sharp, whereas it is subtle for anorthoclase-N phenocrysts. In contrast, the external compositional boundary between rim and matrix alkali-feldspar is consistently sharp.

Plagioclase Grains

Ubiquitous but volumetrically minor, matrix (non-rimming) plagioclase microphenocrysts also occur in Mount Scott Granite. They are typically small, albite-twinned, and anhedral, with embayments of alkali feldspar or quartz. Many are skeletal inclusions in matrix alkali feldspar whereas others are closely associated with mafic and accessory phases. Their modal abundance diminishes with increasing granophyric content. In contrast with other rapakivi granites (Volborth, 1962; Ehrreich and Winchell, 1969) the compositions of discrete plagioclase grains are more albitic (Ab_{83-92}, Or_{1-6}, An_{6-14}) than plagioclase rims on alkali feldspar phenocrysts. These grains exhibit little internal compositional variability and are largely compositionally homogeneous as a group.

Matrix Alkali Feldspar

Modally the most abundant mineral in Mount Scott Granite, matrix alkali feldspar occurs as irregular interstitial crystals. Grains are salmon-pink to red. These grains exhibit patch and ribbon microperthite and appear less exsolved (Figure 2-5C) than ovoid anorthoclase-K phenocrysts with a reintegrated composition of Ab_{29-50}, Or_{58-75} An_{0-3}. These crystals are more potassic than anorthoclase-K phenocrysts and although exsolution is prevalent, lamellae size (<5μ) is smaller than the phenocryst grains. Granophyric alkali feldspar have smaller lamellae (microperthitic).

Matrix alkali-feldspar with abundant inclusions of anhedral to skeletal quartz typically forms a mantle surrounding earlier feldspar phenocrysts, and where present, plagioclase rims. Anhedral quartz inclusions may represent partially resorbed crystals, whereas in samples with increasing granophyre the skeletal to cuneiform morphology suggest crystallization at large undercooling (Gilbert *et al.*, 1990). In granophyre-rich samples this mantle radiates outward from ovoid phenocrysts to gradually merge with the granophyric matrix.

Order of crystallization

The order of feldspar crystallization, based on textural observations of polished slabs and thin sections, and based on the interpretation of our data as discussed below, is summarized in Figure 2-8. As is common in rapakivi granites, Mount Scott Granite exhibits at least two generations of growth for quartz and feldspars. Hogan and Gilbert (1995) divided crystallization of Mount Scott Granite into two periods, partial crystallization at a deeper level temporary crustal magma trap followed by matrix crystallization at the emplacement crustal magma trap. Results of Al-in-hornblende geobarometry and comparison of whole rock compositions with phase relations in the SiO_2-$NaAlSi_3O_8$-$KAlSi_3O_8$ ternary system both yield pressures of 200 MPa and are interpreted to plumb the depth of the earlier period of partial crystallization at 7-8 km (Hogan and Gilbert, 1995). Feldspar crystallization begins with Anorthoclase-N, followed by co-crystallization of Anorthoclase-N and Anorthoclase-K as a solvus pair; reintegrated compositions of these two feldspars plot along the 750 °C, 100 MPa experimentally determined solvus of Seck (1971) and thermodynamically determined solvus near at 750 °C, 200 MPa of Fuhrman and Lindsley (1988). Textures indicate these early phases were accompanied by quartz, amphibole, biotite, oxides and accessory minerals, including titanite and/or fluorite. The final episode of crystallization, represented by the finer-grained to granophyric matrix, occurred at the emplacement level, under subvolcanic conditions, at pressures probably no more than 50 MPa (Hogan and Gilbert, 1997). This was dominated by crystallization of orthoclase and quartz, commonly with a granophyric texture, but also included plagioclase rims and matrix grains, biotite, oxides, apatite, zircon, and fluorite.

Termination of crystallization for some mineral phases (*e.g.*, amphibole) and partial resorption for others (*e.g.*, quartz) separates early deeper-level and later shallow-level periods of crystallization in the Mount Scott Granite magma. Early crystallizing quartz forms subhedral, inclusion-free phenocrysts with rectangular cross-sections diagnostic of β–quartz. These phenocrysts occur as both isolated crystals and in quartz glomerocrysts. Some quartz phenocrysts exhibit irregular to embayed margins indicative of resorption. Other quartz crystals exhibit skeletal forms, a morphology brought on by crystallization at large undercooling (*i.e.*, >50°C, Swanson and Fenn, 1986), and may represent the transition from crystallization as phenocrysts to granophyre. The characteristic ovoid form of rapakivi alkali-feldspar phenocrysts is commonly attributed to resorption by the melt (*e.g.*, Nekvasil, 1991). A similar origin is interpreted here for the ovoid shape of rapakivi-texture feldspar phenocryst in Mount Scott Granite.

Two feldspar geothermometry

Temperatures calculated from various pairings of reintegrated compositions of alkali feldspar phenocrysts and matrix alkali feldspar with compositions of sodic phenocrysts (Anorthoclase-N), plagioclase mantles, or plagioclase phenocrysts, and from pairings of individual exsolved microphases (microperthite and micro-antiperthite) using two-feldspar geothermometry (Fuhrman and Lindsley, 1988) are presented in Table 2-3. Temperatures were calculated at pressure values of 200 MPa, 120 MPa, 50 MPa in order to represent possible equilibration at the deeper crustal magma trap, during magma ascent, and at the emplacement crustal magma trap respectively. This choice of pressures does not include the possibility of partial crystallization at deeper levels related to magma generation at 400 MPa or its ascent to the temporary crustal magma trap at 200 MPa. Variation in pressure has little effect on calculated temperatures for the majority of feldspar pairs.

Anorthoclase-N and -K pairs from individual samples yielded concordant temperatures (those in which all three Ab, Or, and An, geothermometers agree) indicating that these phases did crystallize as solvus pairs early within the crystallization history of the Mount Scott Granite. Calculations yield an average temperature of 764 ± 9.2 °C (2σ). They furthermore indicate the high-temperature of the magma that gave rise to this granite.

Analysis of "disequilibrium pairs" (e.g. cores and rims) yielded few "concordant" temperatures ranging from a low of 471°C for a host and its exsolved lamella to a high of 637 °C for an anorthoclase-K phenocryst and plagioclase rim. Fuhrman and Lindsley (1988) assign an error of 30 - 50°C to concordant temperature estimates. The majority of other pairs yield "close-to-equilibrium" temperature estimates (those in which two out of three geothermometers agree) which range from 577°C for a host and its exsolved lamella to 656°C for matrix alkali feldspar in contact with a plagioclase rim. The average of these temperature estimates is 633°C ± 64°C (2σ).

The experimental work of Clemens *et al.* (1986) indicates liquidus temperatures of A-type felsic melts may well exceed 975°C at low pressures and H_2O activities. Hogan and Gilbert (1995) estimated liquidus temperature of 893°C for felsic melts related to the Southern Oklahoma Aulacogen based on Zr chemical geothermometry (Hogan and Gilbert, 1997). Temperatures calculated from two-feldspar geothermometry for Mount Scott Granite are well below liquidus temperatures and presumed solidus temperature for an H_2O-undersaturated or saturated granite magma crystallizing at pressure less than 50 MPa (*e.g.* Tuttle and Bowen, 1958). However, the presence of additional components such as fluorine can dramatically reduce the solidus of granitic magmas (*e.g.*, Manning, 1981). Webster *et al.* (1987) reported experimentally determined solidus temperatures of 530°C for H_2O-saturated conditions and 630°C for H_2O-undersaturated (1 wt.% H_2O) conditions for a rhyolite vitrophyre ($SiO2\approx72.7$ wt.%) containing 1.2 wt.% F_2 at 50 MPa. Partition coefficients for F_2 between biotite and melt (Icenhower and London, 1993) indicate fluorine contents of ≈0.8 wt.% for Mount Scott magma at the time of biotite crystallization (Hogan and Gilbert, 1993). Melt F_2 contents are likely to increase during crystallization due to its high melt/vapor partition coefficient (Hards, 1978) and the dominant crystallization of anhydrous phases within this magma. Calculated F_2 contents for Mount Scott Granite magma may not represent maximum values attained during crystallization. The average temperatures of 633°C ± 64°C (2σ) recorded by feldspar pairs from Mount Scott Granite is consistent with experimentally determined solidus temperatures for H_2O-undersaturated, F_2-rich magmas crystallizing at low pressures. The relatively high temperatures calculated from compositions of exsolved lamella and host grains (471°C to 615°C) indicate limited subsolidus re-equilibration within grains consistent with the intrinsically low volatile content of the magma and rapid cooling of this shallow level intrusion.

Discussion

Mount Scott Granite exhibits many gross similarities with other rapakivi granites including those of the rapakivi granite-anorthosite association (*e.g.* Emslie, 1991). However, it is notably distinct from other rapakivi granites in that it contains two texturally and compositionally distinct populations of ovoid alkali feldspar cores mantled by plagioclase rims: the anorthoclase-N *antiperthite* as well as anorthoclase-K *perthite*. Where perthitic (*i.e.*, orthoclase) cores are typical of most rapakivi granites, the gray ovoid anorthoclase-N antiperthite (*i.e.*, anorthoclase) cores are the more abundant rapakivi feldspar in Mount Scott Granite. In addition, plagioclase grains in Mount Scott Granite are more albitic than plagioclase rims on alkali feldspar, whereas the reverse is more common for typical rapakivi granites (Volborth, 1962; Ehrreich & Winchell, 1969; Nekvasil, 1991). The origin and petrogenetic significance of rapakivi texture in Mount Scott Granite is considered in the following sections.

Formation of rapakivi texture in granophyre-poor samples (< 35 % Granophyre)

Magma-Mixing

The formation of rapakivi texture in feldspars has previously been attributed to disequilibrium processes resulting from magma mixing (Hibbard, 1981; Bussy, 1990). More recently the presence of rapakivi has been suggested as being *diagnostic* of magma-mixing in silicic rock petrogenesis (Stimac and Wark, 1992). Several lines of evidence suggest interaction with more mafic magma was of limited significance in petrogenesis of Mount Scott Granite. Although recent investigations suggest near contemporaneous compositionally bimodal plutonism within the Wichita Igneous Province (Hogan *et al.*, 1996; Price *et al.*, 1998; Chapters 5 and 6, this dissertation), magma mixing (e.g. Vidrine and Fernandez, 1986) appears to be volumetrically insignificant. Furthermore, samples of Mount Scott Granite are remarkably uniform at both the major and trace element scale, away from the vicinity of contacts, over distances of at least 55 km (Hogan *et al.*, 1992). This uniformity is in marked contrast to the large compositional variations commonly documented for open-system magma chambers. In addition, mineral textures indicative of disequilibrium, other than rapakivi feldspar, that can result from magma-mixing, (*e.g.*, pyroxene coronas on quartz, amphibole/biotite coronas on pyroxene or olivine, compositional reversals in plagioclase) have not been observed. Preservation of amphibole phenocrysts and whole rock compositions yielding ~200 MPa pressure estimates indicate Mount Scott Granite magma ascended *en masse* from the deeper level crustal magma trap to the emplacement level crustal magma trap (Hogan and Gilbert, 1995). Finally, even if interaction with a mafic melt were to have occurred while ponding at a deeper level crustal magma trap, it is unlikely that the effects of such an event could have been filtered out during ascent and emplacement.

<u>Exsolution</u>

Gates (1953) and more recently Dempster *et al.* (1991) proposed plagioclase mantles of rapakivi feldspar are the result of extensive exsolution of a ternary alkali feldspar. Merritt (1966) described partial rims of albitic plagioclase, generally less than 0.02 mm thick, mantling microperthite in the hypersolvus Quanah Granite of the Wichita Granite Group. He also prescribed an exsolution origin for "*rim-albite*" but noted that it was uncommon or absent in other granites of the Wichita Granite Group (which includes the

Mount Scott Granite). Feldspars in Mount Scott Granite have undergone subsolidus readjustments as indicated by the presence of antiperthite and perthite, and the pink color of many grains, but compositions of plagioclase rims are similar regardless whether they mantle anorthoclase-N and anorthoclase-K, a feature inconsistent with an origin by exsolution from compositionally distinct host phenocrysts. Although plagioclase rims in Mount Scott Granite are interpreted to have precipitated from a melt, their original magmatic compositions have been adjusted along both margins during subsolidus re-equilibration as indicated by both optical and compositional zoning. However, the relatively uniform composition of interior portions of the rims are interpreted to more closely represent original magmatic compositions.

Decompression

Several investigators have proposed variation of feldspar phase relationships during crystallization in response to magma depressurization, either during ascent, fractionation, or degassing, as the cause of rapakivi texture (*e.g.*, Tuttle and Bowen, 1958; Stewart and Roseboom 1962; Whitney, 1975; Abbott, 1978; Stull, 1978; Cherry and Trembath, 1978). The plausibility of depressurization in the formation of rapakivi textures has more recently been analyzed by a computational investigation of equilibrium crystallization paths in the system $NaAlSi_3O_8$-$KAlSi_3O_8$-$CaAl_2Si_2O_8$-SiO_4 (Nekvasil, 1986, 1988) for several granitic bulk compositions, at various H_2O contents, and pressures from 100-800 MPa (Nekvasil, 1991). The normative composition of Crotch Island Granite, the example discussed in detail by Nekvasil (1991), is similar to Mount Scott Granite facilitating comparisons with this study.

Results of computations in Nekvasil (1991) indicate rapakivi texture can form in response to depressurization (*i.e.*, ascent) during equilibrium crystallization of granitic magma under the following conditions: 1) Appropriate bulk compositions for multiple early saturation of plagioclase, quartz, and alkali feldspar. 2) Sufficient crystallization of alkali feldspar during higher pressure crystallization to prevent complete resorption of this phase during depressurization. 3) Sufficiently low initial H_2O contents such that magmas do not reach vapor saturation prior to or during ascent. 4) Temperature changes during ascent that are close to adiabatic. Small degrees of undercooling ($\leq 3°C$) result in partial resorption of plagioclase and a greater potential for complete resorption of alkali feldspar. Larger degrees of undercooling ($>10°C$) result in precipitation rather than resorption of alkali feldspar. 5) Although the magnitude of decompression is not a critical factor, conditions for rapakivi formation are favored by smaller pressure drops of a few hundred MPa.

Crystallization conditions of Mount Scott Granite were favorable for formation of rapakivi textures in response to depressurization. Hogan and Gilbert (1995) describe an early period of crystallization for plagioclase, quartz, and alkali feldspar from an H_2O-undersaturated Mount Scott magma at a depth of 7-8 km (~200 MPa). The final period of crystallization, at the emplacement level, occurred under subvolcanic conditions at significantly lower pressure (<50 MPa) beneath and within the lower section of the penecontemporaneous volcanic pile of Carlton Rhyolite. The absence of explosive volcanic activity associated with Mount Scott Granite, as well as the scarcity of pegmatite, aplite, and miraolitic cavities, imply continued crystallization under H_2O-undersaturated conditions even for these relatively low pressures (Hogan and Gilbert, 1997).

Temperature decreases only slightly more than adiabatic during ascent are optimum for resorption of alkali feldspar and rapakivi formation (Nekvasil, 1991). Emplacement of Mount Scott Granite magma was closely preceded by extrusion of the voluminous high-temperature Carlton Rhyolite which may have served to preheat the crustal section traversed by Mount Scott magma minimizing heat loss during ascent. Additionally, the Mount Scott Granite immediately followed ascent and intrusion of the Rush Lake Granite (see Chapter 4), which would have pre-heated the ascent path substantially.

Employing the EQUIPATH.FOR program (Nekvasil, 1990), using the Mount Scott Granite composition, revealed that rapakivi texture may result from equilibrium crystallization as anticipated above. At 200 MPa, the liquidus phase is a calcic plagioclase (Ab_{21}, Or_{01}, An_{78}), that becomes rapidly sodic with decreasing temperature. The absence of this initial feldspar composition in the Mount Scott Granite is reasonable, indicating that equilibrium crystallization occurred early on (at high T), and/or that relatively high fF_2 (not accounted for in the numeric model) concentrations destabilized this phase, and/or that this phase resorbed during ascent. Quartz precipitates secondly, followed by an alkali feldspar (Ab_{28}, Or_{70}, An_{02}) coprecipitating with a plagioclase (Ab_{62}, Or_{06}, An_{32}). Evaluation of the remaining liquid at 50 MPa indicates resorption of the quartz and alkali feldspar, ± plagioclase. Plagioclase (Ab_{69}, Or_{12}, An_{19}) crystallizes first, followed by alkali feldspar (Ab_{70}, Or_{16}, An_{14}). This computational model illustrates that rapakivi textures in Mount Scott Granite are likely to have formed during magma decompression. Phase compositions and trends generated by these calculations generally conform with those seen in the Mount Scott Granite. The possibility that some rapakivi textures formed during ascent of the magma from the site of partial melting at 400 MPa to the temporary crustal magma trap at 200 MPa can not be entirely ruled out.

Formation of Rapakivi Textures in Granophyre-rich Samples (> 35% Granophyre)

Plagioclase rims on ovoid alkali feldspar phenocrysts are either incomplete or more commonly absent in Mount Scott Granite where the matrix contains abundant granophyre. Previous investigators have suggested plagioclase rims may be broken or abraded off by other crystals during emplacement (Brown *et al.*, 1992). However, generally wiborgite granites (rounded phenocrysts have plagioclase rims) have lower SiO_2 (65-70 wt.%) and higher CaO contents (1.7-3.1 wt.%) than pyterlite (rounded phenocrysts lack plagioclase rims) granites ($SiO_2 \approx$ 75-77 wt.%; CaO $\approx$ 0.8-1.0 wt.%) suggesting a compositional dependency for crystallization of plagioclase rims (Haapala and Rämö, 1992). This is supported by the experimental studies of Wark and Stimac (1992) who attribute the absence of plagioclase rims on resorbed alkali feldspar in their rhyolite melt compositions to the low anorthite component of the melt inhibiting plagioclase crystallization. Mount Scott Granite is compositionally similar to wiborgite and similar textured granites (Haapala and Rämö, 1992), although exhibiting lower CaO contents. However, the absence of any noticeable difference in whole rock compositions of granophyre-poor and granophyre-rich samples (Myers *et al.*, 1981; Table 2-1) suggest this explanation is unlikely to account for the presence or absence of plagioclase rims in the different textural facies of Mount Scott Granite.

Local differences in fluorine activity during crystallization of Mount Scott Granite may account for the absence of plagioclase rims on resorbed alkali feldspar phenocrysts and the coincident development of granophyric texture. The Mount Scott Granite is presumed to have crystallized under elevated fF_2 based on relatively high fluorine contents of amphibole (1.0-1.7 wt.%) and early crystallization of magmatic fluorite (Hogan and Gilbert, 1995). In addition, results of two-feldspar geothermometry reported in this study suggest significantly depressed solidus temperatures for Mount Scott Granite, a feature consistent with crystallization of a relatively F_2-rich magma. At relatively high fF_2 the stability of amphibole/biotite and titanite are limited by reactions of the type

$$\text{Amphibole/biotite} + F_{2(melt)} \leftrightarrow CaF_2 + Fe_3O_4 + SiO_2 + H_2O \quad (2\text{-}1)$$

and

$$CaTiSiO_5 + F_{2(melt)} \leftrightarrow CaF_2 + TiO_{2(melt)} + SiO_2 + \tfrac{1}{2}O_{2(melt)} \quad (2\text{-}2).$$

Granophyre-rich samples are characterized by lower modal abundance of mafic silicates and titanite consistent with their crystallization under relatively higher fF_2 compared to granophyre-poor samples (Hogan and Gilbert, 1993; Chapter 3 of this dissertation).

Bohlen and Essene (1978) noted the relatively high fF_2 calculated for fayalite-ferrohedenbergite-fluorite granites exceeds the stability of intermediate plagioclase. As the fluorine content of the melt increases during crystallization the anorthite component of plagioclase will react with melt:

$$2\ CaAl_2Si_2O_8 + 2\ F_{2(melt)} \leftrightarrow 2\ CaF_2 + 2\ Al_2SiO_{5(melt)} + 2\ SiO_2 + O_{2(melt)} \quad (2\text{-}3)$$

leaving a more albitic plagioclase (Bohlen and Essene, 1978; Burt, 1981), or perhaps a continuous subsolvus reaction to produce an Ab-rich alkali feldspar (Hogan, personal comm.). Unfortunately, the Mount Scott Granite does not preserve evidence of a continuous reaction. The matrix alkali feldspar grains within the granophyre rich sample W738 contain higher Or than their granophyre-poor counterparts (see Appendix 2).

Equation 2-3 reflects the instability of plagioclase rims in magma domains characterized by greater fF_2, explaining the presence of rare plagioclase rims, and more commonly their complete absence, on anorthoclase-N and anorthoclase-K phenocrysts in granophyre-rich samples (Price *et al.*, 1996). If the plagioclase microphenocrysts crystallized late, their increased sodic content may reflect increased fF_2 in comparison to the magma in equilibrium with the plagioclase rims in Mount Scott Granite.

Variation in mineral assemblages between granophyre-poor and granophyre-rich samples also suggest these rock types crystallized under different fO_2. Granophyre-rich samples commonly contain magnetite, alkali feldspar, and quartz with little to no amphibole, biotite, and titanite indicating crystallization under higher fO_2 (*e.g.*, Wones, 1981). At constant fF_2, the stability of plagioclase is increased with increasing fO_2 (Bohlen and Essene 1978). Therefore, Price *et al.* (1996) suggested that the absence of magmatic plagioclase in granophyre-rich samples implies that the fF_2 in this magma must have been sufficient enough to exceed the stability field of plagioclase despite higher fO_2.

However, equation 2-3 indicates only that the rims will increase in Ab under higher fF_2, it does not explain the complete absence of plagioclase within granophyre-rich samples. Furthermore, it does not explain why fluorite-dominant (and therefore higher fF_2) portions of the Mount Scott Granite are granophyre-rich. The distribution of granophyre throughout the pluton is irregular, interspersed, and generally does not correlate to contact proximity, precluding development of granophyre-rich and -poor portions of the Mount Scott Granite magma through variable cooling rates. Instead, textural variation is the likely result of compositional variability, and once again the only documented variable compositional parameter is fluorine.

Although Swanson and Fenn (1992) were unable to resolve an effect of F on the kinetics of albite growth in the system $NaAlSi_3O_8$-H_2O-F, experimental work in more complex systems indicates that increasing F increases the crystallization lag time (London, unpublished data). For the Mount Scott Granite, sluggish kinetics may have prevented crystallization of feldspar post-ascent, so that plagioclase mantles would not form. Crystallization may have been locally inhibited until the system was sufficiently undercooled to where rapid, cellular growth of quartz and feldspar developed directly on the ovoid phenocrysts.

Conclusions

Mount Scott Granite is unique among rapakivi granites in that it contains two compositionally distinct ovoid alkali feldspar phenocrysts; a sodic anorthoclase that exsolved to antiperthite, and the more typical potassic orthoclase that exsolved to perthite. These ovoid feldspar phenocrysts are rimmed by a thin layer of plagioclase where the matrix is granophyre-poor while plagioclase rims may be incomplete or absent in samples with abundant granophyre. The decrease in the number of plagioclase rims on ovoid alkali feldspar phenocrysts is attributed to crystallization in a relatively fluorine-rich magma. Involvement of a contemporaneous mafic magma and its possible role in formation of rapakivi textures (*e.g.*, Wark and Stimac, 1992) do not seem likely here. Rapakivi textures in Mount Scott Granite formed in response to decompression of an H_2O-undersaturated magma during ascent (*e.g.*, Nekvasil, 1991). The presence of rapakivi textures provides additional information that can be used to track the ascent of Mount Scott magma from temporary ponding at a crustal magma trap at a depth 7-8 km (Hogan and Gilbert, 1995), or possibly partial crystallization at deeper levels, to emplacement along a crustal magma trap beneath the penecontemporaneous Carlton Rhyolite volcanic pile.

References

Abbott, R. N., Jr., 1978, Peritectic reactions in the system An-Ab-Or-H_2O. Canadian Mineralogist, 16, p. 245-256.

Bates, R. L., and Jackson, J. A., 1987, Glossary of geology, 3rd. edition. Alexandria, Virginia, American Geological Institute, 788 p.

Bohlen, S. R., and Essene, E. J., 1978, The significance of metamorphic fluorite in the Adirondacks. Geochimica et Cosmochimica Acta, 42, p. 1669-1678.

Blacklund, H. G., 1938, The problems of the rapakivi granites. Journal of Geology, 46, p. 339-396.

Brown, P. E., Dempster, T. J., Harrison, T. N., and Hutton, D. H. W., 1992, The rapakivi granites of S Greenland - Crustal melting in response to extensional tectonics and magmatic underplating. Transactions of the Royal Society of Edinburgh: Earth Science, 83, p. 173-178.

Burt, D. M., 1981, Acidity-salinity diagrams - application to greisen and porphyry deposits. Economic Geology, 76, p. 832-843.

Bussy, F., 1990, The rapakivi texture of feldspars in a plutonic mixing environment: a dissolution-recrystallization process? Geology Journal, 25, p. 319-324.

Cherry, M. E., and Trembath, L. T., 1978, The pressure quench formation of rapakivi texture. Contributions to Mineralogy and Petrology, 68, p. 319-324.

Clemens, J. D., Holloway, J. R., and White, A. J. R., 1986, Origin of an A-type granite: Experimental constraints. American Mineralogist, 71, p. 317-324.

Dempster, T. J., Hutton, D. H. W., Harrison, T. N., Brown, P. E., and Jenkin, G. R. T., 1991, Textural evolution of other rapakivi granites, south Greenland - Sr, O, and H isotopic investigations. Contributions to Mineralogy and Petrology, 107, p. 459-471.

Ehrreich, A. L., and Winchell, R. E., 1969, Rapakivi texture in rhyolite. Nature, 224, p. 905-906.

Elliston, J. N., 1985, Rapakivi texture: An indication of the crystallization of hydrosilicates, II. Earth Science Reviews, 22, p. 1-92.

Emslie, R. F., 1991, Granitoids of rapakivi-anorthosite and related associations. Precambrian Research, 51, p. 173-192.

Fuhrman, M. L. and Lindsley, D. H., 1988, Ternary feldspar modeling and thermometry. American Mineralogist, 73, p. 201-215.

Gates, R. M., 1953, Petrogenetic significance of perthite., *in* R. C. Emmons, ed., Selected petrogenic relationships of plagioclase. Geological Society of America Memoir 52, p. 55-70.

Gilbert, M. C., 1983, Timing and Chemistry of igneous events associated with the southern Oklahoma Aulacogen. Tectonophysics, 94, p. 439-455.

Gilbert, M. C., and Myers, J. D., 1986, Overview of the Wichita granite group, *in* M. C. Gilbert, ed., Petrology of the Cambrian Wichita Mountains Igneous Suite. Oklahoma Geological Survey Guidebook 23, p. 107-116.

Gilbert, M. C., Hogan, J. P., and Myers, J. D., 1990, Geology, geochemistry and structure of low-pressure sheet granites, Wichita Mountains, Oklahoma. Guidebook for Field Trip #5, Annual Meeting of the Geological Society of America, Dallas Geological Society, 65 p.

Haapala, L. and Rämö, O. T., 1992, Petrogenesis of the Proterozoic rapakivi granites of Finland. *in* H. J. Stein and J. L. Hannah, eds., "Ore-bearing granite systems: Petrogenesis and mineralizing processes", Geological Society of America Special Paper 246, p. 266-328.

Ham, W. E., Denison, R. E., and Merritt, C. A., 1964, Basement rocks and structural evolution of southern Oklahoma. Oklahoma Geology Survey Bulletin, 95, p. 320.

Hards, N., 1978, Distribution of elements between the fluid phase and silicate melt phase of granites and nepheline syenites. NERC Progress in Experimental Petrology, IV, p. 88-90.

Hibbard, M. J., 1981, The magma mixing origin of mantled feldspars. Contributions to Mineralogy and Petrology, 76, p. 158-170.

Hogan, J. P. and Gilbert, M. C., 1993, The role of fluorine in crystallization of A-type sheet granites, Wichita Mountains Oklahoma. Geological Society of America Abstracts with Programs, 25, no. 6, p. 372.

Hogan, J. P., and Gilbert, M. C., 1997, The intrusive style of A-type sheet granites from the Southern Oklahoma Aulacogen. *in* R. W. Ojakangas, A. B. Dickas, and J. C. Green, eds., Middle Proterozoic to Cambrian Rifting. Mid-North America, Geological Society of America Special Paper, 312, p. 299-311.

Hogan, J. P., and Gilbert, M. C., 1995, The A-type Mount Scott Granite Sheet. Importance of crustal magma traps. Journal of Geophysical Research, 100, B 8, p.15,779 - 15,793.

Hogan, J. P., Gilbert, M. C., and Price, J. D., 1994, Shallow drilling investigations of the Mount Scott Granite - Sandy Creek Gabbro Contact, Wichita Mountains, Oklahoma. Geological Society of America Abstracts with Programs, 26, 1, p. 9.

Hogan, J. P., Price, J. D. and Gilbert, M. C., 1994, Rapakivi feldspars in the Mount Scott Granite. International Mineralogical Association 16th General Meeting, Pisa, Italy, p. 363.

Hogan, J. P., Gilbert, M. C., Weaver, B. L., and Myers, J. D., 1992, A-type sheet granites of the Wichita Mountains Igneous Province, Oklahoma, U.S.A. Transactions of the Royal Society of Edinburgh: Earth Science, 83, p. 491-492.

Hogan, J. P., Gilbert, M. C., Price, J. D., Wright, J. E., and Deggeller, M., and Hames, W. E., 1996, Magmatic evolution of the Southern Oklahoma Aulacogen. Geological Society of America, Abstracts with Programs, 28, p. 19.

Icenhower, J. P. and London, D., 1993, An experimental study of the partitioning of fluorine between biotite and silicic melts. Geological Society of America Abstract with Programs, 25, no. 6, p. 372.

Manning, D. A. C., 1981, The effect of fluorine on liquidus phase relationships in the system Qz-Ab-Or with excess water. Contributions to Mineralogy and Petrology, 76, p. 206-215.

McConnell, D. A., and Gilbert, M. C., 1990, Cambrian extensional tectonics and magmatism within the Southern Oklahoma Aulacogen. Tectonophysics, 174, p. 147-157.

Merritt, C. A., 1965, Mt. Scott Granite, Wichita Mountains, Oklahoma. Oklahoma Geology Notes, 25, p. 263-272.

Merritt, C. A., 1966, Rim albite in coarse-grained Quanah Granite, Wichita Mountains Oklahoma, Oklahoma Geology Notes, 26, p. 211-213.

Merritt, C.A., 1967, Names and relative ages of granites and rhyolites in the Wichita Mountains, Oklahoma. Oklahoma Geology Notes, 27, p. 45-53.

Myers, J. D., Gilbert, M. C., and Loiselle, M. C., 1981, Geochemistry of the Cambrian Wichita Granite Group and Revisions of its lithostratigraphy. Oklahoma Geology Notes, 41, p. 172-195.

Nekvasil, H., 1986, A theoretical thermodynamic investigation of the system Ab-Or-An-Qz(-H_2O) with implications for melt speciation. Ph.D. thesis, The Pennsylvania State University, University Park.

Nekvasil, H. , 1988, Calculated effect of anorthite component on the crystallization paths of H_2O-undersaturated haplogranitic melts. American Mineralogist, 73, p. 966-981.

Nekvasil, H., 1990, EQUIPATH.FOR, program for calculating equilibrium crystallization paths based on thermodynamic constraints. FORTRAN 77 format.

Nekvasil, H., 1991, Ascent of felsic magmas and formation of rapakivi. American Mineralogist, 76, p. 1279-1290.

Powell, B. N., and Phelps, D. W., 1977, Igneous cumulates of the Wichita Province and their tectonic implications. Geology, 5, p. 52-56.

Powell, B. N., Gilbert, M. C., and Fischer, J. F., 1980, Lithostratigraphic classification of basement rocks of the Wichita Province, Oklahoma. Geological Society of America Bulletin, part I, 509-514, part II, 91, p. 1875-1994.

Price, J. D., Hogan, J. P., and Gilbert, M. C., 1996, Rapakivi-texture feldspar within the Mount Scott Granite, Wichita Mountains, Oklahoma. European Journal of Mineralogy, v. 8, p. 435-451.

Price, J. D., Hogan, J. P., Gilbert, M. C., and Denison, R. E., 1998, Field guide to the basement rocks of the Southern Oklahoma Aulacogen. South Central Meeting of the Geological Society of America, 76 p.

Seck, H. A.,1971, Koexistierende Alkalifeldspäte und Plaioklase im System $NaAlSi_3O_8$-$KAlSi_3O_8$-$CaAl_2Si_2O_8$-H_2O bei Temperaturen von 650 °C bis 900 °C. Neues Jahrbuch für Minerologie Abhandlungen, 115, p. 315-345.

Sederholm, J. J., 1891, Uber die finnlandischen Rapakiwigesteine. Tschermak's Mineralogische und Petrographische Mittheilungen, 12, p. 1-31.

Stewart, D. B. and Roseboom, E. H., Jr., 1962, Lower temperature termination of the three-phase region plagioclase-alkali feldspar-liquid. Journal of Petrology, 3, 280-315.

Stimac, J. A., and Wark, D. A., 1992, Plagioclase mantles on sanidine in silicic lavas, Clear Lake, California: implications for the origin of rapakivi texture. Geological Society of America Bulletin, 104, p. 728-744.

Stull, R. J., 1978, Mantled feldspars from the Golden Horn batholith, Washington. Lithos, 11, p. 243-249.

Stull, R. J., 1979, Mantled feldspars and synneusis. American Mineralogist, 64, p. 514-518.

Swanson, S. E., and Fenn, P. M., 1986, Quartz crystallization in igneous rocks. American Mineralogist, 71, p. 331-342.

Swanson, S. E., and Fenn, P. M., 1992, The effect of F and Cl on the kinetics of albite crystallization: a model for granitic pegmatites? Canadian Mineralogist, 30, p. 549-559.

Tuttle, O. F., and Bowen, N. L., 1958, Origin of granite in light of experimental studies in the system $NaAlSi_3O_8$-$KAlSi_3O_8$-SiO_2. Geological Society of America Memoir 74, 153 p.

Vidrine, D. M., and Fernandez, L. A. , 1986, Geochemistry and petrology of the Cold Springs Igneous Breccia, Wichita Mountains, Oklahoma. *in* M. C. Gilbert, ed, Petrology of the Cambrian Wichita Mountains Igneous Suite, p. 86-106.

Volborth, A., 1962, Rapakivi-type granites in the Precambrian Complex of Gold Butte, Clark County, Nevada. Geological Society of America Bulletin, 73, p. 813-832.

Wark, D. A., and Stimac, J. A., 1992, Origin of mantled (rapakivi) feldspars: experimental evidence of a dissolution- and diffusion-controlled mechanism. Contributions to Mineralogy and Petrology, 111, p. 345-361.

Webster, J. D., Holloway, J. R., and Hervig, R. L., 1987, Phase equilibria of a Be, U, and F-enriched vitrophyre from Spor Mountain, Utah. Geochimica et Cosmochimica Acta, 51, p. 389-402.

Whitney, J. A., 1975, The effects of pressure, Temperature, and X_{H2O} on phase assemblages in four synthetic rock compositions. Journal of Geology, 83, p. 1-31.

Wones, D. R., 1981, Mafic silicates as indicators of intensive variables in granitic magmas. Mining Geology, 31, p. 191-212.

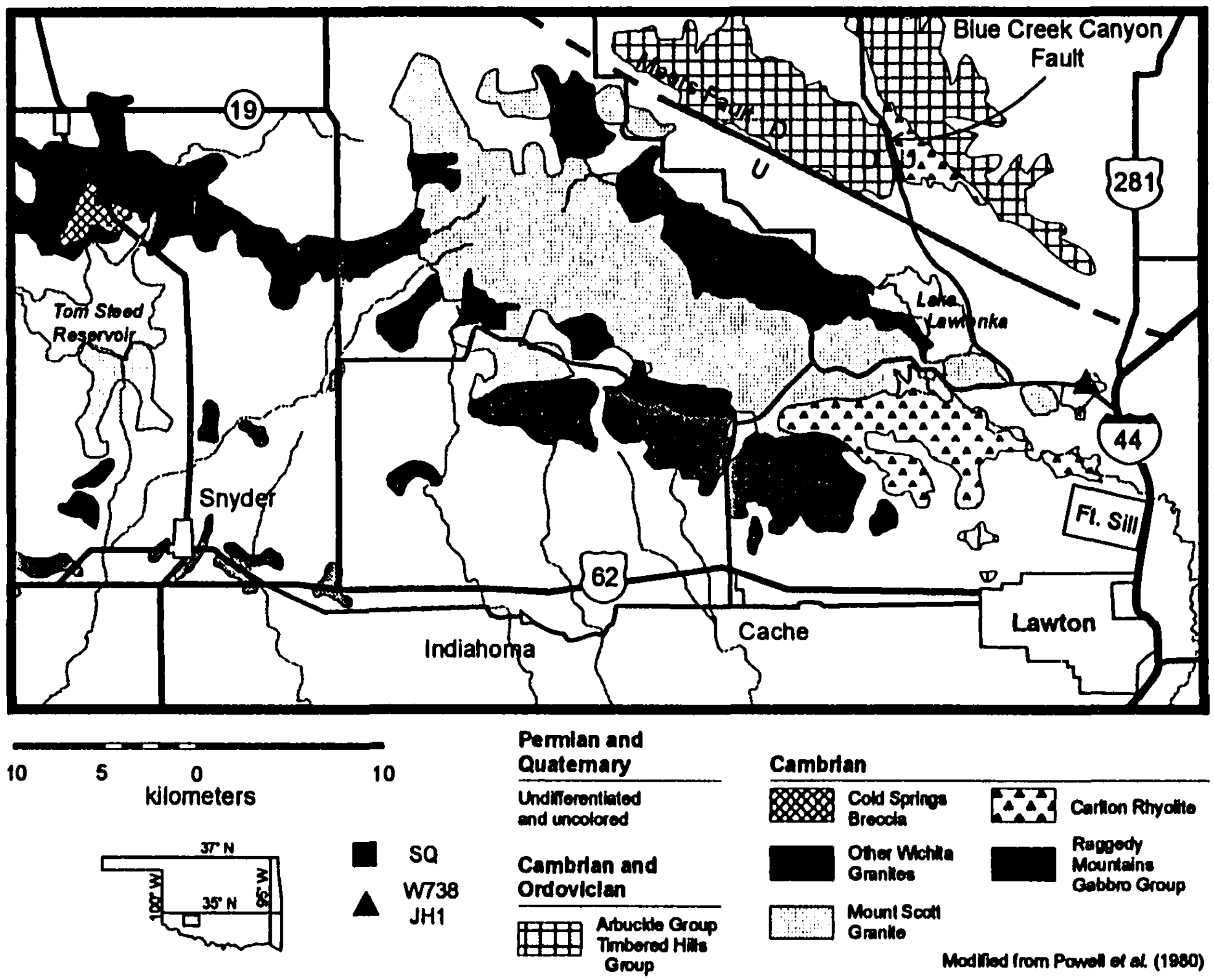

Figure 2-1 Index map showing the location and the extent of outcrop of the Mount Scott Granite. A square marks the location of SQ and triangle marks the location of W738 (JH1-94).

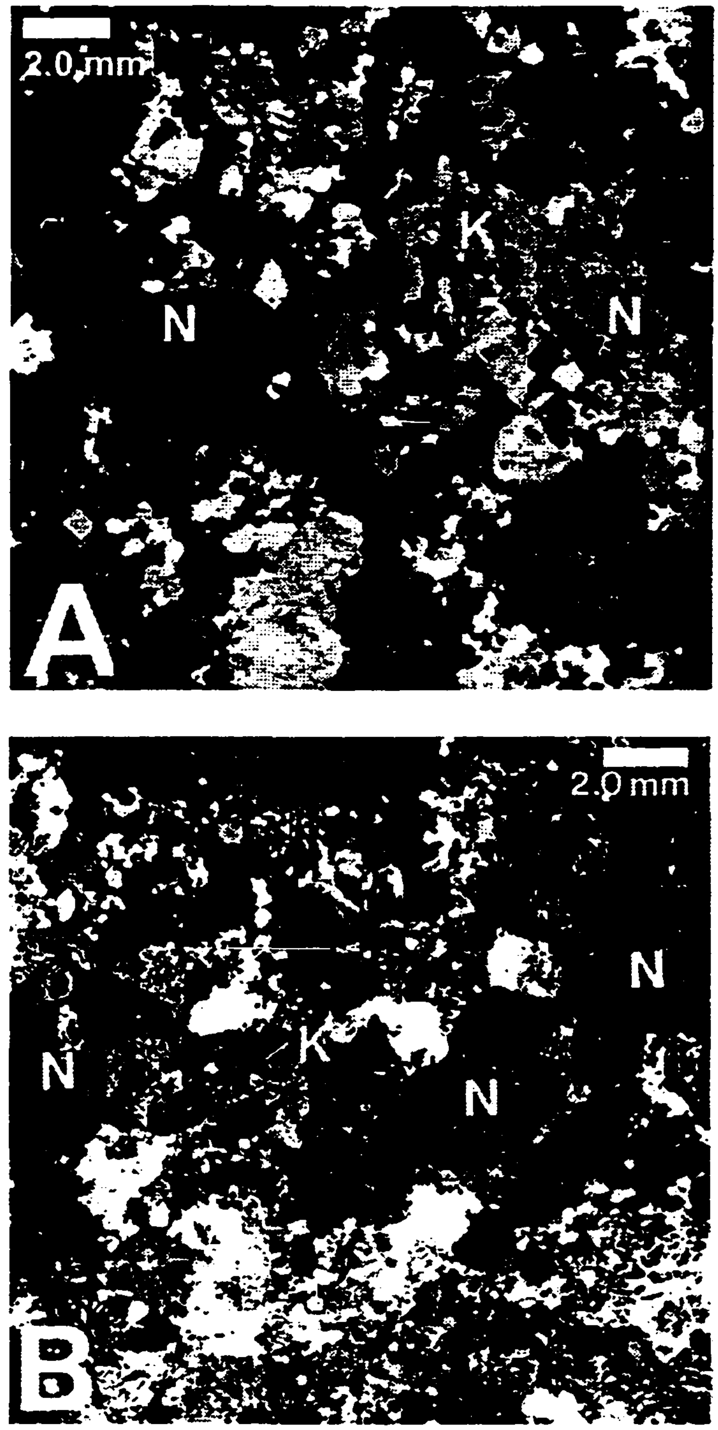

Figure 2-2. Photomicrographs of thin sections of Mount Scott granite (crossed-nichols). Note the presence of ovoid- and block-shaped feldspar phenocrysts. N denotes anorthoclase-N grains, K denotes anorthoclase-K grains. Note variation in feldspar morphology. A.) Sample SQ1, a granophyre-poor (absent) sample. B.) Sample W738 (JH1-94)is a rock with nearly 70% granophyre texture. For whole-rock chemical description see Table 2-1.

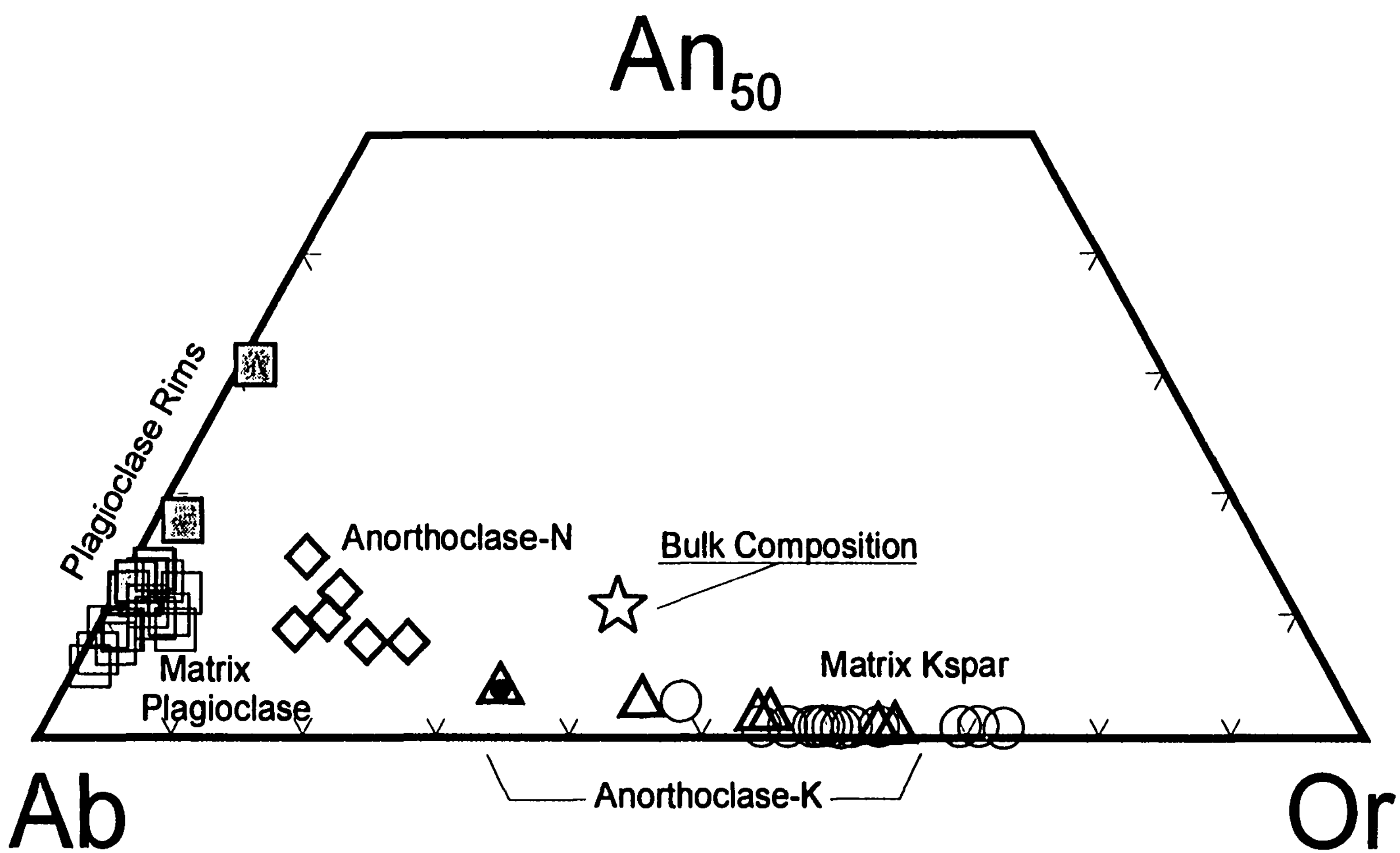

Figure 2-3. Partial ternary feldspar diagram for the Mount Scott Granite in mol.%. Star indicates bulk composition based on the CIPW norm (mol.%) of the average of six analytical samples (Table 1). Open triangles are anorthoclase-K phenocrysts from SQ (granophyre-poor), triangle with dot is from JH1-94 (W738) (granophyre-abundant), open diamonds are anorthoclase-N phenocrysts, filled squares are plagioclase rims found on phenocrysts, open squares are matrix plagioclase microphenocrysts, and open circles are matrix alkali feldspar.

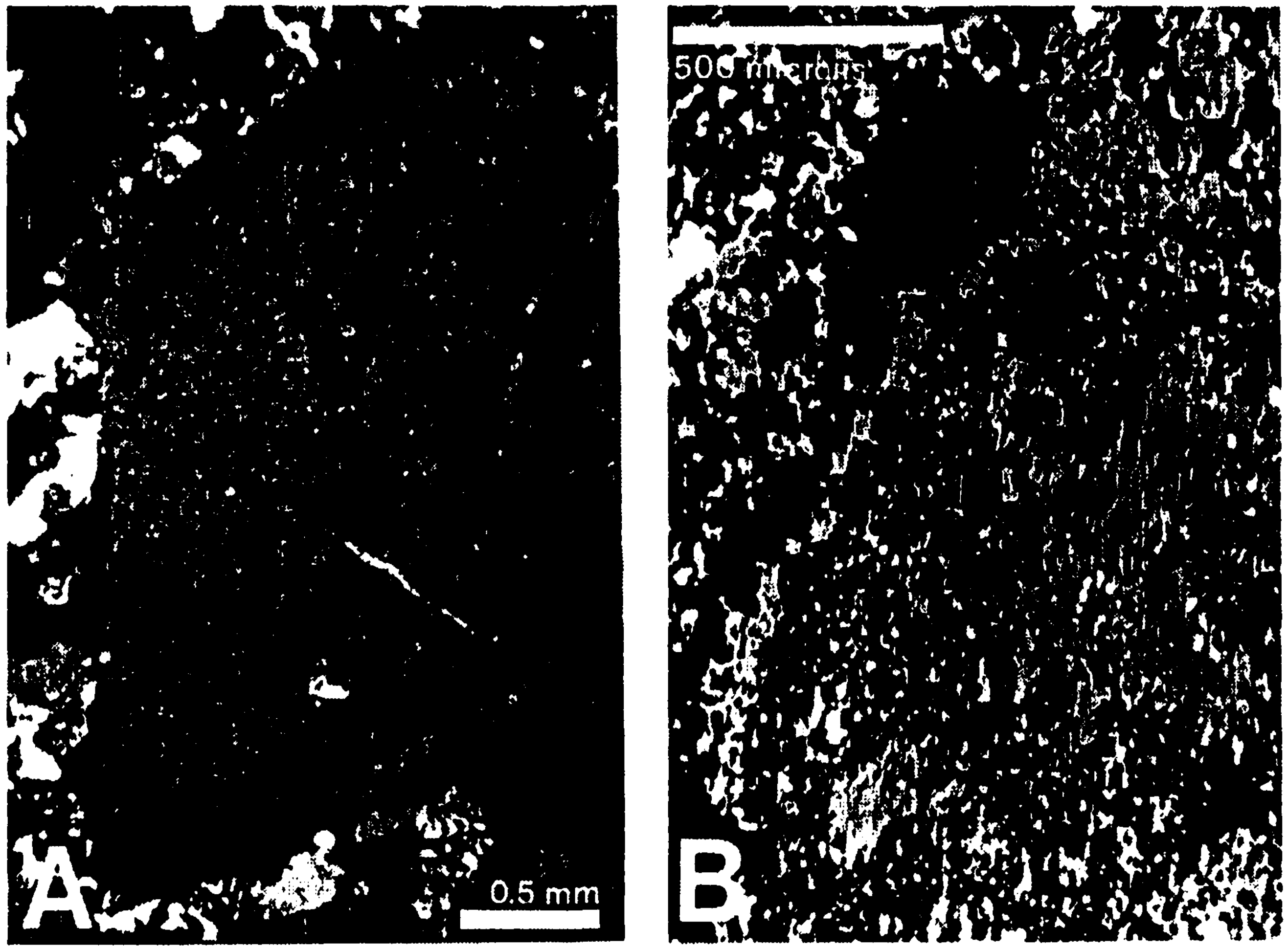

Figure 2-4. Anorthoclase-N phenocrysts. Optical image (A) and chemical image (B) are similar. A.) Photomicrograph of anorthoclase-N ovoid phenocryst under crossed-nichols (sample W728). Ovoid is 3.23 mm long and rimmed by a 200 μm thick layer of plagioclase feldspar. B.) BSE image of an anorthoclase-N crystal from JH1-94 (W738). Plagioclase rim is absent from this specimen, and it is mantled by matrix alkali feldspar. Many of the bright inclusions within the grain are fluorite.

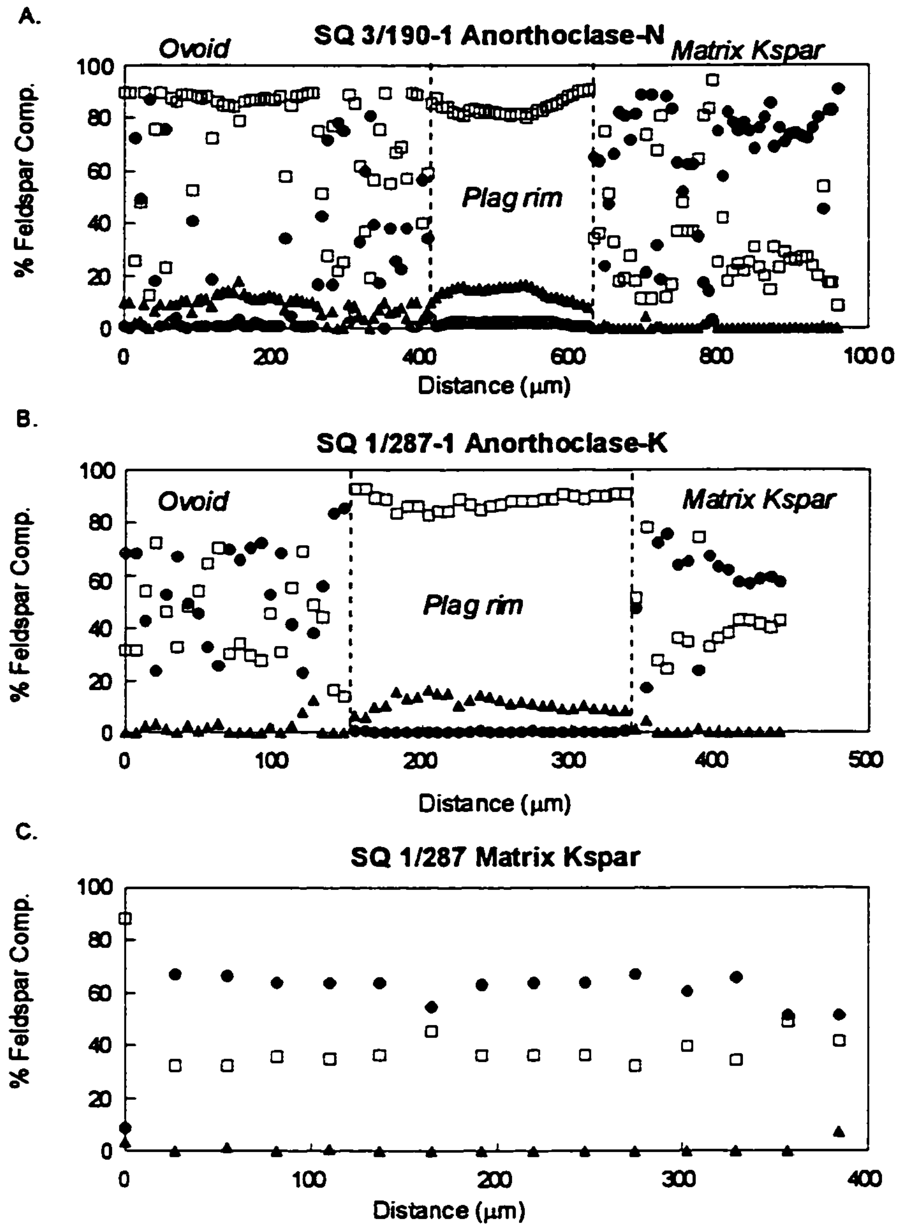

Figure 2-5. Geochemical traverse plots for representative samples of the Mount Scott Granite. Filled squares are albite (mol.%), filled circles orthoclase (mol.%), and filled triangles are anorthite (mol.%). A.) Sample SQ3-19/1, an anorthoclase-N from the exploration drill core at SQ locality. Traverse begins in core, proceeds through plagioclase rim, and then into the surrounding matrix alkali feldspar. Although the rim has a similar composition to the grain, there is a sharp break, and curve in the rim composition. B.) Sample SQ1-287/1, an anorthoclase-K feldspar from the bottom (86 m below surface) of drill core. Traverse starts in the core, goes through rim, and then out into a matrix alkali feldspar. C.) SQ1 287/MK1 is a matrix alkali feldspar grain. Exsolution is less extensive and lamellae are smaller, so chemical variation appears to be minimal.

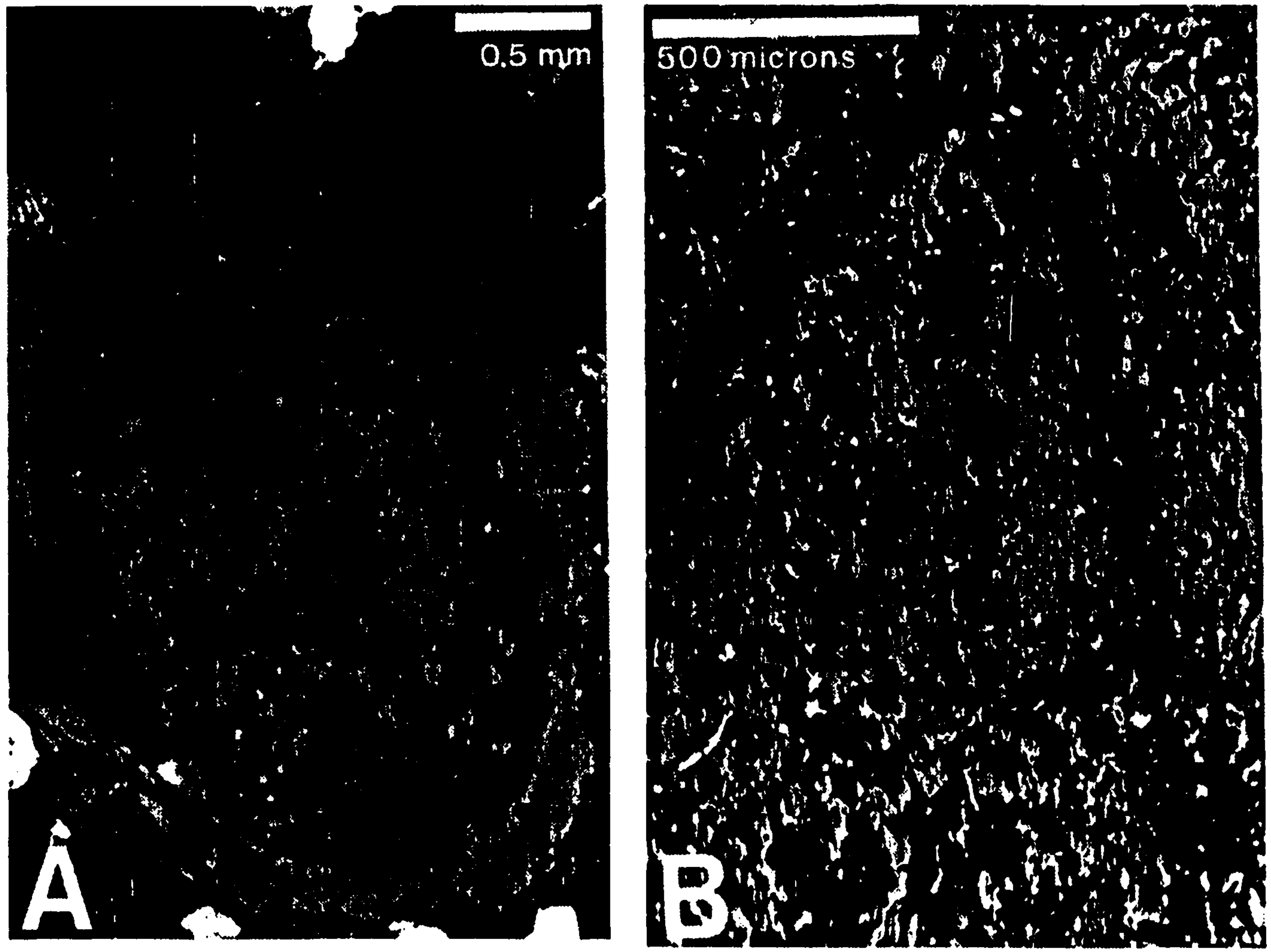

Figure 2-6. Anorthoclase-K ovoid feldspars. Optical image (A) and chemical image (B) are similar. A.) Photomicrograph of anorthoclase-K ovoid phenocryst under crossed-nichols from sample SQ1-150. Ovoid is 3.33 mm long and has a rim of plagioclase (50 - 200 μ thick). These grains are less abundant and smaller than anorthoclase-N. B.) BSE image of anorthoclase-K ovoid from JH1-94 (W738). Grain is rimmed by ~100 μ of plagioclase feldspar.

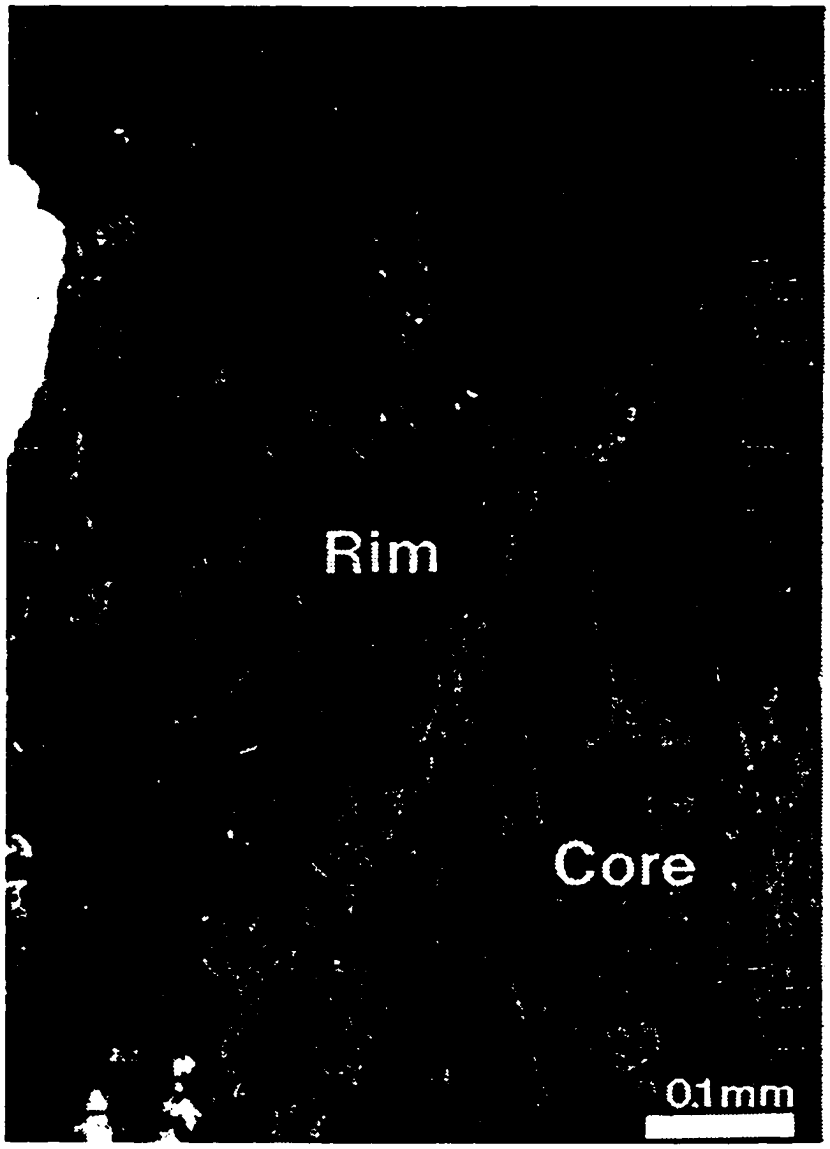

Figure 2-7. Photomicrograph of plagioclase rim surrounding an anorthoclase-K in SQ1-150 (pictured in figure 2-6A). Rims are optically zoned; the extinction converges on the center of the rim. This convergence corresponds with an increase in the Ca component towards the middle of the rim.

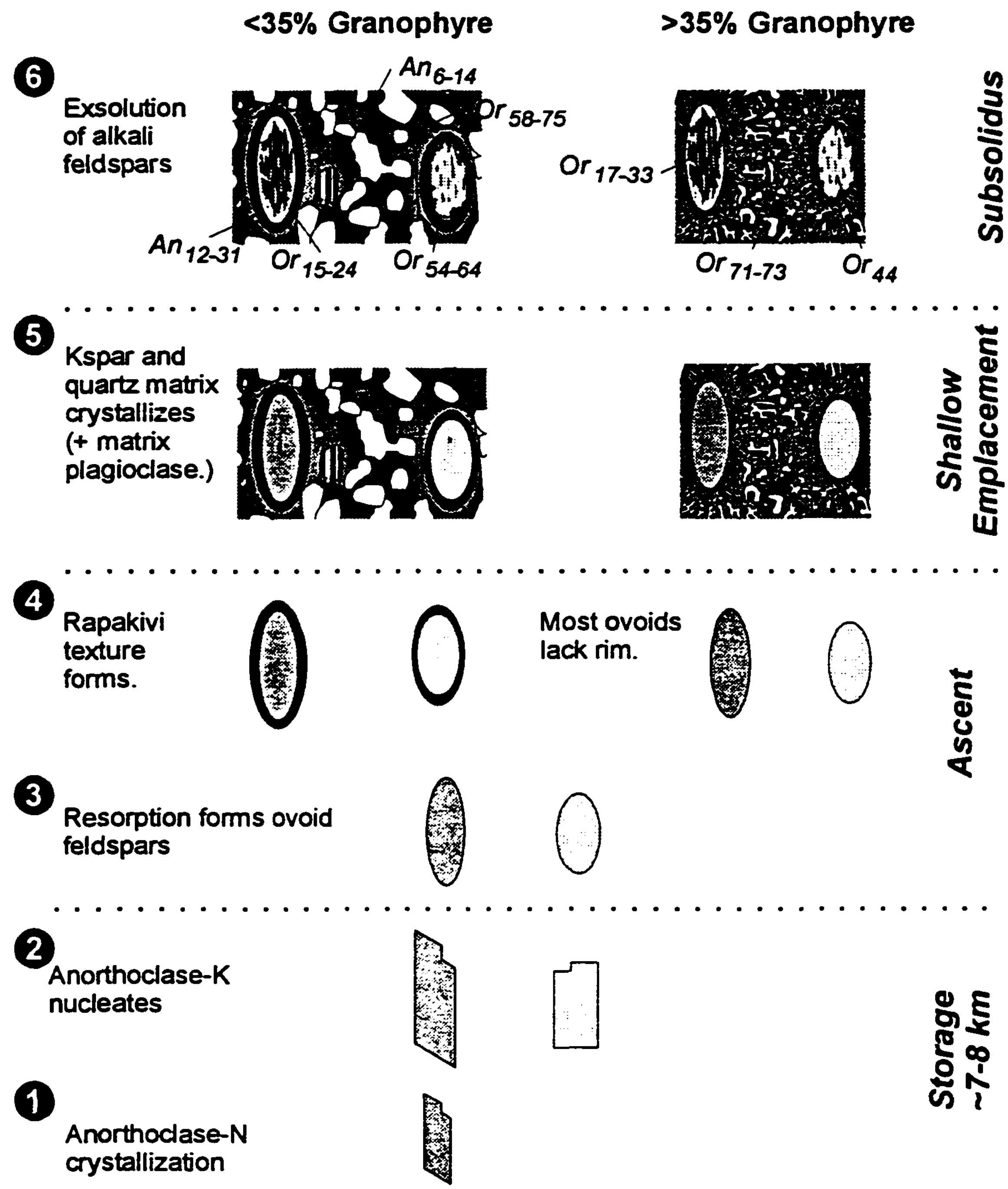

Figure 2-8. Feldspar lineage diagram summarizing the conclusions drawn from textural and geochemical analysis of the Mount Scott Granite. The figure is presented in "stratigraphic" fashion, with oldest feldspar features towards the bottom of the diagram.

Table 2-1. Major element abundances in the Mount Scott Granite.*

Wt.% Oxide	SQ-1	W738 (JH1)	Average† (n=6)	
SiO_2	73.7	73.5	73.6	± 0.60‡
TiO_2	0.42	0.47	0.45	± 0.05
Al_2O_3	12.4	12.7	12.6	± 0.20
Fe_2O_3	3.62	3.83	3.82	± 0.48
MgO	0.36	0.28	0.34	± 0.08
MnO	0.08	0.08	0.08	± 0.01
CaO	1.24	1.27	1.17	± 0.18
Na_2O	3.72	3.64	3.73	± 0.58
K_2O	4.35	4.25	4.30	± 0.10
P_2O_5	0.07	0.08	0.08	± 0.01
Total	100.0	100.1		

*All analyses by XRF

†Average of 6 whole-rock analyses of Mount Scott Granite.

‡2σ standard deviation of the mean

Table 2-2. Representative averages of Mount Scott Granite feldspar analyses.

Type	Anorth-N				Anorth-K		Plag Rim				Matrix Kspar				Matrix Plag	
Sample	JH194.a.1†		SQ 3 19.1		SQ1 2817.3		SQ 3 19.1		SQ1 287.3		SQ 3 19.1		JH194.g.n2		SQ 1 114.4	
# pts.*	28		55		36		31		29		38		5		10	
	wt.%	±2σ	wt.%	±2σ	wt.%	±2σ	wt.%	±2σ	wt.%	±2σ	wt.%	±2σ	wt.%	±2σ	wt.%	±2σ
SiO_2	64.0	0.7	65.2	0.7	65.6	0.5	64.7	0.7	65.4	0.7	64.7	0.9	64.2	0.6	65.6	0.4
Al_2O_3	21.3	1.0	21.1	1.0	19.5	0.5	22.3	0.5	22.2	0.5	19.0	0.3	19.0	0.2	21.5	0.1
FeO	0.3	0.1	0.1	0.0	0.1	0.0	0.1	0.0	0.1	0.0	0.1	0.0	0.1	0.0	0.1	0.0
MgO	‡BD		BD		BD		BD		BD		BD		BD		BD	
CaO	2.4	1.0	1.8	0.9	0.3	0.4	3.0	0.5	2.6	0.5	0.1	0.2	0.2	0.1	2.2	0.2
Na_2O	8.0	1.8	8.3	2.9	3.8	2.1	10.0	0.4	10.3	0.3	3.3	1.8	3.2	1.4	10.4	0.1
K_2O	3.0	3.2	3.7	4.5	10.8	3.3	0.4	0.1	0.2	0.1	12.1	2.5	11.9	2.1	0.5	0.2
BaO	0.4	0.3	0.4	0.4	0.5	0.1	BD		BD		0.4	0.1	0.2	0.1	BD	
P_2O_5	BD		BD		BD		BD		BD		BD		BD		BD	
Total	99.4	0.4	100.6	0.5	100.5	0.6	100.6	0.3	100.9	0.7	99.6	0.8	98.7	0.2	100.3	0.3
Cations (8 Oxygen Basis)																
Si	2.9		2.9		3.0		2.8		2.9		3.0		3.0		2.9	
Al	1.1		1.1		1.0		1.2		1.1		1.0		1.0		1.1	
Fe	0.0		0.0		0.0		0.0		0.0		0.0		0.0		0.0	
Ca	0.1		0.1		0.0		0.1		0.1		0.0		0.0		0.1	
Na	0.7		0.7		0.3		0.9		0.9		0.3		0.3		0.9	
K	0.2		0.2		0.6		0.0		0.0		0.7		0.7		0.0	
Ba	0.0		0.0		0.0						0.0		0.0			
Feldspar Components (Mol. Fraction)																
Ab	0.71		0.71		0.35		0.84		0.87		0.29		0.29		0.87	
Or	0.17		0.21		0.64		0.02		0.01		0.70		0.71		0.03	
An	0.12		0.08		0.01		0.14		0.12		0.00		0.01		0.10	

* Indicates number of points averaged

† Analyzed with a 15μ e-beam spot size, all other analyses with 3μ spot size

‡ BD - Data value below the lower limit of detection

A table of averages from Mount Scott Granite feldspar analyses is found in appendix 2

Table 2-3. Two-feldspar geothermometry

Sample	Alkali Feldspar	Plagioclase	*P	†T_{Ab}	T_{An}	T_{Or}	‡T_{Pref}
Granophyre-rich matrix							
JH1	Anorth-K	Anorth-N	200	745	745	795	§*762*
Granophyre-poor matrix							
SQ1 287	Anorth-K	Anorth-N	200	810	816	804	*810*
SQ3 19	Anorth-K	Anorth-N	200	753	754	751	*753*
SQ1 114	Anorth-K	Anorth-N	200	718	718	757	*731*
Granophyre-poor matrix							
SQ3 19	Anorth-K	Rim	120	573	573	568	*567*
SQ3 19	Anorth-K	Rim	120	589	625	518	607
SQ3 19	Anorth-N	Rim	120	591	587	542	599
SQ3 19	Matrix	Rim	50	703	654	653	654
SQ1 114	Anorth-K	Rim	120	620	616	538	618
SQ1 114	Anorth-K	Rim	120	624	663	620	622
SQ1 114	Anorth-K	Rim	120	661	626	603	614
SQ1 114	Matrix	Rim	50	658	653	614	656
SQ1 287	Matrix	Phenocryst	50	652	595	595	595
SQ1 287	Matrix	Phenocryst	50	610	646	556	628
SQ1 287	Matrix	Phenocryst	50	583	764	531	557
SQ1 287	Matrix	Phenocryst	50	631	647	537	639
SQ1 287	Matrix	Rim	50	663	597	495	630
Granophyre-rich matrix							
JH1b f3	Lamella	Host	50	241	579	574	576
JH1b f4	Lamella	Host	50	611	598	559	604
JH1b f4	Host	Lamella	50	486	455	471	*471*
JH1b f6	Host	Lamella	50	600	611	634	*615*
JH1b f6	Host	Lamella	50	618	605	545	612
JH1g f8	Lamella	Host	50	590	593	540	592

*Pressure in MPa

†Temperature in °C (Fuhrman & Lindsley, 1988)

‡Preferred Temperature

§Concordant values shown in italics

Chapter 3. Titanite-fluorite equilibria in the Mount Scott Granite: experimental study and implications for determining F in felsic magmas.

Introduction

Fluorine affects the physiochemical properties of felsic magmas. Fluorine depresses solidi (Koster Van Groos and Wyllie, 1967; Manning, 1981; Dingwell *et al.*, 1985, Webster *et al.*, 1987), reduces viscosities and densities (Dingwell *et al.*, 1985, Dingwell *et al.*, 1993), affects vapor/melt partitioning behavior (Webster, 1990; Webster and Holloway, 1990), and influences crystal/melt element partitioning (Collins *et al.*, 1982; Keppler, 1991). Commonly, elevated fluorine contents in magmas are proposed to explain numerous igneous phenomena including: 1. high field strength element enrichment in A-type melts (Collins *et al.*, 1982), 2. eruption of rhyolite lava flows with high aspect ratios (Dingwell *et al.*, 1985), 3. development of "rimless" rapakivi texture (*i.e.* pyterlite) (Price *et al.*, 1996a), and 4. phase-stability within crystallizing systems (Bohlen and Essene, 1978; Gilbert *et al.*, 1990; Price *et al.*, 1995; this study). Thus, determining F concentration in magmas is crucial to understanding individual igneous systems.

The F content of magma is difficult to estimate directly from its crystalline products. Even though F partitions preferentially in melt over vapor (Webster, 1990, and references therein), F is largely incompatible in the majority of igneous assemblages, and eventually lost to vapor as crystallization progresses (Webster *et al.*, 1991). Thus, whole-rock F contents of phyric rocks reflects variation in the modal abundance of F-bearing phases

(Bailey, 1977), rather than the F content of the magma (see discussion by Christiansen and Lee, 1986). The F contents of biotite and apatite have been used to interpret the F-concentrations of the liquids from which they crystallized (Munoz and Ludington, 1974; Piccoli and Candela, 1994; Stormer and Carmichael, 1971; Ludington, 1978). Unfortunately, these methods are based on equilibration of these crystalline phases with an aqueous-HF fluid, and are not directly applicable to crystal-melt equilibria, as spectroscopic evidence indicates AlF_6^{3-} complexes are the dominant F species in melt (Kohl *et al.*, 1991), and that HF in melt is negligible (Schaller *et al.*, 1992). Application of the biotite-melt relationships developed by Icenhower and London (1997) is hampered in strongly outgassed systems (*e.g.* Morococala volcanics, Morgan *et al.*, 1998). Finally, re-equilibration after solidification, may impede any estimate of magmatic composition. "The F contents of biotite thus can yield information about the characteristics of the magma or about subsolidus exchange" (Wones, 1981), and in systems where the latter applies, which may include a substantial percentage of felsic rocks, magmatic F remains elusive.

Gilbert *et al.* (1990) recognized an antipathetic modal variation in the abundance of titanite and fluorite in the A-type Mount Scott Granite of the Wichita Mountains, Oklahoma. They attributed this change to reflect variability of the fluorine content of the magma, produced through the reaction:

$$CaTiSiO_{5\,(Ttn)} + F_2 \Leftrightarrow TiO_{2\,(melt\ or\ ilm)} + CaF_{2\,(Fl)} + SiO_{2\,(in\ melt\ or\ in\ qtz)} + \tfrac{1}{2}O_2 \quad (3\text{-}1).$$

This paper presents an experimental evaluation of titanite and fluorite stability as functions of F and H_2O content within a metaluminous felsic melt at T=850 °C, P = 200 MPa, $fO_2 \approx$ NNO. It shows that, with provisions, the equilibrium of equation 3-1 is useful as an indicator of magmatic F contents during crystallization of the Mount Scott Granite, Wichita Igneous Province, Oklahoma. Additionally, this monitor is germane to subaluminous (*s.l.*) granitoids, utilizing the presence of fluorite to classify appropriate magmas as "high F." Similar granitoids reported in the literature are classified by their fluorine ± titanite assemblage.

Techniques

Experimental

Experiments employed a finely powdered (<10 μm) unaltered Mount Scott Granite from 37.5 m depth below surface (SQ-1 drill core, Price *et al.*, 1998). Whole-rock analyses for the starting material, SQ-1 123A are given in table 3-1. Fluorine content, determined by ICP-MS, is 0.18 wt.%, and water content (H_2O^+), determined by loss on ignition, is 0.24 wt.%. These values are consistent with wet-chemical analysis of a surface sample from the same locality (Merritt, 1965). The F content is higher than "normal granite" in Bailey (1977).

To the SQ-1 123A powder, fluorine was added as AgF, ground dry in an agate mortar and pestle to create three mixed powders of 0.5 wt.%, 1.0 wt.%, and 1.5 wt.% added F. The total available F (whole-rock fluorine + added F through AgF) for these three compositions was 0.68, 1.18, and 1.68 wt.% respectively.

In water-added experiments, first doubly-distilled H_2O and then a specified amount of one of the four rock ± fluorine powders (to yield starting compositions from nominally 0.24 to 10 wt.% H_2O) were loaded into 20 x 3 mm cylindrical Au capsules, with the mixture confined to the central 10 x 3 mm portion of the capsule. AgF is extremely hygroscopic. Adsorption rates varied with atmospheric relative humidity, and water contents for each series of charges were determined through weight change in ~0.1 gram sample of powder (pre-dried at 120 °C for one hour) simultaneous to loading. Charges with no added water were dried prior to and heated during welding to prevent adsorption. Final compositions ranged from 0.24 to 11.08 wt.% H_2O_T (bulk, including added, adsorbed, and rock H_2O^+). Sealed charges were heated overnight at 120 °C to redistribute the H_2O in the capsule and to test for leaks by weight loss.

Capsules were run subhorizontally in water-pressurized cold-seal vessels at 850 °C, 200 MPa. The temperature was controlled by external and monitored by internal Chromel-Alumel thermocouples with an estimated internal error of ±5 °C. Pressure was monitored by a factory-calibrated Heise Bourdon tube gauge, with fluctuations < ±2 MPa. Experiments were run open to the gauge and a 2 liter pressure buffer of water plus traces of Immunol ™ rust inhibitor. Oxygen fugacity in the experiments was buffered slightly below Ni-NiO_2 (NNO) by the reaction vessels and the small amount of hydrocarbon rust inhibitor within the water pressure medium (*e.g.* Huebner and Sato, 1970). Duration and temperature of experiments were such as to establish fO_2 equilibration by diffusion of H_2 between experiment and pressure reservoir across Au tubing of 0.18 mm (Chou, 1987). Run times varied, ranging from 139 hours to 331 hours, durations previously proven to produce equilibrium conditions in silicate melts within this facility. Upon completion of the run, experiments were quenched isobarically by air-jet to < 300 °C in under five minutes. Following quench, capsules were weighed to check for leaks developed during the runs.

The investigation did not include a traditional assessment of equilibrium through temperature reversal experiments. Nevertheless, it appears that equilibrium was attained in all experiments with respect to equation (3-1). Experiments contained either titanite or fluorite, and always produced new growth of either phase, from a starting material that contained both phases. Although equilibrium with respect to the entire system was not attained within runs with $H_2O_T = 3\text{-}5$ wt.%, as these produced epitaxial overgrowth on relict fragments, typically hornblende, titanite (in runs with $F_t < 1.05$ wt.%), and ilmenite. In most cases, mantles overgrew cores of the same phase (*i.e.* amphibole mantling amphibole). Still, rims were identifiable because of a contrast in the BSE signal, and thus mantles are compositionally distinct from their cores. Additionally, in F-added runs, rimmed amphiboles contained magnetite as small inclusions at the mantle-core interface of hornblende, the likely result of crystallization early in the run as dissolution of AgF buffered $fO2$ higher than NNO. Following AgF dissolution, the system fO_2 approached the bomb-induced NNO buffer, and continued crystallization produced amphibole around the relict hornblende + newly crystallized magnetite. Despite system-wide disequilibrium in some runs, this study outlines equilibrium phase stability in melt because it assesses it through glass compositions in equilibrium with new crystallization, epitaxial or otherwise.

Analytical

Following quench, capsules were checked for vapor content by examination of effused fluids produced upon puncture of the capsule wall, and by weight change after drying the punctured capsule. The run products were then removed from capsules and broken into chips. Chips from each sample were mounted in epoxy, then ground and polished to <1 μm grit for electron microprobe analysis (EMPA). Other chips were crushed to a coarse powder (< 0.1 mm) for optical evaluation and fine-powder (<10 μm) for X-ray diffraction analysis.

Crystalline phases were identified largely through back-scattered electron (BSE) imaging coupled with energy-dispersive x-ray analysis (EDXA) using a Cameca SX-50 electron microprobe equipped with a delta-class Kevex EDXA spectrometer. Additionally, eleven samples were analyzed by powder X-ray diffraction, and all samples were analyzed optically to verify probe results. Reaction within runs was determined by BSE imaging: rimming, skeletal, equant, and euhedral textures were interpreted as growth; pitting and embayment textures were interpreted as dissolution; and mantled or phases exhibiting none of the previous textures were interpreted as relicts.

Experimentally produced glasses in excess of 35 vol.% of the run product were analyzed by wavelength-dispersive X-ray spectrometry via EMPA for Si, Al, Na, K, and Ca. Analyses used an accelerating voltage of 20 kV, 2 nA beam current, and 15-20 μm spot size, and for Fe, Ti, Mg, Mn, Ba, P, Cl, and F using an accelerating voltage of 20 kV, 20 nA beam current, and 15-20 μm spot size following the methods of Morgan and London (1996) to reduce volatilization during analysis. Primary standards were bytownite for Si, Al, and Ca, albite for Na, orthoclase for K, Ba-Fe-aluminosilicate glass for Ba, olivine for Mg, Ti-bearing glass for Ti, rhodonite for Mn, augite for Fe, topaz for F, and tugtupite ($Na_4AlBeSi_4O_{12}Cl$) for Cl. Calibration was checked against secondary standards of synthetic glasses of Spor Mountain and Topaz Mountain rhyolites. Analyses applied the PAP correction to the counting data (Pouchou and Pichoir, 1985). The 3σ minimum detection thresholds (in weight percent) were: 0.05 for SiO_2, 0.02 for Al_2O_3, 0.02 for Na_2O, 0.01 for K_2O, 0.02 for CaO, 0.02 for FeO, 0.02 for TiO_2, 0.02 for MgO, 0.03 for MnO, 0.04 for BaO, 0.04 for P_2O_5, 0.01 for Cl, and 0.13 for F.

Variable components within this paper are expressed in terms of total available content. The term $\mathbf{F_T}$ expresses total F in the system (SQ-1 123A whole-rock F + added F), and the term $\mathbf{H_2O_T}$ expresses the total H_2O in the system (SQ-1 123A loss on ignition + added H_2O + adsorbed H_2O). Additionally, the term $\mathbf{F_m}$ refers to the wt.% value of F in EMPA of glass (glass = melt). Likewise, the term $\mathbf{H_2O_m}$ refers to 100 - EMPA total of glass analysis in wt.% (water by difference). Mineral abbreviations are from Kretz (1983).

Charges with no added H_2O failed to produce sufficient glass volumes for EMPA (<35% glass). In order to include these runs within the phase stability analysis, a function was regressed for H_2O_T and F_T to H_2O_m (for H_2O-undersaturated runs) and F_m of analyzed glasses from this study (Figure 3-1). F_m correlates to F_T over the set of analyzed glasses by a linear equation with a slope of 0.55 (± 0.09), with an intercept at F_m = 0.49 wt.%, and a r^2 value of 0.75. Likewise, with the exception of runs Z48 and Z57 (both H_2O-saturated runs), the H_2O_m and H_2O_T values express a linear correlation, with a slope of 0.66 (± 0.08) and intercept at H_2O_m = 1.22 wt.%, with a r^2=0.86. This function calculated H_2O_m and F_m values for the no H_2O added runs. Errors for these values are significantly greater than determinations by EMPA as they reflect the uncertainty of the regression analysis (standard deviation) as well as analytical precision.

Results

All experiments contained an assemblage of glass + crystals + vapor (air) following quench. The experimental conditions produced either a fluorite-bearing or titanite bearing assemblage within each capsule dependent on F_T.

Glasses

Runs without added F or H_2O ($F_T = 0.19$ and $H_2O_T = 0.24$ wt.%) contained <1 vol.% of glass as thin pools around crystal grain boundaries. The addition of H_2O, and to a lesser extent F, resulted in larger amounts of glass, ranging from 2 vol.% glass, in runs with starting compositions $F_T = 0.69$ wt.% and no H_2O added, to 95 vol.% glass, in starting compositions exceeding $H_2O_T = 5.0$ wt.%.

Runs Z48 and Z57 (Table 3-1) achieved water saturation, as indicated by the precipitation of liquid in the puncture hole during opening and significant weight loss following drying after opening. These two runs fell below the linear correlation between H_2O_T and H_2O_m observed within the rest of the analyzed glasses (see discussion in analytical techniques), containing 7.1 and 4.5 wt.% H_2O for 11.03 and 10.21 H_2O_T respectively.

Compositional analyses of the starting material and experimental glasses are shown on table 3-1. Glass analyses recalculated on an anhydrous (*i.e.* compositions normalized to analysis total minus H_2O^+) and afluorous basis (*i.e.* compositions normalized to analysis total minus F) allow comparison independent of added components. The glass compositions show significant correlation only with increasing H_2O_m (Figure 3-2), and only weak trends but typically no trend with Fm or F_m/H_2O_m. The K_2O concentration is negatively correlated with H_2O_m, while CaO, BaO, MnO, are positively correlated with H_2O_m. The concentrations of Na_2O and Al_2O_3 increase until $H_2O_m > 3$, and then decrease. The SiO_2 concentration decreases until $H_2O_m > 3$, and then increases at higher values, exhibiting the opposite trend seen in Na_2O and Al_2O_3. The concentration of MgO and TiO_2 remain low until $H_2O_m > 3$, and then increase. With regard to increasing F, only

Al_2O_3 and CaO exhibit a slight positive correlation. With regard to the F/OH ratio, Fe# (molecular Fe / [Fe + Mn + Mg]) exhibits a slight positive correlation. The ANCK ratio (molecular Al_2O_3 / [Na_2O + K_2O + CaO]) and the A/NK ratio (molecular Al_2O_3 / [Na_2O + K_2O]) do not fluctuate with added components; ANCK remains near unity for all runs, A/NK averages 1.13.

Crystalline phases

All runs preserved a relict portion of the starting crystalline assemblage and/or produced new phases similar to those of SQ-1 123A: alkali feldspar + quartz ± plagioclase ± amphibole ± biotite ± FeTi-oxide ± titanite ± fluorite, zircon ± apatite ± monazite. Runs >1 wt.% and <6 wt.% H_2O_T contained rimmed, pitted, and embayed phases, indicating reaction with melt. All runs exceeding 1 wt.% H_2O_T also produced new growth as evidenced by rims, skeletal, and euhedral morphologies. Zircon occurred as angular fragments with no evidence of growth or of dissolution.

Feldspar was present in runs with H_2O_T < 6 wt.%. Runs with H_2O_T > 2 wt.% grew small alkalic ternary feldspars (by EDXA) with largely patchy (skeletal?) morphologies (15-20 μm patches with 1-3 μm limbs). Runs with H_2O_T < 2 wt.% contained relict plagioclase. The vol.% of relict plagioclase decreased with increasing F_m.

Quartz crystals were typically rounded grains in all runs. This morphology precluded drawing conclusions about growth or dissolution of quartz. However, quartz was absent in runs with > 4 wt.% H_2O_m. In runs between 2 and 4 wt.% H_2O_m, the vol.% of quartz increased with F_m.

Amphibole crystals grew in runs between 0.4 wt.% and 1.2 wt.% F_m, as typically small (2-5 μm), evenly distributed skeletal crystals, small euhedral crystals (Figure 3-3a), or thin (2 μm) epitaxial overgrowth on relict hornblende cores. Although too small to analyze by EMPA, rimming hornblende appeared to have a higher Mg# than the hornblende cores they mantle (likely relicts of the ferroedenitic hornblende in the starting rock powder, Hogan and Gilbert, 1995). Mantles have a darker BSE signal, and EDXA shows they have a greater intensity Mg peak relative to their cores.

Biotite was absent from runs with $F_m < 1$ wt.%. In the run without added F or H_2O (Z5), the limited amount of melt was generated through dehydration melting of biotite. At $F_m > 1$ wt.%, biotite appeared as 5 μm or smaller grains, in clusters 20-30 μm wide. Cluster morphology resembled domains of hornblende dissolution.

Runs contained either titanite or fluorite (equation 3-1). Titanite is stable in runs with $F_m < 1.05$ wt.% over a range of $H_2O_m = 1.5$ to 7 wt.%. Titanite appeared as euhedral crystals and thin rims on relict titanite and on FeTi-oxides (Figure 3-3b). Runs with higher F_m produced small fluorite crystals (Figure 3-3c), predominantly adjacent to larger tabular biotite grains and magnetite, confined to small domains. Fluorite crystals were numerous and ranged from submicron to > 5 μm in diameter, typically equant and round, rarely euhedral. In H_2O-saturated runs with $F_m > 1$ wt.%, fluorite appeared as submicron crystals distributed throughout the glass.

Figure 3-4 shows the stability of titanite and fluorite as functions of F_m vs. H_2O_m. The diagram demonstrates that the boundary for titanite versus fluorite (equation 3-1) is at 1.05 ± 0.13 wt.% F. The boundary curve is interpreted to be midway between the analyses. It is interpreted to be vertical, as water does not influence equation 3-1. Although the relative stability of OH-titanite to F-titanite may affect this curve, because F and OH are minor components within titanite (*e.g.* Deer *et al.*, 1966), the overall effect to the phase boundary should be minimal.

A small number of runs, using the same starting composition over a similar range of F and H_2O were completed at T = 750 °C, P = 200 MPa, $fO_2 \approx$ NNO. Water-undersaturated runs did not reach near-equilibrium conditions, even for durations in excess of a month. Water-saturated runs did produce glass with crystals, and results indicated a boundary for equation 1 at 0.67 ± 0.13 wt.

Discussion

Fluorine in the Mount Scott Granite

The experimental conditions were designed to simulate those imposed on the magma during initial crystallization of the Mount Scott Granite. Zirconia geothermometry (zircon saturation temperature) yields estimates of 893 ± 11 °C, a likely near-liquidus temperature (Hogan and Gilbert, 1997), and feldspar geothermometry yields estimates of 764 ± 9.2 °C for early crystallizing solvus pairs, and 633 ± 64 °C for exsolution lamellae, the latter being a likely near- but subsolidus temperature (Price *et al.*, 1996a; chapter 2 this dissertation) indicating that 850°C is in the high-temperature end of the crystal + melt field (hypersolidus-subliquidus) for the magma that gave rise to the Mount Scott Granite.

The magma underwent a segmented (*i.e.* two-stage) crystallization history (Hogan and Gilbert, 1995; Hogan and Gilbert, 1997; Hogan *et al.*, 1998), where the bulk of fluorite and titanite crystallization is likely to have occurred near 200 MPa. Amphibole geobarometry indicates crystallization at P ≈ 200 MPa (Hogan and Gilbert, 1995). Euhedral crystals of fluorite and titanite, some mantled by hornblende or biotite, and fluorite inclusions in porphyritic feldspars (Price *et al.*, 1996a), attest to the early crystallization of both these phases, and textures indicate they crystallized along with zircon ± hornblende ± biotite ± feldspar ± magnetite ± ilmenite. The presence of primary ilmenite (Wones, 1981) suggests initial crystallization conditions were reduced relative to NNO. This period of crystallization was followed by ascent to a shallow emplacement depth: porphyritic and rapakivi textures point to early crystallization followed by ascent (Price *et al.*, 1996a), and intrusive relationships with a nearly coeval rhyolite indicate shallow emplacement of crystals + liquid at $P \approx 50$ MPa (Ham *et al.*, 1964). Ascent produced plagioclase mantles on alkali-feldspar phenocrysts within some of the magma (Price *et al.*, 1996a). Crystallization at the emplacement depth produced the matrix of the rock: variably granophyric alkali feldspar (Or_{60}) + quartz and a second generation of magnetite ± titanite. Second generation titanite is found as rims on first-stage oxides (*i.e.* ilmenite) (Gilbert *et al.*, 1990).

Despite compositional homogeneity that extends to the trace element level, there is mineralogical diversity within the Mount Scott Granite pluton (Gilbert *et al.*, 1990; Price *et al.*, 1996b). An antipathetic relationship exists between the modal quantities of fluorite and titanite. Furthermore, fluorite-poor (titanite dominant) samples have greater volume percentages of hornblende and plagioclase, while fluorite-rich samples contain larger volume percentages of biotite and less plagioclase.

Notably, the variation in the fluorite/titanite abundance within the Mount Scott Granite does not produce a significant change in composition Rare earth element (REE) abundances are nearly identical for all samples of the granite, regardless of the mineralogical variation. Although Marshall *et al.*, (1998) successfully demonstrated REE are strongly partitioned into fluorite, particularly the middle REE's (*e.g.* Gd), they also concluded that the low modal abundance of fluorite prevents it from significantly affecting bulk distribution. Likewise, in the Mount Scott Granite, it is the low modal abundance of titanite and fluorite that precludes measurable whole-rock discrepancies between titanite- and fluorite-dominant samples.

The conclusion of Gilbert *et al.* (1990), that the variation in mineralogy results from inconstant F concentrations within the magma, is borne out through the experimental data. The presence of both titanite and fluorite in the Mount Scott Granite suggests that growth of these phases was buffered by equation 3-1. The glass analyses further confirmed this reaction, recording a sharp increase in TiO_2 within fluorite-bearing runs. Thus the magma that gave rise to the Mount Scott Granite initially contained $\approx$ 1 wt.% F, a value much higher than anticipated for the system. It is five times the whole-rock value for the granite, and twice that of the average calculated F-in-melt using D^F bt/melt values from Icenhower and London (1997) (Table 3-2).

Although higher than anticipated, the value is reasonable for natural systems that preserve their magmatic F (*e.g.*, Spor Mountain Vitorphyric Rhyolite, Utah, average whole-rock F = 1.45 wt.%, Christensen *et al.*, 1986). Despite the discrepancy between the experimentally determined fluorine content and that of the whole-rock, there is no documented evidence of fluorine loss (*i.e.*, hydrothermal fluorite, fluorospar, or cryolite) within or adjacent to the Mount Scott pluton, although such products may have been removed by the erosion that exposed the granite.

In addition to the observed variation in modal titanite and fluorite within the pluton, the variations in plagioclase abundance seen in the Mount Scott Granite were observed within the experiments. Bohlen and Essene (1978) showed plagioclase decreases with increasing F, with loss of the calcium component at relatively low fF_2 via

$$An + F_2 \Leftrightarrow Fl + Al_2O_{3(melt)} + 2SiO_{2(Qtz\ or\ melt)} + \tfrac{1}{2}O_2 \qquad (3\text{-}2)$$

and consumption of the sodium component at higher fF_2 via

$$Ab + 3F_2 \Leftrightarrow Na_3AlF_{6(melt)} + Al_2O_3 + 3SiO_{2(Qtz\ or\ melt)} + \tfrac{1}{2}O_2 \qquad (3\text{-}3).$$

Although runs above 6 wt.% H_2O_T produced new alkalic ternary feldspars, grain sizes were too small for EMPA, so it was not possible to monitor change in An or Ab content with added F. Equation 3-2 implies an increase in melt ANCK with increasing F that was not observed in the analyses of the experimental glasses. The impact of An dissolution (Eq. 3-2) to the ANCK ratio is negligible for this system because the composition of the starting material (SQ-1 123A) plagioclase is highly sodic ($An_{5\text{-}10}$, Price *et al.*, 1996a), thus the bulk of plagioclase dissolution in this system is better described by equation 3-3. This may explain the slight positive correlation with increasing F seen in both Al_2O_3 and Na_2O.

Fluorine stabilizes amphibole in the presence of low water (Gilbert and Briggs, 1974; Gilbert *et al.*, 1982). However, with increasing F, amphibole is destabilized in this experimental study by

$$Amp + \tfrac{1}{2}K_2O_{\ (melt\ or\ Kfs)} + 2F_{2\ (melt)} \Leftrightarrow Bt + Mt + 2Fl + 3SiO_{2\ (melt\ or\ Qtz)} + O_2 \qquad (3\text{-}4).$$

Experiments with $F_m > 1$ wt.% produced biotite, magnetite, and fluorite from hornblende, as evidenced by precipitation within domains pseudomorphic after amphibole. The assemblage relationship to F_m is consistent with observations of the Mount Scott Granite: fluorite-poor, titanite-rich samples contain more hornblende relative to biotite, magnetite, and fluorite. However, within the experiments, the corresponding increases in SiO_2 and decreases in K_2O with increasing F implied by equation 3-4 were not observed within the glasses, reflecting the complexities of this system and of biotite and hornblende compositions.

The current experiments were designed to investigate not only the effect of adding F to Mount Scott Granite, but also the effect of adding H_2O. They determined that the presence of amphibole within the Mount Scott Granite may be a function of elevated F and need not imply early water saturation. In these experiments, amphibole is stable at low water concentrations (H_2O_T = 0.24 wt.%), far below water saturation. Despite relatively higher ANCK, Johnson and Rutherford (1989) also experimentally determined that amphibole is stable at low (0.3) XH_2O at 200 MPa for the Fish Canyon Tuff. This contrasts the experiments of Naney (1983) on synthetic Fe-Mg granite at T = 850 °C, P = 200 MPa, NNO $< fO_2 <$ HM, and Clemens *et al.* (1986) on the A-type Watergums Granite (Australia) at T= 850 °C, P = 100 MPa, $fO_2 \approx$ QFM. The discrepancy is likely explained by higher F contents in the Mount Scott Granite and the Fish Canyon Tuff. The Mount Scott Granite employed in this study (SQ-1 123A) contains 0.18 wt.% F and although the whole-rock F content of the Fish Canyon tuff is unreported, amphiboles from that starting material contain 0.47 wt.% F, compared to 0.12 wt.% F in the Watergums Granite study (GIG-1) and nil in the synthetic Fe-Mg granite.

Application to other felsic rocks

The current experiments constrain the concentration of F and H_2O in the magma that gave rise to the Mount Scott Granite, and therefore the results should generally constrain the concentration of F in other systems with similar compositions and mineral assemblages. The presence of fluorite within an igneous rock may be used to indicate high initial fluorine contents in much the same way that muscovite is used to indicate peraluminosity, or ilmenite is used to indicate low fO_2.

This fluorine monitor is best applied to systems similar in composition to the Mount Scott Granite. They should be subaluminous (*s.l.*, ANCK < 1.1), as strongly peraluminous systems contain the assemblage topaz ± fluorite instead of titanite ± fluorite. Additionally, the precipitation of muscovite will also slightly affect F distribution. The concentration of TiO_2 concentrations should fall between 1 and 0.1 wt.%; low αTiO_2 prohibits titanite growth and increased αTiO_2 increases titanite stability with respect to fluorite (equation 3-1).

Intensive variables affect fluorite-titanite equilibrium, thus the results of this study best apply to systems with crystallization conditions known to be similar to those of the experiments. Increases in temperature, pressure, and oxygen fugacity increase titanite stability. Experimental data at T = 750 °C suggests with decreasing temperature, fluorite tends to precipitate at lower F_m. Thermodynamic calculations (following Bohlen and Essene, 1978) show a positive slope for the titanite-fluorite boundary with increasing pressure (Price, unpublished data) and fO_2 (Bohlen and Essene, 1978) at constant fF_2. Furthermore, at constant temperature and pressure, lower fO_2 enhances ilmenite stability at the expense of titanite (Wones, 1981; Wones, 1989; Xirouchakis and Lindsley, 1998). Employing the equations of Wones (1989) at T = 850 °C and P = 200 MPa, the calculated stability limit for titanite is near NNO (the conditions of this study). Calculations place the NNO buffer at $\log fO_2$ = -1.28 MPa, and the titanite + magnetite + quartz ⇒ wollastonite + ilmenite reaction at $\log fO_2$ = -1.23 MPa. Experiments by Xirouchakis and Lindsley, 1998 indicate that this boundary is actually lower (FMQ boundary at 0.1 MPa), suggesting magmas reduced relative to NNO may produce titanite. However, a magma capable of producing titanite + fluorite above the buffer should produce ilmenite + fluorite below it, thus fluorite remains indicative of elevated magmatic F.

A gross comparison of granitoids with similar compositions to the Mount Scott granite (Table 3-2) placed these rocks into one of three groups, low-F, moderate-F, and high-F, based on the primary titanite fluorite assemblage. Two examples of calcic I-type granites, (Ca / [Na+K] > 0.5) contained titanite only. A-type granitoids fell into all three groups, indicating high-F concentrations may not be an intrinsic characteristic of this granite type as previously thought (*e.g.* Collins *et al.*, 1982; Anderson, 1983; Whalen *et al.*, 1987; Eby, 1990). King *et al.* (1997) reached the same conclusion, that A-type granites need not contain elevated-F concentrations, because the Lachlan Fold Belt (LFB) A-types contained low F values in whole-rock and in amphibole. But in contrast to that study, the presence of fluorite without titanite suggests the LFB A-types were high-F granites. The Sherman and Drammen batholiths are better examples of F-poor A-type granites.

This classification belied some of the details within individual groups of samples. For example, the southwestern U.S. granites data were from plutons both low and high F, due to changes in crustal source (Anderson and Bender, 1989). The three westernmost plutons of this series contained titanite only, and are therefore low-F, while the two easternmost contained titanite + fluorite and crystallized at higher fO_2 (as high as $\log fO_2 = -1.1$ MPa, for the Hualapai Granite, see Figure 11, Anderson and Bender, 1989) and are high-F.

The F concentration in biotite and hornblende documented relative initial F concentrations of magmas within certain groups (*e.g.* Ague and Brimhall, 1988; Anderson and Bender, 1989). The fluorite-bearing easternmost plutons of the Southwestern U.S. granites contained more fluorous hornblende in comparison to the fluorite-absent plutons to the west, indicating that limited preservation of magmatic F values are borne out by the F content in hornblende. However, within the Mount Scott Granite pluton, the F concentrations of the whole rock, hornblende, and biotite do not correlate with the presence of fluorite and within other granitoids. This may result from subsolidus adjustment of F in the F-bearing phases. This is best illustrated by the Drammen batholith, which underwent localized metasomatic alteration (Trønnes and Brandon, 1992), which may include the addition of F by these metasomatic fluids. Further analysis at various scales is required to determine whether preservation of F within the rock and its phases is the exception or rule.

On table 3-2, granitoids with higher F concentrations in whole-rock averages ($F > 0.1$ wt.%) contain fluorite. However, the fluorite and titanite bearing Mount Scott and Saint François Mountains fall in the range titanite-absent granitoids for both whole rock F, and hornblende F. The sparse biotite data suggest that D_F Bt/melt calculations (Icenhower and London, 1997) are a better indicator of initial F. Sierra Nevada and Drammen (titanite-only) granite bodies contain lower calculated F than the Southwestern U.S. and Mount Scott granite bodies (titanite + fluorite), and these granites contain lower calculated F than the Redbluff Suite (fluorite-only). Further data is required, but it seems likely that the D_F Bt/melt calculations might be useful in conjunction with biotite-titanite equilibria for determining F-loss in granitoids

All of the whole-rock averages and biotite calculations are lower than the experimentally determined 1 wt.% initial F value of the Mount Scott Granite, with the exception of the Redbluff Suite (Shannon *et al.*, 1997), whose biotite data indicate magmatic levels nearly 4 times that value. Fluorine loss is preserved in the St. Lawrence Granite (Newfoundland), which contains substantial miarolitic and vein fluorospar thought to be derived from the granite in the latter stages of cooling (Teng and Strong, 1986). In this case, fluorite is thought to have been impounded within the granite by an impermeable layer overlying hornfels (see Teng and Strong, 1986, p. 1383). In contrast, the other examples from table 3-2 (excluding the Redbluff Suite) may have lost significant amounts fluorine into the overlying and surrounding lithologies. Numerous greisen deposits are the result of vapor phase separation from F-rich magmas (e.g. Burt, 1981). Although this is not documented for these granitoids, like the Mount Scott Granite, this information is perhaps missing at the present level of erosion.

Works Cited

Ague, J. J., and Brimhall, G. H., 1988, Magmatic arc asymmetry and distribution of anomalous plutonic belts in the batholiths of California: effects of assimilation, crustal thickness, and depth of crystallization. Geological Society of America Bulletin, 100, p. 912-927.

Anderson, J. L., 1983, Proterozoic anorogenic granite plutonism of North America. Geological Society of America, Memoir 161, p. 133-152.

Anderson, J. L., and Bender, E. E., 1989, Nature and origin of Proterozoic A-type granitic magmatism in the southwestern United States of America. Lithos, 23, p. 19-52.

Anderson, J. L., and Smith, D. R., 1995, The effects of temperature and fO_2 on the Al-in-hornblende barometer. American Mineralogist, 80, p. 549-559

Bailey, J. C., 1977, Fluorine in granitic rocks and melts: a review. Chemical Geology, 19, 1-42.

Barker, F., Wones, D. R., Sharp, W. N., and Desborough, G. A., 1975, The Pikes Peak batholith, Colorado Front Range, and a model for the origin of the gabbro-anorthosite-syenite-potassic granite suite. Precambrian Research, 2, p. 97-160.

Bateman, P. C., Clark, L.D., Huber, N. K., More, J. G., and Rinehart, C. D., 1963, The Sierra Nevada batholith - a synthesis of recent work across the central part. U. S. Geological Survey Professional Paper 414-D, 46 p.

Bateman, P. C., 1992, Plutonism in the central part of the Sierra Nevada Batholith, California. U. S. Geological Survey Professional Paper 1483, 186 p.

Bickford, M. E., Sides, J. R., and Cullers, R. L., 1981, Chemical evolution of magmas in the Proterozoic Terrane of the St. François Mountains, southeastern Missouri. Journal of Geophysical Research, 86, B11, p. 10365-10386.

Bohlen, S. R., and Essene, E. J., 1978, The significance of metamorphic fluorite in the Adirondacks. Geochimica et Cosmochimica Acta, 42, p. 1699-1678.

Bowden, P., and Turner, D. C., 1974, Peralkaline and associated ring-complexes in the Nigeria-Niger Province, west Africa. in Sørensen, H. ed., The Alkaline Rocks. New York, John Wiley and Sons, p. 330-351.

Burt, D. M., 1981, Acidity-salinity diagrams - application to greisen and porphyry deposits. Economic Geology, 76, p. 832-843.

Chappell, B. W., White, A. J. R., and Williams, I. S., 1991, A traverse section through granites of the Lachland Fold Belt, Excursion Guide, Second Hutton Symposium on Granites and Related Rocks. Bureau of Mineral Resources, Geology and Geophysics Record 1991/22, 125 p.

Chou, I. M., 1987, Oxygen buffer and hydrogen sensor techniques at elevated pressures and temperatures, *in* Ulmer, C. G., and Barnes, H. L., eds., Hydrothermal experimental techniques. John Wiley and Sons, New York, p. 61-99.

Christiansen, E. H., and Lee, D. E., 1986, Fluorine and chlorine in granitoids from the Basin and Range Province, western United States. Economic Geology, 81. p. 1484-1494.

Christiansen, E. H., Sheridan, M. F., and Burt, D. M., 1986, The geology and geochemistry of Cenozoic topaz-rhyolites from the western United States, Geological Society of America. Special Paper 205, 82 p.

Clemens, J. D., Holloway, J. R., and White, A. J. R., 1986, Origin of an A-type granite: experimental constraints. American Mineralogist, 71, p. 317-324.

Collins, W. J., Beams, S. D., White, A. J. R., and Chappell, B. W., 1982, Nature and origin of A-type granies with particular reference to southeastern Australia. Contributions to Mineralogy and Petrology, 80, p. 189-200.

Deer, W.A., Howie, R.A., Zussman, J., 1966, An introduction to the rock-forming minerals. Harlow, Longman House, 528 p.

Dingwell, D. B., Knoche, R., and Webb, S. L., 1993, The effect of F on the density of haplogranite melt. American Mineralogist, 78, p. 325-330.

Dingwell, D. B., Scarfe, C. M., and Cronin, D. J., 1985, The effect of fluorine on viscosities of melts in the system Na_2O-Al_2O_3-SiO_2. Implications for phonolites, trachytes, and rhyolites; American Mineralogist, 70, p. 80-87.

Dodge, F. C. W., Smith, V. C., and Mays, R. E., 1969, Biotites from granitic rocks of the central Sierra Nevada Batholith, California. Journal of Petrology, 10, p. 250-271.

Eby, G. N., 1990, The A-type granitoids: a review of their occurrence and chemical characteristics and speculations on their petrogenesis. Lithos, 26, p. 115-134.

Eggler, D. H., 1968, Virginia Dale Precambrian ring-dike complex, Colorado-Wyoming. Geological Society of America Bulletin, 79, p. 1545-1564.

Glibert, M. C., and Briggs, D. F., 1974, Comparison of stabilities of OH- and F-Potassic Richterites - a preliminary report. EOS, Transactions of the American Geophysical Union, 55, p. 480-481.

Gilbert, M. C., Hogan, J. P., and Myers, J. D., 1990, Geology, geochemistry, and structure of low-pressure sheet granites, Wichita Mountains, Oklahoma: Guidebook of Filed Trip no. 5, Geological Society of America Annual Meeting, Dallas Geological Society, 65 p.

Gilbert, M.C., Helz, R. F., Popp, R. K., and Spear, F. S., 1982, Experimental studies of amphibole stability, *in* Veblen, D. R., and Ribbe, P. H., eds., Amphiboles, Petrology and Experimental Phase Relations. Mineralogical Society of America, Reviews in Mineralogy, 9b, p. 229-347.

Greenwood, R., 1951, Younger intrusive rocks of Plateau Province, Nigeria compared with the alkalic rocks of New England. Bulletin of the Geological Society of America, 62, p. 1151-1178.

Ham, W. E., Denison, R. E., and Merritt, C. A., 1964, Basement Rocks and structural evolution of southern Oklahoma. Oklahoma Geological Survey, Bulletin 95, 302 p.

Hogan, J.P., and Gilbert, M.C., 1995, The A-type Mount Scott Granite Sheet. Importance of Crustal Magma Traps: Journal of Geophysical Research, 100, B8, p. 15779-15792.

Hogan, J.P., and Gilbert, M.C., 1997, The intrusive style of A-type sheet granites from the Southern Oklahoma Aulacogen. *in* R.W. Ojakangas, A.B. Dickas, and J.C. Green, eds., Middle Proterozoic to Cambrian Rifting: Mid-North America. Geological Society of America Special Paper, 312, p. 299-311.

Hogan, J. P., Price, J. D., and Gilbert, M. C., 1998, Crustal magma traps and magma driving pressure:consequences for pluton shape and level of emplacement. Journal of Structural Geology, in press.

Holloway, J. R., and Ford, C. E., 1975, Fluid-absent melting of the fluoro-hydroxy amphibole pargasite to 35 kilobars. Earth and Planetary Science Letters. 25; 1, p. 44-48.

Huebner, J. S., and Sato, M., 1970, The oxygen fugacity-temperature relationship of manganese oxide and nickel oxide buffers. American Mineralogist, 55, p. 934-952.

Icenhower, J. P., and London, D., 1997, Partitioning of fluorine and chlorine between biotite and granitic melt: experimental calibration at 200 MPa H_2O. Contributions to Mineralogy and Petrology, 127, p. 17-29.

Johnson, M. C. and Rutherford, M. J., 1989, Experimentally determined conditions in the Fish Canyon Tuff, Colorado, magma chamber. Journal of Petrology, 30, p. 711-737.

Kanisawa, S., 1974,Granitic rocks closely associated with the lower cretaceous volcanic rocks in the Kitakami Mountains, northeast Japan. Journal of the Geological Society of Japan, 80, p. 355-367.

Kanisawa, S., 1979, Content and behaviour of fluorine in granitic rocks, Kitakami Mountains, northeast Japan. Chemical Geology, 24, p. 57-67.

Keppler, H., 1991, The influence of fluorine on the enrichment of high field strength trace elements in the differentiation of granitic rocks. Berichte der deutschen mineralogischen Gesellschaft, Beiheft 1 zum European Journal of Mineralogy, 3, p. 131.

King, P. L., White, A. J. R., Chappell, B. W., and Allen, C. M., 1997, Characterization and origin of alumionous A-type granties from the Lachlan Fold Belt, Southeastern Australia. Journal of Petrology, 38, p. 371-391.

Kisvarsanyi, E. B., Hebrank, A. W., and Ryan, R. F., 1981, Guidebook to the geology and ore deposits of the St. Francois Mountains, Missouri. Missouri Department of Natural Resources Division of Geology and Land Survey, Report of Investigations 67, p. 119.

Koster Van Groos, A. F. K., Wyllie, P. J., 1967, Melting relationships in the system Na $AlSi_3O_8$-NaF-H_2O to 4 kb pressure. Journal of Geology, 76, p. 50-70.

Kohn, S. C., Dupree, R., Mortuza, M. G., and Henderson, C. M. B., 1991, NMR evidence for five- and six-coordinated aluminum fluoride complexes in F-bearing aluminosilicate glasses. American Mineralogist, 76, p. 309-312.

Kretz, R., 1983, Symbols for rock-forming minerals. American Mineralogist, 68, p. 277-279.

Loiselle, M. C., and Wones, D. R., 1979, Characteristic and origin of anorogenic granites. Geological Society of America, Abstracts with Programs, 11, p. 468.

Ludington, S. R., 1978, The biotite-apatite geothermometer revisited. American Mineralogist, 63, p. 551-553.

Manning, D. A. C., 1981, The effect of fluorine on liquidus phase relationships in the system Qz-Ab-Or with excess water at 1 kb. Contributions to Mineralogy and Petrology, 76, p. 206-215.

Marshall, A. S., Hinton, R. W., and Macdonald, R., 1998, Phenocrystic fluorite in peralkaline rhyolites, Olkaria, Kenya Rift Valley. Mineralogical Magazine, 62, p. 477-486.

Merritt, C. A., 1965, Mt. Scott Granite, Wichita Mountains, Oklahoma. Oklahoma Geology Notes, v. 25, p. 263-272.

Morgan, G. B., VI, and London, D., 1996, Optimizing the electron microprobe analysis of hydrous alkali aluminosilicate glasses. American Mineralogist, 81, p. 1176-1185.

Morgan, G. B., VI, London, D., and Luedke, R. G., 1998, Petrochemistry of late Miocene peraluminous silicic volcanic rocks from the Morococala Field, Bolivia. Journal of Petrology, 39, p. 601-632.

Munoz, J. L., and Ludington, S. D., 1974, Fluoride-hydroxyl exchange in biotite. American Journal of Science, 279, p. 396-413.

Naney, M. T., 1983, Phase equilibria of rock-forming ferromagneisan silicates in granitic systems. American Journal of Science, 283, p. 993-1033.

Piccoli, P. and Candela, P., 1994, Apatite in felsic rocks: a model for the estimation of initial halogen concentrations in the Bishop Tuff (Long Valley) and Tuolumne intrusive suite (Sierra Nevada Batholith) magmas. American Journal of Science, 294, p. 92-135.

Pouchou, J. L., and Pichoir, F., 1985, "PAP" (f-r-Z) correction procedure for improved quantitative microanalysis, *in* Armstong, J. T., ed., Microbeam Analysis, San Francisco Press, San Francisco, p 104-106.

Price, J. D., Hogan, J. P., and Gilbert, M. C., 1996a, Rapakivi-texture in the Mount Scott Granite Wichita Mountains, Oklahoma. European Journal of Mineralogy, 8, p. 435-451.

Price, J. D., Hogan, J. P., and Gilbert, M. C., 1996b, Mineralogical variation within the compositionally homogeneous Mount Scott Granite; Geological Society of America, Abstracts with Programs, v. 28, n. 7, p. 42.

Price, J. D., Hogan, J. P., Gilbert, M. C., and Payne, J. D., 1998, Surface and near-surface investigation of the alteration of the Mount Scott Granite and geometry of the Sandy Creek Gabbro pluton, Hale Spring Area, Wichita Mountains, Oklahoma. Basement Tectonics, 12, p. 79-122.

Price, J. D., Hogan, J. P., Gilbert, M. C., London, D., and Morgan, G. B., IV, 1995, Fluorine in A-type granites: experimental Studies on the Mount Scott Granite. Geological Society of America, Abstracts with Programs, v. 27, no. 6, p. 431.

Rämö:, O. T., and Haapala I., 1995, One hundred years of Rapakivi Granite. Mineralogy and Petrology, 52, p. 129-185.

Schaller, T., Dingwell, D. B., Keppler, H., Knoeler, W., Merwin, L., and Sebald, A., 1992, Fluorine in silicate glasses; a multinuclear resonance study. Geocosmica and Geochimica Acta, 56, p. 701-707.

Shannon, W. M., Barnes, C. G., and Bickford, M. E., 1997, Grenville magmatism in west Texas: petrology and geochemistry of the Red Bluff Granititc Suite. Journal of Petrology, 38, p. 1279-1305.

Speer, J. A., Becker, S. W., and Farrar, S. S., 1980, Field relations and petrology of the postmetamorphic, coarse-grained granitoids and associated rocks of the southern Appalachian Piedmont, *in* Wones, D. R., ed., proceedings, the Caledonides in the USA.. Virginia Polytechnic Institute and State University, memoir 2, p. 137-148.

Speer, J. A., and Hoff, K., 1997, Elemental composition of the Alleghanian granitoid plutons of the southern Appalachians, *in* Sinha, A. K., Whalen, J. B., and Hogan, J. P., eds., The nature of magmatism in the Appalachian Orogen. Geological Society of America, Memoir 191, p. 287-308.

Stormer, J.C., and Carmichael, I.S.E., 1971, Fluorine-hydroxyl exchange in apatite and biotite, a potential igneous geothermometer. Contributions to Mineralogy and Petrology, 31, p. 121-131.

Taylor, R. P., Strong, D. F., and Kean, B. F., 1980, The Topsails igneous complex: Silurian-Devonian peralkaline magmatism in western Newfoundland. Canadian Journal of Earth Sciences, 17, p. 425-439.

Teng, H. C., and Strong, D. F., 1976, Geology and geochemistry of the St. Lawrence peralkaline granite and associated fluorite deposits, southeast Newfoundland. Canadian Journal of Earth Sciences, 13, p. 1374-1385.

Trønnes, R. G., and Brandon, A. G., 1992, Mildly peraluminous high-silica granites in a continental rift: the Drammen and Finnemarka batholiths, Oslo Rift, Norway. Contributions to Mineralogy and Petrology, 109, p. 275-294.

Webster, J. D., 1990, Partitioning of F between H_2O and CO_2 fluids and topaz rhyolite melt, Implications for mineralizing magmatic-hydrothermal fluids in F-rich granitic systems. Contributions to Mineralogy and Petrology, 104, p. 424-438.

Webster, J. D., and Holloway, J. R., 1990, Partitioning of F and Cl between magmatic hydrothermal fluids and highly evolved granitic magmas. Geological Society of America, Special paper 246, p. 21-35.

Webster, J. D., Holloway, J. R., and Hervig, R. L., 1987, Phase equilibria of Be, U, and F-enriched vitrophyre from Spor Mountain, Utah. Geochimica et Cosmochimica Acta, 51, p. 389-402.

Webster, J. D., Burt, D. M., Duffield, W. A., Nash, W. P., Gavigan, T., and Aguillon, R. A., 1991, Constraints from glass inclusions in tin/topaz rhyolites on magma evolution, volatile element degassing, and mineralization. Geological Society of America Abstract with Programs, 23, p. 46.

Whalen, J. B., Currie, K. L., and Chappell, B. W., 1987, A-type granites: geochemical characteristics, discrimination and petrogenesis. Contributions to Mineralogy and Petrology, 95, p. 407-419.

Wones, D. R., 1981, Mafic silicates as indicators of intensive variables in Granite Magmas. Mining Geology, 331, p. 191-212.

Wones, D. R., 1989, Significance of the assemblage titanite + magnetite + quartz in granitic rocks. American Mineralogist, 74, p. 744-749.

Xirouchakis, D., and Lindsley, D. H., 1998, Equilibria among titanite, hedenburgite, fayalite, quartz, ilmenite, and magnetite: experiments and internally consistent thermodynaic data for titanite. American Mineralogist, 83, p. 712-725.

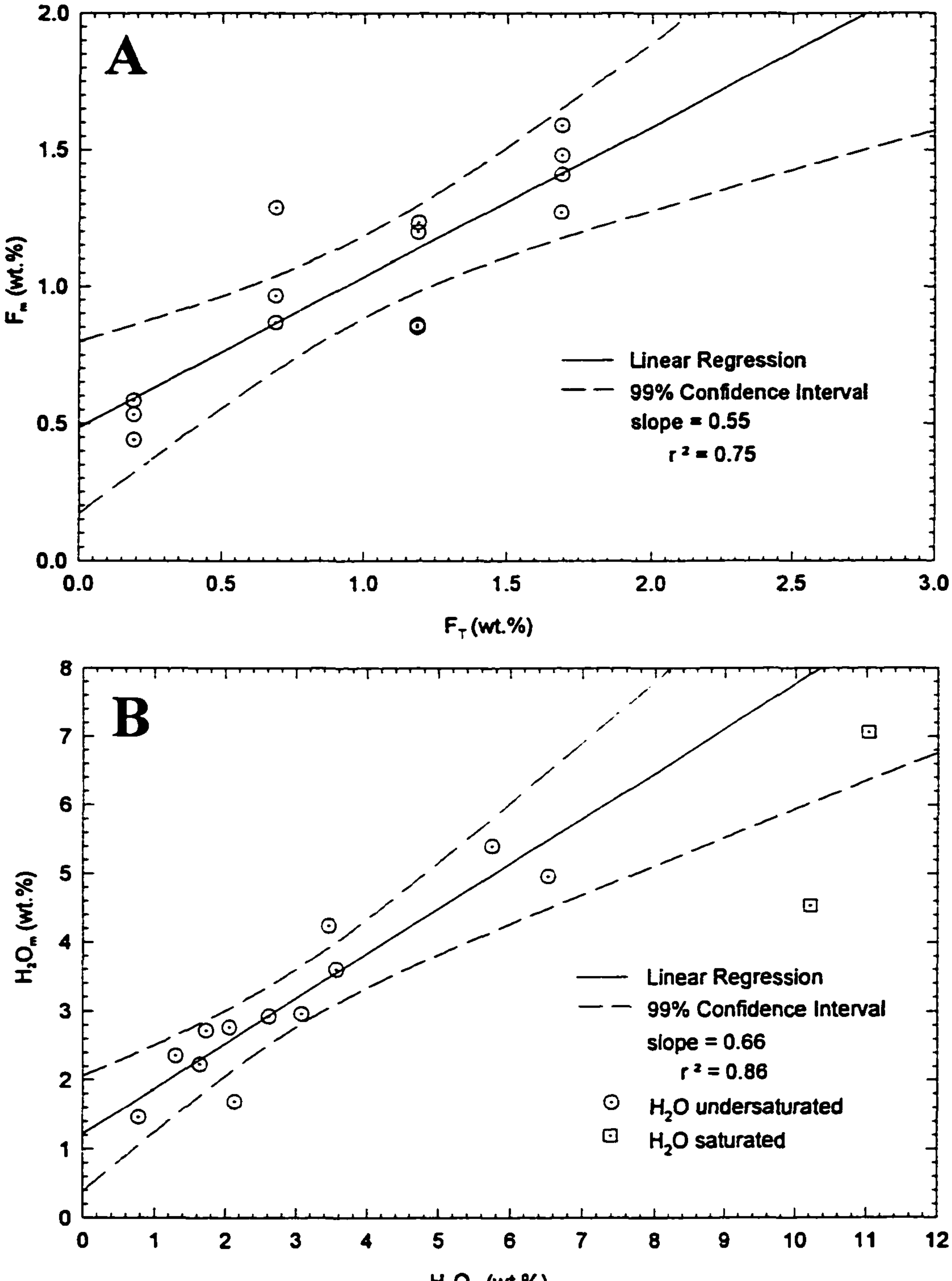

Figure 3-1. Plots of components added versus glass analyses with calculated linear regression. Regression provided equation for plotting runs in terms of melt composition that produced insufficient amounts of glass for analysis (figure 3-3). A.) Fluorine added (F_T) versus fluorine in glass (F_m). B.) Water added (H_2O_T) versus water in glass by difference (H_2O_m); regression excludes water saturated runs. See text for further description.

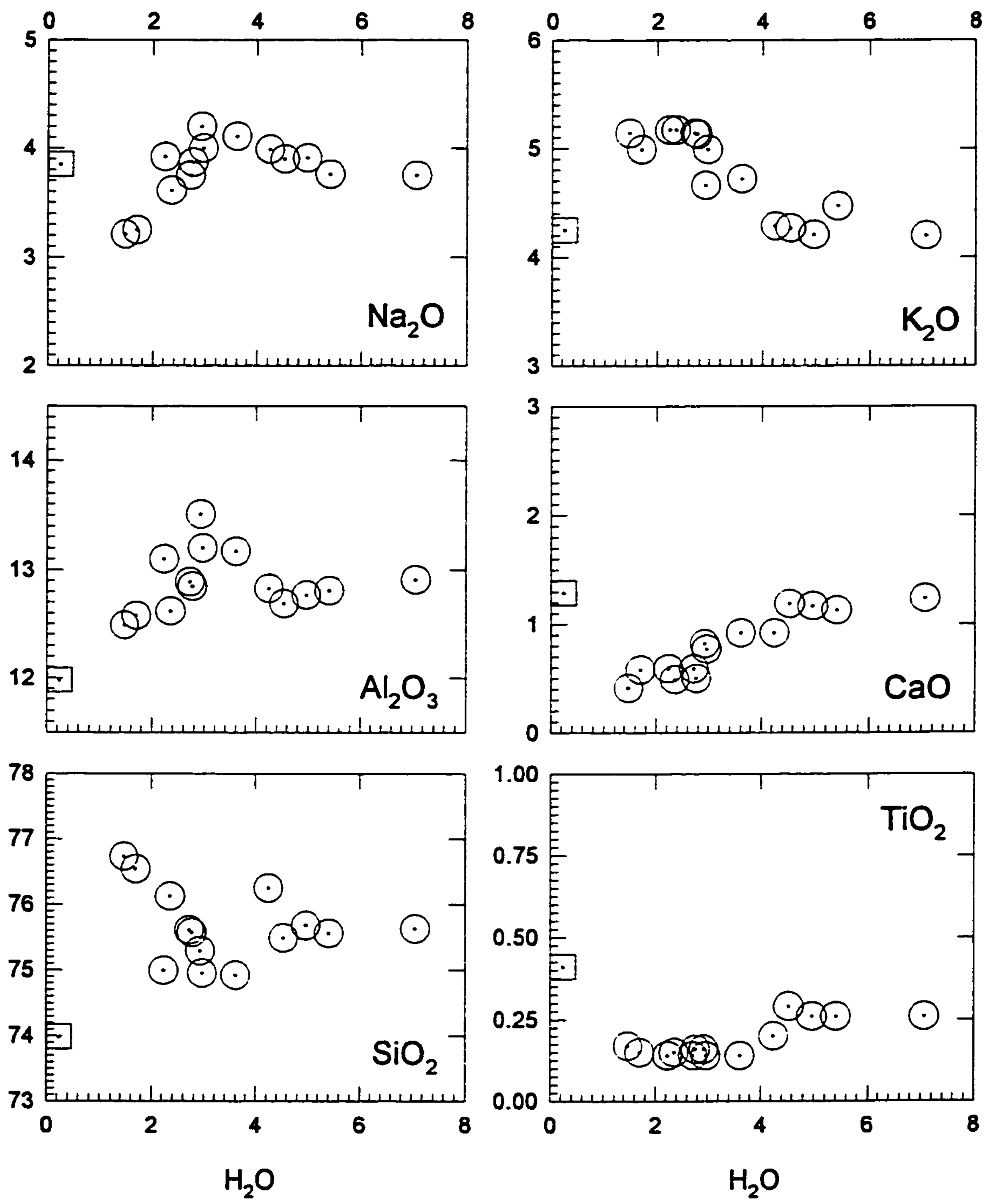

Figure 3-2. Plots of anhydrous and afluorous normalized element oxides (in wt.%) versus water (H_2O_m in wt.%). Experimental glass analyses (oxides vs. H_2O_m) plot as circles, SQ-123A starting material analysis (oxides vs. H_2O by L.O.I.) plots as a square.

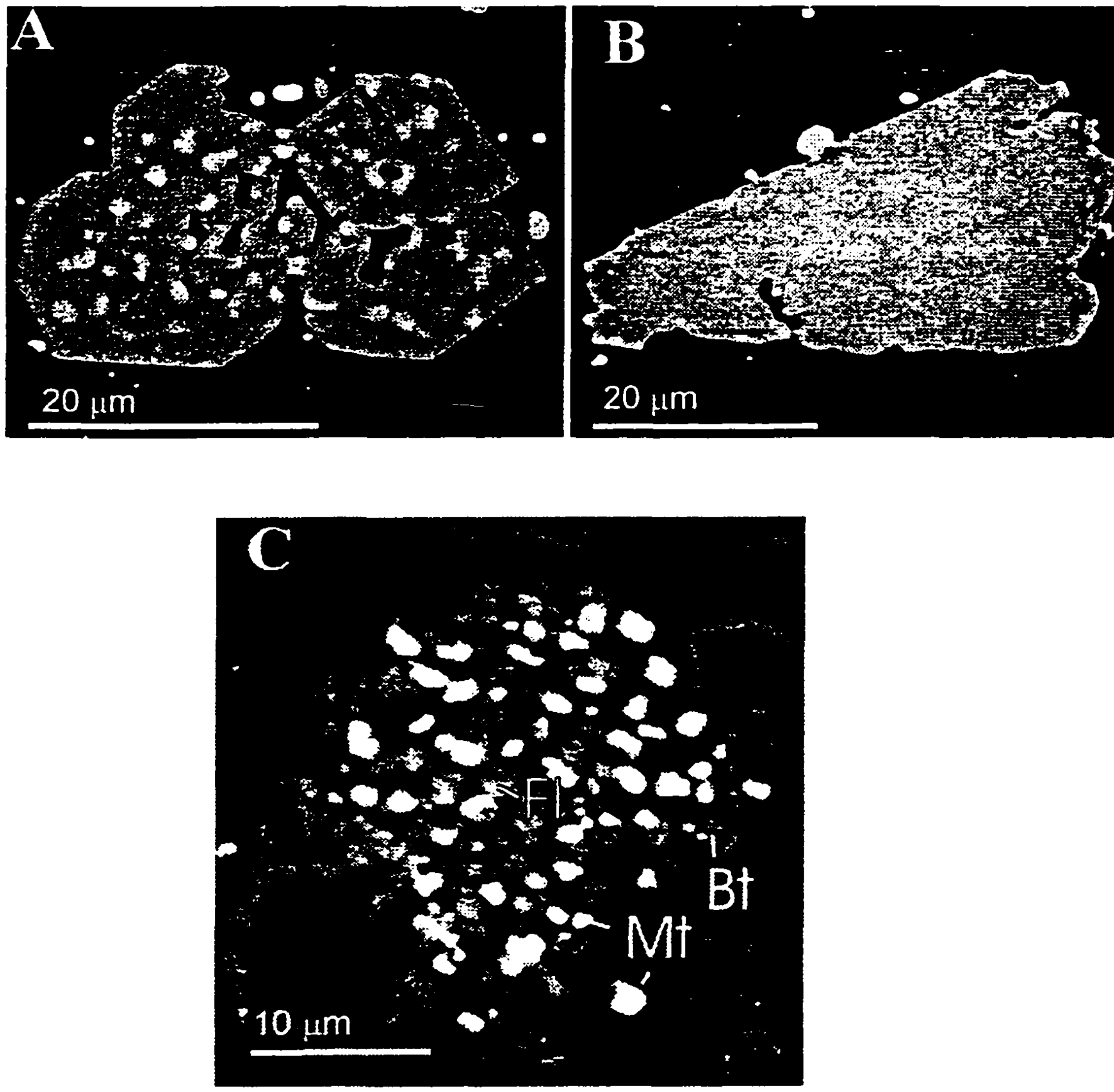

Figure 3-3. Electron micrographs of crystalline phases in run products. A.) BSE image of newly grown euhedral hornblende crystal in glass from run Z11, 0.97 wt.% F_m, 1.7 wt.% H_2O_m. Small bright crystals are magnetite. B.) BSE image of titanite relict grain with mantle of new titanite surrounded by glass and bright grains of magnetite from run Z13, 0.87 wt.% F_m, 2.7 wt.% H_2O_m. Titanite grew in runs with low F_m < 1.1 wt.%. C.) BSE image of small domain (presumably after hornblende) of biotite, magnetite, and fluorite in glass from run Z46, 1.41 wt.% F_m, 2.9 wt.% H_2O_m. Morphology of grains here is typical of new growth of these phases at F_m > 1.1 wt.%.

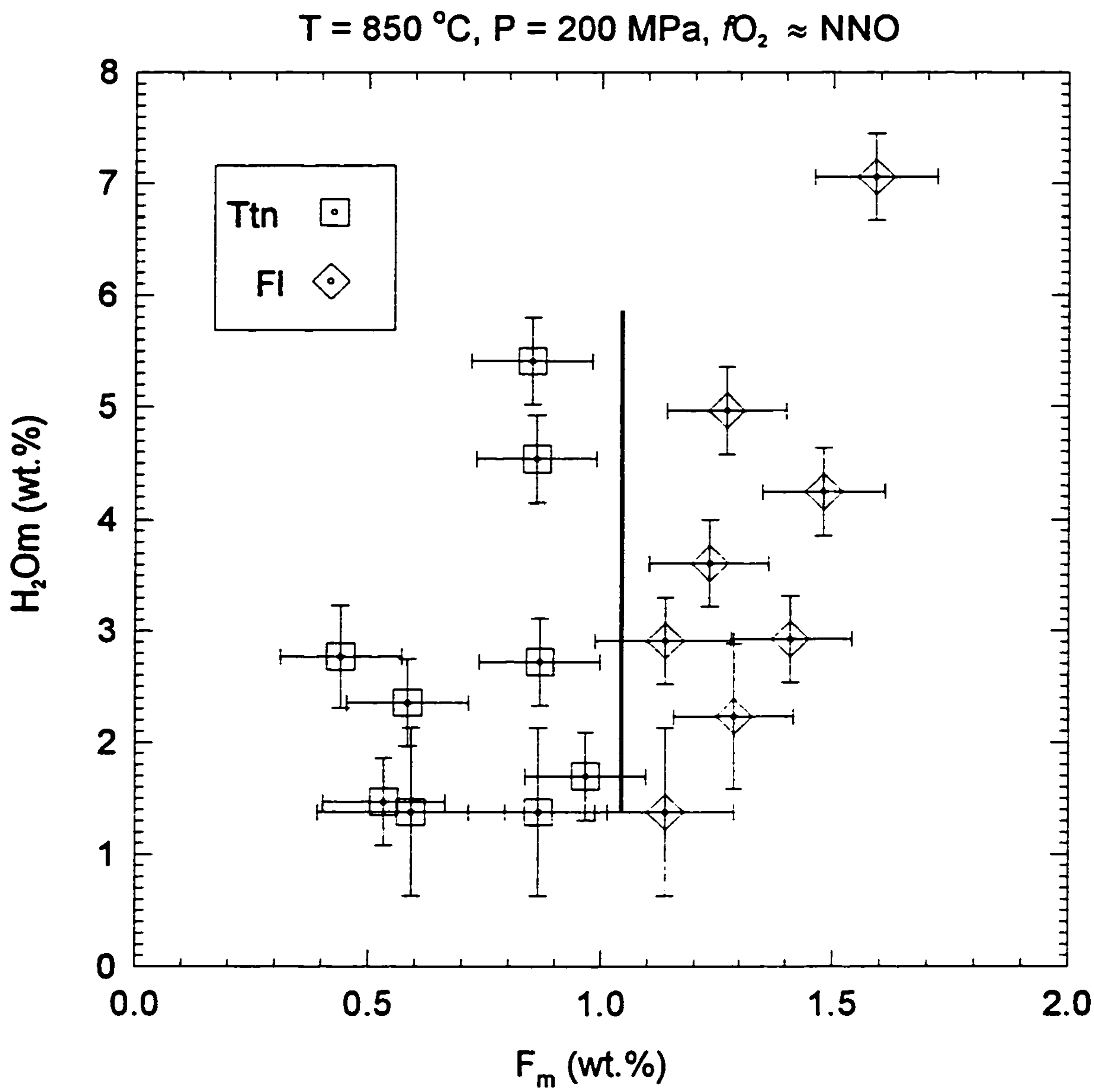

Figure 3-4. Plot of glass analyses and calculated compositions of glass-poor runs (larger error bars) in F (wt.%), H_2O (wt.%) space. Runs precipitated either titanite or fluorite. A boundary (solid line) defines the reaction in equation 3-1 and the stability field for titanite versus fluorite. The line is drawn vertically because equation (3-1) does not involve H_2O. Relative F- and OH-titanite stabilities could change the slope by small amounts (see text for further explanation).

Table 3-1. Starting material and glass analyses for T= 850 °C, P=200 MPa, $fO_2 \approx$ NNO experiments (wt.%).

	SQ-1 123A*	Z6	Z7	Z8	Z11	Z12	Z13	Z14	Z15	Z46	Z47	Z48	Z55	Z56	Z57
F_T‡		0.19	0.19	0.19	0.69	1.19	0.69	1.19	0.69	1.69	1.69	1.69	1.19	1.69	1.19
H_2O_T†		1.30	2.06	0.78	2.13	3.08	1.73	3.57	1.64	2.62	3.46	11.03	5.74	6.52	10.21
SiO_2	73.0	74.1	73.3	75.4	74.8	72.2	73.2	71.7	72.8	72.5	72.4	69.6	71.1	71.4	71.7
Al_2O_3	11.8	12.3	12.5	12.3	12.3	12.7	12.5	12.6	12.7	13.0	12.2	11.9	12.1	12.0	12.1
Na_2O	3.80	3.51	3.75	3.15	3.18	3.85	3.62	3.93	3.80	4.04	3.78	3.45	3.54	3.69	3.70
K_2O	4.19	5.03	4.97	5.04	4.88	4.80	4.98	4.52	5.02	4.48	4.07	3.87	4.20	3.97	4.06
CaO	1.27	0.48	0.48	0.40	0.57	0.74	0.57	0.88	0.57	0.79	0.88	1.14	1.07	1.10	1.13
BaO	0.12	0.08	0.12	0.05	0.12	0.11	0.12	0.11	0.08	0.12	0.10	0.14	0.12	0.10	0.11
MgO	0.32	0.09	0.09	0.09	0.06	0.08	0.09	0.09	0.11	0.08	0.11	0.20	0.16	0.16	0.21
TiO_2	0.40	0.15	0.16	0.17	0.14	0.13	0.14	0.13	0.14	0.15	0.19	0.24	0.24	0.25	0.28
MnO	0.08	0.05	0.04	0.04	0.05	0.06	0.06	0.06	0.07	0.05	0.06	0.06	0.06	0.07	0.06
FeO**	1.62	1.47	1.52	1.56	1.54	1.59	1.49	1.61	1.69	1.04	1.14	1.40	1.51	1.51	1.64
F	0.18	0.58	0.44	0.53	0.97	1.20	0.87	1.23	1.29	1.41	1.48	1.59	0.85	1.27	0.86
Cl	b.d.	0.03	0.02	0.04	0.02	0.02	0.02	0.02	0.03	0.02	0.02	0.02	0.02	0.02	0.02
P_2O_5	0.08	0.04	0.04	b.d.	0.04	b.d.	b.d.	b.d.	b.d.	b.d.	b.d.	b.d.	b.d.	b.d.	b.d.
F=O	-0.07	-0.25	-0.19	-0.22	-0.41	-0.50	-0.37	-0.52	-0.54	-0.59	-0.62	-0.67	-0.36	-0.53	-0.36
Cl=O	0.00	-0.01	-0.01	-0.01	-0.01	-0.01	-0.01	-0.01	-0.01	-0.01	-0.01	-0.01	-0.01	0.00	0.00
Total	96.8	97.6	97.2	98.5	98.3	97.0	97.3	96.4	97.7	97.1	95.8	92.9	94.6	95.0	95.5
H_2O§	*0.24*	2.4	2.8	1.5	1.7	3.0	2.7	3.6	2.2	2.9	4.2	7.1	5.4	5.0	4.5
ANCK#	0.91	1.01	1.00	1.08	1.06	0.99	1.01	0.97	1.00	1.01	1.00	1.00	0.98	0.97	0.96
A/NK	1.09	1.09	1.08	1.15	1.17	1.10	1.10	1.11	1.09	1.13	1.15	1.21	1.16	1.16	1.15

*SQ-1 123A, starting material, Mount Scott Granite from SQ-1 drill core (Price et al., 1998).

‡F_T = fluorine added to SQ-123A powder + F in SQ-123A

†H_2O_T = H_2O added to SQ-123A powder + L.O.I. for SQ-123A

**All Fe as FeO

§SQ-123A H_2O by loss on ignition, glass H_2O by difference from EMPA

#ANCK - molecular Al_2O_3 / Na_2O + CaO + K_2O

Table 3-2. Relative magmatic F of subaluminous granitoids based on phase stability with comparison to F analyses.

	Type	Phase	ANCK			Whole Rock F wt.%			Biotite (22 oxygen) F		Fe#			‡ Bt F-in-melt	Amphibole (24 oxygen) F		Fe/Soct		
			avg	*std*	(n)	avg	*std*	(n)	avg	*std*	avg	*std*	(n)		avg	*std*	avg	*std*	(n)
Low magmatic F																			
Kitakami Mtns	I	Ttn	1.02	*0.07*	(14)	0.04	*0.01*	(15)	0.47	*0.15*			(8)		--	--	--	--	--
Sierra Nevada	I	Ttn	1.05	*0.04*	(9)	--	--	--	0.21	*0.11*	0.53	0.08	(19)	0.10	--	--	--	--	--
S. Appalachians	I-A	Ttn	1.03	*0.35*	(609)	0.09	*0.06*	(48)	--	--	--	--	--		--	--	--	--	--
Sherman batholith	A	Ttn	0.98	*0.02*	(5)	0.04	*0.03*	(5)	--	--	--	--	--		--	--	--	--	--
Drammen batholith	A	Ttn	1.06	*0.05*	(37)	0.10	*0.06*	(61)	1.66	*0.09*	0.41	*0.12*	(6)	0.32	--	--	--	--	--
Moderate magmatic F																			
Southwestern U.S.	A	Ttn±Fl	0.96	*0.06*	(10)	--	--	--	0.86	*0.39*	0.57	*0.13*	(8)	0.45	--	--	--	--	--
Mount Scott Granite	A	Ttn+Fl	0.93	*0.02*	(8)	0.21	*0.03*	(2)	0.59	*0.26*	0.73	*0.04*	(20)	0.41	0.71	*0.07*	0.69	*0.03*	(12)
St. François Mnts	A	Ttn+Fl	1.02	*0.04*	(4)	0.13	*0.08*	(4)	--	--	--	--	--	--	0.55	--	0.45	--	(1)
High magmatic F														--					
Pikes Peak batholith	A	Fl	0.97	*0.03*	(28)	0.43	*0.18*	(29)	--	--	--	--	--	--	--	--	--	--	--
Finnish Rapakivi	A	Fl	0.98		(187)	0.35	*0.26*	(154)	--	--	--	--	--	--	--	--	--	--	--
Redbluff suite	A	Fl	0.92	*0.10*	(13)	--	--	--	0.37	*0.73*	0.96	*0.03*	(5)	3.70	0.50	*0.40*	0.88	*0.02*	(7)
Newfoundland	A	Fl	0.95	*0.06*	(14)	0.16	*0.24*	(14)	--	--	--	--	--	--	--	--	--	--	--
L.F.B. A-type	A	Fl	1.02		(55)	0.10	*0.04*	(17)	--	--	--	--	--	--	0.20	*0.08*	0.83	*0.09*	(24)
Younger Granites	A	Fl	0.90	*0.13*	(6)	0.31	*0.36*	(6)	--	--	--	--	--	--	1.03	*0.44*	0.86	*0.08*	(4)

References - Kitakami Mountains, Japan: Kanisawa, 1974; 2. Kanisawa, 1979. Sierra Nevada, California: Bateman et al., 1963; Dodge et al., 1969; Bateman, 1992. Southern Appalachians: Speer et al., 1980; Speer and Hoff, 1997. Sherman Batholith, Colorado-Wyoming, Eggler, 1968. Drammen Batholith, Oslo Rift, Trønnes and Brandon, 1991. Southern U.S. Proterozoic Granites: Anderson and Bender, 1989. Mount Scott Granite, Oklahoma: Hogan and Gilbert, 1995; Hogan, unpublished data; Price, in prep; Saint François Moutains, Missouri: Kisvarsanyi et al., 1981; Bickford et al., 1981; Anderson and Smith, 1995. Pikes Peak batholith, Colorado: Barker et al., 1975. Finnish Rapakivi, Fennoscandia: Ramo and Haapala,1995. Redbluff Suite, Texas: Shannon et al., 1997. Newfoundland suites: Whalen et al., 1987; Taylor et al., 1980; Teng and Strong, 1986; Lachland Fold Belt (LFB) A-type, Australia: Clemens et al, 1986; Chappell et al., 1991; King et al., 1997. Younger Granites, Nigeria: Bowden and Turner, 1974; Greenwood, 1951

‡ Calculated using Icenhower and London, 1997.

CHAPTER 4. CCC GRANITES OF THE EASTERN WICHITA MOUNTAINS

Introduction

The term *CCC granites* (formerly paired granites; Price *et al.*, 1997, 1998a) is introduced by this chapter to describe two or more *contiguous, consanguineous,* and *coeval* intrusive units. They are individual but related plutons confined to an area of the crust, exhibiting interactions that arise from emplacement over a short period of time.

During the Cambrian, extensional magmatism within the Wichita Igneous Province of Oklahoma produced at least three shallowly-emplaced granites that exhibit connections in time, space, and composition. Although very similar, the Mount Scott Granite, the Rush Lake granite, and the Medicine Park Granite have important but subtle differences.

The following chapter documents the occurrence, physical appearance, and compositional nature of the Wichita Mountains example of CCC granites. It will show why these individual bodies are thought to be genetically related, show that they are spatially associated, and contemporaneous, and it will describe the processes that produced these CCC granites. One purpose of documenting this example is to illustrate the occurrence of CCC granites and one mode of origin so that additional examples can be recognized elsewhere.

Regional Geology

The discussion focuses on igneous rocks from the eastern Wichita Igneous Province, which underlies the rocky promontories and hills of the Wichita Mountains, southwestern

Oklahoma (Figure 4-1). The exposures are dominated by compositionally bimodal intrusives and felsic extrusives, products of magmatism within the Southern Oklahoma Aulacogen, the result of late Proterozoic to Cambrian rifting of the supercontinent, Pannotia (Hogan *et al.*, 1998). The development and subsequent tectonic history of the province, summarized below, is found in Ham *et al.* (1964), Gilbert (1982), and Gilbert (1983) and references therein.

The Glen Mountains Layered Complex represents igneous activity associated with the early stages of rifting. Intrusion of the layered complex is separated from a second stage of magmatism by a hiatus, marked by extensive erosion of the GMLC enhanced through normal faulting and block rotation of the brittle upper crust during rifting (McConnell and Gilbert, 1990). Later stages of activity are represented by the voluminous Carlton Rhyolite Group, the sheet-granites of the A-type Wichita Granite Group, some of the Roosevelt Gabbros, and the volumetrically minor dikes of Late Diabase. The tabular granite plutons chiefly exploited the unconformity of the overlying rhyolites on the Glen Mountains Layered Complex (Ham *et al.*, 1964; Hogan and Gilbert, 1997), at a depth of 1 to 2 kilometers.

The Cambrian igneous rocks were later buried by 4 to 5 km of Paleozoic clastics and carbonates. Subsequently, the Wichita Mountains were uplifted during the Pennsylvanian. Erosion during uplift removed the overlying early Paleozoic cover, and the igneous rocks became exposed by the Permian. Permian erosion produced much of the topography seen in the modern Wichita Mountains. An influx of Permian clastics buried these older mountains, with burial possibly continuing through the Cretaceous. Regional uplift uncovered the Permian landforms in the later Cenozoic (Gilbert, 1983). Recent stream incisement has produced some modification to the Permian topography.

Characteristics of the CCC granites

Three distinct granites, the Medicine Park Granite, the Rush Lake granite (formerly Mount Scott Granite, Facies B, Myers *et al.*, 1981), and the Mount Scott Granite, underlie the mountains around Medicine Park, north Fort Sill, and the high peaks and flat area north of Hwy 49 and east of Hwy. 115 south (road to Cache, OK). Specific outcrop location and general characteristics of these units are found in chapter 6 of this dissertation. Outcrop extent is shown on figure 4-1, and detailed spatial distribution of exposures of the Mount Scott Granite, the Rush Lake granite, and the Medicine Park Granite is shown on Plates II and III. Cross-sections showing the inferred stratigraphic relationships of these and adjacent lithologies are presented in Plates IV and V.

Mineralogical and textural properties of the units

The Medicine Park Granite is a fine to medium grained alkali-feldspar granite, red in highly fractured outcrops, with a pinkish-purple hue in "fresh" samples (Myers *et al.*, 1981). It is porphyritic with orangish-pink alkali feldspar crystals set in a granophyric matrix of quartz and feldspar (Figure 4-2A). Most of the alkali feldspar phenocrysts are angular and microperthitic; all feldspars (phenocrysts and matrix) are altered. Samples contain 1-2 vol.% altered mafic silicates (pseudomorphic after hornblende) and oxides. Many oxides are rounded in form, and rimmed by titanite. Other accessory phases include apatite and zircon, which occur together in glomerocrysts with magnetite ± altered hornblende. Small quartz veins (2-6 mm wide) commonly cut exposures.

The Rush Lake granite is red weathering to brick red, medium- to fine-grained, and porphyritic with angular to slightly rounded orangish-pink altered microperthitic feldspars and rounded quartz phenocrysts in a matrix of variably granophyric quartz and feldspar (Figure 4-2B). Matrix grain size becomes smaller proximal to contacts with the Medicine Park Granite and with the metarhyolite which floors the unit (Davidson Metarhyolite unit of the Carlton Rhyolite Group). Quartz commonly forms "chains" of crystals at the terminus of granophyre domains. Color index varies from << 1 vol.% to 5 vol.% altered amphibole ± biotite ± oxide phases. Accessory minerals include fluorite, titanite, and apatite. Miarolitic cavities are common, ranging in size from 2 to 50 mm. Quartz veins, ranging from microscopic to 3 cm wide, are ubiquitous.

The Mount Scott Granite is a medium grained, pink weathering to brick red, porphyritic, variably granophyric alkali-feldspar granite, with rounded quartz and distinctive rounded gray alkali feldspar (ovoid) phenocrysts (Figure 4-2C). Typically, the ovoid feldspar crystals are microperthitic and variably altered anorthoclase, whose compositions fall into two populations - a predominately sodic group (avg.= Or_{16}) and a relatively potassic group (Or_{52}). Some ovoid feldspars, particularly those in granophyre-poor specimens, are mantled with plagioclase (An_{14}) (Price *et al.*, 1996). A matrix of variably (0 -70 vol.%) granophyric quartz and potassic feldspar (Or_{60}) surrounds the phenocrysts. Also present is a minor amount of primary sodic plagioclase (An_8). The color index of this rock is 4-6 vol.% mafic minerals, which includes ferroedenitic hornblende (Hogan and Gilbert, 1995) and Fe-rich biotite (Price *et al.*, 1998b). Oxide phases include magnetite altered to hematite where the granite is fractured (Price *et al.*, 1998c), and volumetrically smaller amounts of ilmenite. Primary accessory phases include titanite, fluorite, apatite, zircon, and allanite. Overall, there is little evidence of early vapor-saturation or high H_2O activity in the Mount Scott Granite; it contains few examples of miarolitic cavities, pegmatites, or aplites.

Distribution, lithological contacts, and stratigraphy

The Medicine Park Granite and the Rush Lake granite crop out in a small area of the Wichita Mountains. The Medicine Park Granite crops out within the upper elevations immediately east of the village of Medicine Park, and it is additionally exposed further east at Welsh Hill (Johnson and Denison, 1973; Gilbert and Powell, 1988). Outcrops of the Rush Lake Granite also occur in the Medicine Park area, as well as just east of Rush Lake (near Holy City). In contrast, the Mount Scott Granite is exposed over a much larger area, starting with its easternmost exposures at Welsh Hill and continuing west for a distance of 55 km to Tom Steed Reservoir. Roughly half this distance is continuous exposure (Figure 4-1).

Field data suggest that all of the lithological contacts between these Wichita Mountains CCC granites are the result of igneous (intrusive) processes. There is no evidence that any of these units have been juxtaposed by substantial faulting. The Mount Scott Granite sharply contacts the Medicine Park Granite. The matrix grain size of the Mount Scott Granite fines proximal to the contact (T&R: NW SE NW NW 17 3N 12W, UTM: 3843800, 547720), and a fine-grained Mount Scott Granite dike cuts the fine-grained Medicine Park Granite above Big Rock Estates, west of Mount Cummins (T&R: SW SW NW NW 17 3N 12W, UTM: 3843720 546520). Contacts between the Medicine Park Granite and Mount Scott Granite at Welsh Hill (T&R: NE SE SE SW 13 3N12W, UTM: 3842570, 553620) are obscured by cover, but the Mount Scott Granite does not appear to fine with proximity to the Medicine Park Granite at this locality. The Mount Scott Granite, Rush Lake granite contact is sharp, commonly intimate, interdigitating, and irregular in places, particularly in the Holy City area (T&R: SE SE SW SE 7 3N 13W, UTM: 3844030, 536380), and is gradational and poorly defined in others, such as exposures on Mount Cummins, (T&R: SW SE NE NW 17 3N12W, UTM: 3843750, 547130). Medicine Park Granite - Rush Lake granite contacts are rarely exposed, but the boundary can be inferred to an area of 1-3 m between outcrops. Rush Lake granite samples are finer-grained proximal to this contact.

The Mount Scott Granite was emplaced as a sub-horizontal sheet (Gilbert *et al.*, 1990; Hogan and Gilbert, 1995; Hogan and Gilbert 1997). Despite the regional Pennsylvanian tectonism associated with this area, the current outcrop morphology, particularly the subhorizontal contact between the Mount Scott Granite and the Glen Mountains Layered Complex, indicates that current lithological orientations are similar to emplacement orientations with only slight amendments (*e.g.*, Gilbert, 1982). Thus, current outcrop elevations roughly correspond to the igneous stratigraphy.

The stratigraphy of the CCC granites is complex (Figure 4-3), which is typical of intrusive lithologies. Overall relationships show the Medicine Park granite overlies the Mount Scott Granite (see Plate V), which overlies the Rush Lake granite (see Plate IV). However, the Mount Scott granite occurs at the same elevation as the Medicine Park Granite at Welsh Hill, and it is seen at the same elevations as Rush Lake granite at Mount Cummins, indicating that locally these plutons have steep vertical walls.

These units overly members of the Carlton Rhyolite Group (Figure 4-3), indicating that locally, the Mount Scott Granite cut upsection from the unconformity between the

Carlton Group and the underlying Glen Mountains Layered Complex (Price and Gilbert, 1998; Chapter 6, this dissertation). The intrusion of the Mount Sheridan Gabbro, a member of the Roosevelt Gabbros, modified the Mount Scott Granite basal contact on the north and northeast flanks of Mount Scott (for discussion on the relationship between the Roosevelt Gabbros and the Mount Scott Granite, see chapters 5 and 6 of this dissertation). The stratigraphy above these units is not preserved, but should be Carlton Group (Ham *et al.*, 1964). Thus the CCC granites intruded into the rhyolites of the lower Carlton Group

Age relationships

The Mount Scott Granite is the only one of the CCC granites to have a determined absolute age, measured at 533.4 ± 1.7 Ma from zircon $^{206}Pb/^{207}Pb$ data (Hogan *et al.*, 1996). Relative ages between the CCC granites are determined by the contacts, by crosscutting relationships, and by granite textures proximal to contacts. The contact-proximal fining texture (*i.e.*, chilled margin) of both the Rush Lake granite and the Mount Scott Granite against the Medicine Park Granite (at Medicine Park), along with the dike of Mount Scott Granite in Medicine Park Granite, show the Medicine Park Granite is the relatively older unit. However, the Mount Scott Granite does not exhibit a chilled margin at the contact with the coarser-grained variety of the Medicine Park Granite at Welsh Hill. Perhaps the coarser-grained texture of Medicine Park Granite at this location indicates this exposure is more towards the interior of the pluton. In comparison to the intrusive relationships near Medicine Park, the Mount Scott Granite intrusion might experience relatively lesser undercooling intruding a still-cooling portion of the Medicine Park Granite pluton, and therefore not show a chill, provided that the two intrusions were not separated by any great length of time. The Rush Lake granite appears to be only slightly older than the Mount Scott Granite. Xenoliths of the Rush Lake granite occur in the Mount Scott Granite, indicating an older age for the former. However, the intimate-irregular and gradational contacts between the Rush Lake granite and the Mount Scott Granite imply a ductile rheology for both units, suggestive of simultaneous emplacement.

The exact length of time between the Medicine Park intrusion and the Mount Scott Granite and Rush Lake granite intrusions remains unconstrained. Nevertheless, for the purposes of discussion, it is assumed that the Medicine Park only precedes the other two granite plutons by a short period of time. This assumption is not unfounded as recent geochronological evidence indicates that much of the Wichita Igneous Province magmatism occurred briefly (Hogan *et al.*, 1996; Price *et al.*, 1998b).

Chemical composition

The CCC granites from the Wichita Mountains exhibit subtle compositional differences (Table 4-1) between units. The Mount Scott Granite and the Rush Lake Granite are compositionally homogenous, and are represented well by an averaged composition. In contrast, the sample of Rush Lake granite from the Holy City area (Sample JPMS0197) differs substantial from the two from the Medicine Park area , and complicates discussing the Rush Lake granite as a whole. Therefore JPMS0197 is considered separately from the other two samples, and is not included in the Rush Lake granite average composition.

For comparison, the Saddle Mountain Granite is presented with the CCC granite data. Myers *et al.* (1981) and Gilbert (1986) demonstrated that the Saddle Mountain Granite is a hypabyssal to extrusive facies of the Mount Scott Granite. Although compositionally related, it is not a member of the CCC granite group comprised of the Mount Scott Granite, the Rush Lake granite, and the Medicine Park Granite as it is significantly younger than and not spatially related to the Rush Lake granite and the Medicine Park granite. It is presented to illustrate late-stage fractionation of the Mount Scott Granite for comparison against a possible earlier fractionation that produced the CCC granites.

Because of the very low color index of all of these rocks, these granites plot close to the system SiO_2-$NaAlSi_3O_8$-$KAlSi_3O_8$ (Qtz-Ab-Or). Normative calculations of whole-rock analyses plotted on Qtz-Ab-Or illustrate the similar compositions the CCC granites and the Saddle Mountain Granite. Figure 4-4 shows samples and averages plot within Qtz_{31-37}, Or_{25-32}, and Ab_{32-41}.

Weaver and Gilbert (1986) noted that the Mount Scott Granite is not as evolved as the Medicine Park Granite, and Table 4-1 indicates that the Mount Scott Granite is relatively primitive compared to the Medicine Park Granite, the Rush Lake granite (particularly sample JPMS0197), and the Saddle Mountain Granite. Because the Mount Scott Granite is 1.) relatively primitive, 2.) largely compositionally homogeneous (Appendix 1), and 3.) more voluminous, the following discussion will compare the Medicine Park Granite and the Rush Lake granite to its composition.

The Medicine Park Granite is unique among the granites discussed here, because it alone contains normative corundum (1%; Myers *et al.*, 1981). Despite differences, the overall trends of depletion and enrichment relative to the Mount Scott Granite are constant throughout the CCC granites. Both the Rush Lake granite and the Medicine Park Granite are relatively enriched in Rb, K_2O ,and SiO_2. The Rush Lake Granite sample from the Holy City area (JPMS0197) shows minor enrichment of Nb, La, Ce relative to the Mount Scott Granite, deviating from the trend of the other CCC granite samples, but showing affinity with the trend of the Saddle Mountain Granite. The Rush Lake granite and the Medicine Park Granite are relatively depleted in TiO_2, MnO, MgO, CaO, Ba, Sr, Zr, P_2O_5, Y, Zn, and rare earth elements compared to average Mount Scott Granite (Table 4-1, Figure 4-5). Sample JPMS0197 also shows the greatest decrease in Ba (43%) and Sr (82%) relative to the Mount Scott Granite. Rare earth element plots normalized to chondrite (Nakamura, 1974) illustrate both depletion of rare earth elements and the increase of Eu/Eu*(anomaly) (Figure4-6) for the Saddle Mountain Granite, the Medicine Park Granite, and the Rush Lake Granite (all samples) relative the Mount Scott Granite.

Because of the subtle compositional variation, there are only slight mineralogical differences between the three CCC granites. The most striking feature is the higher color index (2-6 vol.% mafic minerals) of the Mount Scott Granite. Furthermore, the proportion of amphibole and biotite to oxides is higher in the Mount Scott Granite than in the other granites. And although the three granites all carry quartz and feldspar phenocrysts, the Mount Scott Granite contains a larger volume of phenocrysts than the Rush Lake Granite, which contains a larger volume than the Medicine Park Granite. Lastly, magmatic plagioclase has only been identified in the Mount Scott Granite.

Compositional relationships

The similar composition, mineralogy, and texture of the Mount Scott Granite, the Medicine Park Granite, and the Rush Lake Granite suggests some genetic relationship exists between these units. Weaver and Gilbert (1986) previously suggested a genetic relationship between Medicine Park and Mount Scott Granites, but the nature of this relationship, and the relationship of these two units with the Rush Lake Granite requires constraint.

The Mount Scott Granite is the more primitive of the granites (lower SiO_2, K_2O, Rb, and Eu/Eu*, higher CaO, MgO, Fe_2O_3, Y, and rare earth elements), and for this discussion, its composition will be used as a proxy for the parent magma from which the other CCC granites are derived. Although the Mount Scott Granite is largely homogeneous, it exhibits some limited compositional variation, best seen in the abundant trace elements (*e.g.* Ba, Rb, Sr). Trace element plots of the Medicine Park Granite, the Rush Lake granite, and the Saddle Mountain granite fall along trends that point to the low-Rb Mount Scott Granite samples, particularly W738. Therefore, fractional crystallization models employed the Mount Scott Granite sample W738 as a parent composition for daughter magmas now represented by the CCC granites.

Least square models of major-element fractionation were applied using the composition of the whole-rock sample W739 and minerals from the Mount Scott Granite. Mount Scott Granite amphibole (Hogan and Gilbert, 1995), feldspar (Price *et al.*, 1996, Appendix 2 of this dissertation), biotite (Price *et al.*, 1998b), and oxide (Hogan *et al.*, 1998) compositional data have been determined through EMPA. Compositions of the accessory phases are not available, therefore models employ relevant compositions from other examples in Deer *et al.*, (1966).

Major Element Modeling

Major element (least-squares) models (*e.g.* Wright and Doherty, 1970) for this system specify that *Mount Scott Granite crystals + liquid = Mount Scott Granite sample W738*. Models employing all of the Mount Scott Granite's phenocryst (plagioclase + alkali feldspar (Na-ovoids + K-ovoids)) and glomerocrystic (hb + bt + ap + ttn + fl) phases as independent variables produce negative coefficients for some phases. Such a result requires that those phases be added to (instead of fractioned out of) the daughter composition The rocks contain no evidence of crystals being added into the daughter products. Instead, the smaller phenocryst volume of the Medicine Park and Rush Lake Granites relative to the Mount Scott Granite argues against the addition of crystalline phases. Final least-squares calculations were performed excluding the phases yielding negative coefficients (crystal phases) found in prior models.

The models indicate the CCC granites can be related through fractional-crystallization of largely hornblende and plagioclase (Table 4-2). Using the W738 (P) composition as parent composition, modeling for the Medicine Park Granite sample W017 (I) produces 6.4 wt.% crystallization of plagioclase, 5.9 wt.% hornblende and 0.6 wt.% titanite. The fit of the model is moderately good (sum $r^2 = 0.388$), with discrepancies in the alkalis contributing the majority of the error. Modeling the Rush Lake Granite JPMS0197 (II) as daughter results in 10.6 wt.% crystallization of plagioclase and 7.3 wt.% crystallization of hornblende, and 0.8 wt.% titanite. The calculated parent composition yields a good fit (sum $r^2 = 0.171$). For comparison, modeling the Saddle Mountain Granite, a unit previously determined to be related to the Mount Scott Granite (Myers *et al.*, 1981; Gilbert, 1986), sample W7125 (IV), results in a smaller amount of fractionation over a greater number of phases, 2.6 wt.% hornblende, 5.8 wt.% sodic alkali feldspar, 0.4 wt.% titanite, 0.6 wt.% apatite, and 0.9 wt.% biotite, and an excellent fit between the calculated parent composition and the actual value (sum $r^2 = 0.082$).

Most of the models produce calculated parental compositions with alkali concentrations excessive of the W738 (parental) composition. The discrepancy (≈0.5 wt.%) may result from 1.) employing an inadequate proxy for the parental composition, and/or 2.) incorrectly assuming alkali contents of the Rush Lake and Medicine Park granites are representative of their respective magmas. Models using other samples from the Mount Scott Granite, produce similar results, and perhaps the true parent composition is not represented by the Mount Scott Granite. The problem could be further compounded if the Rush Lake and Medicine Park Granites analyses overestimate the weight percent of alkali oxides because of unaccounted SiO_2 loss. Quartz veins are prominent in these units, suggesting they lost magmatic SiO_2 to vapor late prior to solidification. Admittedly, such veins make up a small («1 vol.%) fraction of any given outcrop. However, although volumetrically small, such macroscopic veins are excluded in analytical sampling. Thus analyzed sample compositions may misrepresent the magma as they contain lower SiO_2 wt.% (assuming the quartz veins are not formed later), and therefore higher alkali oxide and alumina wt.%. values (the four most abundant components). Additionally, all of these granites have undergone some subsolidus alteration (*e.g.* feldspars in the Medicine Park Granite), which might have affected the alkali content of these rocks.

Trace Element Modeling

A comparison of fractionation trends in Rayleigh trace element fractionation models supports the fractional crystallization process determined by the major element modeling. Instead of calculating a fractionation scheme for each data point, vectors are plotted on relevant trace-element ratio diagrams to illustrate the trends of hornblende and plagioclase fractionation. Only the general analysis is applied here because 1.) appropriate distribution coefficients (K_Ds) for this system are unavailable, 2.) these rocks contain relatively small deviations in concentration, therefore small changes in K_Ds could result in significant error, and 3.) the uncertainty expressed in the alkalis within the major element models extends to the trace element level. In felsic systems, the distribution of elements is greatly influenced by small changes in composition and in intensive parameters (Pitcher, 1993). Published K_Ds for felsic rocks are highly variable, and the values used here were selected from felsic rocks compositionally similar to these CCC granite.

Figure 4-7 A and B are ratios of the abundant and strongly depleted (relative to the Mount Scott Granite) elements Ba and Sr, and the abundant and variably depleted elements Y and La (Figure 4-5), plotted against Rb (differentiation) for these units. Distribution coefficients show that hornblende incorporates La over Y for increasing Rb producing a downward curve, while plagioclase illustrates the opposite behavior. Hornblende incorporates Ba/Sr at similar amounts with Rb, while plagioclase shows a strong partitioning Ba relative to Sr.

The Medicine Park and Rush Lake granites largely plot between the two vectors, suggesting fractionation of both plagioclase and hornblende. There is discrepancy with the major element models in the degree of fractionation. For example, the highest Rb Rush Lake granite (sample JPMS0197 - see I on Table 4-2) is reached by 11 wt.% plagioclase, equivalent with the values predicted by the major element model. But it requires 16 wt.% crystallization hornblende, which is double that of the major element prediction. Additionally, the low Rb Medicine Park Granite sample is inconsistent between the Y/La and Ba/Sr models, exhibiting an affinity for plagioclase fractionation on the Ba/Sr plot, and an affinity for hornblende fractionation within Y/La.

Cumulate phases in the Mount Scott Granite

The phase assemblages of the members of the CCC granites indicate amphibole and plagioclase fractionation. Whereas the Mount Scott (parent) has plagioclase and more amphibole, the Rush Lake and Medicine Park (daughters) contain no plagioclase and lesser amphibole.

All of the mafic phases in the Mount Scott Granite are typically glomerocrystic, and hornblende- and plagioclase-bearing enclaves are common to the granite, suggesting that the cumulate is entrained within the Mount Scott Granite. If the cumulate is in the Mount Scott Granite, then its bulk composition is actually parent + crystals, which seemingly limits its use as a parent composition in modeling. However, Mount Scott Granite is so much more voluminous than the other two CCC granites that adding the cumulate into its bulk composition has little effect. Specifying a 125 km^3 volume for the Mount Scott Granite (a conservative estimate based on outcrop) and a 5 km^3 volume for the Rush Lake and Medicine Park granite magmas (a generous estimate that assumes these units are continuous between the large outcrops), calculations show the addition of the cumulate phases back into the Mount Scott Granite composition produces negligible changes in its composition.

Despite discrepancies in the alkali oxides in major element models, and a lack of precision in the trace element models, the data do point to a consanguineous relationship between all of these units. The degree of fractionation and the crystals that participate in the fractionation scheme are controlled by the timing of magmatic segregation within the ascent history of these CCC granites.

Ascent and Emplacement of the CCC granites

Hogan and Gilbert (1995), Hogan and Gilbert (1997), and Hogan *et al.* (1998) detailed the mechanics and attributes of ascent and emplacement of the magma that gave rise to the Mount Scott Granite. Crystallization of this magma is thought to commence during ascent at a depth of 7-8 km at a crustal magma trap (Hogan and Gilbert, 1997; Hogan *et al.*, 1998). This is evidenced by the porphyritic texture (Merritt, 1965), hornblende geobarometry (Hogan and Gilbert, 1995), and feldspar rapakivi texture (Price *et al.*, 1996).

Because the Medicine Park Granite and the Rush Lake granites are now recognized to have arisen from the same parental magma as the Mount Scott Granite, and to intrude the same crustal horizon at the same time, the history of the development of the Mount Scott Granite needs to include the details of the CCC granites. The following is an account of a simplified scenario for the generation of this example of CCC granites.

Key to the process of generating this example of CCC granites is the idea of segmented crystallization. Segmented crystallization implies that the magma underwent two or more stages of crystallization at separate conditions. For this example, the intrusion of the magmas as separate bodies, that are related through fractionation, requires some crystallization prior to emplacement.

The CCC granite parental magma ascended to a primary crustal magma trap at a depth of 7-8 km. At this level, the magma arrested ascent and crystallized 12 wt.% of a portion of the magma (presumably near the walls), producing subequal amounts hornblende and plagioclase. The fractionated liquid coalesced, and presumably the slight density contrast separated it from the rest of the magma (Figure 4-8a). Eventually a parcel of this fractionated liquid ascended to the shallow crust, and intruded as a small tabular body along a shallow crustal magma trap within the layers of the Carlton Group, resulting in the Medicine Park Granite (Figure 4-8b). Meanwhile, within the chamber, continuing crystallization of 7 wt.% hornblende and 11 wt.% plagioclase produced additional fractionated liquids. These ascended to the same level in the crust (Figure 4-8c), displacing the Medicine Park Granite through uplift, and intruded as sills at the same crustal magma trap exploited by the Medicine Park Granite, resulting in the Rush Lake Granite. The bulk of the magma within the chamber at 7-8 km immediately followed ascent of this Rush Lake Granite magma (Figure 4-8d). The bulk of the chamber, which would become the Mount Scott Granite, interacted with the still liquid Rush Lake pluton along its margins, producing irregularities and gradation between the two units. To the west, the Mount Scott pluton overran the Rush Lake pluton, while to the east, it pushed the still-plastic Rush Lake granite aside, while uplifting Medicine Park Granite. Further east, the granite pushed aside a thicker, and perhaps still cooling, Medicine Park Granite.

Despite the similar composition of these CCC granites, particularly in Qtz-Ab-Or (Figure 4-3), the rapakivi feldspars seen in the Mount Scott Granite (Merritt, 1965; Price *et al.*, 1996) are noticeably absent from the Rush Lake granite and the Medicine Park Granite. This absence may result from the evolving conditions surrounding the near simultaneous intrusion of these CCC granites. The rapakivi-texture seen in the Mount Scott Granite resulted from ascent depressurization of its magma (Price *et al.*, 1996; chapter 2 of this dissertation). However, such depressurization will only produce rapakivi if the ascent is near adiabatic (Nekvasil, 1990; Nekvasil, 1991), implying a rapid ascent though warm crust for the ascent of the Mount Scott Granite magma. However, because the Rush Lake and Medicine Park Granites have a similar composition to the Mount Scott Granite without rapakivi-texture, it follows that these earlier granites did not ascend adiabatically and perhaps intruded through colder crust and/or at a slower rate than the Mount Scott Granite. Because their ascent is just prior to that of the Mount Scott Granite, these rapakivi-less granites may have pre-warmed and/or opened the ascent path for the Mount Scott Granite magma.

Conclusions

The Mount Scott Granite, the Medicine Park Granite, and the Rush Lake Granite exhibit a threefold relationship. They contact each other, are exposed over a small area, and occupy the same stratigraphic horizon, thus they are contiguous. The Rush Lake granite and the Mount Scott Granite share intimate contacts that imply simultaneous emplacement, and are therefore coeval. The Medicine Park Granite is clearly older in places, but the close relationships exhibited with the other two units suggest that no great amount of time (*i.e.*, millions of years) passed between intrusions. Finally, these three granites are compositionally similar and can be related to a common parent through small amounts of hornblende and plagioclase crystallization, and therefore are consanguineous.

This example within the Wichita Mountains provides a good look at CCC granites. The suggested processes that gave rise to this example of CCC granites are not unique, and are not the only mechanisms postulated to generate these related intrusives. It is likely that further examples exist in other shallow plutonic settings.

References Cited

Deer, W. A., Howie, R. A., Zussman, J., 1966, An introduction to the rock-forming minerals. Harlow, Longman House, 528 p.

Gilbert, M. C., 1982, Geologic setting of the eastern Wichita Mountains, with a brief discussion of unresolved problems, *in* Gilbert, M.C., and Donovan, R.N., eds., Geology of the Eastern Wichita Mountains Southwestern Oklahoma. Oklahoma Geological Survey, Guidebook 21, p. 118-119.

Gilbert, M. C., 1983, Timing and chemistry of igneous events associated with the Southern Oklahoma Aulacogen. Tectonophysics, 94, p. 439-435.

Gilbert, M. C., 1986, Stop 6: Saddle Mountain Granite, *in* Gilbert, M. C., ed., Petrology of the Cambrian Wichita Mountains Igneous Suite, Oklahoma Geological Survey, Guidebook 23, p. 169-171.

Gilbert, M. C., and Powell, B. N., 1988, Igneous geology of the Wichita Mountains, southwestern Oklahoma, *in* Hayward, O. T., ed., Geological Society of America Centennial Field Guide - South-Central Section, p. 109-126.

Gilbert, M. C., Hogan, J. P., and Myers, J. D., 1990, Geology, geochemistry, and structure of low-pressure sheet granites, Wichita Mountains, Oklahoma: Guidebook of Field Trip no. 5, Geological Society of America Annual Meeting, Dallas Geological Society, 65 p.

Ham, W. E., Denison, R. E., and Merritt, C. A., 1964, Basement Rocks and Structural Evolution Southern Oklahoma. Oklahoma Geological Survey, Bulletin 95, 302 p.

Hogan, J. P., and Gilbert, M. C., 1995, The A-type Mount Scott Granite Sheet: importance of crustal magma traps. Journal of Geophysical Research, 100, B 8, p.15,779 - 15,793.

Hogan, J. P., and Gilbert, M. C., 1997, The intrusive style of A-type sheet granites from the Southern Oklahoma Aulacogen, *in* R. W. Ojakangas, A. B. Dickas, and J. C. Green, eds., Middle Proterozoic to Cambrian Rifting: Mid-North America. Geological Society of America Special Paper, 312, p. 299-311.

Hogan, J. P., Price, J. D., and Gilbert, M. C., 1998, Crustal magma traps and magma driving pressure: consequences for pluton shape and level of emplacement. Journal of Structural Geology. in press.

Hogan, J. P, Gilbert, M. C., Price, J. D., Wright, J. E., Degeller, M., and Hames, W. E., 1996, Magmatic evolution of the Southern Oklahoma Aulacogen. Geological Society of America, Abstracts with Programs, 28, no. 1, p. 19.

Johnson , K, and Denison, R. E., 1973, Igneous geology of the Wichita Mountains and economic geology of Permian rocks in southwest Oklahoma: Oklahoma Geological Survey Special Publication 73-2, Guidebook for field trip 6, Geological Society of America annual meeting, Dallas, 33 p.

McConnell, D. A., and Gilbert, M. C., 1990, Cambrian extensional tectonics and magmatism within the Southern Oklahoma Aulacogen. Tectonophysics, 174, p. 147-157.

Merritt, C. A., 1965, Mt. Scott Granite, Wichita Mountains, Oklahoma. Oklahoma Geology Notes, v. 25, p. 263-272.

Myers, J. D., Gilbert, M. C., and Loiselle, M. C., 1981, Geochemistry of the Cambrian Wichita Granite Group and revisions of its lithostratigraphy. Oklahoma Geology Notes, 41, p. 172-195.

Nakamura, N., 1974, Determination of REE, Ba, Fe, Mg, Na, and K in carbonaceous and ordinary chondrites. *Geochimica et Cosmochimica Acta*, 38, p. 757-73.

Nekvasil, H. , 1990, EQUIPATH.FOR, program for calculating equilibrium crystallization paths based on thermodynamic constraints. FORTRAN 77 format.

Nekvasil, H., 1991, Ascent of felsic magmas and formation of rapakivi. American Mineralogist, 76, p. 1279-1290.

Pitcher, W. S., 1993, The nature and origin of granite. New York, Blackie Academic and Professional, 321 p.

Price, J. D., and Gilbert, M. C., 1998, Mapping within the eastern Wichita Mountains, Oklahoma. Geological Society of America Abstracts with Programs, v. 31

Price, J. D., Hogan, J. P., and Gilbert, M. C., 1996, Rapakivi texture in the Mount Scott Granite, Wichita Mountains, Oklahoma. European Journal of Mineralogy, 8, p. 435-451.

Price, J. D., Hogan, J. P., and Gilbert, M. C, 1997, Paired granites - an example from the Wichita Mountains, Oklahoma. Geological Society of America Abstracts with Programs, v. 30, no. 7, p 390.

Price, J. D., Hogan, J. P., and Gilbert, M. C, 1998a, Paired granites: further evidence from the Wichita Mountains, Oklahoma. Geological Society of America Abstracts with Programs, v. 31, in press.

Price, J. D., Hogan, J. P., Gilbert, M. C., and Denison, R. E., 1998b, Field guide to the basement rocks of the Southern Oklahoma Aulacogen. South Central Meeting of the Geological Society of America, 76 p.

Price, J. D., Hogan, J. P., Gilbert, M. C., and Payne, J. D., 1998c, Surface and near-surface investigation of the alteration of the Mount Scott Granite and geometry of the Sandy Creek Gabbro pluton, Hale Spring Area, Wichita Mountains, Oklahoma. Basement Tectonics, 12, p. 79-122.

Steiner, J. C., Jahns, R. H., and Luth, W. C., 1975, Crystallization of alkali feldspar and quartz in the haplogranitic system $NaAlSi_3O_8$-$KAlSi_3O_8$-SiO_2-H2O at 4kb. Geological Society of America Bulletin, 36, p. 359-364.

Weaver, B. L., and Gilbert, M. C., 1986, Reconnaissance geochemistry of silicic igneous rocks of the Wichita Mountains: the Wichita Granite Group and the Carlton Rhyolite Group, *in* Gilbert, M. C., ed., Petrology of the Cambrian Wichita Mountains Igneous Suite. Oklahoma Geological Survey, Guidebook 23, p. 117-125.

Wright, T. L., and Doherty, P. C., A linear programming and least squares computer method for solving petrologic mixing problems. Geological Society of America Bulletin, 81, p. 1995-2008.

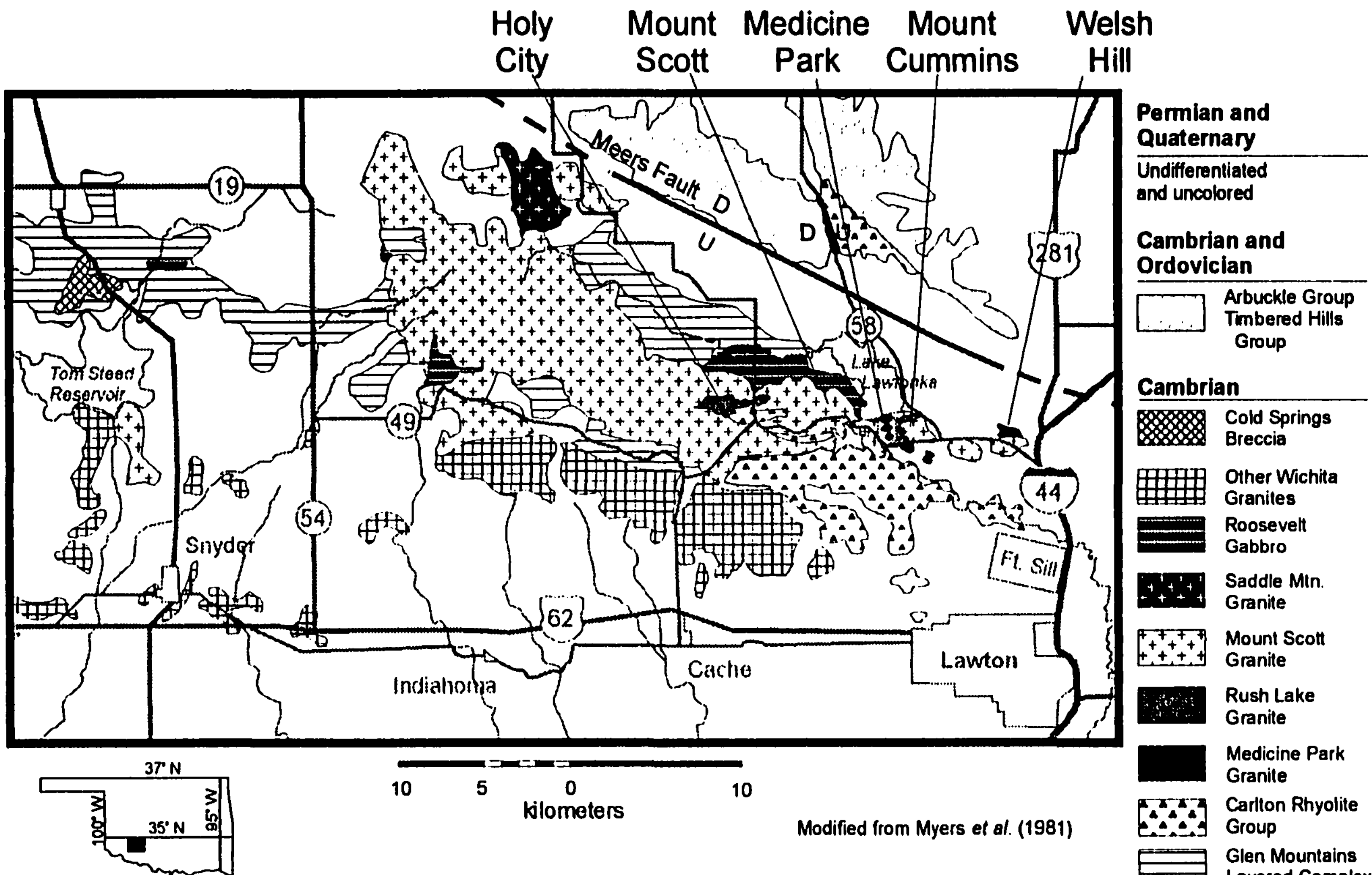

Figure 4-1. Geologic map of the eastern Wichita Mountains, Oklahoma. Areas (top of the map) correspond to stratigraphic columns on figure 4-3.

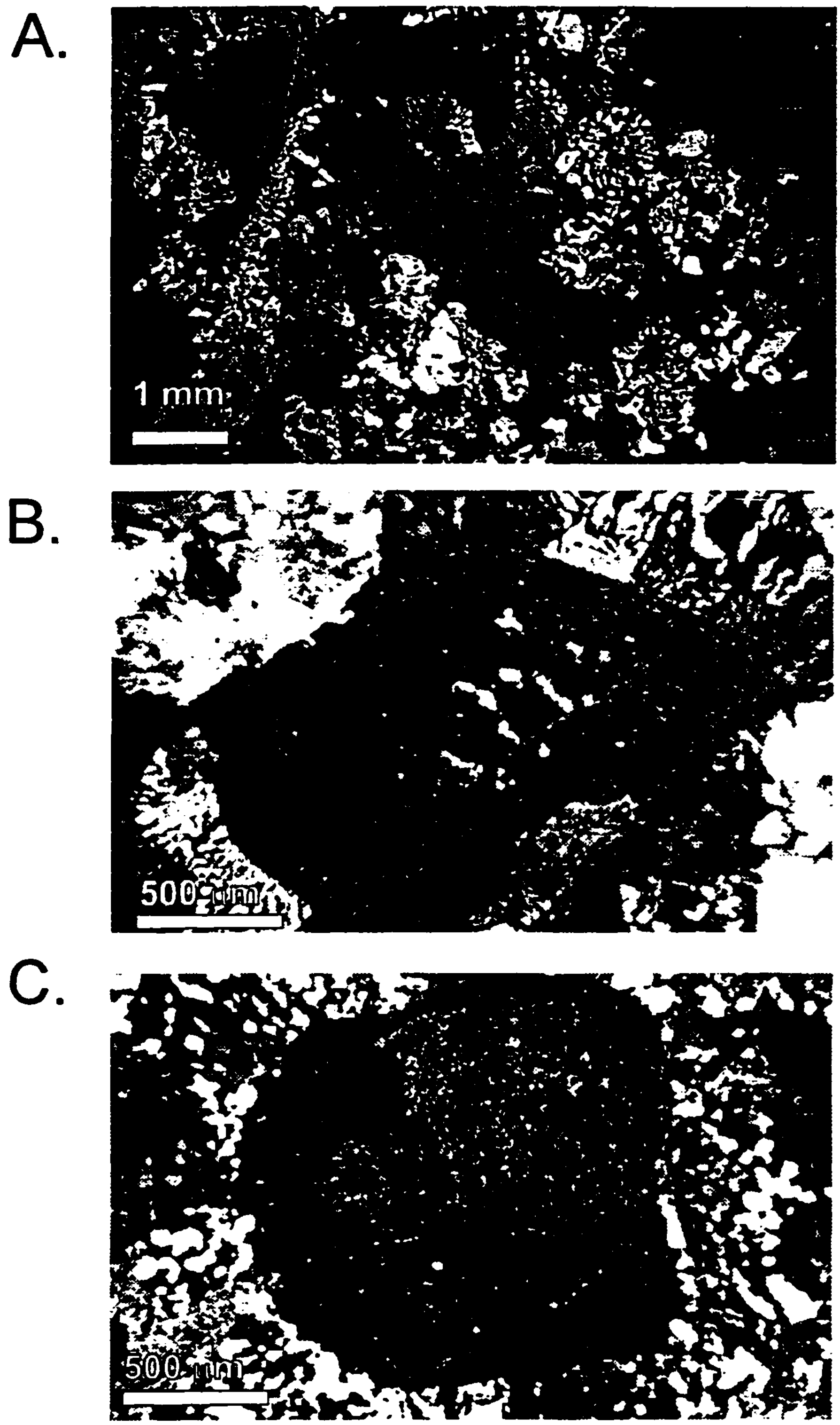

Figure 4-2. Photomicrographs (crossed-Nichols) of alkali feldspar phenocrysts within the CCC granites. A.) Ovoid crystals within the Mount Scott Granite. B.) Angular crystal within the Rush Lake granite. C.) Angular crystal within the Medicine Park Granite.

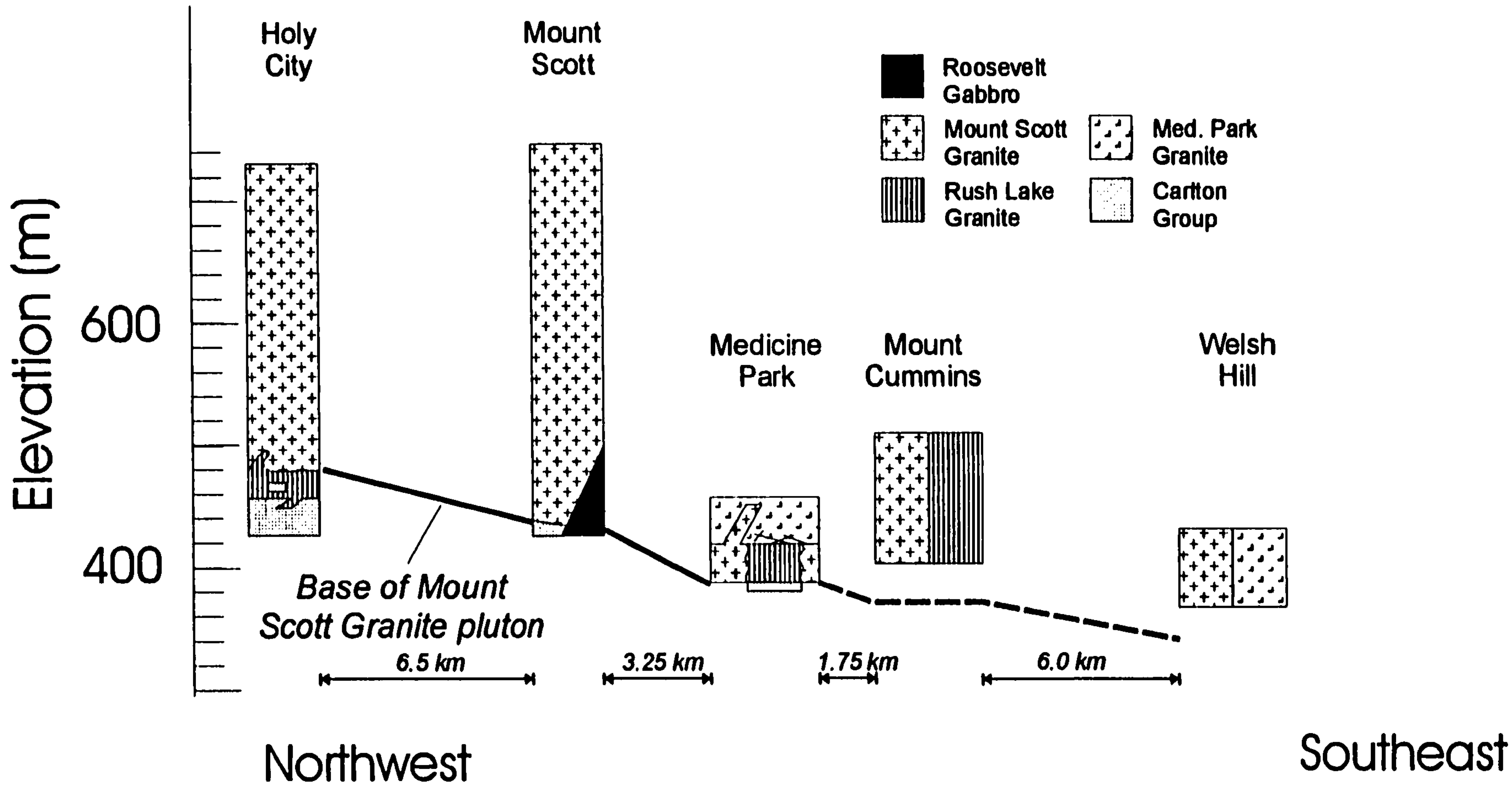

Figure 4-3. Stratigraphic columns showing the Wichita Mountains CCC granites and other contacting units. Locations of sections shown on figure 4-1.

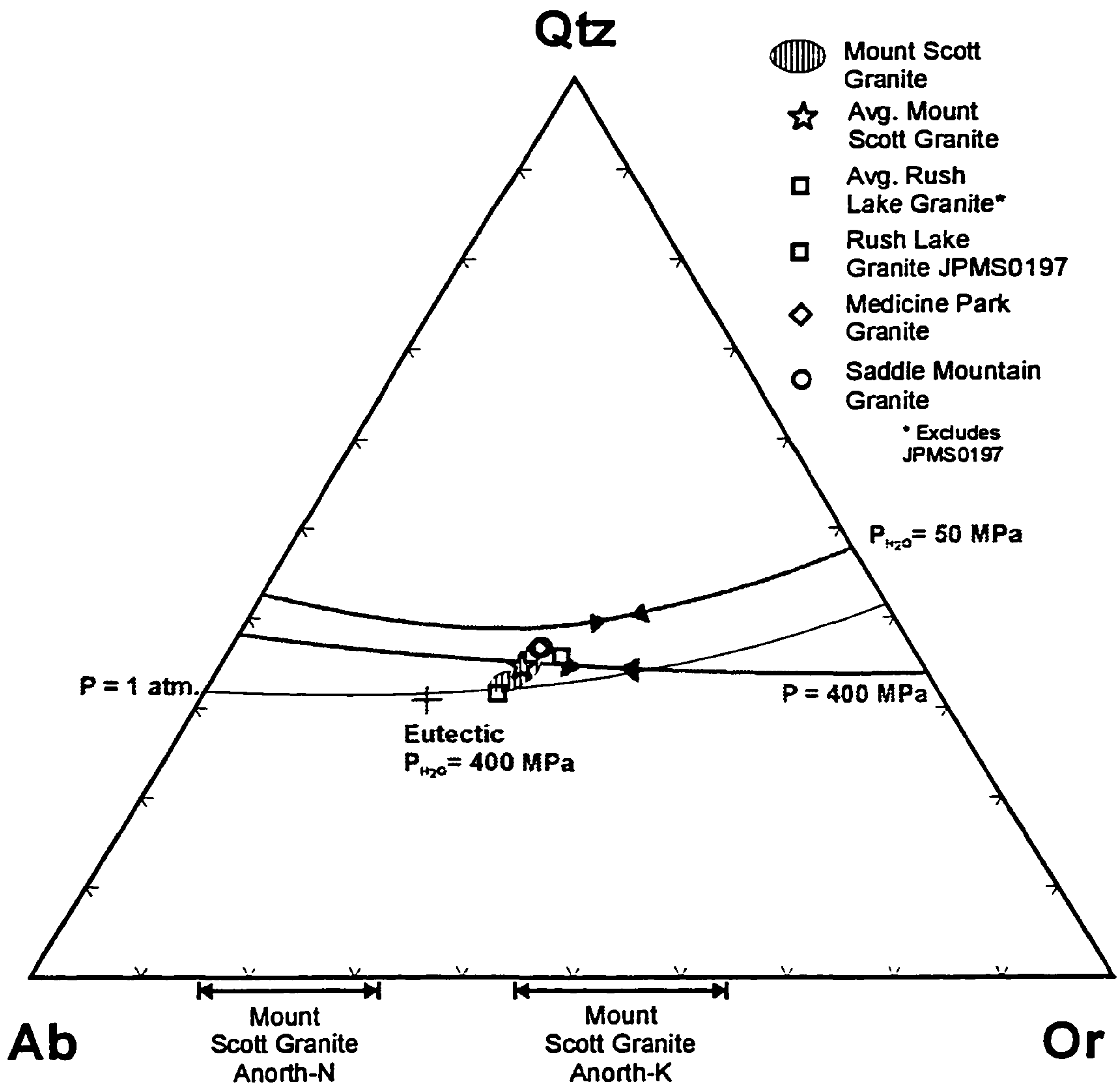

Figure 4-4. Qtz-Ab-Or plot for the CCC granites. Saddle Mountain granite is shown for comparison. Data fall within a small area on the plot, illustrating the gross similarity between these rocks. Compositional ranges for early-crystallizing feldspars from the Mount Scott Granite are shown on Ab-Or join. Boundary curves from Steiner *et al.* (1975) shown for reference.

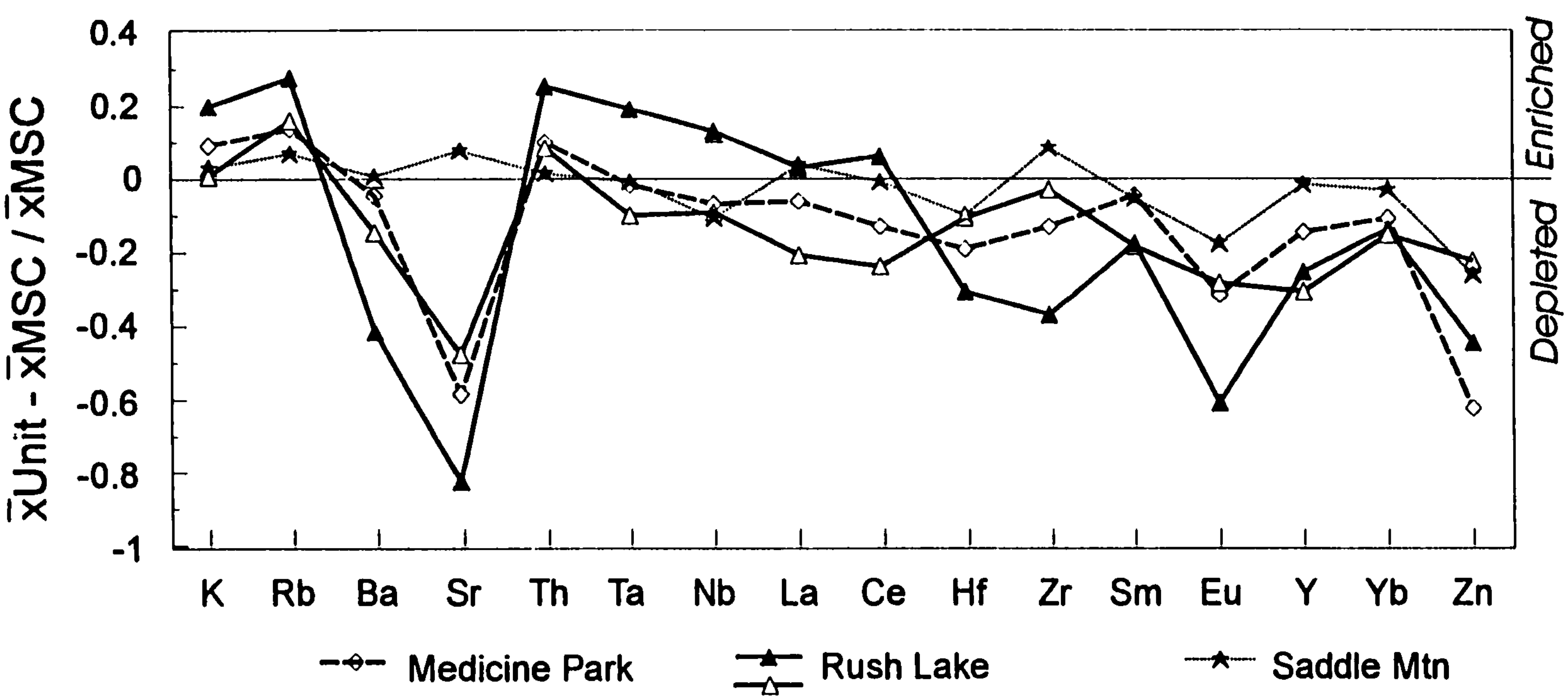

Figure 4-5. Trace-element variation of the Medicine Park Granite, Rush Lake granite, and Saddle Mountain Granite. Values are the difference of unit composition normalized to average Mount Scott Granite. Negative values indicate depletion fraction, positive values indicate enrichment fraction. The Saddle Mountain Granite, the Rush Lake granite, and the Medicine Park Granite show increasing differences from the Mount Scott Granite. Average of the two Rush Lake granite samples from the Medicine Park area are plotted separately from the sample from the Rush Lake-Holy City area (Dark Triangle) because the latter has a distinct composition (see Table 4-1).

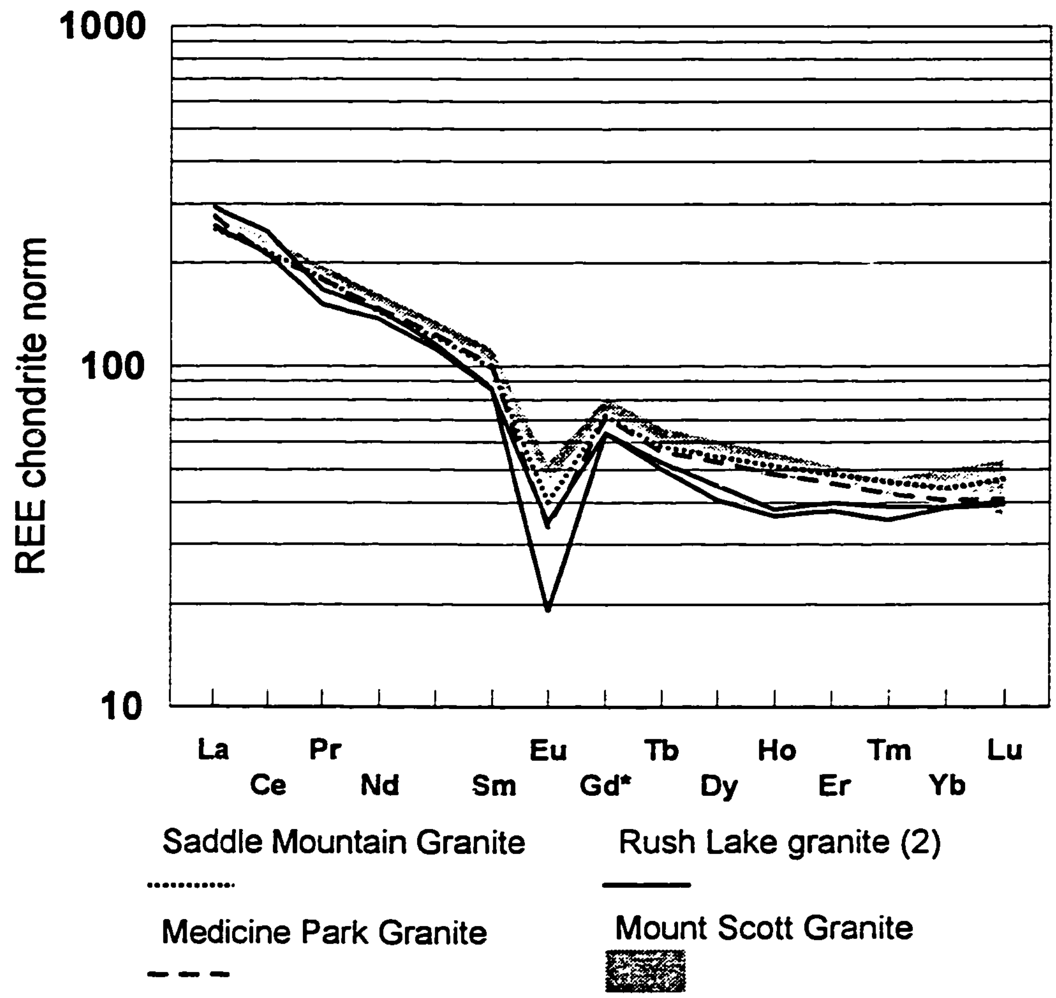

Figure 4-6. Rare earth element diagram for the CCC granites and the Saddle Mountain Granite, a Mount Scott Granite differentiate. Although all trends are similar, an overall depletion in all elements and development of an Eu anomaly are seen from Saddle Mountain Granite, to Medicine Park Granite, to Rush Lake granite. Values normalized to chondrite analyses from Nakamura (1974).

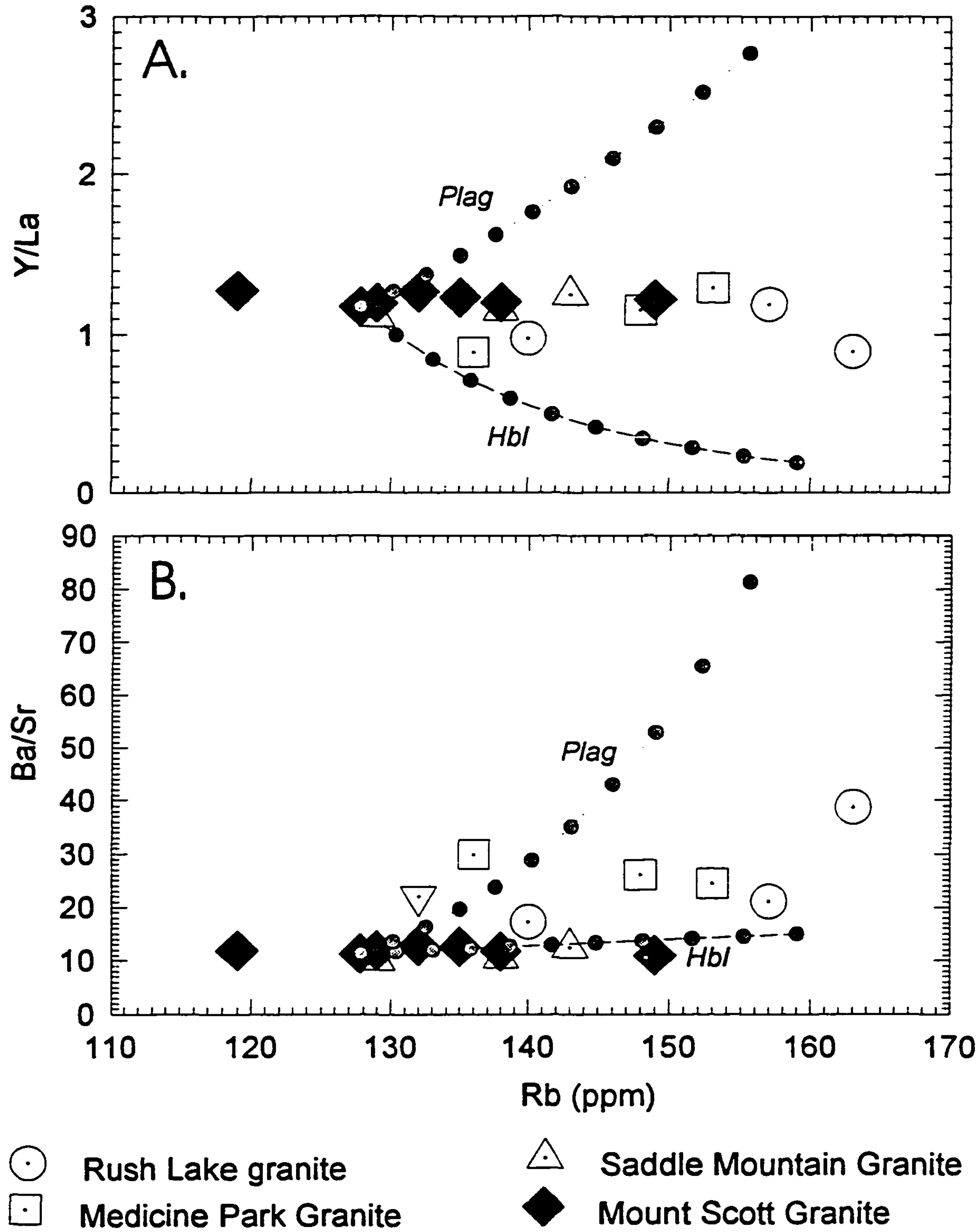

Figure 4-7. Plots of element ratios versus Rb for the CCC granites and the Saddle Mountain Granite. Small points on lines are Rayleigh fractionation curves, points are F = 0.2 apart. Plots agree with major element models that minor amounts of fractionation of plagioclase and hornblende give rise to the Rush Lake and Medicine Park granites. See text for discussion.

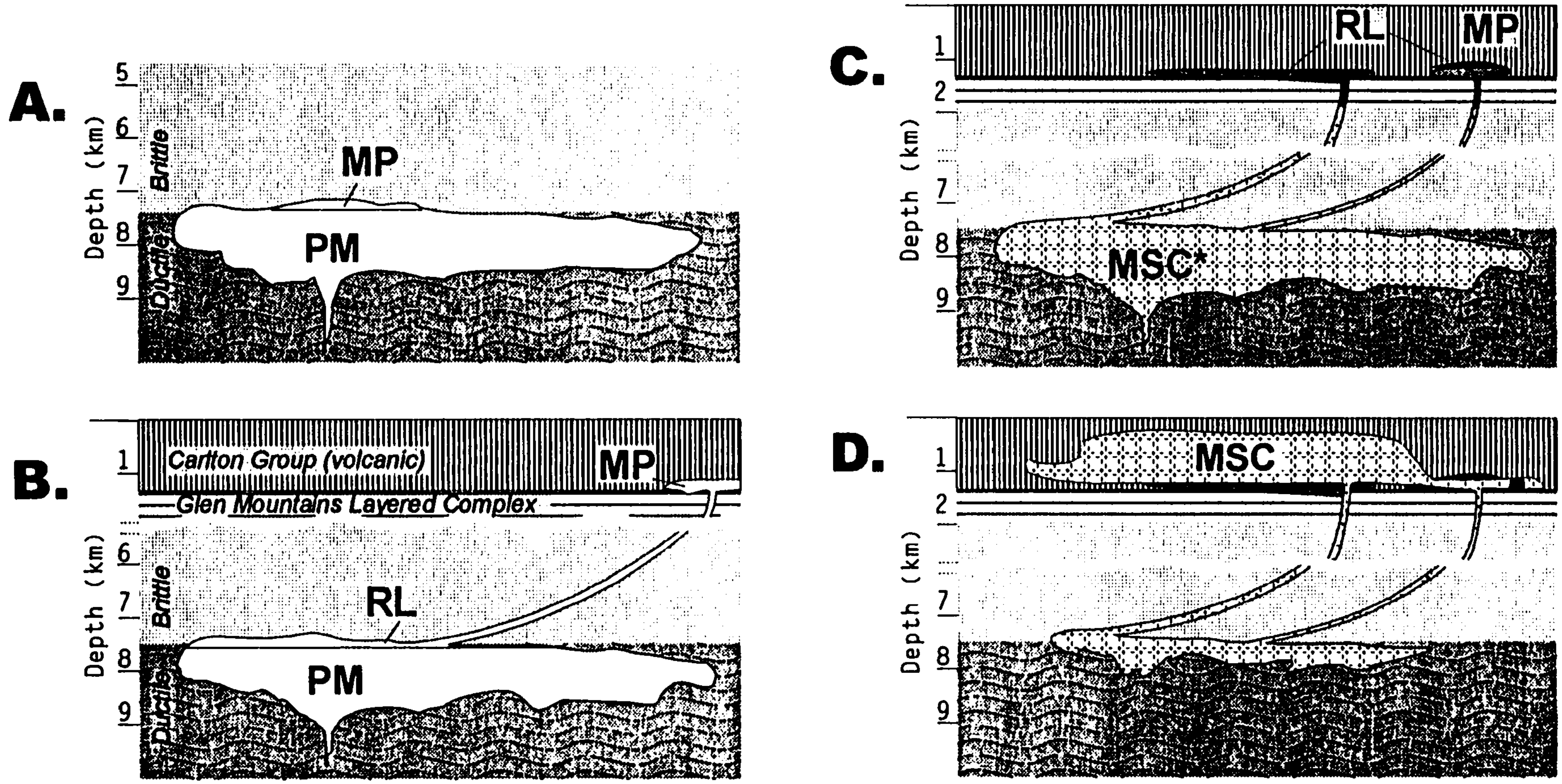

Figure 4-8. Development of the CCC granites within the Wichita Mountains. A.) The CCC granite parental magma (PM) arrests at the brittle-ductile transition zone; begins to fractionate. B.) Fractionated magma ascends to near-surface, stops at crustal magma trap in Carlton Rhyolite, and forms tabular Medicine Park Granite pluton (MP), chamber below continues to fractionate. C.) Fractionate ascends to the same level; uplifts cold MP; forms Rush Lake granite (RL). D.) Chamber empties immediately following RL ascent, and is emplaced at same horizon, overrunning and shouldering aside RL to make Mount Scott Granite (MSC) pluton.

Table 4-1. Compositional data from the CCC granites and the Saddle Mountain Granite.

	Mount Scott Granite W738	Mount Scott Granite Avg	Medicine Park Granite Avg	Rush Lake granite JPMS0197	Rush Lake granite Avg*	Saddle Mtn. Granite Avg.
Major element oxides in wt.%						
SiO_2	72.9	72.8	75.6	75.8	73.0	72.8
TiO_2	0.46	0.44	0.21	0.15	0.31	0.46
Al_2O_3	12.3	12.5	11.9	11.6	12.1	12.5
Fe_2O_3	3.73	3.54	2.35	1.87	2.76	3.88
MnO	0.08	0.08	0.02	0.01	0.02	0.08
MgO	0.28	0.35	0.05	0.06	0.26	0.38
CaO	1.30	1.22	0.45	0.28	0.63	1.11
Na_2O	3.93	3.96	3.84	3.76	4.46	3.62
K_2O	4.15	4.24	4.61	5.07	4.27	4.35
P_2O_5	0.08	0.07	0.01	0.02	0.06	0.07
LOI	0.49	0.17	n.d.	0.64	0.85	n.d.
Total	99.64	99.30	99.03	99.28	98.73	99.27
Trace elements in ppm.						
Ba	1141	1130	1080	664	963	1135
Rb	127.8	128.3	145.5	163.4	148.5	136.5
Nb	90	90	84	101	82	81
Ta	8	8	8	9	7	8
Sr	100	97	41	17	51	104
Zr	528	547	476	344	529	594
Y	107	109	93	81	75	107
Sc	5	5	3	2	5	n.d.
Cr	2	8	5	b.d.l.	4	8
V	11	10	3	b.d.l.	16	8
Zn	147	128	48	71	99	94
La	90.9	88.6	82.9	90.9	70.2	91.5
Ce	197.3	190.7	165.9	201.5	145.3	189.0
Pr	20.3	20.5	n.d.	20.6	18.7	
Nd	97.5	97.4	88.3	91.4	77.2	91.0
Sm	20.4	21.4	20.4	17.5	17.4	20.2
Eu	3.6	3.8	2.6	1.5	2.7	3.1
Gd	20.7	20.6	n.d.	17.8	17.6	n.d.
Tb	3.3	3.3	3.0	2.8	2.6	3.0
Dy	18.2	19.5	n.d.	15.5	14.0	n.d.
Ho	3.7	4.0	n.d.	3.0	2.9	n.d.
Er	10.7	11.7	n.d.	9.1	8.5	n.d.
Tm	1.5	1.6	n.d.	1.3	1.2	n.d.
Yb	9.8	10.0	8.9	8.6	8.5	9.8
Lu	1.6	1.4	1.4	1.4	1.3	1.6
Hf	16	17	14	12	16	16
Th	13	13	15	17	15	14
Pb	17	17	10	16	7	14
U	4	3	n.d.	4	3	n.d.
Cs	3	2	n.d.	3	1	n.d.
F	1670	1785	n.d.	1370	2570	n.d.

*Avg - Rush Lake Granite samples exclusive of JPMS0197

Table 4-2. Major element fractionation models (least squares). All values are in weight percent.

	P Mount Scott Granite	I Medicine Park Granite	II Rush Lake Granite	III Saddle Mtn. Granite
Liquid		88.4	82.7	92.4
Hbl		5.9	7.3	2.6
Na-spar				5.8
Pl		6.4	10.6	
Ttn		0.6	0.8	0.4
Ap				0.6
Mt				0.9
Bt				
		Calculated Parent		
SiO_2	72.8	72.8	72.8	72.8
TiO_2	0.47	0.47	0.44	0.45
Al_2O_3	12.5	12.2	12.3	12.6
Fe_2O_3	3.72	3.75	3.72	3.72
MnO	0.09	0.04	0.01	0.05
MgO	0.29	0.28	0.29	0.23
CaO	1.29	1.25	1.33	1.33
Na_2O	3.96	4.48	4.28	3.80
K_2O	4.17	4.12	4.25	4.14
P_2O_5	0.08	-0.03	-0.07	0.28
Σ res^2		0.39	0.17	0.08

Chapter 5. Surface and near-surface investigation of the Mount Scott Granite and the Sandy Creek Gabbro, Hale Spring Area, Wichita Mountains, Oklahoma

Introduction

Spatial and temporal relationships between the Sandy Creek Gabbro, Mount Scott Granite sheet, and Glen Mountains Layered Complex, all located in the Hale Spring Area of the Wichita Mountains, Oklahoma, were investigated through surface mapping, core drilling, and magnetic surveying. Although the subhorizontal contact between the underlying gabbro and overlying granite sheet is regionally well exposed, details of this contact are typically obscured by talus, vegetation, and extensive alteration. Thus, a drilling investigation was designed with two primary goals: 1) retrieve a continuous core across the contact between Mount Scott Granite and Sandy Creek Gabbro for direct observation of the contact relationships between these two units and 2) obtain "fresh" samples of these units in the vicinity of the contact for petrologic investigation. The Ira Smith Quarry location was selected with these goals in mind, particularly with the intent of transecting the contact at a relatively shallow depth, within 20 m of the surface, based on the local spatial distribution of Sandy Creek Gabbro and Mount Scott Granite. The initial result, 87.5 m of continuous core of Mount Scott Granite, was surprising and thus became the impetus for initiating a magnetic survey designed to determine the subsurface morphology of the Sandy Creek Gabbro pluton and the nature of its contact with Mount Scott Granite. The results of this study require important revisions to earlier models of the temporal and spatial evolution of magmatism in the province as a whole. The subsurface spatial relationships between these units are more compatible with the Sandy Creek Gabbro being younger than the Mount Scott Granite rather than *vice versa* as previously thought (*e.g.*, Powell *et al.*, 1982).

Regional Geology

The geology of the Wichita Mountains is summarized here from Ham *et al.* (1964), Powell *et al.* (1980), Gilbert (1982), and Hogan and Gilbert (1997) and references therein. The Wichita Mountains are a series of rounded hills and rocky promontories located in southwestern Oklahoma, extending northwest from the city of Lawton, past the town of Granite. They are the fault-bounded geomorphic expression of the Wichita Igneous Province, a northwest-southeast trending zone of Cambrian bimodal igneous activity. This igneous activity is believed to be related to crustal extension and formation of the Southern Oklahoma Aulacogen during the breakup of the Laurentian supercontinent (see Hogan and Gilbert, 1998).

The mountains result from a complex tectonic history. Subsequent to the rifting event, the province underwent extensive thermal subsidence and was buried by clastic and carbonate sediments from the early Paleozoic to the Mississippian. This was followed by uplift and exhumation of the igneous rocks as a result of the Wichita Orogeny (Ham and Wilson, 1967) in the Pennsylvanian. The resulting mountain range had a similar form to the currently exposed Wichita Mountains. Permian clastics, largely sediments shed from the Ouachita Mountains to the east, but also locally derived sediments (*e.g.*, Post Oak Conglomerate) buried these early mountains. Re-exhumation of the mountains began in the Tertiary and continues today; all that covers these ancient mountains is a veneer of westward thickening Permian clastics.

Exposed igneous units in the eastern Wichita Mountains (east of Oklahoma Hwy. 54, Figure 5-1), are compositionally stratified: mafic units are overlain by silicic units. In near vertical exposures, the larger mafic bodies (GMLC and Roosevelt Gabbros) crop out below the sheet granites, which in turn typically crop out beneath Carlton Rhyolite. The major mafic bodies (GMLC and Roosevelt Gabbros) were previously interpreted to have been uplifted and eroded, and then covered by rhyolite prior to intrusion of the granite (Ham *et al.*, 1964; Hogan and Gilbert, 1995). The granite magmas then spread out laterally along the rhyolite-gabbro contact resulting in sheet-like plutons (Hogan and Gilbert, 1997). These units are crosscut by later dikes of diabase (Late Diabase), locally abundant pegmatite (*e.g.*, Hale Spring Pegmatite), aplite, and rhyolite (Figure 5-2).

Recent geochronologic investigations suggest that some members of the Roosevelt Gabbros may not have been part of the eroded mafic substrate, but rather intruded the GMLC after early silicic magmatism, thus requiring modification of earlier models for the rift. Laser $^{40}Ar/^{39}Ar$ dating of amphibole and biotite from the Mount Sheridan Gabbro, a member of the Roosevelt Gabbros, places its age at 533 ± 2 Ma, whereas amphibole from the Mount Scott Granite yields an age of 539 ± 2 Ma (Hogan *et al.*, 1996). If these hydrous gabbro plutons are indeed younger than the silicic rocks, then the magmas that gave rise to these gabbro plutons were possibly stopped and trapped beneath the silicic cover. Thus, resolving contact relationships between the Mount Scott Granite sheet and the underlying Roosevelt Gabbro plutons is critical to determining the temporal and spatial evolution of magmatism during formation of the Southern Oklahoma Aulacogen. The

Hale Spring Area (Figure 5-1), a region on the western edge of the large, continuous eastern exposure of the Mount Scott Granite (Cooperton 7.5 minute U.S.G.S. quadrangle, Oklahoma Coordinates T.3N. R.15W. Sec. 2-4, 9-11, 98° 45-46.5' West Longitude, 34° 45-46' N Latitude), provides an area where these units crop out and can be readily investigated.

Geology of the Hale Spring area

Many lithologies are exposed within the Hale Spring Area. These include the Meers Quartzite (age uncertain), the Cambrian Glen Mountains Layered Complex (GMLC), Mount Scott Granite, Sandy Creek Gabbro, Hale Spring Pegmatite, a hybrid rock unit, Permian Post Oak Formation (granite conglomerate), and Quaternary alluvial sediments. The following geologic description is summarized from Johnson (1955), Gilbert (1982), Powell *et al.* (1982), Stockton and Giddens (1982), Stockton (1984), Diez de Medina (1988), and references therein. Figure 5-3 is a "bedrock" (Permian and Quaternary sediments removed) geologic map of the area.

The Sandy Creek Gabbro of the Roosevelt Gabbro Group crops out in the lower elevations (< 600 m), mostly on the valley floor and adjacent to the stream cuts of the Hale Spring Area. The rock is hard and dense. Weathered surfaces are dark-reddish black and scalloped; the weathering does not appear to penetrate the rock more than two or three centimeters. The gabbro is largely composed of plagioclase, with variable amounts of olivine, typically exhibiting pyroxene coronas. Olivine-rich exposures appear layered. Lamination of plagioclase in the southern portion of the area dips ESE 20-30°. Primary interstitial pink-brown amphibole and red-brown mica are common. Exposures to the north of Big Four Mountain also contain quartz and alkali feldspar. Work by Powell *et al.* (1982) and Diez de Medina (1988) found that the samples in the south are compositionally more primitive than those collected from Hollis Canyon, north of Big Four Mountain. Exposures of altered gabbro with sericite- and calcite-replaced plagioclase crystals, chlorite, epidote-zoisite, and calcite and fibrous or acicular amphibole replacing mafic grains (Powell *et al.*, 1982) occur within the central portion of the Hale Spring area.

The Mount Scott Granite crops out in the higher elevations (>500 m). On the surface, the rock is variably fractured and weathers to an orange-red color. Weathered exposures commonly contain spheroidal boulders that are substantially altered to their cores, the result of weathering below the groundwater table along fractures in the granite (Gilbert, 1982). The rock texture is porphyritic, with gray ovoid anorthoclase phenocrysts, many with rapakivi-texture albitic rims of plagioclase, set in a matrix largely of alkali feldspar and quartz (Price *et al.*, 1996). Although many localities contain abundant granophyre, here matrix quartz and feldspar are seriate (Merritt, 1965). Minor and accessory minerals comprise less than 5 modal percent. Typically, the following minerals occur together in clots throughout the matrix: ferroedenitic amphibole, biotite, magnetite, ilmenite, along with titanite, fluorite, zircon, apatite and rare allanite, Secondary minerals include hematite, calcite, sericite, titanite, epidote, and clays.

The contact between the Sandy Creek Gabbro and the Mount Scott Granite is not easily observed; the faster weathering rate of the gabbro relative to the granite results in steep granite hill slopes, with granite talus covering much of the contact. However, the exposure is typically sufficient to allow placement of the contact to within several meters. The regional shape of the contact between the Sandy Creek Gabbro and the Mount Scott

Granite sheet can be inferred from elevations of the contact within the area, provided that there has been no significant offset by faulting. Based on the Mount Scott Granite's sheet-like morphology, its exposure on hill tops, and the Sandy Creek Gabbro exposure in valleys, Powell *et al.* (1982) concluded that the area is an erosional window, where Sandy Creek is dissecting a subhorizontal granite/gabbro contact, stripping away the overlying granite to expose the gabbro.

Cropping out largely within the Mount Scott Granite, and only locally in contact with the gabbro, is a rock of highly variable appearance called hybrid rock. The outcrop pattern of the hybrid rock trends east-west from Sandy Creek Valley across Big Four Mountain (Figure 5-3). The hybrid rock is variable in color index, grading from pink and gray to dark gray. It is medium-grained, with quartz and pink feldspar phenocrysts, and contains xenoliths of biotite gabbro. Similar rocks are found elsewhere in the Wichita Mountains, and workers have attributed their origin to partial melting of the gabbro's weathered erosional surface (*i.e.*, saprolitic regolith) during granite intrusion over and along this surface (Powell *et al.*, 1982). Alternatively, if the gabbro is younger than the granite, it is plausible that the hybrid rock originated along the contact between these two units as a partial melt of the granite that may have mingled with the gabbroic magma. The exposure on Big Four Mountain therefore may represent a "dike" of this contaminated partial melt which intruded the overlying granite.

Exposures of Hale Spring Pegmatite crop out over much of the area in the lower elevations (<550 m) as dikes and elongate pods that cross cut both Sandy Creek Gabbro and Mount Scott Granite. The Hale Spring pegmatite has aplitic to pegmatitic texture, is largely composed of quartz, albite, and microcline, and contains large crystals of sodic amphibole (arfvedsonite) along with magnetite and acmite (Scofield and Gilbert, 1982). Hale Spring Pegmatite is mineralogically similar to the nearby Quanah Granite, and this has led previous workers to infer its derivation from this granite.

The Glen Mountains Layered Complex crops out as small (1-30 m^2) blocks within the Sandy Creek Gabbro. Powell *et al.* (1982) concluded these blocks are xenoliths, confirming the younger age of the Sandy Creek Gabbro relative to the layered complex. The blocks are composed of anorthositic gabbro, and are similar to nearby exposures of the GMLC to the east and the west of the Hale Springs Area.

Also present as xenoliths within the Sandy Creek Gabbro are several exposures of Meers Quartzite, some of which are spatially associated with xenoliths of GLMC, a relationship which may be preserving an unconformable relationship between these two units. Here, the Meers Quartzite is largely composed of quartz, abundant sillimanite, and lesser muscovite. Xenoliths of Meers Quartzite, entirely within the Mount Scott Granite, also occur nearby. This quartzite contains only trace sillimanite and muscovite.

Covering much of the valley floor is Post Oak Conglomerate, composed largely of granite clasts in a matrix of calcrete, clay, and ferric oxides (Donovan, 1982). Elsewhere, this unit has been assigned a Permian age based on gradational contacts into Permian clastics (Chase, 1954). Within the Hale Spring area, stream dissection of this unit is extensive in places, and it is difficult to discriminate between this Permian unit and much younger, reworked fluvial deposits.

This study found scant evidence for faulting within the Hale Spring Area. However, two previous studies have proposed faults. Stockton (1984) placed an east-west fault along the southern base of Black Bear Mountain, although more recent magnetic data argue against its existence (discussed below). McLean and Stearns (1986) placed an east-west trending, left-lateral fault, and a smaller, northeast-southwest trending, left-lateral fault through the southern portion of the Hale Spring area, related to Pennsylvanian uplift. These two faults were based on analysis of regional lineaments and linears and the horizontal offset of local quartz veins. Although these quartz veins are indeed offset, the timing of the offset remains speculative. While a Pennsylvanian origin is possible, it is equally likely that the veins record earlier movements within the granite, perhaps even previous to Sandy Creek Gabbro intrusion. Because of the limited amount of evidence regarding timing and nature of faulting within the region, the conclusions presented here minimize the role of faulting in developing a spatial model for the units.

Procedure

Drilling and core retrieval

The drill site is located on the Snell Ranch adjacent to one of several pits of the defunct Ira Smith Quarry on the west slope of Big Four Mountain, (Township-range, Oklahoma Coordinates: SE SE SW NW Sec. 4 T.4N. R.15W.; NAD 27 UTM 14 S 0520394 N, 3845679 E). The site was chosen on the basis of contact relationships to intercept the granite-gabbro contact within 20 m or less, the ability to start drilling in bedrock, and the close proximity to an ample supply of fresh water.

The SQ-1 hole was spudded in the Mount Scott Granite, just west of the quarry pit and less than 50 m east from the contact with the gabbro. Drilling began in the Spring of 1993, and concluded in September of that year. The SQ-1 hole was cored to a total depth of 87.5 m by 2 inch (5.08 cm) I.D. diamond drill bit, using a water-cooled rotary rig. The rig is owned and operated by the Oklahoma Geological Survey.

The second hole, SQ-2, was a short hole spudded in soil and fill and completed in Sandy Creek Gabbro to an estimated depth of 10.4 m. Only a little over 1.67 m of core was retrieved using the same drilling equipment as SQ-1. Both cores were initially examined, logged, and oriented by J.P. Hogan at the drill site.

Color

Color was assessed by visual observation of the interior of dry core samples using the Geological Society of America Rock-Color chart (Goddard *et al.*, 1948). All estimates indicate the bulk color of the sample, unless otherwise noted. Estimates are reported using color names defined in the U.S. National Bureau of Standard's Special Publication #440 on color (Kelly and Judd, 1976) and the corresponding identification number in the Munsell color system: **hue value/chroma** (*e.g.*, **10R 7/4**). Visual estimation of Munsell identification numbers have the following errors: hue ±4, value ±1, chroma ±1.

Magnetic susceptibility (χ)

Magnetic susceptibility readings of the SQ-1 core were taken every 0.5 feet (0.153 m) using an Exploranium™ KT-5 hand-held susceptibility meter. Measurements from the hand-held meter were correlated to selected analyses of the core on a Sapphire Instruments™ SI-2, 5 cm diameter, copper coil susceptibility and anisotropy meter housed in the School of Geology and Geophysics Paleomagnetic Laboratory. The SI-2 meter was calibrated using a known volume and mass of MnO. Readings on the SI-2 were taken in SI mass units. However, a limited number of readings in SI volume units were acquired to verify the mass readings.

Magnetic susceptibility readings on the SQ-2 core were done exclusively on the SI-2 susceptibility meter. Most of the core was analyzed in 4 cm increments in SI volume measurements. SI volume values were converted to SI mass values using the measured density of the core. SI mass units were taken on three 4 cm long pieces with known masses, and were used to check against the volume readings for the same interval. All magnetic susceptibility measurements are reported in SI mass units (dimensionless).

Magnetic surveying

The magnetic survey of the area was conducted to constrain the relative subsurface relationships and geometry of the Sandy Creek Gabbro and Mount Scott Granite. Several traverses were made using an EG&G™ proton-procession magnetometer. Observation points were located 25 ft (7.63 m) apart in early traverses and 20 m (65.6 ft) apart in later traverses. However, when significant changes in total field were observed, surveying employed smaller station interval distances to better characterize the noted change. Direction and distances were measured using compass, measuring tape, and a GPS unit. Stations were carefully plotted on the appropriate U.S. Geological Survey 7.5' quadrangle to ascertain the elevation. Five or more readings were taken at each observation station, and these were then averaged to produce a total field reading. Averages with 2σ standard deviation $> \pm 3.00$ gammas were discarded from the data set. A base-station was reoccupied to monitor drift (observed drift <10 gammas) every two hours or less. The main field was then subtracted from the total field data. Data were then modeled using *GM*, a commercially available MS-DOS software package (Northwest Geophysical Associates) for forward 2-D modeling of gravity and magnetic data.

Fracture density

Fracture density (fractures/cm of core) data were acquired by counting the number of macro-fractures (visible to the unaided eye) over 0.5 ft (0.153 m) sections of the core.

Two types of fractures were observed: 1) *Complete fractures* which transect the entire core, and 2) *Incomplete fractures* which crosscut only a portion of the core.

Petrographic analysis

Thin sections of the core were made every ~15 m and at selected additional depths. Observations were made in both transmitted and reflected light. Selected feldspar phases were analyzed by electron microprobe as part of a separate study published in Price *et al.* (1996), presented in Chapter 2 of this dissertation.

Results

Drill core investigation

Drilling at SQ-1 produced 87.5 m of continuous core, entirely of Mount Scott Granite. The absence of the granite-gabbro contact came as a surprise and prompted a magnetic survey in order to better resolve the subsurface geometry of this contact. The results of this survey are discussed later in the paper. Cursory inspection of the core revealed little if any significant variation with respect to primary igneous texture and mineralogy of the Mount Scott Granite as a function of depth. However, more detailed studies documented systematic variation in oxide mineralogy, fracture density, color, and magnetic susceptibility as a function of depth within the first 30 m of the surface.

The granite of the SQ-1 core is typical of surface exposures of Mount Scott Granite as observed within the Ira Smith Quarry. Although this granite may contain abundant granophyre at other locales (*e.g.*, Mount Scott), here the Mount Scott Granite is porphyritic with a seriate matrix, and granophyre is noticeably absent. Miarolitic cavities were not observed. The granite contains the characteristic gray ovoid rapakivi-textured anorthoclase feldspar phenocrysts discussed by Price *et al.* (1996). These phenocrysts are set in a matrix of red to pink alkali feldspar and quartz, with lessor plagioclase and with glomerocrystic ferroedenitic hornblende + biotite + accessory minerals which include titaniferous oxides, titanite, fluorite, zircon, apatite, ± allanite. The core also contains a substantial amount of mafic enclaves, characteristic of the Mount Scott Granite (Merritt, 1965). Sodic amphibole is present in the very deepest sample from the core (87.5 m) and is observed in surface exposures in vein fillings. A 0.1 m thick aplitic zone is present at 47.05 m depth. The aplite is fine-grained, ~equigranular, and devoid of ovoid feldspars or other phenocrysts. The color index grades from 5% to 0% from 47.05 to 47.11 m depth, and then grades back to 5% over the next 0.04 m.

The primary igneous mineralogy of the Mount Scott Granite is variably altered over the first ~30 m of the SQ-1 core. Largely, it is the titaniferous oxides that are altered, however, many of the silicates are altered to a lesser extent. With increasing depth to 27 m, the proportion of primary titanomagnetite and ilmenite increases and the proportion of secondary hematite decreases. At 20.5 m depth and shallower, oxide grains are largely hematite (Figure 5-4d), with a small amount of ilmenite, and have a martite texture. In samples between 20.5 m and 34.7 m depth (Figure 5-4b, c), hematite, propagating inward from grain boundaries, fractures, and partings, has encroached upon primary magnetite grains leaving only small domains of the original magnetite. This encroachment decreases as a function of depth and by 34.7 m, (Figure 5-4a) and in deeper samples, the oxide assemblage is near-pristine primary titanomagnetite and primary ilmenite. Here magnetite grains typically exhibit only trace amounts of hematite along grain boundaries and partings.

The color changes substantially over the first 30 m of the SQ-1 core (Figure 5-5a). Close to the surface, the color is a grayish reddish orange (2YR 5/6). With increasing depth, the color darkens to a moderate grayish red (8R 4/6) (depth of 10 m). The color becomes lighter and more yellow from 10 to 13 m, ending at a grayish reddish orange (2YR 5/6). Over the next 14 m, the color gradually grades darker, and largely remains a moderate grayish red (8R 4/6) at depths below 27 m. This color is observed above and below the aplitic zone at 47.1 m, although the zone itself is a lighter color (8 R 6/3).

Magnetic susceptibility (χ) increases almost two orders of magnitude (Figure 5-5b and Appendix 3a) in the first 27 m of the SQ-1 core and then remains constant with depth. The lowest susceptibility values, 3×10^{-4} SI, are found at depths less than 2 m. From 2 to 10 m, susceptibility values rise to just below 1×10^{-3} SI, and are ~constant for 2 m. Between 12 m and 19.5 m, susceptibility varies from 3×10^{-4} to 1×10^{-3} SI. From 19.5 m to 27 m, susceptibility values increase to 9×10^{-3} SI. Below 27 m, to a depth of 55 m, values average ~9×10^{-3} SI, with only one notable exception at 47.1 m, where values drop over the corresponding interval of the aplitic-texture zone noted above.

The SQ-1 core is variably fractured, and the fracture density decreases to nil with depth in the first ~30 m from the surface (Figure 5-5c, d and Appendix 3a). Fractures are irregular to planar, exhibit several orientations, and are observed both macroscopically and microscopically. Larger fractures commonly have thin (~1 mm) coatings of secondary minerals (*e.g.*, calcite, pyrite, clays). Fractures contain little evidence of offset but zones of micro-brecciation have been observed. Above 0.9 m depth, the rock is largely incompetent and crumbly as a result of the extremely high number of fractures. Between 0.9 m and 27 m, fracture density varies, but shows an overall decrease with increasing depth. Partial fracture densities between 1 and 3 m are as great as 0.60 cm^{-1}. Complete fracture densities were large in this same interval, with densities above 1.0 cm^{-1}. Complete fracture density dropped to zero from 9.5 m to 14 m, and partial fracture density was low (~0.07 cm^{-1}) for this interval. Fracture densities increase at 14 m, to 0.45 cm^{-1} partial fractures and 0.50 cm^{-1} complete fractures. Below 15 m, fracture densities taper off to 0.0 by 27 m. Below 27 m the core is unfractured, except at 31.5 m, 41.5 m, and 56.5 m.

Color, oxide mineralogy, magnetic susceptibility, and fracture density vary systematically with depth over the first 27 m of SQ-1 core. At depths greater than 27 m the core remains largely homogeneous. In general, from the surface to 27 m, magnetic susceptibility, hue, and modal primary magnetite and ilmenite increase, whereas fracture density and modal secondary hematite decrease. More importantly there is a direct correspondence between these properties and fracture density. For example, at 14.5 m depth and again at 19.5 m depth, magnetic susceptibility decreases drastically, the color lightens, with a corresponding *increase* in fracture density. Conversely, at 11 m depth and again at 18 m depth, magnetic susceptibility increases, the color becomes pinker, with a corresponding *decrease* in fracture density (Figure 5-5).

In contrast to this, the Sandy Creek Gabbro from the near-surface SQ-2 core, although containing a significantly fractured interval (0.70 cm^{-1} partial fractures) from 9.5 to 10 m, shows no alteration of magnetite to hematite (Figure 5-6) and insignificant change in magnetic susceptibility (Appendix 3b). Although the core length is short and perhaps insufficient for documenting trends in mode or susceptibility, it is shallow (<11 m) and one would expect to find magnetite to hematite alteration here if present. However, exsolution of fine ilmenite needles (Figure 5-6b) within magnetite grains was the only observed secondary feature of the SQ-2 oxides. Magnetite crystals are otherwise pristine, showing not even the slightest alteration, including along grain boundaries, fractures, and partings.

Magnetic survey

Magnetic susceptibility of the Mount Scott Granite is considerably lower (at any depth) than for the Sandy Creek Gabbro (Bradley and Jones-Cecil, 1991). Thus, as a result of failing to intersect the granite gabbro contact with the drill, a magnetic survey of the area was initiated in order to better resolve the subsurface geometry of the Sandy Creek Gabbro and Mount Scott Granite contact. The large contrast in magnetic susceptibility ($\Delta\chi$) between these units greatly facilitates modeling the subsurface spatial geometries of these two bodies from geomagnetic data.

Jones-Cecil (1995) presents the results of a detailed aeromagnetic survey of the Wichita Mountains with the total-field data from the survey reduced to the pole. Figure 5-7 places that data over the geology shown in figure 5-3. Substantial magnetic highs on this map should correspond with relatively shallow and/or large bodies of material with a large $\Delta\chi$ with their surroundings. Although the survey indicates there are substantial changes in magnetism within this area, very few coincide with mapped contacts. For instance, the highest readings in the Hale Spring Area are found beneath Black Bear Mountain, the surface of which is composed entirely of Mount Scott Granite. This is likely to correspond to Sandy Creek Gabbro under a thin veneer of Mount Scott Granite.

Several magnetometry ground traverses resolved local details of the magnetic field (see Figure 5-3). Traverses across the contact between the Sandy Creek Gabbro and all of the surrounding and intruding lithologies were always marked by a change in total field.

Total field variations were also noted elsewhere along many of the traverse lines, and, in many cases, direct observation of the geology during such variations was obscured by alluvium. Two extensive traverses are presented in this paper (Table 5-1 and 5-2), and a permissible subsurface geometry for the units was constructed by 2D forward modeling.

Discussion and Conclusions

Variation within the granite

Analysis of the SQ-1 drill core indicates little change in the primary magmatic character of Mount Scott Granite over the 87.5 m hole depth. The majority of variations in the core result from fracture-controlled, fluid induced alteration of the granite (Price *et al.*, 1995).

Magmatic Variation

Magmatic variation refers to changes resulting from igneous processes operating during crystallization of the cooling granite magma. The homogeneous nature of the primary igneous mineralogy and primary texture of the core suggest a largely uniform composition, and a uniform cooling history, for the Mount Scott Granite magma over the interval examined (87.5 m). Detailed investigations of feldspar compositions (Price *et al.*, 1996) and amphibole compositions (Hogan and Gilbert, 1995) from this core revealed little if any compositional variation, indicating rather uniform magma composition and intensive parameters (*e.g.*, T, fO_2) during crystallization of this portion of the granite.

The one exception to the primary mineralogical and textural homogeneity of the core is the aplitic zone observed at 47.1 m. In general aplite dikes are rarely observed within the Mount Scott Granite. This aplite is finer grained and more felsic than the adjacent granite and is free of ovoid phenocrysts. Although currently compositional information is unavailable on this zone, these are interpreted to be a late stage differentiate of the Mount Scott Granite rather than a distinctly separate magma.

<u>Subsolidus Variation (Alteration)</u>

Circulation of presumably meteoric waters through a near-surface fracture network in this crystalline basement has significantly altered the primary mineralogy of the Mount Scott Granite. This alteration has drastically modified both the magnetic susceptibility and color of the Mount Scott Granite.

Fluids altered the primary titanomagnetite grains within the Mount Scott Granite. Samples from depths below 27 m in the core contain primary titanomagnetite, largely free of hematite. With decreasing depth, these grains are increasingly replaced by hematite by the following reaction:

$$2Fe^{2+}Fe_2^{3+}O_4 + \tfrac{1}{2}O_2 \rightarrow 3Fe_2^{3+}O_3 \qquad (5\text{-}1)$$

Hematite growth proceeds from grain boundaries and fractures into the crystals.

Fluids altered the color of Mount Scott Granite through hydration of chromophores in alkali feldspar. Based on cathodoluminescence studies of other samples of Mount Scott Granite (Price, unpublished data), and what is known about feldspar chromophores (Smith, 1974), the color of matrix alkali-feldspars results from submicroscopic hematite flakes as inclusions. If water-rich fluid were to permeate the crystals, perhaps along perthite boundaries or cleavage planes, it could react with the inclusions, to produce iron hydroxide (*e.g.*, goethite) at the expense of hematite:

$$Fe_2^{3+}O_3 + H_2O \rightarrow 2(Fe^{3+}O(OH)) \qquad (5\text{-}2)$$

Hydration of red hematite flakes to yellow iron hydroxide turns the alkali feldspar grains from pink to orange. Since alkali feldspar comprises over 80 percent of the rock, the entire color of the rock is changed when alteration is thorough.

The oxidation of primary magnetite to hematite and the hydration of hematite to iron hydroxide diminish the magnetic susceptibly of the rock. Magnetic susceptibility is a function of the concentration, size, shape, and type of the ferromagnetic (*s.l.*) minerals (*i.e.*, magnetite, hematite, ilmenite) within a rock (Tarling and Hrouda, 1993). Changes in concentration, size, shape are not significant here: the mode of oxides remains unchanged throughout the upper portion of the core, and replacement appears to be largely pseudomorphic. However, the secondary alteration of magnetite to hematite and hematite to iron hydroxide, can readily account for the decrease in the magnetic susceptibility. The mass magnetic susceptibility values of magnetite are ten times those of hematite, and the values for hematite are one hundred times those for the iron hydroxide, goethite (Tarling and Hrouda, 1993).

All of the above alteration features, changes in color, oxide mineralogy, and magnetic susceptibility, correlate with fracture density. The greater alteration occurs closer to the surface, as do the greater numbers of fractures. In highly fractured intervals (*i.e.*, near surface) alteration was more pervasive because of enhanced permeability and because of the increased surface area for fluid/rock interaction.

The exact origin, timing, or temperature of the fluid(s) that altered the Mount Scott Granite remains unknown. However, because of the decrease in intensity of alteration as a function of depth, and because of the oxidizing nature of the reaction, it is likely that relatively recent circulation of meteoric water through this near surface fracture system explains the alteration. Since many of the observed fractures within the core and on the surface of the granite are open, it is likely that the oxidation and hydration of the granite are ongoing phenomena. However, because of the previous exposure of the Wichita Mountains to surface conditions in the Permian, multiple alteration events cannot be ruled out. The presence of rare sulfide mineralization along some fractures indicates interaction with low-fO_2 fluid(s). This suggests more complicated scenarios involving more than one alteration period with fluids of differing composition.

The ultimate origin of the fractures and their distribution is poorly constrained at this time. The region was subjected to several episodes of compression during the late Paleozoic, and faults have been located proximal to the core site (Stockton and Giddens, 1984; McLean and Stearns, 1986). However, the lack of offset and the presence of only minor brecciation argues against a compressional tectonic origin for the fractures observed in the core. Moreover, the decreasing fracture density with depth is more indicative of sheet fracturing developed during overburden unloading (Holtzhausen, 1989; Turcotte and Schubert, 1982). Because of the early Paleozoic burial level of this region, removal of overburden would have had a pronounced effect on the structural integrity of the Mount Scott Granite. Some 4-5 km of volcanic and sedimentary rocks once covered the Mount Scott Granite, and these were stripped away during the late Paleozoic. Additionally, the region returned to a depth of 1 km during the Mesozoic (Gilbert, 1982), and the current re-exhumation provides a second opportunity for sheet fracture genesis.

Perhaps the most significant conclusion from this portion of the study is the depth to which significant alteration of the granite is observed. To obtain what would be pristine igneous rock, one must penetrate >30 m below the surface. Typically, compositional analyses from granites are performed on near-surface samples. The effect of alteration on major-elements appears to be negligible, based on the lack of mineral mode variation. The possible effect on trace element chemistry is unknown, but may be substantial for elements easily mobilized by the fluids described here.

The Mount Scott Granite - Sandy Creek Gabbro contact

Based on the regional relationships, the granite-gabbro contact was inferred to be subhorizontal and should have been encountered within ~15 m of the surface at the drill site. However, the contact was not encountered with 87 m of drilling through solid Mount Scott Granite. Clearly, within the immediate vicinity of the drill hole the contact is neither subhorizontal nor does it dip shallowly to the east. Thus, forward 2-D modeling of the magnetic survey data was employed to resolve the subsurface geometry of this contact. Modeling provides a calculated profile that fits the observed data. This is largely dependent on the contrast in magnetic susceptibility, the shape of the boundary between the units, and the depth of the units. Although by themselves such models produce non-unique solutions, when augmented by detailed surface mapping, known regional relationships, and, albeit limited, drill hole data, the result is a reasonable geologic model of the subsurface.

As previously discussed, the magnetic susceptibility of the Mount Scott Granite gradually increases through a zone of fracturing and alteration to a depth of 27 m where it remains largely uniform. Thus, the Mount Scott Granite was subdivided into two units: a 27 m thick altered cap, with an average susceptibility of 1.23×10^{-3} SI, and an unaltered subsurface unit with a susceptibility of 7.60×10^{-3} SI. In construction of the models, it is assumed the boundary between altered and unaltered granite parallels topography.

Although a more complicated geometry reflecting fracture intensity and paleo-groundwater circulation is likely, significant variation to the depth of this contact will not drastically alter the conclusions presented here.

Magnetic susceptibilities for the Sandy Creek Gabbro core (SQ-2) are quite consistent (Appendix 3b), and magnetite grains throughout the core appear pristine and largely unaltered. It appears that the Sandy Creek Gabbro does not share the same alteration profile as the Mount Scott Granite. This is evidenced by the difference in the weathering of the gabbro, as seen on surface outcrops. Whereas exposed Mount Scott Granite weathers completely, producing meter-sized boulders of crumbly rock that are completely altered to their cores, the Sandy Creek Gabbro produces a weathering rind that is a few centimeters thick, with pristine-appearing rock below this surface. There are at least two possible reasons for this: 1.) there are fewer fractures and joints within surface exposures of the Sandy Creek Gabbro relative to the Mount Scott Granite so there is less surface area for fluid interaction; 2.) the diffusion rate of fluid through the rock is much slower than that of the Mount Scott Granite.

Although weathering will have created little to no variation in magnetic susceptibility of the Sandy Creek Gabbro, some variation, including higher values than those observed in the SQ-2 core, should be anticipated as the gabbro exhibits pronounced layered mineralogical variation throughout the body, including apatite-pyroxene-titaniferous oxide cumulates in the central portion of the Hale Spring Area (Powell, 1986; Diez De Medina, 1988). Furthermore, other Roosevelt Gabbro bodies contain appreciable amounts of high magnetic susceptibility rocks: there is a magnetite-ilmenite-olivine body (21-60% modal magnetite, Powell and Gilbert, 1982) exposed within the Glen Creek Gabbro, and some

Mount Baker Gabbro float contains magnetite crystals as large as 15 cm in diameter (Stockton and Giddens, 1982). In many parts of the pluton, it is likely that overall susceptibility of the gabbro is much greater than that measured from the core.

Modeling attempted to use the collected susceptibilities (average = 1.64×10^{-2} SI) from the core SQ-2. These were employed for the construction of Trav. 1 (Figure 5-8), as the core hole penetrates much of the modeled section, and the susceptibility satisfied the observed magnetic readings. However, the observed susceptibilities precluded modeling the gabbro in Trav. 2 (Figure 5-9) with this susceptibility: the calculated magnetic profile falls far below the observed data. It was therefore necessary to increase the susceptibility to produce the observed magnetic anomaly. In comparison to Trav. 1, Trav. 2 crosses a more mafic section of the pluton (Diez de Medina, 1988). The mineralogy may differ substantially from that observed in the SQ-2 core. Additionally, if the gabbro extends to great depths (500 m), as has been modeled, more mineralogical (and susceptibility) variation is likely, and should be accounted for within the model. Therefore, models of the gabbro in Trav. 2 employed a much greater susceptibility (5.00×10^{-2} SI) for the gabbro, chosen because it produces the intensity of magnetism necessary to fit the profile and because it is a reasonable estimate of a gabbro pluton with small magnetite-dominated layers or zones.

The susceptibility data for the other modeled units was taken from literature sources, where available, or approximated based on rock composition. The magnetic susceptibility value for the GMLC (5.7×10^{-3} SI) was taken from Bradley and Cecil-Jones, (1991). This value does not significantly differ from that of unaltered Mount Scott Granite. Because of the lack of contrast, the contact between the Mount Scott Granite and GMLC within the subsurface was interpolated from exposures to the north and east of the Hale Spring Area. Its presence in the near subsurface is likely, as xenoliths or possibly roof pendants of GMLC are present within the Sandy Creek Gabbro. No data are available for the Hale Spring Pegmatite. Its felsic mineral composition indicates that its susceptibility is quite low, and was modeled with values similar to the altered Mount Scott Granite. Likewise, there are no available data for the Post Oak Conglomerate or younger alluvium. Altered Mount Scott Granite susceptibility values were used for these units, as they are largely comprised of detrital grains and cobbles from the granite.

Figure 5-8 displays the modeled results for an ~east-west magnetic survey across the southern portion of the Sandy Creek Gabbro (Trav. 1, Figure 5-3). The traverse begins 15 m east of the SQ-1 drill hole in Mount Scott Granite, transects the gabbro, and ends 100 m into exposed Mount Scott Granite on the western side of the body. Beneath this traverse, the Sandy Creek Gabbro is relatively thin with an irregular floor. The eastern contact dips shallowly to the west, readily explaining why the granite-gabbro contact was not intersected by the SQ-1 drill hole. The western contact is near vertical. An anomaly of low-susceptibility material is present roughly in the middle of the traverse, and although not exposed at the surface, its location, shape, and low susceptibility are indicative of Hale Spring Pegmatite. The subhorizontal contact between the Mount Scott Granite and the underlying GMLC is interpreted from regional map patterns and appears to be truncated by emplacement of the Sandy Creek Gabbro.

A south-north traverse (Figure 5-9) beginning on Mount Scott Granite at Bell Mountain, crosses Sandy Creek Gabbro, and terminates on a small exposure of pegmatite within the gabbro. The Sandy Creek Gabbro displays considerable thickness, and the floor of the pluton is not imaged by this data. The contacts between the Sandy Creek Gabbro and the Mount Scott Granite along this traverse are near vertical, dipping only slightly to the north. The Sandy Creek Gabbro contact is again interpreted to truncate an older contact between the GMLC and Mount Scott Granite in the subsurface. No compelling evidence for faulting was observed in surface exposures of nearby Mount Scott Granite, suggesting that this geometry is the direct result of intrusion of the magma which gave rise to the Sandy Creek Gabbro. Numerous Hale Spring Pegmatite dikes crop out along this traverse, and thus, regions with low magnetic anomalies were modeled as pegmatite.

Magnetic data indicate that shape of the gabbro-granite contact varies. The models show that in the southern portion of the area, the surface contact outlines the furthest extent of the gabbro into the granite. The areomagnetic data (Jones-Cecil, 1995, figure 5-6) indicate the gabbro extends beneath the granite to the northeast. This may indicate that the contact is indeed subhorizontal for a short distances in the less eroded regions of the eastern Hale Spring Area.

The shape of the Sandy Creek Pluton

The subsurface geometry of the Sandy Creek Gabbro and its spatial relationships with adjacent units were evaluated from a series of north-south cross-sections, spaced 1 km apart, constructed on the basis of the results of this study (*i.e.*, surface mapping, drill-hole core data, and magnetic surveys), aeromagnetic data from Jones-Cecil (1995); Figure 5-7), and the surface geologic data from Powell *et al.* (1982), and Stockton (1984) and are shown in figure 5-10. Additional field data from exposures elsewhere in the Wichita Mountains aided in constraining this geologic model.

Cross sections A and B on figure 5-10 reveal that the present erosional surface is just beginning to expose the subhorizontal roof of the Sandy Creek Gabbro pluton in the vicinity of Hollis Canyon. The gabbro is interpreted to extend back beneath Black Bear Mountain where it is capped by a relatively thin veneer of Mount Scott Granite on the basis of the large regional magnetic anomaly associated with this mountain (see Figure 5-7). The hybrid rock, present along the southern contact of the gabbro, is interpretively depicted here as a dike-like body, generated by partially melting Mount Scott Granite (see Big Four Mountain, Figure 5-3). The Sandy Creek Gabbro is also shown to lip over, and, to an extent, exploit the GMLC-Mount Scott Granite contact. This is an interpreted extension of the Sandy Creek Gabbro ledge that protrudes out from the main body to the south seen on magnetic surveys further west (see cross section C).

Section C crosses the most eroded portion of Sandy Creek Valley. The surface geology is mostly Permian and younger sediments, but exposures of gabbro are found throughout the valley. Additionally, small blocks of GMLC and Meers Quartzite crop out: xenoliths, possibly roof pendants, suggesting the level of exposure is proximal to the former unconformity, that is the GMLC-Mount Scott Granite sheet contact. The southern end of section C is perpendicular to the E-W geophysical traverse (Trav. 1, Figure 5-8). Here the Sandy Creek Gabbro is relatively thin, with inwardly dipping margins, interpreted as a protruding subhorizontal ledge of gabbro that exploited the preexisting GMLC-Mount Scott Granite contact. Such lateral spreading occurs when the overlying strata (*e.g.*, Mount Scott Granite and Carlton Rhyolite) are lifted by the driving pressure of the intruding magma (Hogan and Gilbert, 1995). Although much of the Sandy Creek Gabbro pluton has steep sides, and it probably made room for itself largely through stopping or displacing the crust horizontally, a small amount of magma had sufficient driving pressure to exploit the horizontal discontinuity and form a shallow ledge.

Section D is ~0.3 km west and parallel to the S-N geophysical profile (Trav. 2) in Figure 5-9. The moderately eroded profile has similar geometry to that seen in the other sections. However, geophysical data indicate that the southern contact of the Sandy Creek Gabbro pluton is best modeled as a steep, near-vertical wall that truncates, rather than spreading laterally along, the older contact between the GMLC and the Mount Scott Granite sheet. As previously discussed, evidence of faulting was not observed at the surface. Thus this geometry is attribute to intrusion of a younger gabbroic magma that gave rise to the Sandy Creek Gabbro. Additional support for this conclusion includes a recently determined younger crystallization age for another Roosevelt Gabbro pluton, the Mount Sheridan Gabbro, than that determined for the Mount Scott Granite (Hogan *et al.*, 1996).

The Sandy Creek Gabbro pluton may have made room for itself through a combination of stoping, passive lifting of the overburden, and partial melting of its roof rocks. The pluton is typically a steep walled, >300 m deep roughly oval shape, with a short axis ~1.5 km wide, and a long axis excessive of 5 km. However, minor amounts of spreading occurred along the anisotropy created by the GMLC-Mount Scott Granite contact (*i.e.*, the 100 m thick subhorizontal gabbro ledge along the southern margin of the body; see Figure 5-8).

Work by Diez de Medina (1988) shows the gabbro fractionated after emplacement, producing a general distribution of relatively high MgO, cumulitic gabbro adjacent to highway 49 in the southern portion of the area and moderate, less cumulitic, moderate to low MgO gabbro located to the north in the drainage of Sandy Creek. Her work concluded that the gabbro adjacent to the creek results from fractional crystallization of the gabbro to the south and assimilation of crustal materials. This is consistent with our model, in that the gabbro to the south, crystallizing within a thin ledge, would cool prior to the rest of the body, and preserve a more primitive composition. Additionally, granite assimilation would occur in the bulk of the body to the north, producing the observed contamination.

Powell *et al.* (1982) and Powell (1986) concluded that the Sandy Creek Gabbro is tilted to the east with respect to the nearly horizontal Mount Scott Granite on the basis of dipping lamination and compositional differentiation within the gabbro. Such an interpretation is only valid for a scenario where the Sandy Creek Gabbro is much older than the Mount Scott Granite, and is emplaced and tilted prior to the Carlton unconformity. As mentioned above, the evidence from this study precludes this case. Instead these features arise from floor irregularity and assimilation of the granite. Powell *et al.* (1982) report 20-30° ESE dips on plagioclase lamination within the olivine gabbro in the southern portion of the Hale Spring area. However, no additional layering is observed elsewhere in the exposed gabbro, so it is doubtful that laminations continue for any great distance. Furthermore, the observed lamination occurs within the thin ledge of our model, and since lamination is the likely result of crystal settling, probably reflects the irregular floor of the ledge (see Figure 5-8). In addition to the evolution of the gabbro pluton noted in Diez de Medina (1998), the olivine gabbro grades into quartz gabbro adjacent to the contact with the Mount Scott Granite in Hollis Canyon. Differentiation away from the ledge, as mentioned above, should be expected, so that the gabbro becomes increasingly evolved in the uppermost portions of the main body (*i.e.* the roof). Additionally, although the degree of chemical contamination of the gabbro by the granite remains unconstrained at this time, it is likely that the gabbro becomes more pronouncedly evolved adjacent to the contact because of interaction with partially melted Mount Scott Granite (hybrid rock).

Summary

Combined surface and subsurface methods have been used to image the spatial relationships of the Sandy Creek Gabbro and the Mount Scott Granite. The upper portion of the Sandy Creek Gabbro pluton can be modeled as an oval cylinder with steep-walls and a relatively flat roof. The southern contact, as modeled from magnetic surveying, is best interpreted with the Sandy Creek Body intruding the Mount Scott Granite. Other contacts of the pluton are inferred to truncate in the subsurface a preexisting contact between Mount Scott Granite and Glen Mountains Layered Complex, implying a younger age for the Sandy Creek Gabbro than either of these two units. The presence of xenoliths, or possibly roof pendants, of Glen Mountains Layered Complex and Meers Quartzite within the Sandy Creek Gabbro, and the geometry of the surrounding contacts with Mount Scott Granite, suggest the roof of this pluton is spatially associated with an older regional unconformity that developed on the layered complex. This unconformity and associated sediments (*i.e.*, Meers Quartzite) were subsequently buried by the Carlton Rhyolite Formation prior to intrusion of the Mount Scott Granite along this surface. Limited subhorizontal protrusion of gabbro out from the main body of the pluton along this older contact suggests that locally accommodation of the gabbroic magma was achieved by passive lifting of the overburden.

Alteration of the Mount Scott Granite core, presumably by meteoric fluids, is fractured controlled. Macro-fracture density is variable but overall, decreases with depth, from an intensely fractured surface to unfractured rock at 30 m depth. Interaction with these fluids has changed the rock color and oxidized primary titanomagnetite to hematite and hydrated hematite to iron hydroxide. This change in magnetic mineralogy of the granite resulted in a drastic reduction of the magnetic susceptibility of Mount Scott Granite. This was incorporated into construction of subsurface models from magnetic field data. Changes in color, magnetic susceptibility, and oxide mineralogy are directly correlated to changes in fracture density. Domains of intense fracturing correspondingly exhibit more intense alteration. Thus, brittle fractures provided conduits for fluid-flow and subsequent alteration of the crystalline basement. The extent of alteration reflects the fluid/rock ratio which in part is a function of fracture density and connectivity. The exact timing of the fracturing and the composition of fluid(s) is unconstrained, but fluids likely include groundwater in equilibrium with atmospheric conditions. Circulation of these fluids has been restricted to depths less than 30 m below the present erosional surface. Thus, opening of these fractures is likely to be directly related to unroofing of this basement and the timing of alteration may be a relatively recent phenomenon. However, because the Wichita Mountains were previously exposed to atmospheric conditions in the Permian, the possibility for multiple alteration events is not excluded.

References Cited

Bradley, L., and Jones-Cecil, M., 1991, Density and magnetic susceptibility measurements of the rocks in the Wichita uplift and Slick Hills, southwestern Oklahoma. United States Geological Survey Open-File Report 91-269, 31 p.

Chase, G. W., 1954, Permian conglomerate around Wichita Mountains, Oklahoma. Bulletin of the American Association of Petroleum Geologists, v. 38, p. 2028-2035.

Diez de Medina, D. M., 1988, Geochemistry of the Sandy Creek Gabbro, Wichita Mountains, Oklahoma. Unpublished M.S. Thesis, University of Oklahoma, Norman, 163 p.

Donovan, R. N., 1982, Geology of Blue Creek Canyon Wichita Mountains Area, *in* Gilbert, M. C., and Donovan, R. N., eds., Geology of the Eastern Wichita Mountains Southwestern Oklahoma. Oklahoma Geological Survey, Guidebook 21, p. 65-77.

Gilbert, M. C., 1982, Geologic setting of the Eastern Wichita Mountains, with a brief discussion of unresolved problems, *in* Gilbert, M. C.; and Donovan, R. N., eds., Geology of the Eastern Wichita Mountains Southwestern Oklahoma. Oklahoma Geological Survey, Guidebook 21, p. 1- 28.

Goddard, E. N., Trask, P. D., De Ford, R. K., Rove, O. N., Singewald, J. T., and Overbeck, R. M., 1948, Rock Color Chart. Geological Society of America, Boulder, Colorado, 16 p.

Ham, W. E.; Denison, R. E., and Merritt, C. A., 1964, Basement rocks and structural evolution of Southern Oklahoma. Oklahoma Geological Survey, Bulletin 95, 302p.

Ham, W. E., and Wilson., J. L., 1967, Paleozoic epeirogeny and orogeny in the Central United States. American Journal of Science, 265, p. 332-407.

Hogan, J. P., and Gilbert, M. C., 1995, The A-type Mount Scott Granite Sheet. Importance of crustal magma traps: Journal of Geophysical Research, 100, B 8, p.15,779 - 15,793.

Hogan, J. P., and Gilbert, M. C., 1997, The intrusive style of A-type sheet granites from the Southern Oklahoma Aulacogen: *in* R. W. Ojakangas, A. B. Dickas, and J. C. Green ,eds., Middle Proterozoic to Cambrian Rifting. Mid-North America. Geological Society of America Special Paper, 312, p. 299-311.

Hogan, J. P., and Gilbert, M. C., 1998 The Southern Oklahoma Aulacogen. A Cambrian analog for Mid-Proterozoic AMCG (Anorthosite-Mangerite-Charnockite-Granite) complexes? Basement Tectonics, 12, p.39-78.

Hogan, J. P., Gilbert, M. C., Price, J. D., Wright, J. E., and Deggeller, M., and Hames, W. E., 1996, Magmatic evolution of the Southern Oklahoma Aulacogen. Geological Society of America, Abstracts with Programs, 28, p. 19.

Holtzhausen, G. R., 1989, Origin of sheet structure, 1. Morphology and boundary conditions, *in* A.M. Johnson, C. W. Burham, C. R. Allen, and W. Muehlberger, eds., Richard H. Jahns Memorial Volume. Engineering Geology, 27, 225-278.

Johnson, E. L., 1955, Geology of the pegmatite in the Hale Spring Area, Wichita Mountains, Oklahoma. Unpublished M.S. Thesis, University of Oklahoma, Norman, 87 p.

Jones-Cecil, M., 1995, Total-field Aeromag and Derivative Maps of the Lawton Area, Southwestern Oklahoma. United States Geological Survey, Map GP-998-A, 2 plates, 1:100000.

Kelly, K. L., and Judd, D. B., 1976, Color, universal language and dictionary of names. National Bureau of Standards, Special Publication 440, 158 p.

Merritt, C. A., 1965, Mt. Scott Granite, Wichita Mountains, Oklahoma. Oklahoma Geology Notes, 25, p. 263-272.

McLean, T. R., and Stearns, D. W., 1986, Stop 7: Hale Spring Locality, *in* Gilbert, M. C., ed., Petrology of the Cambrian Wichita Mountains Igneous Suite, Oklahoma. Geological Survey, Guidebook 23, p. 172-178.

Powell, B.N., 1986, The Raggedy Mountain Gabbro Group, *in* Gilbert, M.C., ed, Petrology of the Cambrian Wichita Mountains Igneous Suite. Oklahoma Geological Survey, Guidebook 23, p. 21-52.

Powell, B. N. and Gilbert, M. C., 1982, Stop 1 - Reid's Pit, *in* Gilbert, M. C.; and Donovan, R. N., eds., Geology of the Eastern Wichita Mountains Southwestern Oklahoma. Oklahoma Geological Survey, Guidebook 21, p. 79-96.

Powell, B. N., Gilbert, M. C., and Fischer, J. F., 1980, Lithostratigraphic classification of basement rocks of the Wichita province, Oklahoma: Summary. Geological Society of America Bulletin, Part I, vol. 91, p. 509-514, Part II, v. 91, p. 1875-1994.

Powell, B. N., Stockton, M. L., Giddens, J. D., III., and Gilbert, M. C., 1982, Stop 3 - Hale Spring Locality, *in* Gilbert, M. C.; and Donovan, R. N., eds., Geology of the

Eastern Wichita Mountains Southwestern Oklahoma. Oklahoma Geological Survey, Guidebook 21, p. 102-117.

Price, J. D., Hogan, J. P., Payne, J., and Gilbert, M. C., 1995, Investigation of the Mount Scott Granite Drill Core, Wichita Mountains, Oklahoma, Abstracts from the 12th International Conference on Basement Tectonics '95. International Basement Tectonics Association, Norman, Oklahoma, p. 65.

Price, J. D., Hogan, J. P., and Gilbert, M. C., 1996, Rapakivi-texture feldspar within the Mount Scott Granite, Wichita Mountains, Oklahoma. European Journal of Mineralogy, v. 8, p. 435-451.

Scofield, N., and Gilbert, M.C., 1982, Alkali amphiboles of the Wichita Mountains, *in* Gilbert, M. C.; and Donovan, R. N., eds., Geology of the Eastern Wichita Mountains Southwestern Oklahoma. Oklahoma Geological Survey, Guidebook 21, p. 60-64.

Smith, J. V., 1974, Feldspar Minerals II. Springer-Verlag, Heidelberg, 627 p.

Stockton, M. L.,1984, Geology of the gabbroic rocks in southern Cooperton Quadrangle and northern Odetta Quadrangle, Oklahoma. University of Texas, Arlington, unpublished M.S. thesis, 83 p.

Stockton, M. L., and Giddens, J. D., III., 1982, Igneous Geology of Cooperton Quadraqngle, Wichita Mountains, *in* Gilbert, M. C., and Donovan, R. N., eds., Geology of the Eastern Wichita Mountains Southwestern Oklahoma. Oklahoma Geological Survey, Guidebook 21, p. 47-50.

Tarling, D. H., and Hrouda, F., 1993, The magnetic anisotropy of rocks. Chapman and Hall, New York, 217 p.

Turcotte, D. L., and Schubert, G., 1982, Geodynamics, Applications of continuum physics to geological problems. John Wiley & Sons, New York, 450 p.

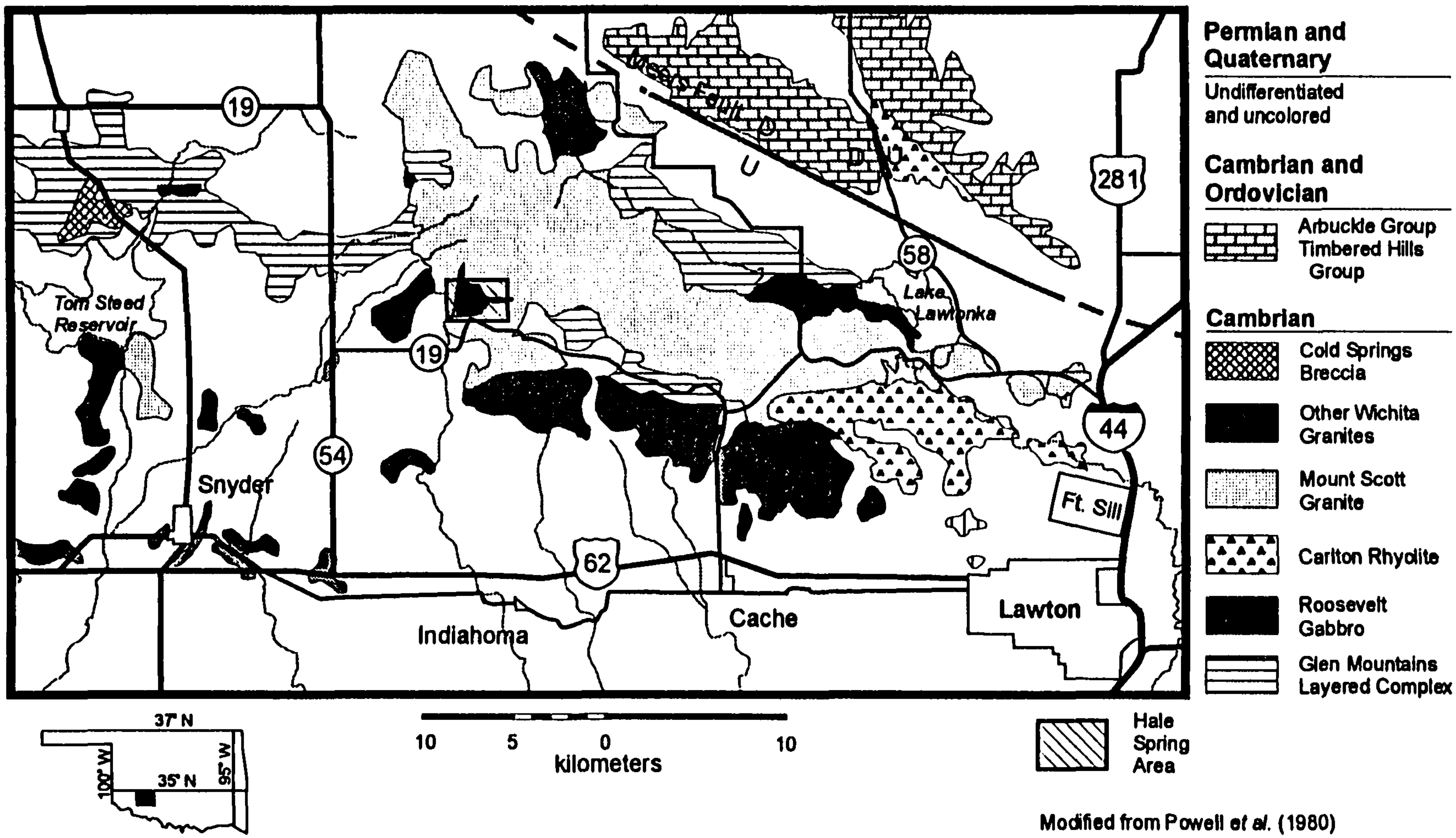

Figure 5-1. Generalized geologic map of the eastern Wichita Mountains, Oklahoma. Hale Spring Area, within the box, is enlarged in figure 5-3.

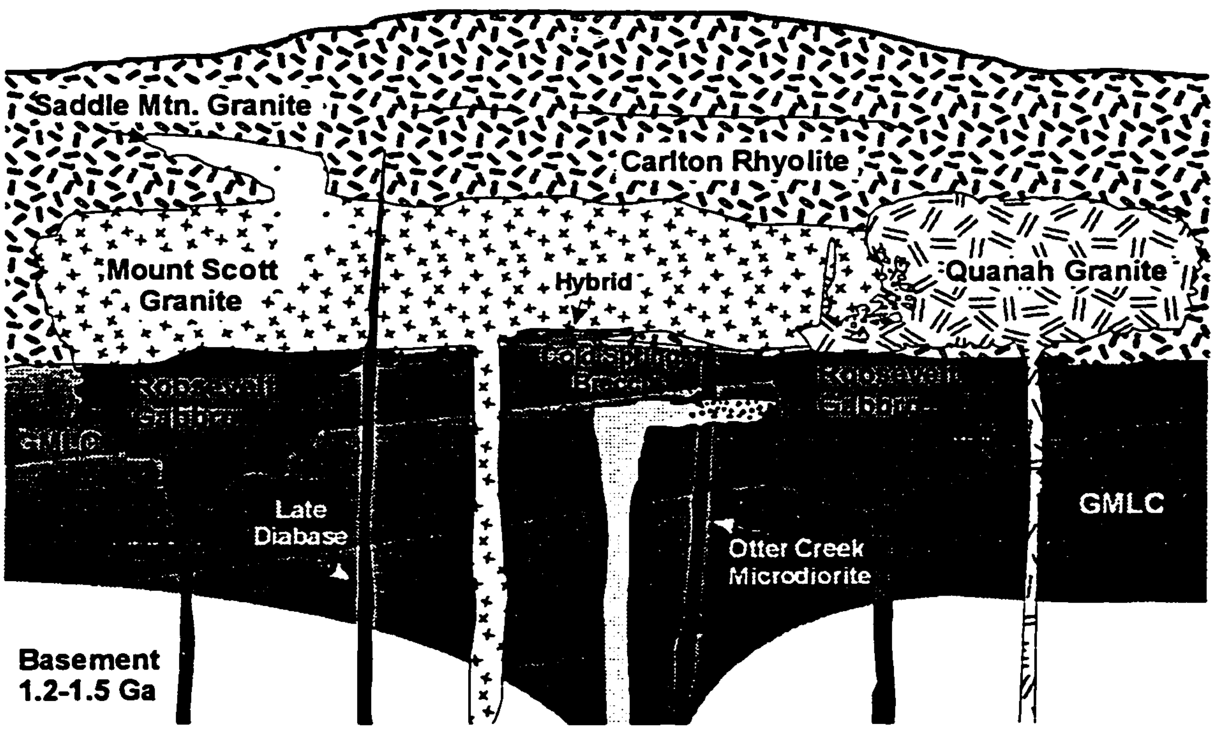

Figure 5-2. Schematic stratigraphic cross-section through the eastern Wichita Igneous Province illustrating the Cambrian contact relationships between the observed units. No erosion or faulting shown. This study examines the relationship between the Sandy Creek Gabbro, one of the Roosevelt Gabbros and the Mount Scott Granite.

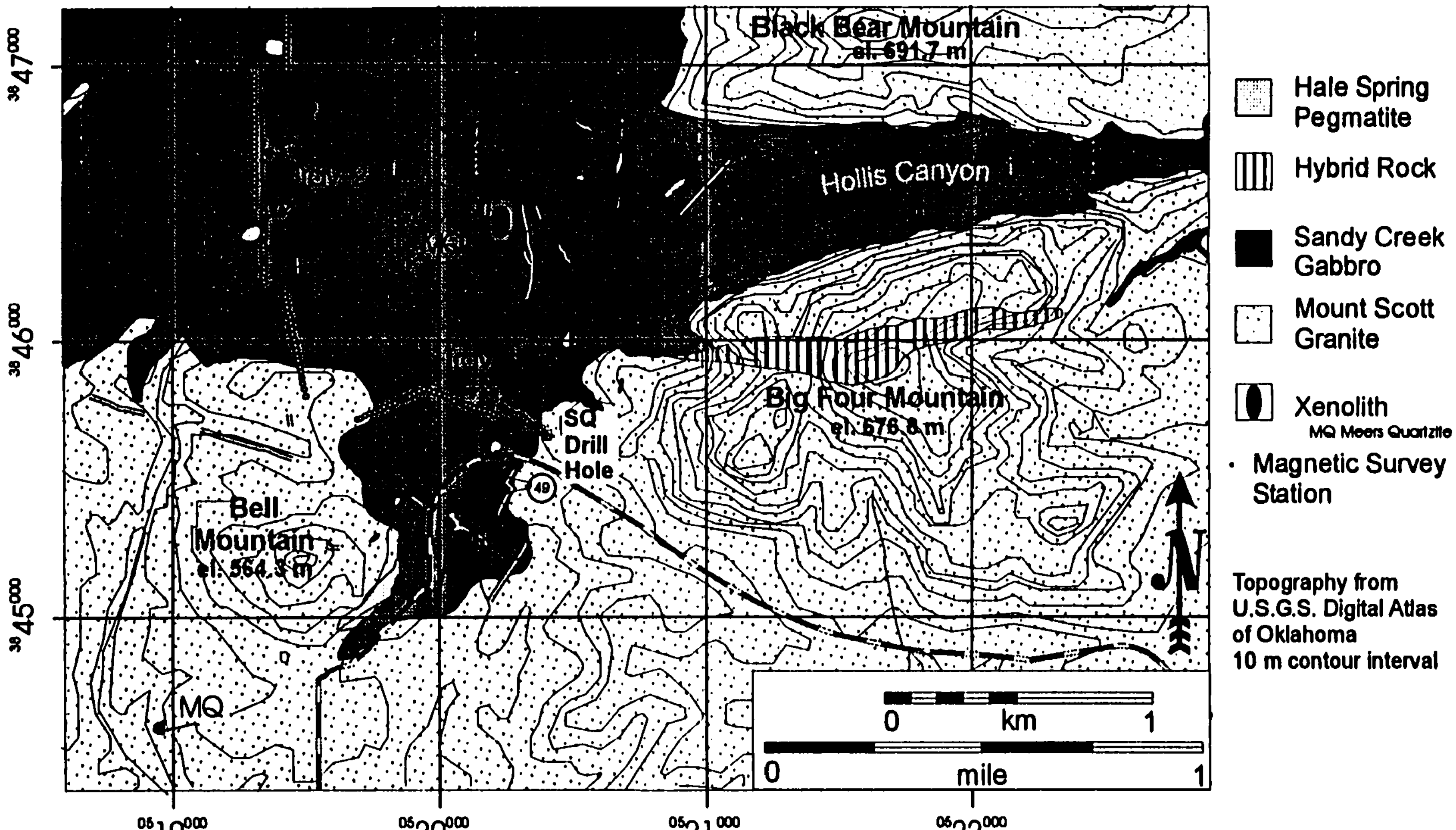

Modified from Powell et al., 1982

Figure 5-3. Geologic map of the Hale Spring Area with Permian and Quaternary removed. Surface magnetic traverses are plotted as a series of points that correspond with reading stations. Trav. 1 and Trav. 2 refer to two modeled traverses presented in this paper (Figs. 5-8 and 5-9 respectively).

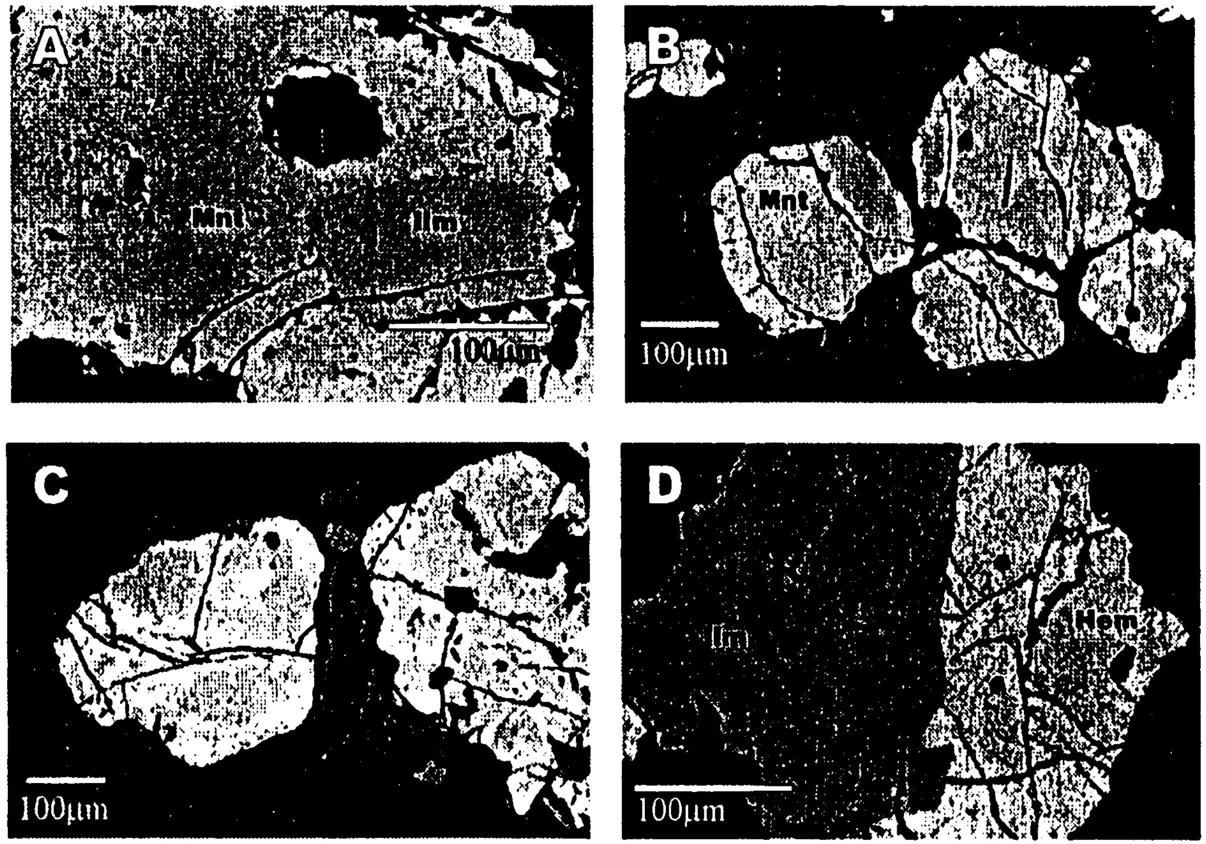

Figure 5-4. Four photomicrographs of the SQ-1 drill core (reflected light) documenting a change in the oxide mineralogy as a function of depth. A.) An example of near-pristine (unaltered) oxides: magnetite (Mnt) and euhedral ilmenite (Ilm) from 34.7 m depth. B.) Hematite (highest reflectivity) replacing magnetite grains along fractures at 27.5 m depth. C.) Hematite (highest reflectivity) replacing magnetite along fractures and grain boundaries at 23.3 m. Note alteration is more extensive than at 27.5 m. D.) Ilmenite (Ilm) and hematite (Hem) at 20.5 m depth.

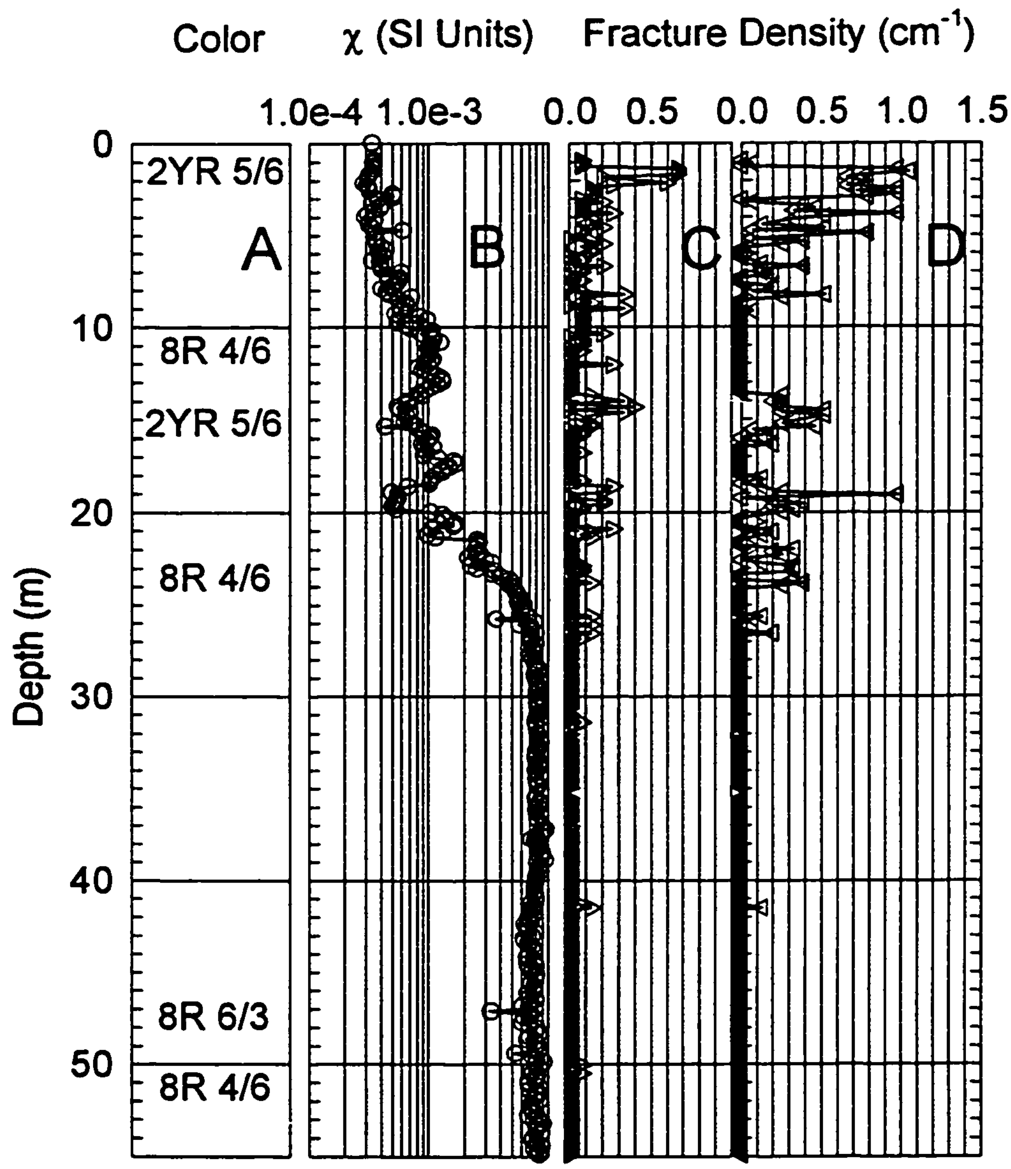

Figure 5-5. Variation of A.) color (reported as **hue value/chroma**), B.) magnetic susceptibility (χ), C.) complete fracture density, and D.) incomplete fracture density with depth. Lowest hue, lowest susceptibility, and highest fractures density values occur near the surface, grading to higher hue, higher susceptibility and lower fracture density values by 27 m depth. Between 0 and 27 m, increases in hue, susceptibility, correspond to increases in fracture density. Below 27 m, all of these measured parameters are largely constant, with the exception of a change in color (increased value, decreased chroma) and a drop in susceptibility at 47.1 m corresponding to aplite in the core. See text for further description.

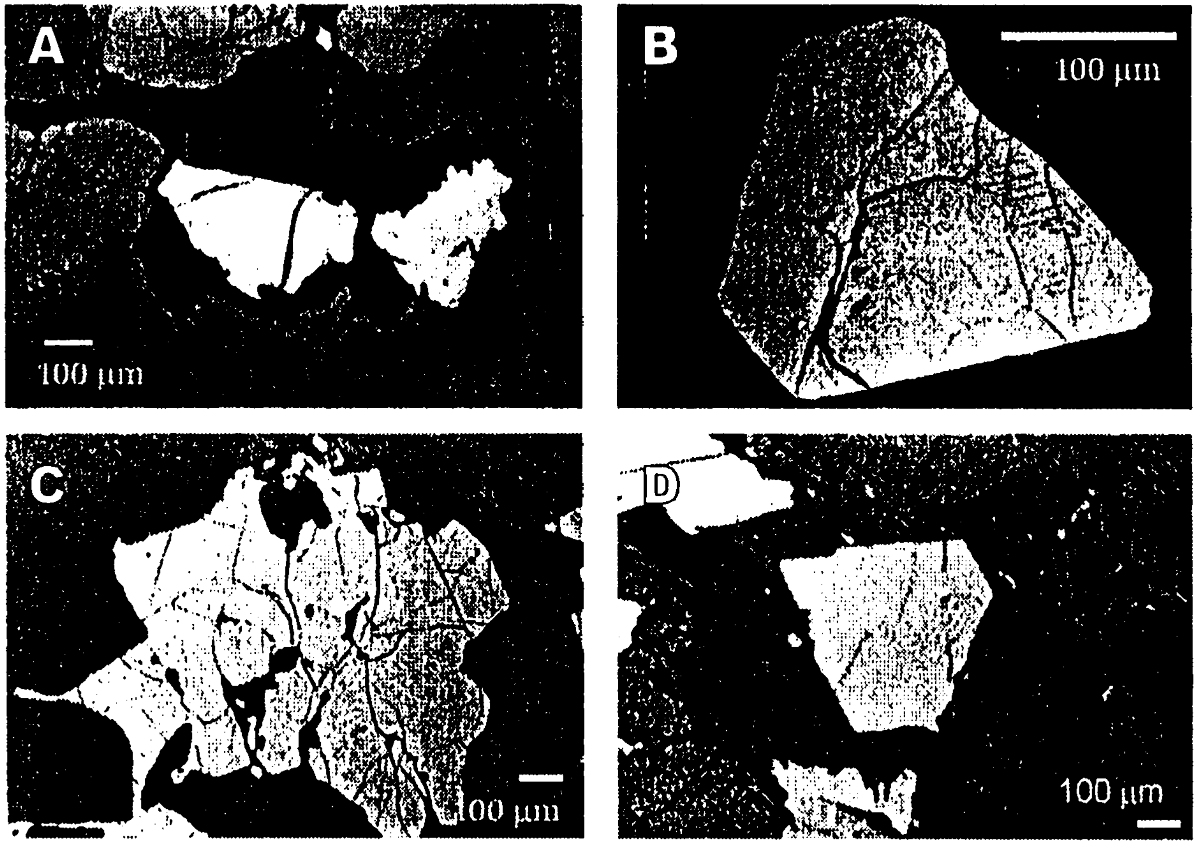

Figure 5-6. Four photomicrographs of the Sandy Creek Gabbro drill core SQ-2 (reflected light) from depths less than 11 m. Despite the shallow depth, there is no visible alteration of these oxides. A.) A sample from 10.7 m containing near-pristine (unaltered) magnetite. B.) Magnetite with ilmenite exsolution needles with no alteration to hematite at 9.7 m depth, perhaps the most fractured interval of the SQ-2 core. C.) Another pristine magnetite at 9.7 m depth. D.) An exsolved oxide (magnetite with ilmenite) from 9.4 m depth with no hematite.

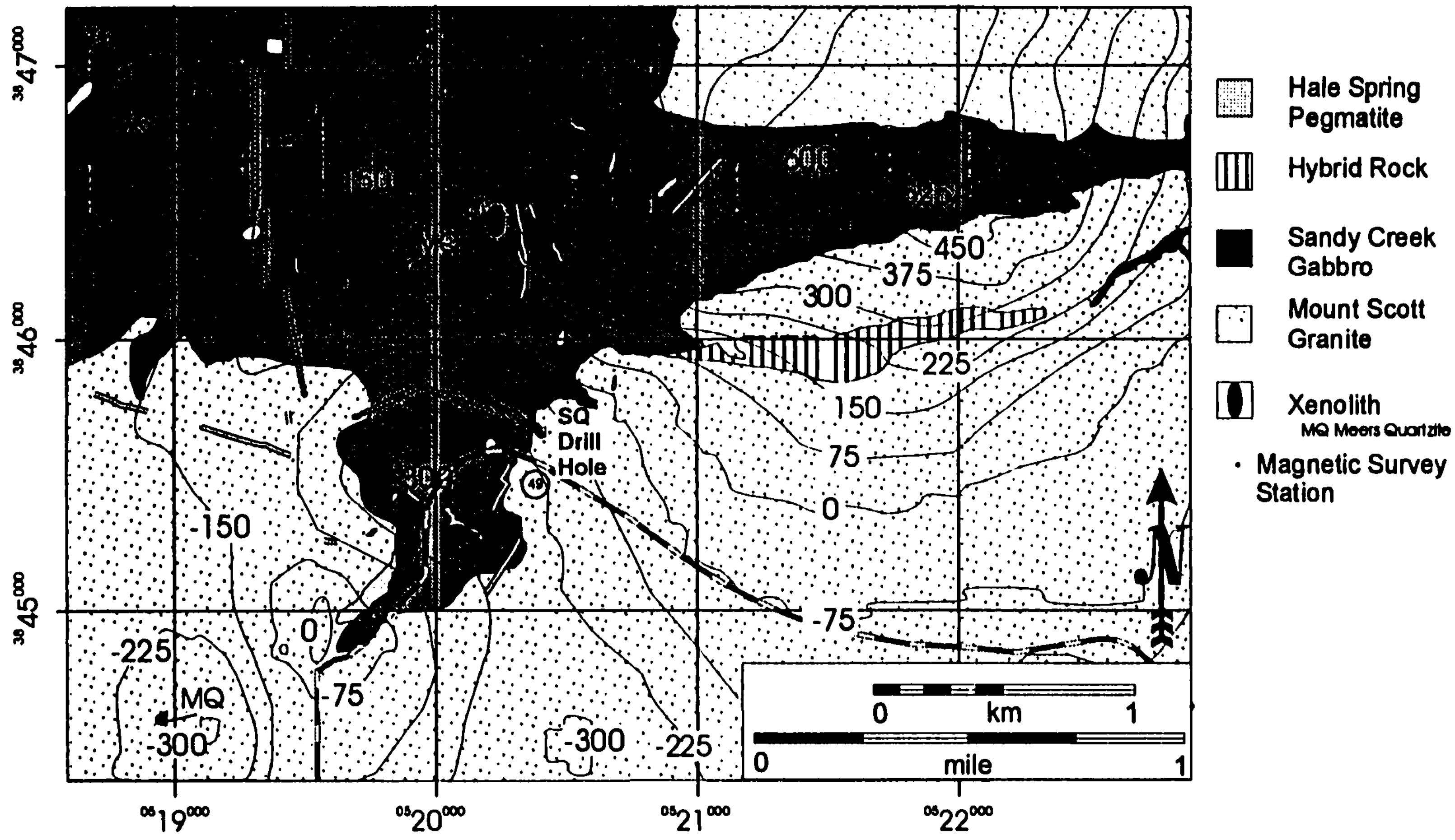

Figure 5-7. Geomagnetic map superimposed on geologic map (Figure 5-3). High values indicate near-subsurface domains of higher magnetic susceptibility (*e.g.*, Sandy Creek Gabbro), while low values indicate domains of lower susceptibility (*e.g.*, Mount Scott Granite). Data from Jones-Cecil (1995) reduced to the pole with 75 gamma contour line spacing.

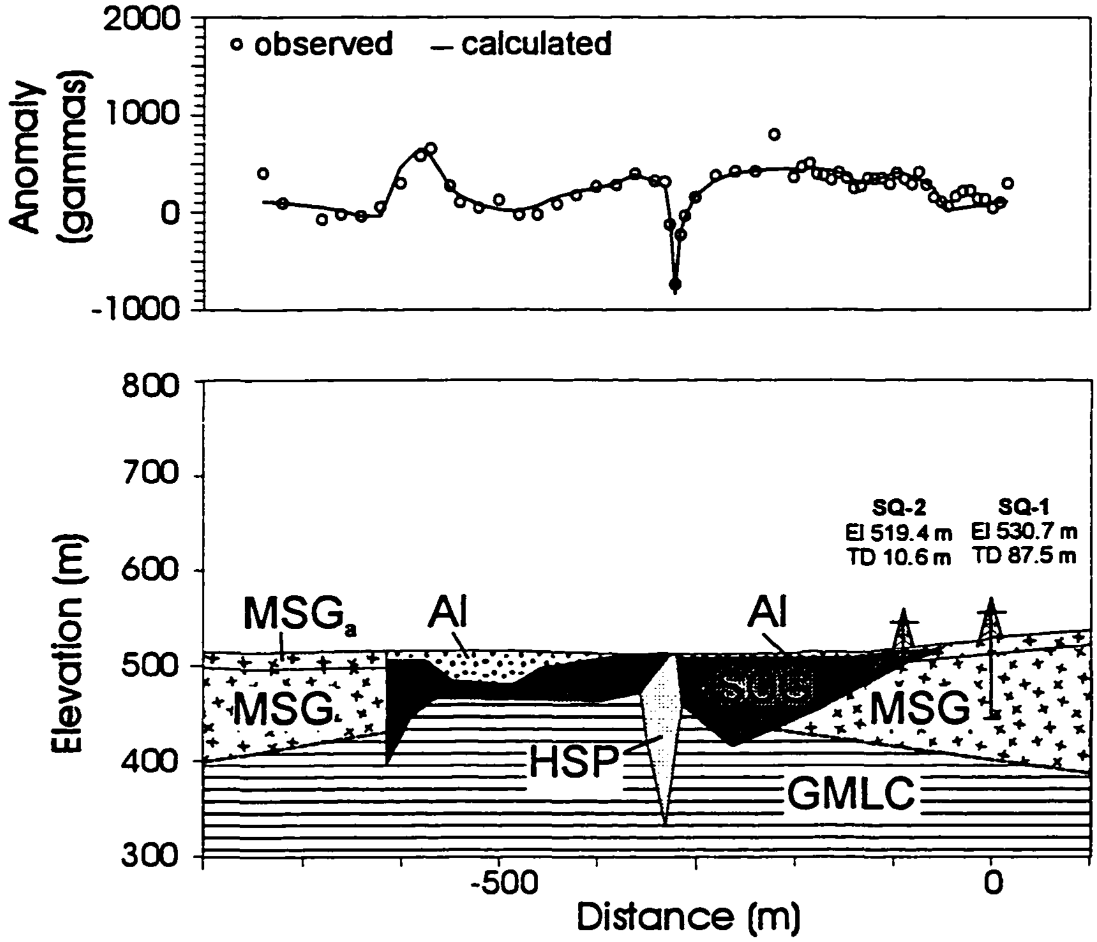

Figure 5- 8. Two dimensional forward magnetic model of Trav. 1, a traverse extending west from the Smith Quarry to the slopes of Bell Mountain. Observed anomaly marked by open circles, modeled profile marked by a line. Drill sites SQ-1 and SQ-2 are marked, along with total depth of penetration. Modeled lithologies include MSG - Mount Scott Granite; MSG_a - Altered Mount Scott Granite; SCG - Sandy Creek Gabbro; GMLC- Glen Mountains Layered Complex; Al - Post Oak Formation, alluvium, fill, and soil; and HSP - Hale Spring Pegmatite.

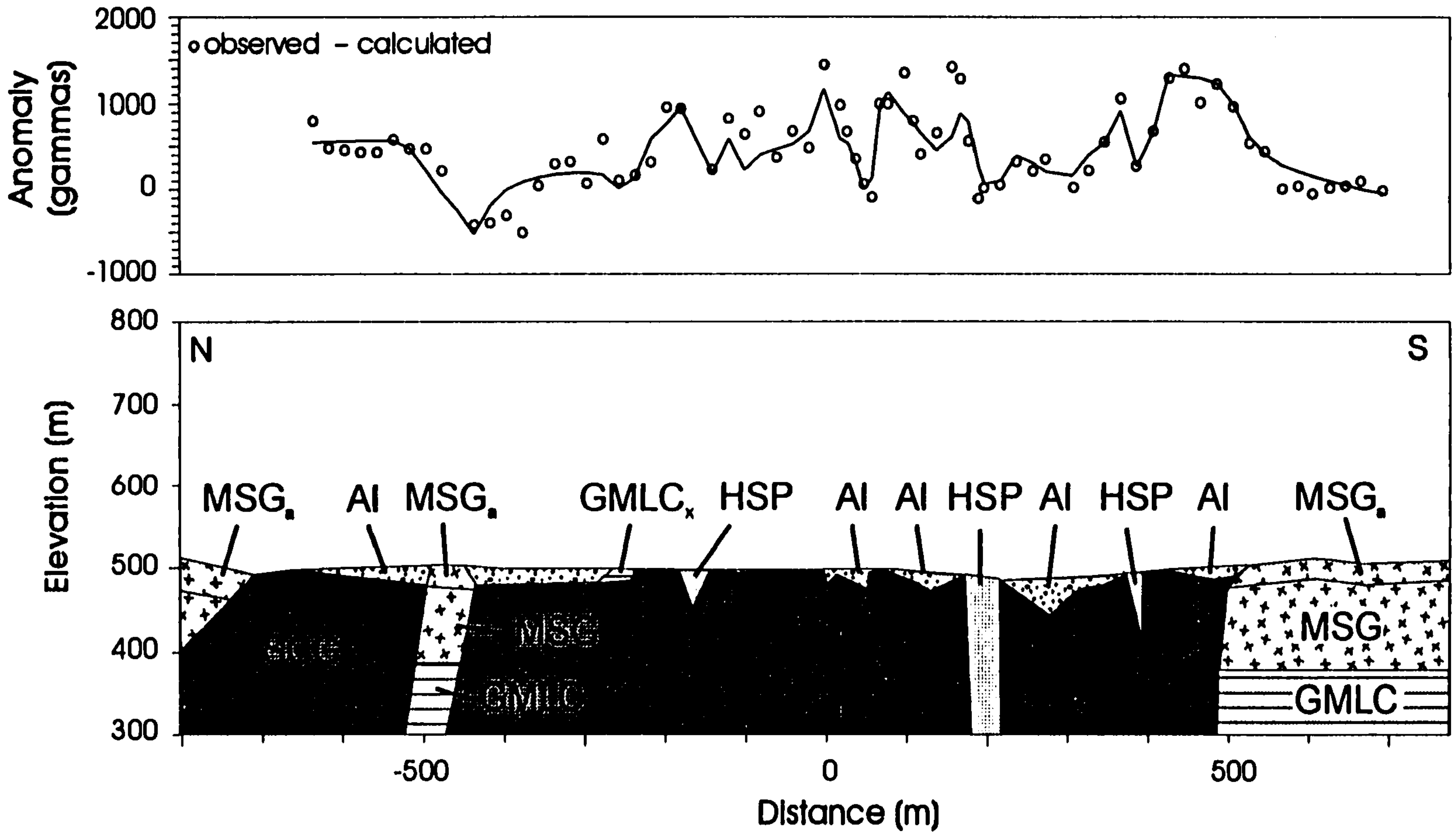

Figure 5-9. Two dimensional forward magnetic model of Trav. 2, a traverse extending north from Bell Mountain, across Sandy Creek. Observed magnetic anomaly marked by open circles, modeled anomaly by a line. Modeled lithologies include Al - Post Oak Formation, alluvium, fill, and soil; MSG - Mount Scott Granite; MSG$_a$ - Altered Mount Scott Granite; SCG - Sandy Creek Gabbro; GMLC- Glen Mountains Layered Complex; GMLC$_x$- Xenolith of Glen Mountains Layered Complex; and HSP - Hale Spring Pegmatite.

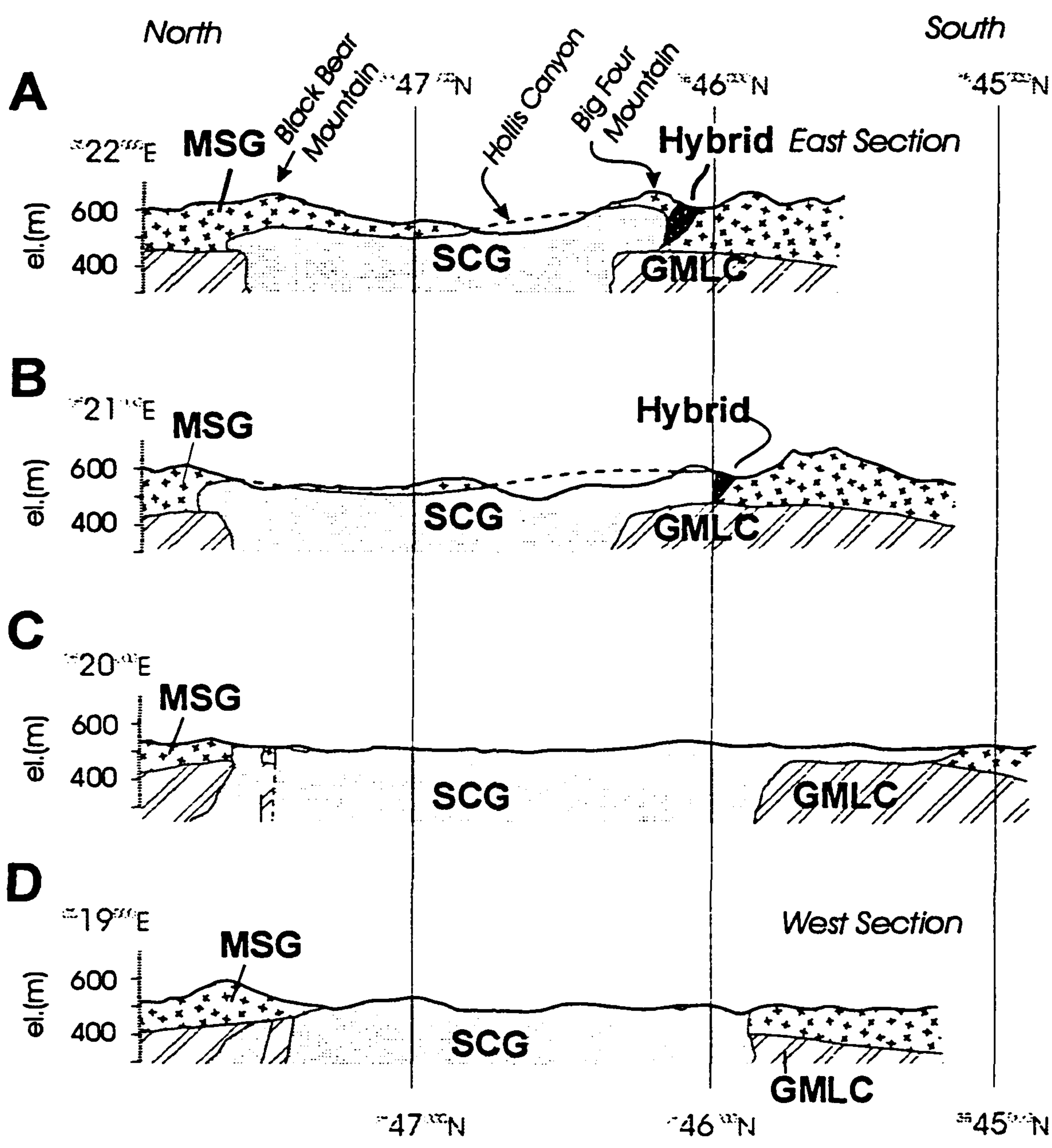

Figure 5-10. North-south cross sections of the Hale Spring Area. Sections follow UTM coordinates (see fig. 4-3) and are spaced 1 km apart. See text for description.

Table 5-1. Position of stations, distance and angle from origin, and anomalous field values for East to West traverse from SQ to Bell Mountain for Trav. 1.

NAD 27 UTM		Elevation	Distance	Azimuth	Anomaly
Easting	Northing	(meters)	(meters)	(degrees)	(gammas)
520408	3845673	531	15	115	302
520401	3845676	531	8	115	104
520394	3845679	531	0	318	51
520389	3845685	528	-4	318	140
520384	3845690	527	-8	318	140
520379	3845696	526	-23	318	226
520374	3845702	525	-31	318	219
520367	3845705	525	-38	313	173
520360	3845708	523	-45	310	68
520353	3845711	522	-52	308	114
520346	3845714	521	-60	306	162
520340	3845719	521	-67	306	287
520334	3845724	520	-75	307	415
520328	3845728	520	-83	307	299
520322	3845733	520	-90	307	351
520318	3845739	519	-98	308	402
520313	3845746	519	-105	309	299
520306	3845748	518	-112	308	350
520298	3845750	515	-119	306	348
520291	3845752	514	-126	305	357
520284	3845755	514	-134	305	273
520277	3845757	514	-141	304	248
520269	3845759	515	-148	303	356
520263	3845763	515	-156	303	411
520256	3845766	515	-163	302	338
520249	3845770	515	-171	302	389
520243	3845774	516	-179	302	400
520236	3845778	516	-186	302	503
520230	3845782	515	-194	302	469
520205	3845752	514	-203	302	362
520188	3845762	514	-222	300	807

Table 5-1. Continued

NAD 27 UTM		Elevation	Distance	Azimuth	Anomaly
Easting	Northing	(meters)	(meters)	(degrees)	(gammas)
520168	3845765	514	-242	290	420
520149	3845771	513	-262	288	417
520130	3845776	513	-282	288	376
520112	3845786	513	-302	290	160
520103	3845789	513	-312	290	-23
520098	3845791	513	-317	290	-224
520093	3845792	513	-322	290	-736
520088	3845794	512	-327	290	-123
520084	3845795	513	-332	290	326
520074	3845799	513	-342	290	331
520055	3845804	514	-362	289	401
520036	3845812	514	-382	290	292
520018	3845820	515	-401	290	271
520000	3845829	515	-421	291	182
519981	3845834	516	-441	290	94
519962	3845841	518	-461	290	-16
519943	3845846	518	-481	290	-19
519924	3845838	518	-501	287	132
519906	3845830	518	-521	285	48
519888	3845822	517	-541	282	110
519879	3845817	517	-551	281	281
519861	3845809	517	-571	279	654
519851	3845805	516	-581	279	590
519833	3845797	516	-601	277	301
519815	3845789	516	-621	275	57
519797	3845781	516	-641	274	-34
519778	3845773	515	-661	273	-20
519760	3845765	515	-681	272	-70
519723	3845748	515	-721	270	100
519705	3845740	515	-741	269	407

Table 5-2. Position of stations, distance and angle from origin, and anomalous field values for South to North traverse from Bell Mountain for Trav. 2.

NAD 27 UTM		Elevation	Distance	Azimuth	Anomaly
Easting	Northing	(meters)	(meters)	(degrees)	(gammas)
519428	3847230	489	-655	0	799
519428	3847210	489	-635	0	482
519428	3847190	488	-615	0	457
519428	3847170	487	-595	0	435
519428	3847150	487	-575	0	440
519428	3847130	486	-555	0	578
519428	3847110	485	-535	0	473
519428	3847090	488	-515	0	478
519428	3847070	488	-495	0	218
519428	3847050	488	-475	0	-615
519428	3847050	488	-455	0	307
519317	3846973	482	-455	0	-412
519317	3846953	482	-435	0	-387
519317	3846933	482	-415	0	-298
519317	3846913	482	-395	0	-503
519317	3846893	482	-375	0	46
519317	3846873	482	-355	0	302
519317	3846853	482	-335	0	340
519317	3846833	482	-315	0	75
519317	3846813	482	-295	0	597
519317	3846793	482	-275	0	103
519317	3846773	482	-255	0	168
519317	3846753	482	-235	0	
519317	3846733	482	-215	0	319
519317	3846713	482	-195	0	953
519317	3846713	482	-195	0	959
519317	3846697	482	-179	0	945
519317	3846657	482	-139	0	236
519317	3846637	482	-119	0	828
519317	3846617	482	-99	0	644
519317	3846597	482	-79	0	913
519317	3846577	483	-59	0	371
519317	3846557	482	-39	0	680
519317	3846537	482	-19	0	482
519349	3846509	501	0	0	1446
519349	3846489	501	20	180	981
519349	3846479	501	30	180	680
519349	3846469	501	40	180	363
519349	3846459	501	50	180	65
519349	3846449	501	60	180	-91

Table 5-2. Continued

NAD 27 UTM		Elevation	Distance	Azimuth	Anomaly
Easting	Northing	(meters)	(meters)	(degrees)	(gammas)
519349	3846439	501	70	180	1005
519349	3846429	500	80	180	994
519349	3846409	499	100	180	1345
519349	3846399	499	110	180	813
519349	3846389	498	120	180	411
519349	3846369	497	140	180	657
519349	3846349	496	160	180	1429
519349	3846339	496	170	180	1282
519349	3846329	496	180	180	559
519349	3846316	495	193	180	-104
519349	3846309	494	200	180	31
519349	3846289	493	220	180	68
519349	3846269	491	240	180	332
519349	3846249	491	260	180	221
519349	3846232	491	277	180	348
519426	3846199	490	310	180	23
519426	3846179	491	330	180	236
519429	3846159	495	350	175	573
519434	3846140	498	370	173	1059
519438	3846120	499	390	171	275
519442	3846101	500	410	171	688
519446	3846081	502	430	170	1295
519450	3846061	503	450	170	1406
519454	3846042	504	470	170	1012
519459	3846022	505	490	170	1235
519463	3846003	506	510	169	957
519467	3845983	507	530	169	538
519471	3845964	509	550	169	445
519475	3845944	510	570	169	13
519479	3845925	512	590	169	51
519484	3845905	513	610	169	-60
519488	3845885	513	630	169	27
519492	3845866	511	650	169	47
519496	3845846	509	670	169	97
519502	3845820	509	696	169	-6

Chapter 6. Geology of the Eastern Wichita Mountains, Oklahoma

Introduction

The eastern Wichita Mountains contain exposures of many of the units typical of the entire geologic province. The exposures exhibit many of the complexities of Cambrian magmatism and associated metamorphism that produce the basement beneath much of southwestern Oklahoma. They also allow examination of late Paleozoic erosion and Permian sedimentation.

The Wichita Mountains are regionally well characterized. The body of knowledge developed through detailed studies of relatively small areas that invariably report complexities understandable only through detailed examination. In order to better understand the finer-scale geologic processes of the far eastern Wichita Mountains (Figure 6-1), geological maps (Plates I, II, III) were constructed for an area covering the northern half of the Fort Sill and the Mount Scott U.S.G.S. 7.5' quadrangles, and portions of the southern Meers and the northern Quanah Mountain U.S.G.S. 7.5' quadrangles. Cross section interpretations of the area adjacent to and west of Mount Scott (Plate IV) and the Medicine Park area (Plate V) present the relationships of the igneous units as revealed from the mapping data. Additionally, high-resolution mapping of a diabase dike at Lake Elmer Thomas (Plate VI) reveals the complexities of magmatism in the region.

The Wichita Mountains Wildlife Refuge (U.S. Fish and Wildlife Service) manages much of the land covered by these maps. While most of the area is open to the public for general use, the northeastern portion of the mapped area is within the special use zone, and access is restricted. The southern portion of the maps is on the Fort Sill Military Reservation, the U.S. Army field artillery school. Access here is restricted as a considerable part of the area is firing range.

State Hwy. 49 approaches this area from the east and State Hwy. 115 approaches from the south. These numeral designations technically do not apply in the Wichita Mountains Wildlife Refuge. However, this report will use the names Hwy. 49 for the road that runs generally east-west through the area, and Hwy. 115 for the road that runs north-south.

Geologic Framework

The geologic framework of the Wichita Mountains is summarized here from Ham *et al.* (1964), Powell *et al.* (1980a, b), Gilbert (1982a), and references therein, with minor amendments from the conclusions of this dissertation. The Wichita Mountains are a northwest-trending series of rocky promontories and rounded hills stretching from just north of Lawton, to Granite, Oklahoma. Most of these mountains are Cambrian igneous rock surrounded by Permian clastics with a contiguous belt of Cambrian to Ordovician sedimentary rocks north of the igneous exposures, and a small outcrop of Cambrian sedimentary rocks to the south.

These mountains are the fault-bounded exposed portion of the Wichita Igneous Province. Crustal extension associated with aulacogen formation during the Cambrian breakup of the Laurentian supercontinent, Pannotia, produced the compositionally bimodal activity of this province. Early igneous activity included the intrusion of the Glen Mountains Layered Complex (GMLC). Local uplift followed, as normal listric faulting and block rotation exposed this complex (McConnell and Gilbert, 1990). Igneous activity resumed with the eruption of Carlton Rhyolite Group lavas, tuffs, and tephras, closely followed by intrusion of Wichita Granite Group sheet-granites, which largely exploited the Carlton - GMLC unconformity. The intrusion of stocky Roosevelt Gabbro plutons may have started previous to and continued after granite emplacement. Activity then waned, last recorded by volumetrically insignificant tholeiitic and rhyolite dikes.

Early Paleozoic thermal subsidence resulted in deep burial of the Wichita Igneous Province under 5 km of carbonate and clastic sediments. By the Pennsylvanian, tectonic collision from the east and south resulted in uplift and exhumation of the Wichita block. By early Permian, erosion had removed the upper and middle Paleozoic cover, and stream incisement resulted in the landforms observed today, with only minor differences. Uplift of the Ouachita Mountains of eastern Oklahoma outpaced that of the Wichita Mountains, and by Hennessey time (late Leonardian), clastics from the east and locally derived sediments began to bury the Wichita Mountains. Burial possibly continued throughout the Cretaceous and early Tertiary, although evidence of this is not locally preserved. Uplift and re-exhumation, beginning in the late Tertiary, removed all but a thin veneer of westwardly thickening Permian clastics surrounding the exposed igneous rock.

Previous Mapping in the Eastern Wichita Mountains

Many researchers have mapped the geology of this region, beginning with Taff (1904), who constructed the first geological map of the Wichita Mountains. Greater detail of the granites was published by Taylor (1915). Hoffman (1930) published a map of the Eastern Wichita Mountains, and Schoonover (1948) mapped the west Fort Sill Military Reservation. G. W. Chase, of the Oklahoma Geological Survey, produced a manuscript geologic map of the eastern Wichita Mountains, and although unpublished, it greatly influenced more recent investigations of this area. Additionally, Chase mapped the Permian Post Oak Formation (Chase, 1954), and recent alluvium deposits within the mountains, including a detailed map immediately adjacent to Mount Scott (Chase, 1952). Ham *et al.* (1964) included this area in their study of the basement rocks of southern Oklahoma. Powell et al, (1980 a, b) defined the major lithodemic units of the area, followed by Myers *et al.* (1981), who further refined the granite terminology through geochemistry. Gilbert mapped much of the area from 1977-1979, and published a map (1:50,000) of T3N-R14W (Gilbert, 1984), and detailed maps (1:12,000) the areas adjacent French Lake (Gilbert, 1982b), Quanah Parker Lake (Gilbert, 1982c), Welsh Hill (Gilbert, 1982e) the west side of Lake Elmer Thomas (Gilbert and Miller, 1982), and the Quetone area (Gilbert and Powell, 1988). In addition to all of these maps specific to the Wichita Mountains, the area is covered by Miser's (1954) state geologic map and Havens' (1977) geologic map of the U.S.G.S. Lawton 1:250,000 quadrangle.

These mapping investigations were complemented by numerous studies on the stratigraphy, geologic history, and petrology of the region. Figure 6-1 attempts to summarize the chronostratigraphy as presented in these various studies, and relate these units to the units presented below.

Geologic Maps and Cross Sections

The 1:12,000 maps are the result of two separate grants from the U.S.G.S. Cooperative Mapping Agreement (EDMAP), completed over two years. Plate I, contains two maps. Plate Ia is the geologic map of the lowermost Meers 7.5' Quadrangle. Plate Ib is the geologic map of the Central Lowland, Quanah Mountain 7.5' quadrangle. Plate II, is the geologic map of the north Mount Scott 7.5' quadrangle. Plate III is the geologic map of the north Fort Sill 7.5' quadrangle. In addition to the 1:12,000 maps of the area, Plate VI is a fine-scale map of the diabase dike at Lake Elmer Thomas Dam.

Three north-south cross sections of the geology from plates Ia and II are presented on plate IV. These are 1:12,000, vertical same as horizontal, and are right aligned to the base of the 19-24 section line for township 3N, range 13 and 14W (34° 42' 37" N latitude). Two north-south and one east-west cross section is presented as a fence diagram on plate V. These correspond to lines across the Medicine Park area on plate III and the northeast corner of plate II.

Lithologic Units

Lithologic nomenclature follows that of Powell *et al.* (1980a, b), Myers *et al.* (1981), and references therein. Deviations are noted within the text. The following descriptions are presented in chronostratigraphic order (Figure 6-2) as determined by this investigation. Each of the following sections begins with a description of the rock with emphasis on field appearance, followed by location of outcrops, location-specific appearance, and contact characteristics, followed by a summary of prior nomenclature, and ending with a discussion on the units origins and relationship to other lithologies, including relative age. Figure 6-2 summarizes the stratigraphic position and emplacement relationships of the igneous lithologies.

Glen Mountains Layered Complex

The color of the Glen Mountains Layered Complex (GMLC) ranges from dark gray to white-gray, weathering to a light gray. Fresh surfaces are visible on exposures with recent spall, and close examination reveals that weathering alteration does not visibly penetrate the rock surface to depths greater than a few centimeters. The GMLC in the eastern Wichita Mountains (the mapped area) is largely anorthositic gabbro, with one exposure of olivine gabbro. The rock is comprised of ophitic clinopyroxene surrounding parallel to subparallel layered plagioclase + Fe-Ti oxides (titnanomagnetite) ± olivine ± local Fe sulfides. Pyroxene crystals are typically large (< 1 cm up to 5 cm diameter), and cleavage-plane reflections are easily spotted on fresh surfaces in bright sunlight. Exposed surfaces of olivine-bearing GMLC are marked with small (0.5 cm) pits, as olivine is removed during weathering. Outcrops adjacent to the Mount Scott Granite and Quanah Granite are commonly altered and contain secondary biotite, chlorite, prehnite, and zeolite.

Within the study area, the GMLC is exposed within the Central Lowland (the Permian valley between the bulk of the Quanah Granite and the Mount Scott Granite-Plate Ib). Here, outcrops typically are masses of large boulders, separated by thicker soils (relative to the granites). In low-lying areas, these soils host groves of post and blackjack oak trees. In addition to the Central Lowland, the saddle north of Central Peak (Table 6-1, #3) contains one small, highly altered xenolithic exposure of GMLC.

All of the previous studies recognized and mapped this gabbro within the Central Lowland. Schoonover (1948) also noted the small outcrop at Central Peak. GMLC stratigraphy was defined by Spencer (1961), and expanded by Stockton (1984) for exposures west of the Wichita Mountains Wildlife Refuge. These workers defined the K, L, M, and N zones of the unit, based on stratigraphy seen within other layered complexes (*e.g.*, Stillwater Complex, Montana). The stratigraphy is incomplete, as the lowermost layers are not exposed, and the uppermost layers, including the roof-sequence, are missing as well.

The exposures in the Central Lowland are a small fraction of the total exposures of GMLC, which is better exposed further to the west in the Glen Mountains. Correlating these exposures to the Central Lowland remains problematic. Regional structural trends, combined with the dominance of anorthositic gabbro, led Gilbert (1982a) to place these Central Lowland outcrops in the N zone. The presence of olivine gabbro (a rock-type not diagnostic of the N-zone) at Panther Creek just north of Hwy. 49., (Table 6-1, #2) led Powell (1986) to disagree with this assignment and suggest these outcrops belong to the L or M zone. Because the Panther Creek olivine gabbro is volumetrically overshadowed by the more typical anorthositic gabbro within the Central Lowland, the olivine gabbro at Panther Creek is in all likelihood a xenolith of less-evolved GMLC from below, or perhaps above. Thus, the Central Lowland are likely to be N-zone.

The GMLC directly underlies the granites and rhyolite (Ham *et al.*, 1964; Powell *et al.*, 1980a, b; Gilbert, 1982a) (see plate VI, A-A'). Its unconformable relationship with the Carlton Rhyolite Group (Ham *et al.*, 1964) suggests the GMLC was locally uplifted, exposed, and eroded prior to subsequent local igneous activity.

Carlton Rhyolite Group

The Carlton Rhyolite Group exposed in the mapped area is part of a 1.5 km thick package of volcanics and related clastics that covers 39,000 km^2 to 44,000 km^2 of southern Oklahoma, both exposed on the surface and in the subsurface (Ham *et al.*, 1964). The units presented below are informal group members, denoting significant change in rock appearance within this area.

Davidson metarhyolite, banded

The banded facies of the Davidson metarhyolite is recognized by its buff color and distinctive dark gray bands, locally contorted into isoclinal folds. The rock contains abundant fine-grained granoblastic quartz and alkali feldspar, and minor glomerocrysts of these two phases. Some of the feldspar exhibit substantial alteration. Feldspars in the matrix are smaller than and interstitial to the matrix quartz crystals. Hematite ± chlorite ± muscovite ± biotite ± zircon are seen within thin sections, but are typically too fine-grained for field observation. Opaque minerals (oxides) and altered mafic-silicate grains are concentrated within the bands; away from the bands, the modes of these minerals decrease.

Exposures of the banded Davidson metarhyolite are largely confined to the lower elevations on plate II. This unit crops out in Little Medicine Creek (Table 6-1, #4) and at the Hideaway area, southwest corner of Elmer Thomas Lake (Table 6-1, #5). Contacts with the Mount Scott Granite are sharp, and with the exception of two highly fractured outcrops adjacent to Little Medicine Creek (Table 6-1, #7, #24), they typically lack any evidence of faulting and thus are assumed to be igneous. Contacts are also shared with the massive Carlton Rhyolite, although most contacts are obscured by thin soils.

In the past, workers assigned different names (and origins) to this rock, and attempted to correlate it with other Wichita Mountains lithologies (see Figure 6-2). Both Hoffman (1930) and Schoonover (1948) grouped these rocks with those of this study's Pratt Hill quartzite and massive Davidson metarhyolite, and termed all Davidson granophyre. Ham *et al.* (1964) also grouped these units together as a hornfelsed member of the Carlton Rhyolite Group. Sides and Miller (1982) included the portion of the Davidson metarhyolite exposed at the southwest corner of Lake Elmer Thomas as part of their Pratt Hill quartzite. However, the accompanying map provided by Gilbert and Miller (1982) mapped these banded rocks and the Pratt Hill quartzite as Meers Quartzite (dirty facies), and suggested they were deposited along the GMLC-Carlton rhyolite unconformity (Gilbert, 1983).

The bands are reminiscent of flow-banding in rhyolite ignembrites or lavas, suggesting an extrusive origin for the banded Davidson metarhyolite. Like the other formations of the Carlton Rhyolite Group, the Pratt Hill quartzite, the massive Davidson metarhyolite and the massive and spherulitic Carlton Rhyolite, it contacts the Mount Scott Granite and exhibits granoblastic texture. All of theses units are likely to have underwent recrystallization. Therefore, it is likely the banded Davidson are Carlton rhyolite (possibly tuffs), metamorphosed by the intrusion of the Mount Scott Granite (Ham *et al.*, 1964).

Davidson metarhyolite, massive (unbanded)

The unbanded Davidson metarhyolite is consistently feldspathic, fine-grained, and highly fractured. It is typically pink color which weathers to buff, largely aphyric and granoblastic, with pink-colored alkali-feldspar glomerocrysts. Samples contain alkali feldspar and quartz, with small, variable amounts of oxides, sericite, and chlorite. The quartz and feldspar are roughly equigranular. Epidote spherules (2-3 mm diameter) are locally prominent, producing scattered dark splotches. The rock is commonly cut by thin veins of pink feldspar or oxide. It is densely cut by linear fractures that are loci for weathering, and dissect the metarhyolite into small rhombohedral blocks, and produce a distinct pavement-like outcrop morphology.

Although float from this unit is seen on the northeast slope of Mount Scott, near the Mount Sheridan Gabbro - Mount Scott Granite contact, the majority of exposures outline a NW-SE trending swath through the easternmost Wichita Mountains. The unbanded Davidson crops out north of Jed Flat (Plate II), on both sides of Hwy. 115, including a small, quarried area east of the Holy City (Table 6-1, #8). Most of the unit here is buried beneath Post Oak Formation, but contacts with the Rush Lake granite and the Mount Scott Granite are clearly exposed in a number of places. Adjacent to the contact at Quetone Overlook (Table 6-1, #9), meter-sized xenoliths are entrained Rush Lake granite. Exposures are seen at the Fish Hatchery near Medicine Park (Table 6-1, #10), and east of the Thomas marker on Fort Sill (Table 6-1, #11). Both localities exhibit clear, angular contacts with the Rush Lake Granite at the former and the Mount Scott Granite and Carlton Rhyolite at the latter. Additional small outcrops occur adjacent to the north shore of Lake Elmer Thomas (Table 6-1, #12), and beneath the dam at Rush Lake (Table 6-1, #13). Xenoliths are found within the Mount Scott Granite at Rabbit Hill on Fort Sill.

With the exception of Gilbert and Powell (1988), most workers have lumped this and the banded Davidson metarhyolite as one unit. This unit has been called the Davidson granophyre (Hoffman, 1930), the Davidson microgranite (Schoonover, 1948), and the Carlton Rhyolite Group hornfels rhyolite (Ham *et al.*, 1964). Ham *et al.* (1964) and Gilbert and Powell (1988), concluded this unbanded unit is metamorphosed Carlton Rhyolite.

Gilbert and Powell (1988) previously proposed the rocks that comprise the massive Davidson metarhyolite served as the floor for the Mount Scott Granite and Rush Lake granite plutons (see Chapter 4, this dissertation). Outcrops are typically lower in elevation and beneath the Mount Scott Granite and Rush Lake granite. Exposed contacts between the massive Davidson metarhyolite and the Rush Lake granite are numerous and sharp. Additionally, the Davidson metarhyolite is included as xenoliths in the Mount Scott and Rush Lake granites. Unfortunately, observable contacts between the Davidson metarhyolite and other Carlton Rhyolite Group members are few in number and ambiguous in nature. Outcrops are stratigraphically equivalent with the rest of the Carlton Rhyolite Group.

Pratt Hill quartzite

Although the appearance and composition of the Pratt Hill quartzite varies slightly, it is identified by its green-gray color, becoming slightly darker adjacent to the contact with the Carlton rhyolite. Quartz and white micas are always the dominant minerals, but vary in modal abundance. Quartz grains are angular, exhibit crystalloblastic texture, and are uniform in size (0.1 to 0.3 mm, Sides and Miller, 1982). The Pratt Hill quartzite contains no feldspar. A large percentage of the mineralogical components are indiscernible to the unaided eye, such as white mica, occurring with variable amounts of chlorite and magnetite. Trace amounts of hematite, epidote, and iron hydroxide are also present.

The quartzite is found only on the north side of Pratt Hill (Table 6-1, #14). Rhyolite caps the hill, but the contact between it and the underlying quartzite occurs near the base. From this slope, the contact dips 10° SE, striking N60E (Sides and Miller, 1982), extending both to the east and west where the hill slope is less steep and becomes concealed under talus. The lower contact with the Davidson metarhyolite of this unit is covered by Lake Elmer Thomas and alluvium.

Sides and Miller (1982) first used the term Pratt Hill quartzite informally to describe this unit and the banded rock found in the "Hideaway" area (the area directly west of Lake Elmer Thomas' southwestern shore). They concluded that the quartzite protolith was a sedimentary rock of a locally-derived quartz and potassium-clay rich (submature) clastic developed from and on an early Carlton rhyolite surface. The alternate classification of this unit as Meers Quartzite (Gilbert and Miller, 1982) implies that it developed on the GMLC-Carlton Rhyolite Group unconformity, as part of a larger package of clastic rocks that include the banded Davidson. In either case, the banded Davidson is older than the Pratt Hill quartzite, as the outcrop suggests channeling of the quartzite into the metarhyolite (Sides and Miller, 1982). The previously discussed Carlton age for the banded Davidson metarhyolite applies here to the quartzite.

<u>Carlton rhyolite, massive</u>

For the most part, the porphyritic Carlton rhyolite is distinguished by orange feldspar phenocrysts set in a dark brown, weathering to a pink brown, matrix. It is massive rhyolite, lacking structures, layers, or bands (Ham *et al.*, 1964). The porphyritic texture results from phenocrysts and glomerocrysts of angular, orange-pink microperthite and smaller phenocrysts of rounded, dark-gray quartz, magnetite, and plagioclase. These are set in a fine-grained granoblastic matrix of largely feldspar and quartz with acicular needles of magnetite.

The rhyolite crops out within the southeastern quarter of the mapped area. It underlies a substantial portion of the hills on the eastern half of the west firing range, Fort Sill, including Medicine Bluffs (Table 6-1, #15). Outcrops within Little Medicine Creek outline a triangular area from just southwest of the Quetone overlook (Table 6-1, #17) to the Mount Scott picnic area (Table 6-1, #16). There are numerous contacts with the Mount Scott Granite. These are typically sharp, and many examples show the granite coarsening away from the contact. Contacts with the Davidson metarhyolite are commonly obscured by thin soils and grass, alluvium, or water (*e.g.*, Lake Elmer Thomas). At Lake Elmer Thomas, the massive Carlton rhyolite stratigraphically overlies the Davidson metarhyolite and the Pratt Hill quartzite. The contact with the Pratt Hill quartzite is sharp but is exposed only for a short distance on Pratt Hill (Sides and Miller, 1982).

Beginning with Taff (1904), who included this unit in his Carlton Mountain Porphyry (granite porphyry and associated aporhyolite), workers recognized this rock as distinct from the other units. Hoffman (1930) renamed this unit the Carlton porphyritic granophyre, interpreting these rocks as a sheet intrusion. Schoonover (1948) recognized the volcanic nature of this rock and termed it Carlton rhyolite. Ham *et al.* (1964) introduced the formal name Carlton Rhyolite Group for the widespread body of lavas and tuffs found in the Arbuckle Mountains, the Slick Hills, the Wichita Mountains, and within the subsurface of southern Oklahoma.

Although the exposures here differ from Carlton rhyolite exposures north of the Meers Fault, where samples clearly preserve many of the volcanic textures (Ham *et al.*, 1964; Bigger and Hanson, 1992), the matrix is fine-grained, suggestive of a volcanic origin. Furthermore, it shares an overall similarity with the volcanic spherulitic-textured rocks, discussed below. The mode of emplacement for all of the Carlton Rhyolite Group within this area remains enigmatic at this time, as any primary characteristics are masked by minor amounts of recrystallization.

Carlton Rhyolite, Spherulitic

Spherulitic Carlton rhyolite is similar to the massive facies of the same unit. The sole difference is that the former contains flame-structured bands of variably spherulitic-textured feldspar (spherules are typically < 1mm diameter). Bands are pink to orange, vary from less than 0.1 cm up to 2 cm long, and 1 cm to over 50 cm in length. Smaller bands are typically more concentrated than larger ones. Large bands tend to exhibit the spherulitic texture, whereas smaller ones contain coarse (relative to the matrix) granoblastic feldspars with lesser quartz. Some examples are tabular, and most appear to be linear features. Margins of bands are irregular, undulating, and flame out into the matrix. Bands frequently include the phenocrysts seen in the matrix: angular alkali feldspar, rounded quartz, and small grains of oxides. Bands are parallel and are typically undeformed, although broad folding is locally observed.

Substantial outcrops of the spherulitic unit are found on Jones Ridge (Table 6-1, #18), with small exposures found throughout the massive Carlton Rhyolite. The spherulitic unit appears to be completely encapsulated by the massive Carlton Rhyolite

The spherulitic bands were previously interpreted as flow banding (Schoonover, 1948) or eutaxitic structures (Sides and Miller, 1982). The appearance of the spherulitic and the massive Carlton rhyolite differs from that of exposures of Carlton rhyolite seen north of the Meers Fault, particularly where it has been examined in detail at Bally Mountain (Ham *et al.*, 1964; Donovan *et al.*, 1988). Whereas north of the fault, the rock preserves volcanic textures (*i.e.*, eutaxitic structure, flow banding) and devitrification textures (Hanson, 1977; Bigger and Hanson, 1992), in the mapping area, the granoblastic matrix of the rock suggest substantial recrystallization presumably the result of subsequent rhyolite eruptions and granite intrusion. It is doubtful that volcanic structures would be preserved following recrystallization. However, their appearance differs in comparison to other fiamme-bearing rocks known to the author (*e.g.*, Fish Canyon Tuff, Colorado). Notable differences include the linear nature of some bands as opposed to the typically tabular nature of most fiamme, and the presence of phenocrysts which are typically absent from eutaxitic structures. Despite the differences between the bands seen in the spherulitic Carlton rhyolite and fiamme observed elsewhere, because spherulitic growth is a texture commonly associated with devitirification, it is most likely these bands formed from glassy zones within an extrusive unit. The origins of glassy zones within this unit requires further constraint before developing conclusions regarding their nature and origin.

Medicine Park Granite

The Medicine Park Granite is a fine grained, alkali-feldspar granite, red in highly fractured outcrops, but has a pinkish-purple hue in "fresh" samples. It is porphyritic with rare orangish-pink alkali feldspar crystals set in a granophyric matrix of quartz and feldspar. Granophyre matrix is fine-grained: crystal domains (defined by simultaneous optical extinction of quartz) are under 1 mm, and intergrowths are very fine. Most of the alkali feldspar phenocrysts are angular, microperthitic, and strongly altered. Likewise, the granophyric alkali feldspar is altered to the same degree. Samples contained 1-2 vol.% altered mafic silicates (pseudomorphic after hornblende) and oxides. Many oxides are rounded, and rimmed by titanite. Other accessory phases include apatite and zircon, occurring together in glomerocrysts with magnetite ± altered hornblende. Small quartz veins are common within exposures.

The Medicine Park Granite is found on the upper elevations of the hills immediately west of the village of Medicine Park (Johnson and Denison, 1973), and particularly good exposures are seen immediately south of Lake Lawtonka (Table 6-1, #19). A coarser grained example of the Medicine Park is found on Welsh Hill (Table 6-1, #28), separated from the Medicine Park area by 1 km of Mount Scott Granite and 5 km of Permian sediments.

These outcrops were mapped as Lugert Granite prior to Myers *et al.* (1981), who demonstrated a difference in composition between this granite and other members of the Wichita Granite Group. Gilbert and Powell (1988) provide the only map of the granite exposures around medicine Park, and Gilbert (1982e) provides the only map of the Welsh Hill outcrops.

Exposures of the granite occur immediately east of Medicine Park, appearing to have a subhorizontal base that overlies the Mount Scott Granite and Rush Lake granite (see Plate V). To the east, at Welsh Hill, the Medicine Park Granite shares a near vertical contact with the Mount Scott Granite. Contacts here are not well exposed, but constrained by outcrop to 2 or 3 m.

Previous work regarded the Medicine Park granite as intrusive into the Mount Scott Granite (Gilbert, 1982e), but within the Medicine Park Area, the Mount Scott Granite and the Rush Lake granite both chill against much of the Medicine Park Granite (Table 6-1, #20). Furthermore, the Mount Scott Granite cuts the Medicine Park (Table 6-1, #27) as a dike north of Big Rock Estates.

Rush Lake granite

The Rush Lake alkali-feldspar granite is pink to pale red, weathering to brick-red. It is medium-grained, grading to fine grained near some contacts, with variable granophyric and porphyritic alkali feldspar and quartz, with lesser hornblende, biotite, and oxides. Exposures exhibit a variable color index, although most examples have a low (<3 %) color index.

Outcrops are found adjacent to Rush Lake, where they show sharp, but intimate, as well as gradational contacts with the Mount Scott Granite (Table 6-1, #21) (Price *et al.*, 1997). The rock crops out continuously for about 1.5 km to the east, where it contacts the massive Davidson metarhyolite (Table 6-1, #8). At least one small dike of Rush Lake granite cuts into the Davidson just east of this contact. A smaller outcrop of Rush Lake granite occurs adjacent to massive Davidson and the Mount Scott Granite further east at Quetone Overlook (Table 6-1, #9), and there it contains two meter-sized xenoliths of Davidson. Additional exposures are seen at the Medicine Park Fish Hatchery (Table 6-1, #22), on the hill to the northeast, and on Mount Cummins. Outcrops containing a fine-grained version are located on the southwest side of Costain Hill, but these are poorly constrained at this time.

Contacts with the Mount Scott Granite in the hills around Medicine Park are gradational and difficult to find, and those with the Medicine Park Granite are typically obscured by talus and soil. Contacts with the Mount Scott Granite close to Rush lake are sharp, but irregular and convoluted. Conversely, sharp, angular contacts with the massive Davidson are very clearly exposed east of the Medicine Park fish hatchery. Also, small xenoliths of Rush Lake Granite are found within the Mount Scott Granite.

This unit was previously mapped as Lugert Granite (Taylor, 1915; Schoonover, 1948). Subsequent mapping efforts have also grouped these outcrops with those of the Mount Scott Granite. Myers *et al.* (1981) separated it as a basal facies of the Mount Scott Granite (facies B).

The origin and emplacement of Rush Lake granite are presented in Chapter 4 of this dissertation. Based on field and petrological evaluation, it is consanguineous with the Mount Scott Granite, and represents a fractionated forerunner of the larger body. While the xenoliths argue that the Rush Lake granite is relatively older than Mount Scott Granite, the observed intimate contacts strongly advocate a plastic rheology for both units during emplacement. Together these indicate that emplacement of Rush Lake granite precedes Mount Scott Granite, but not by any great length of time.

Western exposures do appear to underlie the Mount Scott Granite, sitting between this unit and the Davidson floor (see Plate IV, B-B'). Eastern exposures contain both the Rush Lake and Mount Scott granites at the same elevation, and contacts are near vertical in places (see Plate V). Considering that additional exposures of the Mount Scott Granite are found further east at Welsh Hill, the Mt. Cummins exposure of Rush Lake granite may be a screen between two lobes of the Mount Scott Granite.

Mount Scott Granite

The Mount Scott alkali-feldspar granite is fine to medium grained, red, weathering to brick or orange red and much of the rock is alkali feldspar and quartz, with varying amounts of granophyre. The rock is characterized by gray ovoid perthitic feldspar crystals (Merritt, 1965), which weather to a dull pink, and commonly leave pits following extensive weathering. Some of these have thin, rapakivi-texture plagioclase rims (Price *et* *al.*, 1996a). It contains primary plagioclase, but these are too small to detect without a thin section. The rock is more mafic than the other local granites, containing 4-6 vol.% of biotite + hornblende. Hillsides underlain by the granite are characteristically rocky, and are covered with large boulders.

Another common characteristic of the granite is two types of small (2-5 cm) mafic enclaves, best seen on fresh surfaces (excellent examples are seen at Lake Elmer Thomas Dam, Table 6-1, #39). Type I enclaves are dark, angular, composed of microgranular plagioclase and hornblende, with lesser biotite and magnetite. Magnetite is typically concentrated near margins or in zones of plagioclase alteration. Type II enclaves are round with irregular margins with a relatively high (>50 %) but variable color index, typically appearing as dark patches on the granite. These contain subequal amounts of fine grained plagioclase, alkali feldspar, and subhedral hornblende, with lesser quartz, magnetite, and titanite.

The Mount Scott Granite that crops out within the mapped area, is part of a substantial pluton that is 55 km in exposed length, from Welsh Hill (Table 6-1, #28) to Lake Tom Steed. Merritt (1965) lists two type localities for this unit, including one within the mapping area, at the top of Mount Scott (Table 6-1, #23). Exposures of the granite are not difficult to find within the mapped area. It caps all of the peaks and ridges to the north of Hwy. 49 west of Medicine Park. In addition to the top of Mount Scott, outstanding exposures are seen in a quarry adjacent to Lake Elmer Thomas Dam (Table 6-1, #39), and at a quarry above Rush Lake Dam (Table 6-1, #25).

Contacts with gabbroic units are easily observed from great distances, but are remarkably difficult to examine at close proximity. A tree line on the north slopes of

Mount Scott, Mount Wall, Mount Sheridan, and Mount Tarbone, visible from 10 km away, roughly marks the contact. Likewise, the short drop in elevation and the increased vegetation roughly delineates the Mount Scott Granite - GMLC contact in the Central Lowland. However, close observation of these contacts is obscured by granite talus, thick soils, and alluvium.

Most contacts with the Carlton Rhyolite Group (including metarhyolite) result in subtle changes in topography and outcrop morphology, and local fining of the granite. These contacts are nearly vertical where they are exposed. Contacts with the Medicine Park Granite, north of the Big Rock Estates, Medicine Park (Table 6-1, #27), show a fine-grained (microgranophyric), ovoid-bearing Mount Scott Granite adjacent to the contacts. Contacts with the Rush Lake granite are far more subtle than any other boundary within this area, because of the similarities between the two units.

This granite was first defined by Merritt (1965), whereas previous workers had mapped this as Lugert Granophyre (Hoffman, 1930) or Lugert Granite (Taylor, 1915; Schoonover, 1948). The granite was first separated by Merritt (1965) based on the distinctive ovoids and the mafic enclaves. The spatial extent of the unit was documented by Myers *et al.* (1981).

The granite intruded as a sheet-like, tabular pluton when magma intercepted a crustal magma trap at the Carlton Rhyolite Group - GMLC boundary (unconformity) during ascent (Ham *et al.*, 1964; Hogan and Gilbert, 1995; Hogan *et al.*, in press). The contacts suggest that emplacement followed this horizon to the west, but locally deviated from this boundary to the east. The granite is stratigraphically above some of the Carlton Rhyolite Group in the eastern half of the mapped area (Gilbert, 1982d).

Roosevelt Gabbros

Mount Sheridan Gabbro

The Mount Sheridan Gabbro, the only one of the five Roosevelt Gabbros that is exposed in this area, is best recognized in the field as the (primary) biotite-bearing gabbro. The rock is dark-gray, weathering to dark-reddish brown, and is commonly crosscut by thin white-pink pegmatite dikes which grade with increasing elevation to thicker pods. The rock is composed of plagioclase ± augite ± orthopyroxene ± biotite, with lesser hornblende and trace amounts of olivine or quartz and alkali feldspar. The amount of pyroxene decreases, and the amount of alkali feldspar and quartz increases towards the contact with the Hybrid Rock or Mount Scott Granite (Powell, 1986). Pegmatite dikes and pods are largely alkali feldspar, plagioclase, hornblende, and biotite. Typically, the gabbro is unweathered beneath a thin rind a few centimeters deep. In other exposures, it is extensively weathered to depths >10 meters.

The Mount Sheridan Gabbro has the greatest amount of outcrop area of the five Roosevelt Gabbros. Outcrops include small knobs of boulders that protrude from dark, magnetite rich soils. The exposure on Little Mount Sheridan is enhanced by small quarries on the eastern slope, and contains numerous pegmatite dikes (Table 6-1, #29). More mafic exposures at lower elevations (Table 6-1, #30) typically contain fewer pegmatite dikes.

Originally, this unit, along with the other Roosevelt Gabbros, was included as part of the GMLC (*e.g.*, Taylor, 1915). Gilbert (1960) identified one of the Roosevelt Gabbros within the Glen Mountains, as biotite-olivine gabbro. Subsequent workers have separated out the biotite-gabbro rocks as the Roosevelt Gabbros (Powell *et al.*, 1980a, b), and included these rocks with the GMLC under the term Raggedy Mountains Gabbro Group (see Figure 6-2). For reasons discussed below, the GMLC and Roosevelt Gabbros are now considered temporally separated (Figure 6-2). However, the Raggedy Mountains Gabbro Group remains a valid spatial designator, as these two mafic units are typically found adjacent to one another.

Recent investigations suggest that the Mount Sheridan Gabbro is younger than the granite. Previously, the gabbro was thought to substantially predate the Cambrian unconformity beneath Carlton Rhyolite Group (Ham *et al.*, 1964). Zircon U/Pb data yields an age of 552 ± 7 Ma for the Mount Sheridan Gabbro (Bowering and Hoppe, 1982), and 533±2 Ma for the Mount Scott Granite (Hogan *et al.*, 1996). However, the isotopic systematics of the gabbro zircons are complicated by an older, inherited component and subsequent Pb-loss (Hogan and Gilbert, 1998). Laser $^{40}Ar/^{39}Ar$ geochronologic investigation of primary amphibole and biotite from the gabbro yield 533 ± 2 and 533 ± 4 Ma, respectively, whereas amphibole from the granite yields 539 ± 2 Ma, indicating that the two units are nearly contemporaneous (Hogan *et al.*, 1996). Additionally, the shape and contacts of another Roosevelt Gabbro pluton, the Sandy Creek Gabbro, suggest it intruded into the Mount Scott Granite (see Chapter 5; and Price *et al.*, 1998b). There is only limited field evidence for relative timing of these two units. The increasingly fractionated composition of the pluton with elevation, along with the increased accumulation of pegmatite with proximity to the contact, suggests that the pluton is completely intact. And while neither the Mount Sheridan Gabbro or the Mount Scott Granite exhibit a chilled margin, the granite has chill induced textures elsewhere (see Medicine Park Granite), thus its absence here suggests the granite is older.

Hybrid Rock

Ferrogranitoids of variable composition and appearance are grouped together here as the Hybrid Rock unit. Most outcrops of ferrogranitoid rock are green and light pink in color, and even the most granitic (alkali-feldspar rich) examples contain a rather high color index (30 %). Primary mineralogy includes variable amounts of alkali feldspar, plagioclase, quartz and hornblende, with small amounts of biotite and titanite. A few alkali feldspar crystals are rounded, reminiscent of Mount Scott Granite phenocrysts. Substantial mineralogical alteration includes abundant sericite and chlorite pseudomorphic after biotite.

Small outcrops of this rock are found along the north slope of the Wichita Mountains between outcrops of Mount Scott Granite and Mount Sheridan Gabbro. Specific localities include the drainage on the northwest slopes of Mount Scott (Table 6-1, #32), on Little Mount Sheridan, and in an area adjacent to Mount Tarbone (Table 6-1, #31). Outcrops are small and isolated by talus and soil. Contacts with the underlying gabbro and the overlying granite are not exposed.

Huang's (1955) study of intermediate rocks of the Wichita Mountain included these ferrogranitoids where, in addition to the mineralogy presented above, he observed orthopyroxene and clinopyroxene in some examples. Myers *et al.* (1981) referred to these rocks hybrid, citing to their intermediate and highly variable composition.

Myers *et al.* (1981) attributed the origin of the hybrid rocks to granite-intrusion induced melting of locally produced saprolitic soils developed on the unconformity surface of the Raggedy Mountains Gabbro Group. This assumes that these soils escaped dehydration (baking) during that rhyolite emplacement that covered the GMLC prior to granite intrusion. In light of evidence for a Mount Sheridan Gabbro younger than the Mount Scott Granite (see Mount Sheridan Gabbro), it is likely that these hybrid rocks are melts of the Mount Scott Granite that may have interacted with Mount Sheridan Gabbro magma and pegmatitic liquids. This explains intermediate liquids of varying composition trapped beneath the solid granite body. If these hybrid melts cooled prior to the solidification of the gabbro, they might have altered from interaction with Mount Sheridan Gabbro pegmatite derived fluids.

Quanah Granite

The Quanah alkali-feldspar granite exhibits two textural types within the area: coarse grained granite and fine- to medium-grained granite. The finer-grained subunit locally contains xenoliths of coarse-grained Quanah Granite. Additionally, the rock plays host to numerous aplitic and pegmatitic features, and pegmatitic dikes and apophyses (mapped as Quanah dikes) occur in the GMLC adjacent to the granite within the Central Lowland. Regardless of the texture, the rock is pink (typically much pinker than the other granites in the Wichita Mountains), weathering to orange-pink. Alkali feldspar and quartz are the dominant minerals. Alkali feldspars are perthitic, and coarse-grained examples produced exsolution mantles of rim albite (Merritt, 1966). Unlike the other members of the Wichita Granite Group, the Quanah Granite contains two amphiboles, hornblende and arfvedsonite (Scofield and Gilbert, 1982). Weathering is pervasive on most exposures, and fresh outcrops are rare. Thin soil and grus are common to exposures which therefore typically host little vegetation. The rock also contains xenoliths of Mount Scott Granite, and members of the Carlton Rhyolite Group, increasing in number towards the margins of the pluton. The coarse-grained facies produces a distinct geomorphology of massive rocky promontories, steep slopes, towering tors, smooth exfoliation surfaces, and deep canyons, particularly in the southern portions of the mapped area.

Coarse-grained Quanah Granite comprises the majority of the outcrops exposed directly south of the Central Lowland. One example of relatively unweathered coarse facies is found on the road from Hwy. 49 to Lost Lake, about 1 km south of the contact with the GMLC (Table 6-1, #33, J. P. Hogan, personal comm.). Fine to medium grained Quanah is more abundant to the east, and substantial outcrops occur in a 1 km east-west trending belt on Cross Mountain (Table 6-1, #35) and Mount Sherman, and adjacent to the contact with the GMLC along the Fish Lakes (east of French Lake) (Table 6-1, #36). Most examples are aphyric, although porphyritic granite, dominated by large (~5-10 mm) alkali feldspar crystals, crops out west of Burford Lake.

Because it is the only coarse-grained granite exposed in the eastern Wichita Mountains, previous workers were quick to map these distinctive outcrops as a separate unit called Quanah Granite (*e.g.*, Taylor, 1915). Schoonover (1948) mapped the fine-to medium-grained as Quanah aplite. Gilbert (1982b) mapped the boundary between the coarse and fine grained lithologies around French Lake.

The Quanah Granite here is intrusive into the GMLC and the Mount Scott Granite. Numerous apophyses and dikes of usually supercoarse-grained pink granite and pegmatite cut the GMLC immediately adjacent to the Quanah margin (*e.g.*, north of the Fish Lakes), and are likely to be intrusive from the main body of Quanah Granite, although none are traceable back to the granite at the surface.

Myers *et al.* (1981) established the Quanah as among the younger granites of the Wichita Granite Group. Xenoliths of Mount Scott Granite at French Lake indicate limited stoping into the Quanah Granite. Mount Scott Granite stoping appears to be much more intense further west (Gilbert, unpublished data). Some of the fine-grained facies occurs proximal to contacts, and perhaps is a chilled margin texture. Stoping and possible chilling point to a Quanah younger than the Mount Scott. Also the coarser-grained texture may also indicate a younger age for the Quanah Granite, because the texture may be a response to a warmer emplacement level brought on by previous intrusions (*i.e.*, Mount Scott Granite).

Diabase Dikes

Diabase dikes are identified by their fine-grained, aphyric texture, composed of subparallel plagioclase laths and interstitial augite, and magnetite. Chilled margins have even smaller crystals of roughly the same assemblage with increased amounts of clinopyroxene.

Typically the dikes are difficult to observe in the typical field setting. With the exception of the Mount Sheridan Gabbro, where dikes are largely obscured by thick soils, the diabase typically weathers faster than the rocks it intrudes. This weathering results in eroded trenches, commonly filled in with soils and detritus from the surrounding rock, completely obscuring the dike trace with areas where the host lithology has developed a substantial soil profile. Their presence is best noted in stream cuts, quarries, and exploration pits. Outcrops are limited as dike widths are usually < 1 m. The best exposure is found on the quarry wall and floor at Elmer Thomas Dam (Table 6-1, #39), which has been mapped in detail (Plate VI). Another easily accessible exposure is found on the south side of Beaver Creek at Rush Lake Dam (Table 6-1, #40), occurring half way up the slope between the top of the dam and the creek.

Previous workers beginning with Taylor (1915) recognized these dikes. Prior to that, the dikes were common targets for mineral prospectors. Since the dikes are small, they are difficult to document on larger maps, so most published maps do not include these dikes. Gilbert and Powell (1988) include three dikes with slightly exaggerated widths on their inset map of the Quetone area (*e.g.*, Table 6-1, #17).

Since Taylor (1915), investigators placed these dike as the chronostratigraphically highest igneous unit within the Wichita Mountains, concluding that some are very late in the development of the Wichita Igneous Province (*e.g.*, Gilbert, 1983). They crosscut most of the igneous section, and within the mapped area they intrude the Carlton Rhyolite, the Mount Scott Granite, the Rush Lake granite, the Quanah Granite, and the Mount Sheridan Gabbro contain dikes. Recent studies implicated earlier emplacement of some dikes. Exposures to the west of this area contain fragments of diabase in the Mount Scott Granite, suggesting that dikes are contemporaneous with the Mount Scott Granite (Hogan, unpublished data). At the Lake Elmer Thomas dam quarry, diking partially melted the Mount Scott Granite, generating liquids that re-intruded cooling fractures within the dike (see Plate VI). Thermal modeling stipulates that granite host rock must be significantly above ambient (completely cooled) temperatures to melt (Price *et al.*, 1996b, 1998a), indicating that the granite was still cooling at the time of dike intrusion. Thus, diabase dikes and the Mount Scott Granite are contemporaneous, indicating diabase intrusion occurred much earlier and for a longer period of time than previously acknowledged.

Rhyolite Dike

Post-granite brown-red porphyritic rhyolite contains euhedral pink alkali-feldspar and subhedral to euhedral clear quartz phenocrysts. Altered hornblende is present in small amounts. The groundmass, mostly alkali feldspar and quartz, is granulitic. Small vesicles are common.

The rock occurs as a dike adjacent to Hwy. 49 at the medicine Park Fish Hatchery (Table 6-1, #22), where it cuts the Rush Lake granite. Up the hill to the north, it cuts the massive Davidson metarhyolite and continues back into the Rush lake Granite. Further north it disappears, covered by talus, and presumably capped by the Rush Lake granite, as it is not seen again along strike on the hill slopes to the north.

Ham *et al.* (1964) provide the earliest documentation of the dike. A detailed map of the immediate area is presented in Gilbert and Powell (1998), and revisions are in Price *et al.* (1998a).

Although the rock was employed by Ham *et al.* (1964) to demonstrate granite-rhyolite contemporaiety, the rhyolite must be substantially younger than the Wichita Granite group (Gilbert and Powell, 1988). The fine-grained texture of the groundmass, indicative of shallow emplacement into cold rock, suggests that the Rhyolite dike crystallized under substantially different conditions than the Rush Lake granite it intrudes The dike must follow a hiatus in local felsic magmatism that included thermal loss from the area, and possible erosion of the overlying rhyolite pile.

Post Oak Formation

The Post Oak Formation is Permian (Leonardian), the result of erosion within the late Paleozoic Wichita Mountains. This formation includes the boulder conglomerate and arkosic sandstone that substantially covers much of the eastern Wichita Mountains (Stone, 1977). This study includes an additional facies, Post Oak talus, which occurs in small amounts along the granite highlands.

Post Oak talus

Talus deposits are found on the slopes of the Wichita Mountain peaks. The largest examples occur on Mount Scott, and one is easily observed from the road that climbs the mountain (Table 6-1, #42). Outcrops of talus are comprised of sizable (>3 m) rounded boulders of Mount Scott Granite. These are poorly sorted. On the northern slopes, boulder fields are typically infilled by smaller fragments, sand, and silt. On the southern slopes, boulder fields generally lack substantial infilling. Depth varies with talus boulder size; deposits are only as deep as one layer of the largest boulders.

Boulders develop from the removal of tors, the result of weathering followed by erosion (Gilbert, 1982a). Weathering of the rock is fracture controlled (see Chapter 5, Price *et al.*, 1998b). Fractures commonly intersect each other in the granites, and where three fractures intersect, they form a corner producing three fluid-rock interfaces. Eventually these corners become incompetent. Uplift following this weathering increases erosion rates, and free these blocks each other. They form round boulders, proportional in size to the joint sets they were eroded from.

The youthful appearance of these talus deposits almost warrants the assignment of a Quaternary age. However, they appear to be contemporaneous with the Post Oak conglomerate, which is Permian. The highly variable nature of fracturing within the Mount Scott Granite should produce boulders in a large variety of sizes, but talus piles contain boulders typically greater than 1 m in diameter, suggesting that smaller sizes were removed by gravitational separation in stream flow from the highlands and deposited on the plains below. Such smaller boulders are common to the Permian Post Oak conglomerate (see below), therefore the talus might be contemporaneous with the conglomerate.

Post Oak conglomerate

The appearance of the Post Oak conglomerate in this area is very consistent. The rock is conglomeratic, characterized by the presence of granite boulders 15-65 cm and pebbles 1-7 cm in diameter. Boulders are largely medium-grained granite, with some coarse granite, metarhyolite, and rhyolite. These are set in a matrix of sand-sized granite fragments, quartz, and microperthitic feldspar, and silts (Al-Shaieb *et al.*, 1980). The unit locally contains horizontally stratified color changes of light orange and gray. Matrix grain size varies between the two colors; gray layers are finer-grained than orange layers.

Widespread, thin outcrops of the conglomerate are found on Jed Flat and south in the Fort Sill Reservation around Engineer Pond. Good sections of this unit are found in a small roadside quarry at Quetone overlook (Table 6-1, #43), covering Rush Lake granite and the rhyolite dike at the Fish Hatchery (Table 6-1, #22), in the cut bank of Medicine Creek immediately to the South of the Fish hatchery (Table 6-1, #44), and within Brush Creek on Fort Sill Table 6-1, #45). However, the unit may be found in smaller outcrops throughout the area. Outcrops generally mantle topography on low relief areas with shallow slopes.

The Post Oak Formation found in this area is Chase's (1954) granite-boulder conglomerate that grades laterally into the limestone conglomerate to the north. Al-Shaieb *et al.* (1980), determined that the Post Oak Formation interfingers with the Permian redbeds to the east and documented the textural diversity of the unit, concluding that lithification involved a complex diagenetic history of early caliche formation and breakdown of silicates with subsequent development of clay minerals and ferric oxides.

The outcrops in this area mark the location of a Permian drainage system. Outcrops suggest east-west drainage patterns, like those around Mount Scott, and north-south patterns, such as those south of Lost Lake and at the Cache Wye. Flow direction is unconstrained at this time. The low-relief and gentle slope marked by these deposits most likely reflects the topography of the bedrock, planed by terracing of these Permian streams.

The Post Oak Formation is of hydrological interest, as it is the thickest unit with considerable permeability exposed within this area. Although the exact permeability is unknown, water transport through this unit is evidently substantial: the conglomerate contains few incised channels, occurring only at the unit's margins, where they have cut upsection from fracture-controlled streams in the igneous bedrock. Furthermore, after significant rainfall, water percolates through this unit and seeps forth along the contact between the conglomerate and underlying crystalline rocks. However, despite the relatively high permeability of the unit, significant water storage in Post Oak Formation within this area is unlikely, as all of the outcrops mantle elevations that are drained by major streams. Further west, where streams have yet to dissect the unit, the Post Oak Formation may have potential as small, isolated aquifer units that drain the granite highlands.

Garber -Hennessey Formation

Deep cuts into the Garber-Hennessey formation reveal a gray arkosic sandstone, cut by channels of red arkosic sandstone fining upwards to red shale, that is capped by a buff-colored arkosic sandstone. The shale is commonly cut by small, irregular (<0.5 cm) calcite veins, and fluids within these veins have altered the shale to a white color for small distances around the vein. At some exposures these veins are numerous and exhibit several orientations.

The unit occurs only in the easternmost portion of the area, is largely obscured by grassland soils and is rarely exposed. Erosion of the upper sandstone forms a small ridge (as seen at the intersection of Hwy. 49 and I-44) which outlines the extent of the unit within this area. It is best seen in Ketch Creek south of Hwy. 49, where cuts expose 1 to 2 m of section, as well as the overlying soil profile, and in a cut on Punch Bowl Road (Fort Sill) adjacent to Ketch Creek.

Havens (1977) correlated the Garber Sandstone exposed to the north of this area with other pre-Hennessy deposits within Oklahoma. There are not as yet any detailed correlation of the sandstones and shales on west Fort Sill with those of Havens (1977). The presence of shale (Hennessey) between the two sandstones may indicate interfingering of marine clastics from the east with fluvial deposits sourced from the Wichita Mountains.

Post Oak Formation grades into this unit in the southwestern portions of the Wichita Mountains (Chase, 1954). Within the study area (Plate III), that facies change must occur between Medicine and Ketch Creeks, but the change is only suggested by adjacent outcrops within Ketch Creek, and therefore it is uncertain whether the Post Oak Formation interfingers with the Garber-Hennessey.

Quaternary Alluvium

Quaternary alluvial deposits are present in this area within streams and valleys. Alluvium varies in composition. The stream deposits are strongly dependent on the lithologies the stream drains. Typically, alluvium is comprised of clast, sand, and silt sized grains of orthoclase, plagioclase, quartz, oxides, and clays (Chase, 1952), and is richer in plagioclase, and contains augite and trace amounts of olivine in stream deposits sourced from the gabbros. Exposures adjacent to Carlton Group contain the largest grain size, 2 to 6 cm lithic clasts, somewhat reminiscent of Post Oak conglomerate (rhyolite conglomerate). However, clasts are angular and generally smaller within the alluvium.

With the exception of the alluvium around East Cache Creek on the eastern portions of the Fort Sill sheet, most occurrences are small and limited to the immediate vicinity of modern drainages. Cuts by streams provide good profiles, including those seen in Little Medicine Creek near the Mount Scott picnic ground (Table 6-1, #16), and a contact with the Post Oak Formation in Brushy Creek Table 6-1, #45).

The alluvium deposits definitely indicate that the modern depositional processes differ from those of the recorded Permian within this area. Modern stream deposits contain boulders only when adjacent to or in the Post Oak formation, indicating that conditions of stream flow for the exposed Permian are not being replicated in the modern drainage systems of this area. Such variation may result from differences in Leonardian climate from the modern as well differences in vegetation, although the degree of difference these parameters is currently unconstrained.

Structure

The mapping investigation focused on documenting the spatial distribution of the lithologies within the eastern Wichita Mountains. No formal analysis of rock deformation was undertaken. The lack of *mappable* strain features (*i.e.*, faults and folds that could be documented at a 1:12,000 scale) requires some clarification, particularly in light of other studies which have placed faults within this area.

Without doubt, the rocks of the Wichita Mountains have been subjected to numerous opportunities for deformation including Cambrian rift faulting (*e.g.*, McConnell and Gilbert, 1990), plutonic intrusion (*e.g.*, Hogan and Gilbert, 1997), early Paleozoic subsidence, and Pennsylvanian uplift (*e.g.*, Ham *et al.*, 1964; McLean, 1983; McLean and Stearns, 1986). Even recent (Holocene) movement is evidenced by the fault escarpment and recent earthquakes on the Meers Fault (*e.g.*, Luza *et al.*, 1987) to the north of this area, thus deformation may be ongoing. Because the crystalline rocks of the area were never buried deeper than 5 km, it is likely that any deformation is manifested as brittle rock-failure (*i.e.*, fractures).

Fractures are indeed numerous within the mapped area. Although no attempt was made by this study to statistically quantify the intensity of fracturing, some general observations should be noted. The Cambrian rocks of the eastern Wichita Mountains exhibit a continuum of fracture densities ranging from microscopic to superoutcrop scales. For generalization, five groups of intensities, based on relative fracture densities observable to the unaided eye, are discussed below.

Very high fracture density (VHFD) zones contain breccia with fractures so abundant that they obscure the identity of the rock in hand sample. Only three localities are known within the mapped area, and these are adjacent to Little Medicine Creek, west of the Mount Scott Picnic Grounds. Brecciated Mount Scott Granite is seen along Hwy. 49, both in a road cut west of the picnic grounds exit (Table 6-1, #24) and near the quarry south of the Quetone parking area (Table 6-1, #17). Brecciated Davidson metarhyolite (Carlton Rhyolite Group) is found adjacent to Little Medicine Creek directly south of the first brecciated Mount Scott Granite locality (south of Table 6-1, #24) and on the rise south of Little Medicine Creek, southeast of the Quetone parking area (Table 6-1, #7). With the exception of this latter locality, where the brecciated Davidson contacts the Mount Scott Granite, the breccia rocks contact the massive Carlton rhyolite which is not extensively brecciated. The relatively small distribution of brecciated rocks might result from exposure, a function of cuts from Hwy. 49 and Little Medicine Creek. Otherwise, the brecciation might point to a localized area of deformation currently unconstrained. The three outcrops are separated by exposures with significantly lower fracture densities, thus making it difficult to determine a spatial link between these zones of VHFD.

High fracture density (HFD) zones contain fragmented rocks that typically weather out as pieces between 1-20 cm on a side. HFD zones are abundant and well distributed throughout the area. An example is found within the Mount Scott Granite immediately east of the breccia zone (VHFD) on Hwy. 49 west of the picnic grounds exit (Table 6-1, #24). At this locality, some of the fractures exhibit slickensides. A series of examples within the Mount Scott Granite is found intermittently along Hwy. 49 from the Picnic grounds entrance (south of Table 6-1, #32) east to 0.5 miles west of the Fish Hatchery (Table 6-1, #10), at the Happy Hollow store. Another example is found adjacent to the Medicine Park Granite north of Big Rock Estates (Table 6-1, #27). Other examples are found in the Rush Lake granite east of Rush Lake Dam (Table 6-1, #7), and in the Davidson metarhyolite north of the Quetone Parking Lot (Table 6-1, #9), particularly along the metarhyolite contact with the Rush Lake granite. Like the VHFD zones, some of the HFD zones appear to be isolated and preclude correlation with other zones. Others, like the one seen east of Rush Lake dam, correspond to other fracture zones air-photo lineaments (*i.e.*, lines observed on high-altitude aerial photographs).

Exposures with *moderate fracture density* (MFD) contain relatively more competent rock, weathering out as pieces from 20-50 cm along a side. Such is typical of most exposures of the Carlton Rhyolite Group, which exhibit polygonal fracture patterns. Specifically, massive and spherulitic Carlton rhyolite units exhibit hexagonal and pseudo-hexagonal patterns, reminiscent of columnar jointing. Massive and banded Davidson metarhyolite units exhibit rhombohedral patterns that typically produce flat pavements. Moderate fracture density zones are also observed in the other lithologies, and are more common than the HFD zones. Most are not extensive. Some appear to be isolated from other MFD zones, others correspond to MFD and HFD zones along air-photo lineaments.

Exposures with *low fracture density* (LFD) contain competent rock that weathers out blocks between 50 and 200 cm on a side. This type of fracturing is common in the Mount Scott Granite, the Rush Lake Granite, and the Mount Sheridan Gabbro. Low fracture density zones are found in the Quanah granite, although these are largely confined to the fine- to medium-grained facies.

Exposures with *very low fracture density* (VLFD) are massive and weathering produces boulders larger than 200 cm on a side. This is typical of the coarse-grained

Quanah granite and the GMLC. Examples of VLFD zones are found in the other units, but represent a small volume of those lithologies. For example, most of the highest peaks of the Mount Scott Granite have VLFD zones.

As noted, individual lithologies are largely dominated by one category of fracture density. The average fracture density shows correspondence with average grain size (Gilbert, 1984). The coarse grained rocks, like the Quanah Granite are dominated by VLFD, the medium-grained rocks are largely exposures of LFD, and the extrusive and metaextrusive units are predominantly exposures of MFD.

The average fracture density of each lithology appears to influence topography. Despite being roughly compositionally equivalent (at least from an weathering/erosional standpoint) the Carlton rhyolite, Mount Scott Granite, and the Quanah Granite exhibit vastly different topography. Carlton rhyolite, dominated by MFD, underlies rounded hills. Mount Scott Granite, dominated by LFD, produces rocky knobs. Quanah Granite, dominated by VLFD, has steep peaks and tors, and relatively deeper canyons.

Only a handful of studies have examined the fractures of the area, and these have largely focused on the air-photo linears. The air-photo linears range from 0.1 m to > 5 km in length. These can be divided into two types, those that occur along lithologic boundaries and those that transect one or more lithology. Those that mark lithological boundaries typically delineate significant compositional contrasts (*i.e.*, granite-gabbro). Prominent among these is the GMLC- Mount Scott Granite contact and the GMLC-Quanah Granite contact within the Central Lowland (see Gilbert, 1984 for discussion). The lineament corresponds to a change in elevation, presumably the result of differential weathering rates between the compositionally distinct units. The location of the lithological boundary need not correspond to fracturing, although that may be the case in some examples. The transecting type of air-photo linear is typically a zone a few meters wide recessed into the surrounding lithology. Some have collected soil and host vegetation, others are stream drainages. Some exposed linears are largely HFD or MFD zones. Others are single fractures, particularly in the VLFD units like the coarse-grained Quanah granite. As mentioned above, the scale of fracturing grades from the microscopic to very large. Why some HFD and MFD zones and VLFD fractures become linears and others do not remains a problem. Further investigation on the distribution, orientation, and nature of fracturing within this area is warranted, particularly prior to any further analysis of the linears.

Cursory observations from this study show that rock competency has greatly influenced fracturing in places. The best example is the contact between the Davidson metarhyolite and the Rush Lake Granite, both northeast of the Quetone parking (Table 6-1, #9) area and at the State Fish Hatchery (Table 6-1, #10). A few cm away from straight contacts, fractures within the metarhyolite become listric proximal to the contact, converging at the contact. In most cases they do not appear to continue into the granite. At corners, several fractures in the metarhyolite will converge to produce a single fracture within the granite. Although not quantitatively constrained, presumably this behavior results from a contrast in the brittle behavior of the granite relative to the metarhyolite. The coalescing nature of the fractures at the margin of the metarhyolite increases the fracture density of the metarhyolite adjacent to the contact. This might be the case on an outcrop scale, where lithologies show an increase in fracture densities within a few meters of contacts (*e.g.*, HFD zone, Mount Scott Granite - Medicine Park Granite; Table 6-1, #27).

Some sets of fractures seen in the granite outcrops are curvilinear, exhibit a wide range of orientations, parallel or concentric to one another, and reflect topography, and thus appear to be exfoliation or sheet joints. Good examples are seen at Lake Elmer Thomas Dam, on Rabbit Hill, on Mount Scott, and on Cross Mountain. Exfoliation jointing is understood to develop as a response of crystalline rocks subjected to overburden removal, developing as fractures subparallel to the surface that become more numerous (*i.e.*, higher fracture density) with proximity to the free surface (*e.g.*, Turcotte and Shubert, 1982; Holtzhausen, 1989). The development of the sheet joints in these granites is not well constrained, but these are likely to be early Permian features, developed when much of the current topography was formed, and the granite was unroofed by erosion.

It is assumed that many of the other fractures not associated with exfoliation, record strain from Pennsylvanian uplift. The air-photo linears, perhaps because of their striking prominence, have been previously mapped as faults by Miser (1954) and Havens (1977). Gilbert (1982a; 1984) shows that some of the proposed faults, those that fall along lithological-contact linears, are clearly igneous contacts. This study also found that most lithologic contacts in this mapped area showed evidence that the units shared igneous relationships and were not juxtaposed by faulting. Additionally, there is no evidence of horizontal offset on linears that transect lithologies.

Schoonover's (1948) map of the Fort Sill area documents further (and somewhat extensive) faulting. These appear to explain the distribution of some lithologies. This current work found that the distribution was not as complex as previously thought, and attributes previous error to the difficulty of lithologic identification within the area. The current mapped patterns are not suggestive of faulting.

Despite the great many fractures, this study found only limited evidence for faulting. Slickensides are the only observed kinematic indicators, and these are only seen on the HFD zone on Hwy. 49. Most of the igneous units within the mapped area lack internal structures to use as piercing points. Quartz veins are prominent in most lithologies (some more than others), and have been previously defined offset along a small number of fractures and fracture zones (McLean, 1983; McLean and Stearns, 1986). This study agrees that offsets recorded by these piercing points are small (less than 1 m, McLean, 1983). Although a rigorous effort was not made, this study did not find any offsets greater than 10 cm. The failure to demonstrate offset that are presentable at a 1:12,000 scale precluded recording quartz vein offsets on this mapping effort.

The mapped area is within the Fort Sill Anticline of Gilbert (1982a), a large crustal fold defined by the northward dipping sediments of the Slick Hills north of the mapped area, the southward dipping sediments of Signal Hill, south of the mapped area, and internal structures within the GMLC in the Glen Mountains, west of the mapped area. Evidence of this broad fold within the exposures of the mapped area is scant. Some of the fracturing within the felsic units may result from gentle flexure of the granite (Smart, personal comm., 1998). Additionally, the outcrop pattern of the Davidson metarhyolite, interpreted to be the near-horizontal eastern floor for the granite plutons, delineates a NW-SE tend, consistent with it being the core of a broad anticline.

Conclusion

This mapping area within the eastern Wichita Mountains exhibits numerous lithologies that document much of southern Oklahoma's geological history. The numerous interactions between the largely igneous units of this area are revealed in the contacts between units, indicating a complex story of intrusion, volcanism, and metamorphism.

Specifically, mapping detailed the extent of the Davidson metarhyolite, and the Medicine Park granite, as well as Quanah dikes. Mapping of the diabase dike at lake Elmer Thomas illustrates the complexities of dike intrusion and partial melting of the host rock. Additionally, a new unit, the Rush Lake granite, was broken out from the Mount Scott Granite due to its distinctiveness and the evidence of intrusion as a separate (although simultaneous) unit. Most of the previously established age relationships were verified by this study, with the exception of the Mount Sheridan Gabbro. However, the field evidence for this gabbro postdating the Mount Scott Granite is scant at best. Also the maps document the nature of the Permian unconformity, and the results of stream erosion and deposition during that time, processes that differ from the current erosional and depositional regime ongoing in the modern Wichita Mountains.

Although the area contains numerous fractures, this study was unable to document significant faulting within the mapped area.

Works Cited

Al-Shaieb, Z. F., Hanson, R. E., Donovan, R. N., and Shelton, J. W., 1980, Petrology and diagenesis of sandstones in the Post Oak Formation (Permian), southwestern Oklahoma. Journal of Sedimentary Petrology, 50, p. 43-50.

Bigger, S. E., and Hanson, R. E., 1992, Devitrification texturees and related features in the Carlton Rhyolite in the Blue Creek Canyon area, Wichita Mountains, southwestern Oklahoma. Oklahoma Geology Notes, 53, p. 124-142

Bowering, S. A., and Hoppe, W. J., 1982, U/Pb ages from Mount Sheridan Gabbro, Wichita Mountains, *in* Gilbert, M.C., and Donovan, R. N., eds., Geology of the Eastern Wichita Mountains Southwestern Oklahoma. Oklahoma Geological Survey, Guidebook 21, p. 54-59.

Chase, G. W., 1952, Ilmenite in alluvial sands of the Wichita Mountain System, Oklahoma. Oklahoma Geological Survey, Circular 30, 44 p.

Chase, G. W., 1954, Permian conglomerate around Wichita Mountains, Oklahoma. Bulletin of the American Association of Petroleum Geologists, v. 38, p. 2028-2035.

Chase, G. W., Frederickson, E. A., and Ham, W. E., 1956, Geology of the Wichita Mountains, *in* Hicks, I. C., Westheimer, J., Tomlinson, C. W., Putman, D. M., and Selk, E. L., eds., American Association of Petroleum Geologists Symposium Volume on the Petroleum Geology of Southern Oklahoma, I, p. 36-55.

Donovan, R. N., Ragland, D., Cloyd, K., Bridges, S., and Denison, R. E., 1988, Carlton rhyolite and lower Paleozoic sedimentary rocks at Bally Mountain in the Slick Hills of southwestern Oklahoma, *in* Hawyard, O. T., ed., Geological Society of America Centennial Field Guide - South-Central Section. Geological Society of America, p. 93-98.

Gilbert, M. C., 1960, The geology of the western Glen Mountains, Oklahoma. University of Oklahoma unpublished M.S. Thesis, 48 p.

Gilbert, M. C., 1982a, Geologic setting of the eastern Wichita Mountains, with a brief discussion of unresolved problems, *in* Gilbert, M. C., and Donovan, R. N., eds., Geology of the Eastern Wichita Mountains Southwestern Oklahoma. Oklahoma Geological Survey, Guidebook 21, p. 118-119.

Gilbert, M. C., 1982b, Geologic map for stop six - French Lake Dam, *in* Gilbert, M. C., and Donovan, R. N., eds., Geology of the Eastern Wichita Mountains Southwestern Oklahoma. Oklahoma Geological Survey, Guidebook 21, p. 130-131.

Gilbert, M. C., 1982c, Geologic map for stop five-Quanah Parker lake Area, *in* Gilbert, M. C., and Donovan, R. N., eds., Geology of the Eastern Wichita Mountains Southwestern Oklahoma. Oklahoma Geological Survey, Guidebook 21, p. 124-125

Gilbert, M. C., 1982d, Stop 4 - Mount Scott Campground, *in* Gilbert, M. C., and Donovan, R. N., eds., Geology of the Eastern Wichita Mountains Southwestern Oklahoma. Oklahoma Geological Survey, Guidebook 21, p.118-123.

Gilbert, M. C., 1982e, Stop 8 - Welsh Hill, *in* Gilbert, M. C., and Donovan, R. N., eds., Geology of the Eastern Wichita Mountains Southwestern Oklahoma. Oklahoma Geological Survey, Guidebook 21, p.144-147.

Gilbert, M. C., 1983, Timing and chemistry of igneous events associated with the Southern Oklahoma Aulacogen. Tectonophysics, 94, p. 439-455.

Gilbert, M. C., 1984, Comments on structure within the igneous core, Wichita Mountains Crustal Block. Techinical Proceedings of the 1981 AAPG Mid-Continent Regional meeting, Oklahoma City Geological Soiecty, p. 177 - 190.

Gilbert, M. C., and Miller, J. R., 1982, Geologic map for stops four and eight, *in* Gilbert, M.C., and Donovan, R.N., eds., Geology of the Eastern Wichita Mountains Southwestern Oklahoma. Oklahoma Geological Survey, Guidebook 21, p. 118-119.

Gilbert, M. C., and Powell, B. N., 1988, Igneous geology of the Wichita Mountains, southwestern Oklahoma, *in* Hayward, O. T., ed., Geological Society of America Centennial Field Guide - South-Central Section, p. 109-126.

Ham, W. E., Denison, R. E., and Merritt, C. A., 1964, Basement Rocks and structural evolution of southern Oklahoma. Oklahoma Geological Survey, Bulletin 95, 302 p.

Hanson, R. E., 1977, Petrology and geochemistry of the Carton Rhyolite, southern Oklahoma. Unpublished M.S. thesis, Oklahoma State University, Stillwater 161 p.

Havens, J. S., 1977, Reconnaissance of the water resources of the Lawton Quadrangle, southwestern Oklahoma. Oklahoma Geological Survey Hydrological Atlas 6, sheet 1 of 4, Figure 2, geologic map, scale 1:250,000.

Hoffman, M. G., 1930, Geology and petrology of the Wichita Mountains. Oklahoma Geological Survey, Bulletin 52, 83 p.

Hogan, J. P., and Gilbert, M. C., 1995, The A-type Mount Scott Granite Sheet. Importance of crustal magma traps. Journal of Geophysical Research, 100, B 8, p.15,779 - 15,793.

Hogan, J. P., and Gilbert, M. C., 1997, The intrusive style of A-type sheet granites from the Southern Oklahoma Aulacogen. *in* Middle Proterozoic to Cambrian Rifting: Mid-North America, R. W. Ojakangas, A. B. Dickas, and J. C. Green, eds., Geological Society of America Special Paper, 312, p. 299-311.

Hogan, J. P., and Gilbert, M. C.,1998, The Southern Oklahoma Aulacogen: A Cambrian analog for Mid-Proterozoic AMCG (Anorthosite-Mangerite-Charnockite-Granite) complexes? Basement Tectonics, 12, p. 39-78.

Hogan, J. P., Price, J. D., and Gilbert, M. C., 1998, Crustal magma traps and magma driving pressure:consequences for pluton shape and level of emplacement. Journal of Structural Geology, in press.

Hogan, J. P., Gilbert, M. C., Price, J. D., Wright, J. E., Deggeller M., and Hames, W .E., 1996, Magmatic evolution of the Southern Oklahoma Aulacogen: Geological Society of America, Abstracts with Programs, 28, n. 1, p. 19.

Holtzhausen, G. R., 1989, Origin of sheet structure, 1. Morphology and boundary conditions, *in* A.M. Johnson, C. W. Burham, C. R. Allen, and W. Muehlberger, eds., Richard H. Jahns Memorial Volume. Engineering Geology, 27, p. 225-278.

Huang, W. T., 1955, Occurrences of leucograno gabbro and associated igneous rocks in the Wichita Mountains, Oklahoma. American Journal of Science, 253, p. 341-357.

Johnson, K., and Denison, R. E., 1973, Igneous geology of the Wichita Mountains and economic geology of Permian rocks in southwest Oklahoma. Oklahoma Geological Survey Special Publication 73-2, Guidebook for field trip 6, Geological Society of America annual meeting, Dallas, 33 p.

Luza, K. V., Madole, R. F., Crone, A. J., 1987, Investigation of the Meers Fault, southwestern Oklahoma. Oklahoma Geological Survey, Special Publication 87-1, 75 p.

McConnell, D. A., and Gilbert, M. C., 1990, Cambrian extensional tectonics and magmatism within the Southern Oklahoma Aulacogen. Tectonophysics, 174, p. 147-157.

McLean, T. R., 1983, Structural style of the Wichita Mountains of southern Oklahoma. Unpublished M.S. thesis, University of Oklahoma, Norman, 94 p., 2 pl.

McLean, T. R., and Stearns, D. W., 1986, Hale Spring locality, *in* Gilbert, M. C., ed., Petrology of the Cambrian Wichita Mountains Igneous Suite. Oklahoma Geological Survey, Guidebook 23, p. 172-178.

Merritt, C.A., 1965, Mt. Scott Granite, Wichita Mountains, Oklahoma. Oklahoma Geology Notes, v. 25, p. 263-272.

Merritt, C.A., 1966, Rim albite in coarse-grained Quanah Granite, Wichita Mountains, Oklahoma. Oklahoma Geology Notes, 26, p. 211-213.

Merritt, C.A., 1967, Names and relative ages of granites and rhyolites in the Wichita Mountains, Oklahoma. Oklahoma Geology Notes, 27, p. 45-53.

Miser, H. D., 1954, Geologic map of Oklahoma. U.S. Geological Survey and Oklahoma Geological Survey, scale 1:500,00.

Myers, J. D., Gilbert, M. C., and Loiselle, M. C., 1981, Geochemistry of the Cambrian Wichita Granite Group and revisions of its lithostratigraphy. Oklahoma Geology Notes, 41, p. 172-195.

Powell, B. N., 1986, The raggedy mountain gabbro group, *in* Gilbert, M. C., ed., Petrology of the Cambrian Wichita Mountains Igneous Suite. Oklahoma Geological Survey, Guidebook 23, p. 21-52.

Powell, B. N., Gilbert, M. C., and Fischer, J. F., 1980a, Lithostratigraphic classification of basement rocks of the Wichita province, Oklahoma. Geological Society of America Bulletin Part I, 91, p. 509-514.

Powell, B. N., Gilbert, M. C., and Fischer, J. F., 1980b, Lithostratigraphic classification of basement rocks of the Wichita province, Oklahoma. Geological Society of America Bulletin Part II, 91, p. 1875-1994.

Price, J. D., Hogan, J. P., and Gilbert, M. C., 1996a, Rapakivi texture in the Mount Scott Granite, Wichita Mountains, Oklahoma. European Journal of Mineralogy, 8, p. 435-451.

Price, J. D., Hogan, J. P., and Gilbert, M. C., 1996b, Investigation of Late Diabase Dikes at Lake Elmer Thomas, Wichita Mountains, Oklahoma. Geological Society of America, Abstracts with Programs, 28, n. 1, p.59.

Price, J. D., Hogan, J. P., and Gilbert, M. C., 1997, Plutonic relationships within the Eastern Wichita Mountains, Oklahoma. Geological Society of America, Abstracts With Programs, 29, n. 2, p. 43.

Price, J. D., Hogan, J. P., Gilbert, M. C., and Denison, R. E., 1998a, Field guide to the basement rocks of the Southern Oklahoma Aulacogen. South Central Meeting of the Geological Society of America, 76 p.

Price, J. D., Hogan, J. P., Gilbert, M. C., and Payne, J. D., 1998b, Surface and near-surface investigation of the alteration of the Mount Scott Granite and geometry of the Sandy Creek Gabbro pluton, Hale Spring Area, Wichita Mountains, Oklahoma. Basement Tectonics, 12, p. 79-122.

Scofield, N., and Gilbert, M. C., 1982, Alkali amphiboles of the Wichita Mountains, *in* Gilbert, M. C., and Donovan, R. N., eds., Geology of the Eastern Wichita Mountains Southwestern Oklahoma. Oklahoma Geological Survey, Guidebook 21, p. 60-64.

Schoonover, F. E., 1948, The igneous rocks of the Fort Sill Reservation, Oklahoma: University of Oklahoma, Unpublished M.S. Thesis, 123 p.

Sides, J. R., and Miller, J. R., 1982, Geologic map for stops four and eight, *in* Gilbert, M. C., and Donovan, R. N., eds., Geology of the Eastern Wichita Mountains Southwestern Oklahoma. Oklahoma Geological Survey, Guidebook 21, p. 40-46.

Spencer, A. B., 1961, Geology of the basic rocks of the eastern portion of the Raggedy Mountains, southwestern Oklahoma. University of Oklahoma, unpublished M.S. Thesis, 46 p.

Stockton, M. L., 1984, Geology of the gabbroic rocks in southern Cooperton Quadrangle and north Odetta Quadrangle, Oklahoma. University of Texas, Arlington, unpublished M.S. Thesis, 83 p.

Stone, W. B., 1977, Mineralogic and textural dispersal patterns with the Permian Post Oak Formation of Southwestern Oklahoma. University of Oklahoma, unpublished M.S. Thesis, 117 p.

Taff, J. A., 1904, Preliminary report on the geology of the Arbuckle and Wichita Mountains in Indian Territory and Oklahoma. U.S. Geological Survey, Professional Paper 31, 97 p.

Taylor, C. H., 1915, Granites of Oklahoma. Oklahoma Geological Survey Bulletin, 20, 108 p.

Turcotte, D. L.; and Schubert, G., 1982, Geodynamics, Applications of continuum physics to geological problems. John Wiley & Sons, New York, 450 p.

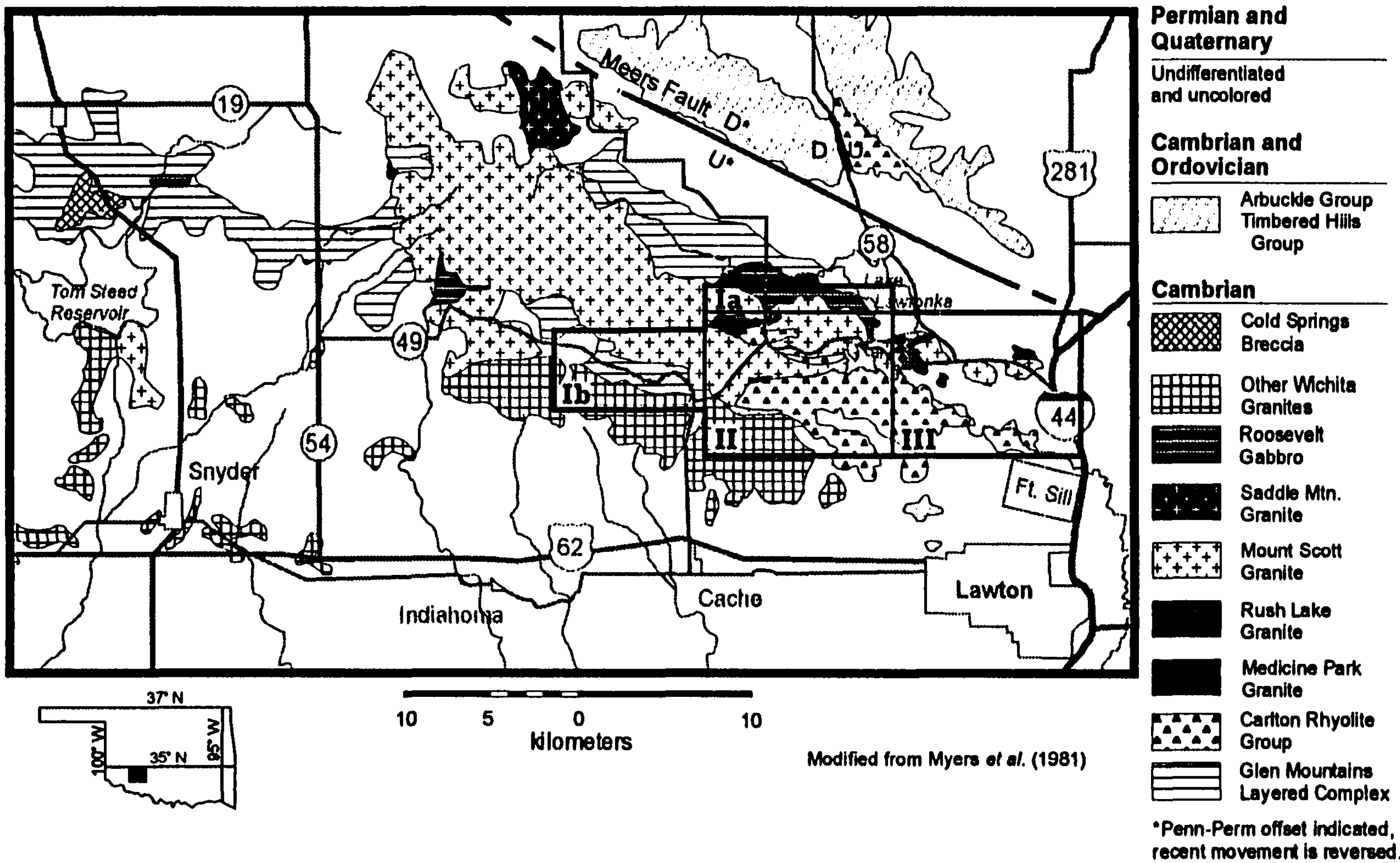

Figure 6-1. Geologic map of the eastern Wichita Mountains, Oklahoma with the mapped area outlined with a bold line. Individual map plates boundaries are marked with a thinner line and enumerated.

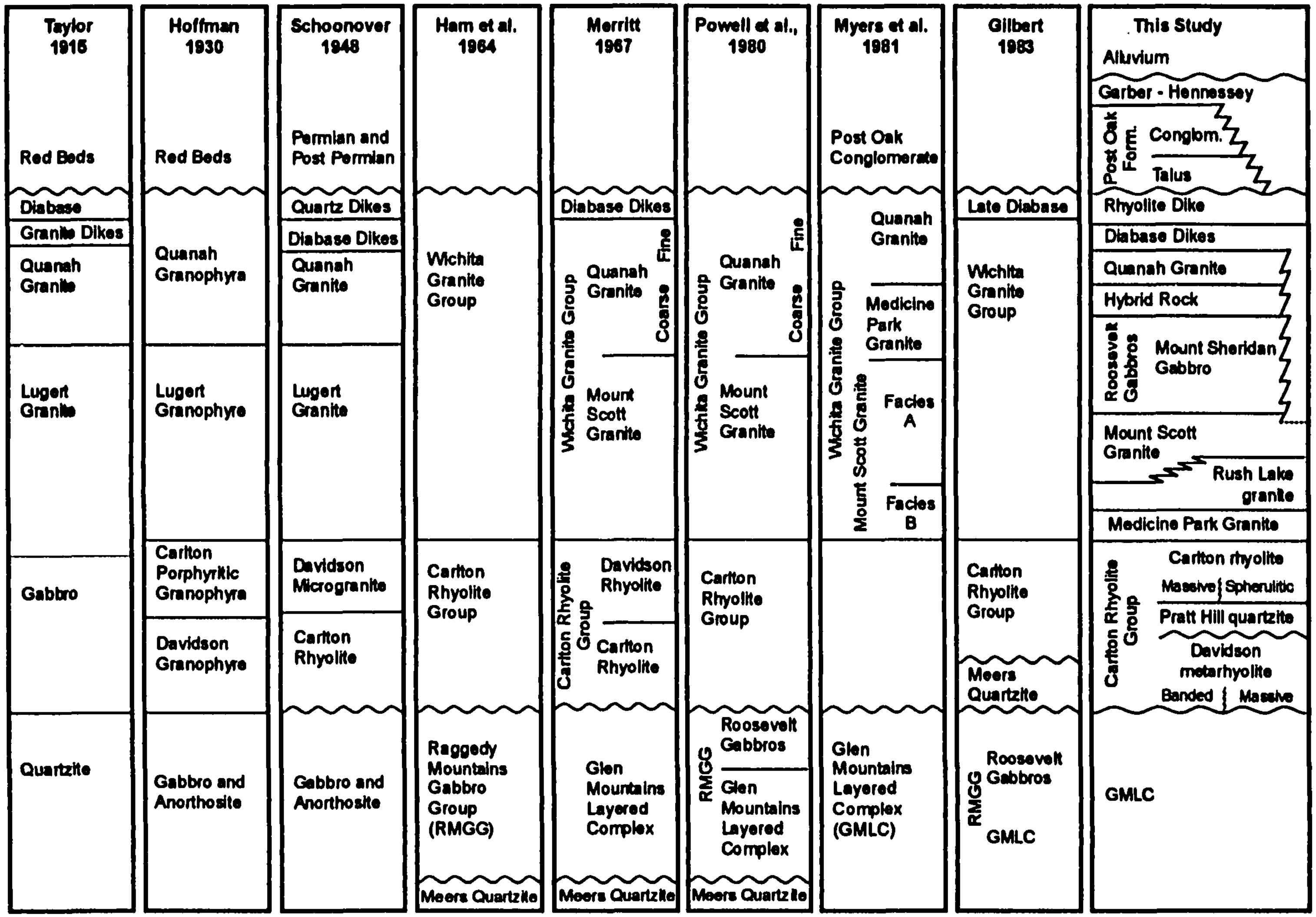

Figure 6-2. Chronostratigraphic correlation chart for the eastern Wichita Mountains showing the units within the mapped area in comparison to previous research. Taylor (1915) did not attempt to assign relative ages, only name units; assignment to chronostratigraphy was provided by the author.

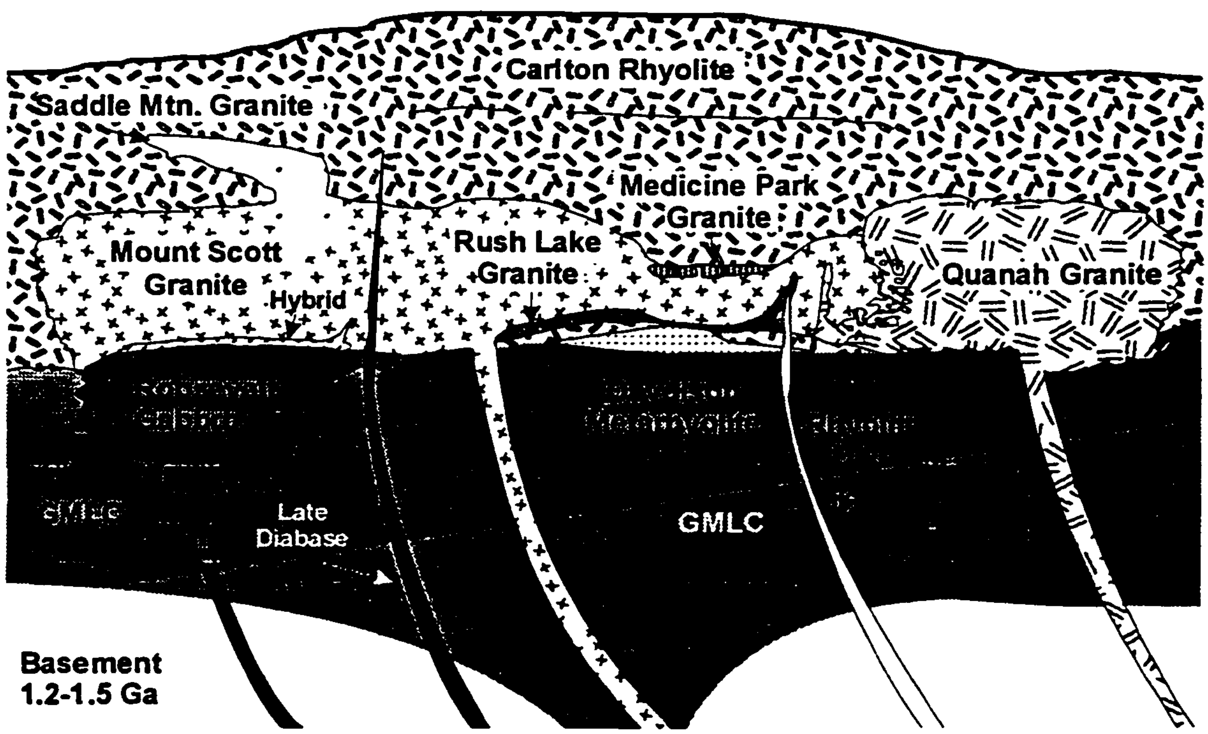

modified from Myers *et al.*, 1981

Figure 6-3. Schematic stratigraphic cross-section through the eastern Wichita Igneous Province illustrating the Cambrian contact relationships between the observed units within the mapping area.

Table 6-1. Representative locations of units described in Chapter 6.

#	Location	Map Plate	Township and Range Quater	S	T	R	UTM** Northing	Easting	Contacts**
Glen Mountains Layered Complex (GMLC)									
➲ 1	Camp Doris	I	NE NW NW SW	23	3N	14W	3841480	532240	Qc
2	Panther Creek	I	NE NE NW NE	21	3N	14W	3842250	530030	
3	Central Peak	II	SE SE NE NW	18	3N	13W	3843680	536050	MSC
Davidson Metarhyolite, Banded (Db)									
➲ 4	E. L Medicine Crk	II	SE NE SW NW	14	3N	13W	3843420	542040	MSC, POc
5	Hideaway	II	NW NW SE NE	23	3N	13W	3843420	542040	MSC
6	W L. Medicine Crk	II	SW SW NE SW	15	3N	13W	3842860	540580	CRm
7	W L. Medicne Creek	II	SE SE SW NE	15	3N	13W	3843250	539700	MSC
Davidson Metarhyolite, Massive (Dm)									
➲ 8	Holy City	II	SE NE SW SE	8	3N	13W	3844310	538000	RL, POc
9	Quetone Overlook	II	NW NW SW NW	15	3N	13W	3843510	540150	MSC, RL
10	Fish Hatchery	III	NE NE NE NE	19	3N	13W	3842350	546360	RL, CRm
11	W of Thomas Pt.	II	NE SW NE NE	22	3N	13W	3841030	541380	MSC, CRm
12	Elmer Thomas Lake	II	SE NE SE NE	14	3N	13W	3843470	543260	MSC
13	Rush Lake Dam	II	SW SW SW SE	7	3N	13W	3844020	536150	RL, MSC
Pratt Hill Quartzite (PH)									
➲ 14	Pratt Hill	II	SE SE NW NW	24	3N	13W	3842040	543610	Db, CRm
Carlton Rhyolite, Massive (Cm)									
➲ 15	Medicine Bluffs	III	Old Fort Sill				3838250	553250	
16	Mt. Scott Picnic Area	II	NE SE SE NE	15	3N	13W	3843350	541650	MSC, Db
17	Quetone Overlook	II	C NE NE SE	16	3N	13W	3843180	539900	MSC
Carlton Rhyolite, Spherulitic (Cs)									
➲ 18	Jones Ridge	III	NE NE SW NE	26	3N	13W	3840450	542850	
Medicine Park Granite (MP)									
➲ 19	Lake Lawtonka	III	SW NW NE NE	18	3N	12W	3843940	546050	
20	Contact w/ MSC	III	NW SE NW NW	17	3N	12W	3843800	547720	MSC
Rush Lake granite (RL)									
➲ 21	Rush Lake	II	SE SE SW SE	7	3N	13W	3844030	536380	MSC, Dm
22	Fish Hatchery	III	SW SW NW NW	20	3N	12W	3842250	546500	Dm, RL,RD
Mount Scott Granite (MSC)									
➲ 23	Mount Scott	II	SE NE NW SE	11	3N	12W	3844600	542870	
24	Hwy. 49 Roadcut	III	SE SE SW NE	15	13 N	13W	3843200	541200	Db, CRm
25	Rush Lake Quarry	II	NE SW SW SE	7	3N	13W	3844100	536200	
26	Mt. Cummins	III	SW SE NE NW	17	3N	12W	3843750	547130	
27	Big Rock Estates	III	SW SW NW NW	17	3N	12W	3843720	546520	MP
28	Welsh Hill	III	NE SE SE SW	13	3N	12W	3842570	553620	MSC
Mount Sheridan Gabbro (MSH)									
➲ 29	Little Mt. Sheridan	Ia	SE SW NE SE	5	3N	13W	3846100	538250	
30	Wall Mountain	Ia	NE NE NE SE	4	3N	13W	3846500	539900	

Table 6-1. Continued

#	Location		Township and Range Quarter	S	T	R	UTM* Northing	Easting	Contacts**
Hybrid rock (Hy)									
➲ 31	Poko Mtn.	Ia	SW SW SE NW	6	3N	13W	3846425	535700	MSC, MSH
32	Mount Scott	II	SW NE SE SW	12	3N	13W	3844220	543980	MSC, MSH
Quanah Granite, Coarse (Qc)									
➲ 33	Lost Lake Road	Ib	C E W SE	21	3N	14W	3841175	529940	
34	Ketch Lake	II	NE SW SW NW	29	3N	13W	3840140	537000	MSC
Quanah Granite, Fine (Qf)									
35	Cross Mtn	II	SE SE NW NW	32	3N	13W	3838840	537180	
36	French Lake	Ib	NW SE SE NW	21	3N	14W	3841750	529440	GMLC
Quanah Dikes (Qd)									
37	West Burford	Ib	SW SW NW NE	15	3N	14W	3842230	529680	GMLC
38	East Burford	Ib	SW SW NE NE	15	3N	14W	3842080	530070	GMLC
Diabase Dikes (DD)									
➲ 39	Elmer Thomas Lk.	II	SW SW NE SE	13	3N	13W	3842850	544540	MSC
40	Rush Lake Dam	II	NW NW NW NE	18	3N	13W	3843950	536130	MSC
41	Wall Mountain	II	S NW SW NE	9	3N	13W	3845030	539280	MSC
Post Oak Fm., Talus (POt)									
➲ 42	Mount Scott	II	SW NW NW NE	14	3N	13W	3843850	542500	MSC
Post Oak Fm., Conglomerate (POc)									
➲ 43	Quetone overlook	II	SW SW SE NE	16	3N	13W	3843250	539700	MSC
44	Medicine Creek	II	NE NW NW SW	20	3N	12W	3841510	546650	CRm
45	Brushy Creek	III	SW SW NW SW	29	3N	12W	3839630	546500	CRm

➲ Type locality for the area in Plates I, II, and III

* 1000 m Universal Transverse Mercator Grid, Zone 14, North American Datum, 1927

** Contacted lithologies in the vicinity of the specified location.

Appendix 1. Averaged available data for the Mount Scott Granite and adjacent felsic units.

This appendix presents compositional data for the felsic rocks of the eastern Wichita Mountains. The data presented here is a newly compiled average of all the available data on the each sample site.

Appendix 1. Averaged available data for the Mount Scott Granite and adjacent felsic units.

SAMPLE	SiO_2	TiO_2	Al_2O_3	Fe_2O_3	MnO	MgO	CaO	Na_2O	K_2O	P_2O_5	LOI	F	Cl	Br	I	Ba
Wichita Granite Group																
Aplites																
WO62B	77.6	0.21	11.4	2.04	0.05	0.15	0.56	3.47	4.11	0.03						1100
Medicine Park Granite																
W017	75.6	0.24	11.9	2.35	0.03	0.05	0.45	3.84	4.61	0.02						1029
JPMS71297		0.21			0.02											1075
JPMS90297		0.19			0.01											1135
Rush Lake granite																
JPMS0197	75.8	0.15	11.6	1.87	0.02	0.06	0.28	3.76	5.07	0.02	0.64	1370	bd	9	bd	664
JPMS0497	73.0	0.33	12.1	2.76	0.03	0.26	0.63	4.46	4.27	0.06	0.85	2570	bd	8	bd	977
JPMS71097		0.30			0.02											950
Mount Scott Granite																
W998	73.3	0.41	12.5	3.40	0.09	0.32	1.03	3.97	4.30	0.07						1158
W738	72.8	0.47	12.5	3.72	0.09	0.29	1.29	3.96	4.17	0.08						1169
W7248	73.1	0.42	12.4	3.70	0.08	0.41	1.09	4.30	4.21	0.07						1126
W78	72.6	0.45	12.4	3.98	0.09	0.35	1.25	3.74	4.27	0.08						1168
W992	72.4	0.47	12.4	3.93	0.10	0.33	1.18	3.99	4.20	0.09						1240
SQ	73.1	0.42	12.3	3.59	0.09	0.34	1.26	3.86	4.30	0.08	0.18	1785	bd	7	bd	1145
196 (Mt.S)	72.0	0.47	12.7	2.49	0.09	0.39	1.43	3.90	4.25							1000
JPMS90197		0.44			0.08											1035
SQ1-123A	73.0	0.36	11.8	3.60	0.08	0.32	1.27	3.80	4.19	0.08	0.24	1870	bd	8	bd	1050

Appendix 1. Averaged available data for the Mount Scott Granite and adjacent felsic units.

SAMPLE	SiO_2	TiO_2	Al_2O_3	Fe_2O_3	MnO	MgO	CaO	Na_2O	K_2O	P_2O_5	LOI	F	Cl	Br	I	Ba
Saddle Mountain Granite																
W060	71.6	0.50	12.6	4.17	0.09	0.35	1.17	4.10	4.20	0.08						1212
W055	72.1	0.49	12.6	4.25	0.10	0.43	1.21	3.55	4.32	0.08						1175
W7125	74.6	0.40	12.5	3.24	0.06	0.35	0.95	3.21	4.53	0.06						1020
Quanah Granite																
W986	75.5	0.15	12.1	1.99	0.04	0.04	0.35	4.09	4.72	0.01						81
W984	75.7	0.21	11.8	2.56	0.02	0.05	0.13	3.72	4.79	0.03						261
Carlton Rhyolite Group																
Davidson Metarhyolite																
W967	75.5	0.29	11.9	3.62	0.05	0.05	0.18	3.72	3.80	0.02						871
W776	69.9	0.42	17.5	3.42	0.13	0.70	0.11	0.68	4.68	0.04						2593
JPMS2596	76.3	0.28	11.4	2.13	0.02	0.02	0.22	3.29	4.46	0.02	0.73	430	2294	6	4	1160
Rhyolite xenoliths																
JH-6-91	76.1	0.18	12.2	2.50	0.04	0.20	0.33	3.99	4.71	0.01						822
JH-4-91	76.6	0.19	12.3	2.53	0.03	0.20	0.24	3.81	4.72	0.01						156
Carlton Rhyolite																
#5028	76.4	0.24	11.7	2.70	0.06	0.11	0.28	3.62	4.45	0.02						1653
W029	74.2	0.33	12.8	3.48	0.02	0.08	0.15	3.90	4.14	0.03						2216
#5022	74.7	0.29	12.7	3.27	0.03	0.49	0.42	3.63	4.63	0.04						893
#5025	80.1	0.27	12.0	3.76	0.01	0.26	0.12	0.20	4.09	0.04						68
W994	72.7	0.59	13.0	4.78	0.10	0.55	0.92	3.22	3.90	0.11						1903
W069	75.2	0.27	12.0	2.33	0.04	0.06	0.27	3.21	5.54	0.02						2379
Rhyolite Dikes																
W71	76.6	0.13	12.0	2.19	0.01	0.05	0.07	4.10	4.30	0.01						110
WO62A	76.2	0.23	11.5	2.45	0.05	0.05	0.41	3.60	4.56	0.02						1600

Appendix 1. Averaged available data for the Mount Scott Granite and adjacent felsic units.

SAMPLE	Rb	Nb	Ta	Sr	Zr	Y	Sc	Cr	Ni	V	Cu	Zn	La	Ce	Pr	Nd	Pm*	Sm	Eu	Gd	Tb
Wichita Granite Group																					
Aplites																					
WO62B	132	99		50	480	110		22													
Medicine Park Granite																					
W017	148	85	8	40	478	111		13	4	2	5	48	96	184		93		20	3		3
JPMS71297	153	96		44	597	102	4	1		4			79	174		93					
JPMS90297	136	71		38	354	65	3	2		3			73	140		79					
Rush Lake granite																					
JPMS0197	163	101	9	17	344	81	2	-5	bd	-3	22	71	91	201	21	91		18	1	18	3
JPMS0497	140	82	7	57	534	76	5	6	11	16	-10	99	78	172	19	84		17	3	18	3
JPMS71097	157	82		45	524	74		2					62	119		70					
Mount Scott Granite																					
W998	132	92	8	91	577	110	5	9			9	116	87	187		99		21	4		3
W738	126	88		104	535	113		9			10	133	93								
W7248	135	93	8	90	511	109	5	11			10	148	89	188		93		20	4		3
W78	119	88	8	99	522	114	6	9			9	101	89	195		103		22	4		3
W992	129	91	8	104	561	113		10			8	136	94	212		100		23	4		3
SQ	138	93	8	98	549	107	5	3	bd	10	16	132	89	195	21	98		21	4	21	3
196 (Mt.S)	100																				
JPMS90197	149	87		94	575	97		4					80	167		92					
SQ1-94							4	2		11			94	199		103					
SQ1-123A	140	88		95	517	102	5	-3	24	10	13	138	89	191	21	93		21	4	21	3

Appendix 1. Averaged available data for the Mount Scott Granite and adjacent felsic units.

	Rb	Nb	Ta	Sr	Zr	Y	Sc	Cr	Ni	V	Cu	Zn	La	Ce	Pr	Nd	Pm*	Sm	Eu	Gd	Tb
Saddle Mountain Granite																					
W060	129	77		120	605	110		11	5	8	10	78	99								
W055	138	76		111	606	103		10	5	8	11	114	89								
W7125	143	89	8	82	571	108		2	6	8	6	91	87	189		91		20	3		3
Quanah Granite																					
W986	166	128	11	5	468	169		11	5	2	2	220	66	172		91		27	1		5
W984	185	97	9	19	582	93	1	10	5	2	4	55	92	248		94		20	2		3
Carlton Rhyolite Group																					
Davidson Metarhyolite																					
W967	102	85		33	715	105		11	4	2	2	92	65								
W776	241	117		11	1028	142		9	6	2	6	148	134								
JPMS2596	126	83	7	30	705	64	2	30	12	1	11	200	48	111	12	52		11	3	10	2
Rhyolite xenoliths																					
JH-6-91	153	83	7	12	672	108	0	2	0	2	0	128	89	199		103		23	4		3
JH-4-91	158	80	7	10	721	101	1	2	0	1	0	105	90	197		99		21	2		3
Carlton Rhyolite																					
#5028	103	63		31	617	93		2	5	2	8	106	83								
W029	120	66		62	721	113		12	5	2	4	49	131								
#5022	99	94		17	759	86		2	3	2	4	54	99								
#5025	105	84		8	628	63		2	5	7	4	10	82								
W994	103	62		103	695	87		2	4	26	11	148	72								
W069	139	61		31	647	98		10	3	2	23	69	105								
Rhyolite Dikes																					
W71	167	58		7	319	89		11	6	2	4	91	58								
WO62A	129	58		16	560	85		19													

Appendix 1. Averaged available data for the Mount Scott Granite and adjacent felsic units.

SAMPLE	Dy	Ho	Er	Tm	Yb	Lu	Hf	Th	Pb	U	Cs	Be	Mo	Ag	In	Sn	Sb	W	Tl	Bi	Co	Ga	Ge	As
Wichita Granite Group																								
Aplites																								
WO62B																								
Medicine Park Granite																								
W017					9	1	14	15	10															
JPMS71297																								
JPMS90297																								
Rush Lake granite																								
JPMS0197	16	3	9	1	9	1	12	17	16	4	3	5	3	bd	0	11	0		1	bd	111	26	2	bd
JPMS0497	14	3	9	1	9	1	16	15	7	3	1	3	4		0	12	0		1	bd	85	27	1	bd
JPMS71097																								
Mount Scott Granite																								
W998					10	1	19	14	16	3	2													
W738								13	18															
W7248					10	1	15	14	19	3	2													
W78					10	1	19	13	18	3	2													
W992					11	2	17	14	17															
SQ	19	4	12	2	10	2	18	13	17	4	4	5	4		0	9	0		1	bd	30	28	2	bd
196 (Mt.S)																								
JPMS90197																								
SQ1-89																								
SQ1-123A	19	4	11	2	10	2	17	14	15	4	4	5	3		0	10	0	19	1	bd	2	27	2	bd

Appendix 1. Averaged available data for the Mount Scott Granite and adjacent felsic units.

	Dy	Ho	Er	Tm	Yb	Lu	Hf	Th	Pb	U	Cs	Be	Mo	Ag	In	Sn	Sb	W	Tl	Bi	Co	Ga	Ge	As
Saddle Mountain Granite																								
W060								13	16															
W055								13	16															
W7125					10	2	16	15	11															
Quanah Granite																								
W986					14	2	21	7	10															
W984					9	1	19	14	10	3	2													
Carlton Rhyolite Group																								
Davidson Metarhyolite																								
W967								11	14															
W776								17	21															
JPMS2596	13	3	9	1	9	2	19	11	20	3	2	2	3		0	8	0		0	-0	87	29	1	bd
Rhyolite xenolith																								
JH-6-91					9	1	17	13	14	3	2													
JH-4-91					9	1	18	16	13	4	4													
Carlton Rhyolite																								
#5028								12	14															
W029								11	12															
#5022								14	7															
#5025								13	4															
W994								11	16															
W069								12	34															
Rhyolite Dikes																								
W71								16	5															
WO62A																								

Appendix 2. Table of averaged compositions of feldspars from Mount Scott Granite (by EMPA)

	Anorthoclase-K										Anorthoclase-N			
	SQ 1 114 3.1		SQ 3 19 2.1		SQ 1 287 1.1b		SQ1 287 3.1		SQ1 287 2.1		JH194.a 3.1		SQ 1 114 2.1	
pts	17		15		21		36		15		10		82	
	wt.%	STD	wt.%	STD	wt.%	STD	wt.%	STD	wt.%	STD	wt.%	STD	wt.%	STD
SiO_2	65.7	0.8	64.3	0.5	65.3	0.8	65.6	0.5	65.5	0.6	64.2	0.8	64.4	0.7
Al_2O_3	19.2	0.49	19.6	0.8	19.5	0.5	19.4	0.5	19.6	0.5	20.1	0.8	20.9	1.0
FeO	0.09	0.03	0.09	0.03	0.11	0.05	0.10	0.02	0.13	0.03	0.50	0.28	0.11	0.05
MgO	bd		bd		bd		bd		bd		bd		bd	
CaO	0.14	0.38	0.45	0.62	0.50	0.76	0.26	0.39	0.59	0.67	0.89	0.56	1.67	0.88
Na_2O	4.12	1.93	5.00	2.68	5.15	2.02	3.81	2.13	6.08	2.49	7.08	3.32	8.34	2.98
K_2O	10.9	2.8	9.4	4.0	9.3	2.7	10.8	3.3	7.8	3.6	5.6	5.0	3.7	4.8
BaO	0.27	0.06	0.97	0.42	0.36	0.10	0.48	0.14	0.30	0.11	0.37	0.30	0.42	0.49
P_2O_5	bd		bd		bd		bd		bd		bd		bd	
Total	100.5	0.83	99.7	0.41	100.3	0.83	100.5	0.65	100.0	0.67	98.8	0.31	99.5	0.50
Cations (8 oxygen)														
Si	2.98		2.94		2.89		2.97		2.95		2.87		2.89	
Al	1.02		1.05		1.10		1.04		1.04		1.13		1.10	
Fe	0.00		0.00		0.00		0.00		0.00		0.01		0.00	
Ca	0.01		0.02		0.08		0.01		0.03		0.12		0.08	
Na	0.36		0.44		0.71		0.33		0.53		0.70		0.73	
K	0.63		0.55		0.21		0.62		0.45		0.17		0.21	
Ba	0.00		0.02		0.01		0.01		0.01		0.01		0.01	
Feldspar Components (Mol. Fraction)														
Ab	0.36		0.44		0.71		0.35		0.53		0.71		0.71	
Or	0.63		0.54		0.21		0.64		0.44		0.17		0.21	
An	0.01		0.02		0.08		0.01		0.03		0.12		0.08	

bd - below detection
STD - standard deviation

Appendix 2. Table of averaged compositions of feldspars from Mount Scott Granite (by EMPA).

	Anorthoclase-N												Plag rim	
	SQ 3 19 1.1		SQ 3 19 1.1		JH194.a 1.1		JH194.a 2.1		JH194.a 4.1		JH194.a 5.1		SQ 1 114 1.1	
pts	55		68		28		34		10		42		58	
	wt.%	STD	wt.%	STD	wt.%	STD	wt.%	STD	wt.%	STD	wt.%	STD	wt.%	STD
SiO_2	65.2	0.7	65.2	0.4	64.0	0.7	64.3	0.9	62.9	0.6	64.6	0.9	64.0	0.7
Al_2O_3	21.1	1.03	21.3	1.0	21.3	0.9	21.1	1.1	21.8	1.2	20.8	1.1	22.1	0.4
FeO	0.10	0.02	0.14	0.05	0.27	0.11	0.25	0.09	0.35	0.14	0.36	0.22	0.12	0.06
MgO	bd		bd		bd		bd		bd		bd		bd	
CaO	1.76	0.87	1.88	0.84	2.44	0.95	2.07	0.97	3.10	1.22	1.59	1.00	2.80	0.41
Na_2O	8.30	2.88	8.90	2.42	8.04	1.81	8.45	2.09	8.21	1.93	7.71	2.64	10.06	0.33
K_2O	3.7	4.5	2.6	4.1	3.0	3.2	3.0	3.8	2.3	3.8	4.1	4.3	0.4	0.2
BaO	0.39	0.43	bd		0.36	0.31	0.25	0.28	0.16	0.18	0.30	0.30	bd	0.49
P_2O_5	bd		bd		bd		bd		bd		bd		bd	
Total	100.6	0.53	100.1	0.40	99.4	0.40	99.4	0.57	98.8	0.23	99.57	0.4	99.6	0.51
Cations (8 oxygen)														
Si	2.89		2.89		2.87		2.88		2.83		2.90		2.84	
Al	1.10		1.11		1.13		1.11		1.16		1.10		1.15	
Fe	0.00		0.01		0.01		0.01		0.01		0.01		0.00	
Ca	0.08		0.09		0.12		0.10		0.15		0.08		0.13	
Na	0.71		0.76		0.70		0.73		0.72		0.67		0.87	
K	0.21		0.15		0.17		0.17		0.13		0.23		0.02	
Ba	0.01		0.00		0.01		0.00		0.00		0.01		0.00	
Feldspar Components (Mol. Fraction)														
Ab	0.71		0.76		0.71		0.73		0.72		0.68		0.85	
Or	0.21		0.15		0.17		0.17		0.13		0.24		0.02	
An	0.08		0.09		0.12		0.10		0.15		0.08		0.13	

Appendix 2. Table of averaged compositions of feldspars from Mount Scott Granite (by EMPA).

	Plagioclase rim															
	SQ 1 114		SQ 1 114		SQ 3 19		SQ 3 19		SQ1 287		SQ1 287		SQ1 287		SQ 1 114	
	3.1		2.1		1.1		2.2		1.1		3.1		2.1		4.1.2 rim	
pts	58		21		31		28		24		29		29		81	
	wt.%	STD	wt.%	STD	wt.%	STD	wt.%	STD	wt.%	STD	wt.%	STD	wt.%	STD	wt.%	STD
SiO_2	65.3	0.6	63.5	0.6	64.7	0.7	64.0	0.7	65.1	0.9	65.4	0.7	64.7	0.9	65.2	0.9
Al_2O_3	21.9	0.35	21.9	0.4	22.3	0.5	22.5	0.5	22.1	0.5	22.2	0.5	22.4	0.7	21.9	0.6
FeO	0.12	0.05	0.11	0.02	0.10	0.02	0.10	0.02	0.06	0.05	0.13	0.05	0.11	0.04	0.11	0.01
MgO	bd		bd		bd		bd		bd		bd		bd		bd	
CaO	2.49	0.36	2.73	0.43	2.97	0.50	3.13	0.53	2.56	0.55	2.56	0.49	2.75	0.61	2.57	0.53
Na_2O	10.30	0.30	10.04	0.37	10.03	0.42	9.96	0.46	10.59	0.31	10.28	0.34	10.20	0.43	10.20	0.45
K_2O	0.3	0.1	0.4	0.1	0.4	0.1	0.4	0.2	0.1	0.0	0.2	0.0	0.3	0.2	0.4	0.2
BaO	bd		bd		bd		bd		bd		bd		bd		bd	
P_2O_5	bd		bd		bd		bd		bd		bd		bd		bd	
Total	100.5	0.46	98.8	0.19	100.6	0.31	100.2	0.33	100.5	0.49	100.87	0.7	100.49	0.5	100.47	0.44
Cations (8 oxygen)																
Si	2.86		2.84		2.84		2.83		2.86		2.86		2.84		2.87	
Al	1.13		1.16		1.15		1.17		1.14		1.14		1.16		1.13	
Fe	0.00		0.00		0.00		0.00		0.00		0.00		0.00		0.00	
Ca	0.12		0.13		0.14		0.15		0.12		0.12		0.13		0.12	
Na	0.88		0.87		0.85		0.85		0.90		0.87		0.87		0.87	
K	0.02		0.02		0.02		0.02		0.01		0.01		0.01		0.02	
Ba	0.00		0.00		0.00		0.00		0.00		0.00		0.00		0.00	
Feldspar Components (Mol. Fraction)																
Ab	0.87		0.85		0.84		0.84		0.88		0.87		0.86		0.86	
Or	0.02		0.02		0.02		0.02		0.01		0.01		0.01		0.02	
An	0.12		0.13		0.14		0.14		0.12		0.12		0.13		0.12	

Appendix 2. Table of averaged compositions of feldspars from Mount Scott Granite (by EMPA).

	Matrix alkali feldspar													
	SQ 3 19 6.1		JH194.a 2		JH194.g 1		JH194.g 7		SQ1 114 1.1		SQ 1 114 3.1		SQ1 114 2.1	
pts	61		18		7		10		32		19		20	81
	wt.%	STD	wt.%	STD	wt.%	STD	wt.%	STD	wt.%	STD	wt.%	STD	wt.%	STD
SiO_2	65.4	0.6	59.1	1.4	62.5	0.7	64.4	0.3	64.7	0.4	65.5	0.4	64.4	0.5
Al_2O_3	22.2	0.43	25.2	0.9	23.0	0.4	21.6	0.7	19.0	0.1	19.3	0.4	19.0	0.3
FeO	0.11	0.02	0.37	0.18	0.32	0.13	0.17	0.03	0.10	0.05	0.10	0.08	0.18	0.11
MgO	bd		bd		bd		bd		bd		bd		bd	bd
CaO	2.62	0.42	6.29	0.99	3.74	0.36	2.97	0.40	0.07	0.05	0.17	0.29	0.09	0.13
Na_2O	10.12	0.35	7.64	0.59	9.06	0.17	9.71	0.25	4.05	0.78	4.98	1.69	4.61	1.95
K_2O	0.4	0.2	0.2	0.0	0.4	0.1	0.3	0.0	11.0	1.0	9.8	2.5	10.3	2.6
BaO	bd		bd		0.13	0.02	bd		0.27	0.06	0.29	0.09	0.27	0.07
P_2O_5	bd		bd		bd		bd		bd		bd		bd	bd
Total	100.8	0.47	99.0	0.69	99.2	0.24	99.3	0.10	99.22	0.40	100.2	0.44	98.9	0.40
Cations (8 oxygen)														
Si	2.86		2.66		2.79		2.86		2.97		2.97		2.97	2.87
Al	1.14		1.34		1.21		1.13		1.03		1.03		1.03	1.13
Fe	0.00		0.01		0.01		0.01		0.00		0.00		0.01	0.00
Ca	0.12		0.30		0.18		0.14		0.00		0.01		0.00	0.12
Na	0.86		0.67		0.78		0.84		0.36		0.44		0.41	0.87
K	0.02		0.01		0.02		0.02		0.64		0.57		0.60	0.02
Ba	0.00		0.00		0.00		0.00		0.00		0.01		0.00	0.00
Feldspar Components (Mol. Fraction)														
Ab	0.86		0.68		0.80		0.84		0.36		0.43		0.40	
Or	0.02		0.01		0.02		0.02		0.64		0.56		0.59	
An	0.12		0.31		0.18		0.14		0.00		0.01		0.00	

Appendix 2. Table of averaged compositions of feldspars from Mount Scott Granite (by EMPA).

	Matrix alkali feldspar															
	SQ 3 19 1.1		SQ 3 19 1.2.1		SQ1 287 1.1		SQ1 287 2.1		SQ1 287 3.1		SQ1 287 1.1		SQ1 287 3.1		SQ1 287 4.1	
pts	38		31		13		20		10		41		50		20	
	wt.%	STD	wt.%	STD	wt.%	STD	wt.%	STD	wt.%	STD	wt.%	STD	wt.%	STD	wt.%	STD
SiO_2	64.8	0.8	65.0	0.9	66.2	0.6	64.9	0.8	66.1	0.8	65.0	0.6	65.9	0.5	65.4	0.5
Al_2O_3	19.0	0.34	19.8	1.0	19.4	0.3	19.0	0.2	19.2	0.2	19.1	0.2	19.1	0.3	18.9	0.2
FeO	0.09	0.03	0.10	0.03	0.08	0.01	0.12	0.06	0.12	0.07	0.14	0.05	0.13	0.05	0.12	0.04
MgO	bd		bd		bd		bd		bd		bd		bd		bd	
CaO	0.07	0.16	0.63	0.71	0.17	0.27	0.02	0.03	0.01	0.01	0.15	0.24	0.17	0.31	0.11	0.19
Na_2O	3.30	1.77	5.84	4.14	5.19	1.81	3.09	1.82	4.00	1.90	4.12	1.40	4.50	1.13	3.43	1.07
K_2O	12.1	2.5	8.3	6.0	9.4	2.6	12.3	2.5	10.5	2.8	11.0	1.9	10.4	1.7	12.0	1.5
BaO	0.37	0.09	0.25	0.19	0.28	0.06	0.31	0.06	0.31	0.08	0.25	0.05	0.26	0.07	0.29	0.05
P_2O_5	bd		bd		bd		bd		bd		bd		bd		bd	
Total	99.7	0.82	99.9	0.89	100.7	0.58	99.7	0.63	100.2	0.73	99.70	0.6	100.6	0.4	100.2	0.49
Cations (8 oxygen)																
Si	2.97		2.94		2.97		2.98		2.99		2.97		2.98		2.98	
Al	1.03		1.05		1.03		1.03		1.02		1.03		1.02		1.01	
Fe	0.00		0.00		0.00		0.00		0.00		0.01		0.00		0.00	
Ca	0.00		0.03		0.01		0.00		0.00		0.01		0.01		0.01	
Na	0.29		0.51		0.45		0.27		0.35		0.36		0.39		0.30	
K	0.71		0.48		0.54		0.72		0.61		0.64		0.60		0.70	
Ba	0.01		0.00		0.00		0.01		0.01		0.00		0.00		0.01	
Feldspar Components (Mol. Fraction)																
Ab	0.29		0.50		0.45		0.28		0.37		0.36		0.39		0.30	
Or	0.70		0.47		0.54		0.72		0.63		0.63		0.60		0.69	
An	0.00		0.03		0.01		0.00		0.00		0.01		0.01		0.01	

Appendix 2. Table of averaged compositions of feldspars from Mount Scott Granite (by EMPA).

	Matrix alkali feldspar															
	SQ1 287 5.1		SQ1 287 5.2		SQ1 287 7.2.1		SQ1 114 1.5		SQ1 114 3.1		SQ1 114 4.1		SQ1 114 5.2		SQ1 114 6.1.1	
pts	30		30		20		3		30		40		3		18	
	wt.%	STD	wt.%	STD	wt.%	STD	wt.%	STD	wt.%	STD	wt.%	STD	wt.%	STD	wt.%	STD
SiO_2	65.5	0.4	65.7	0.4	65.7	0.5	65.4	0.4	66.0	0.4	65.8	0.5	66.2	0.0	65.9	0.3
Al_2O_3	19.1	0.20	19.2	0.1	19.2	0.2	19.1	0.1	19.1	0.2	19.1	0.2	19.3	0.1	19.2	0.2
FeO	0.12	0.04	0.11	0.05	0.11	0.04	0.15	0.03	0.12	0.03	0.14	0.06	0.17	0.07	0.10	0.03
MgO	bd		bd		bd		bd		bd		bd		bd		bd	
CaO	0.14	0.07	0.12	0.11	0.09	0.09	0.09	0.06	0.11	0.07	0.10	0.12	0.17	0.07	0.14	0.09
Na_2O	4.67	0.85	4.61	0.41	4.40	0.93	3.58	0.76	4.60	0.59	4.26	0.95	4.51	0.27	4.71	0.53
K_2O	10.2	1.1	10.3	0.6	10.7	1.3	11.5	1.1	10.2	0.9	10.6	1.4	10.1	0.5	10.0	0.8
BaO	0.25	0.04	0.26	0.05	0.27	0.06	0.26	0.02	0.27	0.04	0.28	0.06	0.29	0.01	0.25	0.06
P_2O_5	bd		bd		bd		bd		bd		bd		bd		bd	
Total	99.9	0.29	100.3	0.38	100.5	0.56	100.1	0.37	100.4	0.40	100.32	0.3	100.7	0.3	100.3	0.45
Cations (8 oxygen)																
Si	2.98		2.98		2.98		2.98		2.98		2.98		2.98		2.98	
Al	1.02		1.02		1.02		1.03		1.02		1.02		1.02		1.02	
Fe	0.00		0.00		0.00		0.01		0.00		0.01		0.01		0.01	
Ca	0.01		0.01		0.00		0.00		0.01		0.00		0.01		0.01	
Na	0.41		0.40		0.39		0.32		0.40		0.37		0.39		0.39	
K	0.59		0.59		0.62		0.67		0.59		0.61		0.58		0.58	
Ba	0.00		0.00		0.00		0.00		0.00		0.01		0.01		0.01	
Feldspar Components (Mol. Fraction)																
Ab	0.41		0.40		0.38		0.32		0.41		0.38		0.40		0.40	
Or	0.58		0.59		0.61		0.68		0.59		0.62		0.59		0.59	
An	0.01		0.01		0.00		0.00		0.01		0.00		0.01		0.01	

Appendix 2. Table of averaged compositions of feldspars from Mount Scott Granite (by EMPA)

	Matrix alkali feldspar													
	SQ1 114		SQ3 19		SQ3 19		SQ3 19		SQ3 19		JH194.g		JH194.g	
	7.1.2		2.1		4.1		5.1		6.1.1		nr2		7	
pts	26		45		31		26		23		5		10	
	wt.%	STD	wt.%	STD	wt.%	STD	wt.%	STD	wt.%	STD	wt.%	STD	wt.%	STD
SiO_2	65.2	0.3	64.7	0.5	63.7	1.2	65.7	0.5	64.5	0.7	64.2	0.6	64.5	0.9
Al_2O_3	19.2	0.14	19.1	0.2	18.8	0.4	19.3	0.2	19.0	0.3	19.0	0.2	19.0	0.3
FeO	0.11	0.04	0.11	0.05	0.10	0.03	0.12	0.05	0.11	0.05	0.11	0.04	0.19	0.11
MgO	bd		bd		bd		bd		bd		bd		bd	
CaO	0.14	0.09	0.09	0.07	0.11	0.07	0.12	0.12	0.06	0.08	0.15	0.09	0.14	0.10
Na_2O	4.49	0.44	3.83	0.90	4.05	0.78	4.34	1.12	2.71	1.49	3.17	1.37	2.94	2.22
K_2O	10.3	0.6	11.3	1.3	10.4	1.2	10.7	1.6	12.8	2.3	11.9	2.1	12.3	3.1
BaO	0.28	0.05	0.24	0.05	0.25	0.06	0.25	0.07	0.32	0.07	0.24	0.06	0.28	0.06
P_2O_5	bd		bd		bd		bd		bd		bd		bd	
Total	99.8	0.30	99.4	0.48	97.5	2.05	100.5	0.40	99.6	0.34	98.72	0.1	99.3	0.5
Cations (8 oxygen)														
Si	2.97		2.97		2.97		2.97		2.97		2.97		2.97	
Al	1.03		1.03		1.03		1.03		1.03		1.04		1.03	
Fe	0.00		0.00		0.00		0.00		0.00		0.00		0.01	
Ca	0.01		0.01		0.01		0.01		0.00		0.01		0.01	
Na	0.40		0.40		0.37		0.38		0.24		0.28		0.26	
K	0.60		0.60		0.62		0.62		0.75		0.70		0.72	
Ba	0.00		0.00		0.00		0.00		0.01		0.00		0.01	
Feldspar Components (Mol. Fraction)														
Ab	0.40		0.40		0.37		0.38		0.24		0.29		0.27	
Or	0.60		0.60		0.63		0.61		0.75		0.71		0.73	
An	0.01		0.01		0.01		0.01		0.00		0.01		0.01	

Appendix 2. Table of averaged compositions of feldspars from Mount Scott Granite (by EMPA)

	Matrix plagioclase microphenocrysts															
	SQ1 287 1.p1		SQ1 287 1.p2		SQ1 287 2.p1		SQ1 287 2.p2		SQ1 287 3.p1		SQ1 287 3.p2		SQ1 287 3.p4		SQ1 287 3.p5	
pts	3		3		3		3		3		3		3		4	
	wt.%	STD	wt.%	STD	wt.%	STD	wt.%	STD	wt.%	STD	wt.%	STD	wt.%	STD		
SiO_2	65.9	1.1	65.1	0.4	65.7	1.2	63.8	0.8	65.2	0.4	65.6	0.7	64.4	1.3	65.5	0.6
Al_2O_3	21.5	0.14	21.4	0.2	21.2	0.3	21.5	0.4	21.1	0.3	21.4	0.2	21.5	0.1	20.9	1.4
FeO	0.15	0.15	0.02	0.00	0.11	0.02	0.10	0.02	0.14	0.02	0.11	0.01	0.19	0.09	0.12	0.02
MgO	bd		bd		bd		bd		bd		bd		bd		bd	
CaO	1.86	0.29	2.77	0.71	1.71	0.35	2.34	0.44	1.85	0.13	2.01	0.12	2.11	0.38	1.66	0.96
Na_2O	10.94	0.05	10.92	0.04	10.63	0.28	10.39	0.29	10.46	0.28	10.71	0.23	10.28	0.29	8.35	4.12
K_2O	0.1	0.0	0.1	0.0	0.4	0.1	0.2	0.0	0.4	0.2	0.3	0.2	0.8	0.4	3.9	6.5
BaO	bd		bd		bd		bd		bd		bd		bd		bd	
P_2O_5	bd		bd		bd		bd		bd		bd		bd		bd	
Total	100.5	0.75	100.4	0.19	99.7	0.81	98.4	0.24	99.2	0.50	100.16	1.1	99.3	0.8	100.4	0.64
Cations (8 oxygen)																
Si	2.89		2.87		2.90		2.86		2.90		2.89		2.87		2.90	
Al	1.11		1.11		1.10		1.14		1.10		1.11		1.13		1.09	
Fe	0.01		0.00		0.00		0.00		0.01		0.00		0.01		0.00	
Ca	0.09		0.13		0.08		0.11		0.09		0.09		0.10		0.08	
Na	0.93		0.93		0.91		0.90		0.90		0.91		0.89		0.72	
K	0.01		0.01		0.02		0.01		0.02		0.02		0.04		0.22	
Ba	0.00		0.00		0.00		0.00		0.00		0.00		0.00		0.00	
Feldspar Components (Mol. Fraction)																
Ab	0.91		0.87		0.90		0.88		0.89		0.89		0.86		0.71	
Or	0.01		0.01		0.02		0.01		0.02		0.02		0.04		0.22	
An	0.09		0.12		0.08		0.11		0.09		0.09		0.10		0.08	

Appendix 2. Table of averaged compositions of feldspars from Mount Scott Granite (by EMPA)

	Matrix plagioclase microphenocrysts															
	SQ1 287 4.p1		SQ1 287 4.p2		SQ1 287 5.p1		SQ1 287 6.p1		SQ1 287 7.p1		SQ1 287 7.p2		SQ1 287 7.p4		SQ1 114 2.p1	
pts	3		3		3		4		3		3		3		3	
	wt.%	STD	wt.%	STD	wt.%	STD	wt.%	STD	wt.%	STD	wt.%	STD	wt.%	STD		
SiO_2	67.0	1.8	67.0	1.8	66.6	1.0	64.8	0.4	65.3	0.2	65.4	0.3	65.6	0.3	65.2	0.9
Al_2O_3	20.9	0.67	20.9	0.7	20.9	0.6	22.2	0.0	21.6	0.0	21.6	0.1	21.4	0.4	22.0	0.3
FeO	0.13	0.03	0.13	0.03	0.15	0.05	0.12	0.01	0.10	0.00	0.11	0.01	0.17	0.04	0.10	0.01
MgO	bd		bd		bd		bd		bd		bd		bd		bd	
CaO	1.36	0.96	1.36	0.96	1.57	0.56	2.63	0.31	2.31	0.13	2.35	0.20	1.87	0.25	2.71	0.26
Na_2O	10.91	0.63	10.91	0.63	10.85	0.43	10.16	0.12	10.55	0.10	10.52	0.16	10.72	0.03	10.07	0.06
K_2O	0.2	0.0	0.2	0.0	0.3	0.2	0.3	0.2	0.3	0.1	0.2	0.0	0.2	0.0	0.6	0.1
BaO	bd		bd		bd		bd		bd		bd		bd		bd	
P_2O_5	bd		bd		bd		bd		bd		bd		bd		bd	
Total	100.6	0.78	100.6	0.78	100.4	0.17	100.2	0.54	100.2	0.17	100.28	0.2	99.9	0.7	100.7	0.65
Cations (8 oxygen)																
Si	2.93		2.93		2.92		2.85		2.88		2.88		2.89		2.86	
Al	1.08		1.08		1.08		1.15		1.12		1.12		1.11		1.13	
Fe	0.00		0.00		0.01		0.00		0.00		0.00		0.01		0.00	
Ca	0.06		0.06		0.07		0.12		0.11		0.11		0.09		0.13	
Na	0.92		0.92		0.92		0.87		0.90		0.90		0.91		0.86	
K	0.01		0.01		0.01		0.01		0.02		0.01		0.01		0.03	
Ba	0.00		0.00		0.00		0.00		0.00		0.00		0.00		0.00	
Feldspar Components (Mol. Fraction)																
Ab	0.92		0.92		0.91		0.86		0.88		0.88		0.90		0.84	
Or	0.01		0.01		0.01		0.01		0.02		0.01		0.01		0.03	
An	0.06		0.06		0.07		0.12		0.11		0.11		0.09		0.13	

Appendix 2. Table of averaged compositions of feldspars from Mount Scott Granite (by EMPA)

	Matrix plagioclase microphenocrysts															
	SQ1 114 3.p1		SQ1 114 4.p1.1		SQ1 114 5.p1		SQ1 114 5.p2		SQ1 114 6.p1		SQ3 19 2.p1.1		SQ3 19 2.1.3		SQ3 19 1.p1	
pts	2		10		3		3		40		30		20		4	
	wt.%	STD	wt.%	STD	wt.%	STD	wt.%	STD	wt.%	STD	wt.%	STD	wt.%	STD		
SiO_2	64.9	1.3	65.6	0.3	66.2	0.3	66.9	0.2	64.9	0.6	65.2	0.7	65.1	0.4	65.5	0.5
Al_2O_3	22.4	0.86	21.5	0.1	21.5	0.0	21.1	0.2	21.8	0.6	21.4	0.5	21.7	0.3	21.9	0.1
FeO	0.12	0.00	0.11	0.02	0.13	0.02	0.12	0.01	0.10	0.02	0.11	0.03	0.12	0.02	0.10	0.01
MgO	bd		bd		bd		bd		bd		bd		bd		bd	
CaO	2.92	0.83	2.20	0.15	1.99	0.12	1.56	0.16	2.58	0.56	1.83	0.56	2.24	0.21	2.38	0.06
Na_2O	10.03	0.71	10.37	0.14	10.68	0.05	10.87	0.30	9.78	1.21	10.55	0.37	10.22	0.25	10.05	0.16
K_2O	0.4	0.1	0.5	0.2	0.3	0.1	0.3	0.2	0.9	1.7	0.3	0.4	0.5	0.2	0.5	0.2
BaO	bd		bd		bd		bd		bd		bd		bd		bd	
P_2O_5	bd		bd		bd		bd		bd		bd		bd		bd	
Total	100.7	0.16	100.3	0.31	100.8	0.24	100.9	0.48	100.3	0.57	99.46	0.4	100.0	0.4	100.5	0.57
Cations (8 oxygen)																
Si	2.84		2.88		2.89		2.92		2.86		2.89		2.87		2.87	
Al	1.16		1.11		1.10		1.08		1.13		1.12		1.13		1.13	
Fe	0.00		0.00		0.00		0.00		0.00		0.00		0.00		0.00	
Ca	0.14		0.10		0.09		0.07		0.12		0.09		0.11		0.11	
Na	0.85		0.88		0.90		0.92		0.84		0.91		0.87		0.85	
K	0.02		0.03		0.01		0.02		0.05		0.02		0.03		0.03	
Ba	0.00		0.00		0.00		0.00		0.00		0.00		0.00		0.00	
Feldspar Components (Mol. Fraction)																
Ab	0.84		0.87		0.89		0.91		0.83		0.90		0.87		0.86	
Or	0.02		0.03		0.01		0.02		0.05		0.02		0.03		0.03	
An	0.14		0.10		0.09		0.07		0.12		0.09		0.10		0.11	

Appendix 2. Table of averaged compositions of feldspars from Mount Scott Granite (by EMPA)

	Matrix plagioclase microphenocrysts					
	SQ3 19 3.1		SQ3 19 4.1.3		SQ3 19 6.1.2	
pts	15		20		41	
	wt.%	STD	wt.%	STD	wt.%	STD
SiO_2	65.8	0.4	65.3	0.4	65.9	0.7
Al_2O_3	21.7	0.59	19.1	0.2	21.5	0.7
FeO	0.12	0.02	0.11	0.02	0.12	0.02
MgO	bd		bd		bd	
CaO	2.14	0.48	0.07	0.03	1.88	0.56
Na_2O	9.99	1.27	3.82	0.73	9.98	2.09
K_2O	1.0	1.9	11.4	1.0	1.1	3.2
BaO	bd		0.29	0.05	bd	
P_2O_5	bd		bd		bd	
Total	100.7	0.27	100.1	0.57	100.7	0.75
Cations (8 oxygen)						
Si	2.88		2.97		2.89	
Al	1.12		1.02		1.11	
Fe	0.00		0.00		0.00	
Ca	0.10		0.00		0.09	
Na	0.85		0.34		0.85	
K	0.05		0.66		0.06	
Ba	0.00		0.01		0.00	
Feldspar Components (Mol. Fraction)						
Ab	0.85		0.34		0.85	
Or	0.05		0.66		0.06	
An	0.10		0.00		0.09	

Appendix 3a. Magnetic susceptibility and fracture density data for the SQ-1 drill hole core.

Depth	Magnetic Susceptibility	Standard Deviation	Fracture Density	
			Complete	Incomp.
(m)	(SI mass)	(SI mass)	(Cm^{-1})	(Cm^{-1})
0.00				
0.15				
0.31				
0.46				
0.61				
0.76				
0.92	1.19E-04	5.16E-06	0.07	0.00
1.07	1.08E-04	1.21E-05	0.07	0.07
1.22	1.16E-04	1.39E-05	0.07	0.00
1.37	1.15E-04	1.23E-05	0.66	0.98
1.53	1.03E-04	8.16E-06	0.66	1.05
1.68	8.52E-05	8.56E-06	0.66	0.79
1.83	8.00E-05	4.47E-06	0.20	0.66
2.14	5.51E-05	1.29E-05	0.59	0.79
2.29	7.36E-05	9.91E-06	0.26	0.66
2.44	8.52E-05	9.31E-06	0.13	0.98
2.59	8.95E-05	6.44E-06	0.13	0.72
2.75	2.68E-04	1.22E-04	0.13	0.98
2.90	2.81E-04	1.10E-04	0.13	0.79
3.05	1.45E-04	4.19E-05	0.07	0.00
3.20	1.05E-04	5.63E-06	0.20	0.07
3.36	1.77E-04	4.06E-05	0.07	0.39
3.51	1.61E-04	2.23E-05	0.07	0.46
3.66	1.20E-04	1.77E-05	0.07	0.33
3.81	8.00E-05	1.48E-05	0.26	0.98
3.97	6.32E-05	7.64E-06	0.07	0.52
4.12	1.24E-04	6.32E-06	0.13	0.33
4.42	8.52E-05	1.29E-05	0.13	0.13
4.58	1.05E-04	3.15E-05	0.20	0.52
4.73	3.75E-04	1.51E-04	0.07	0.07
5.19	1.28E-04	9.22E-06	0.00	0.07
0.00	1.30E-04	1.18E-05	0.07	0.79
5.34	1.39E-04	8.16E-06	0.13	0.39
5.49	1.38E-04	6.71E-06	0.20	0.26
5.64	1.72E-04	1.48E-05	0.07	0.07
5.80	2.09E-04	5.08E-05	0.13	0.00
5.95	1.50E-04	1.46E-05	0.13	0.00
6.10	1.85E-04	8.78E-06	0.00	0.00
6.25	1.62E-04	2.32E-05	0.00	0.00
6.41	1.03E-04	1.21E-05	0.07	0.07
6.56	1.61E-04	4.45E-05	0.00	0.13
6.71	1.66E-04	1.88E-05	0.20	0.39
6.86	1.70E-04	2.22E-05	0.07	0.13
7.02	3.59E-04	8.10E-05	0.07	0.13
7.17	2.18E-04	1.38E-05	0.00	0.20

Appendix 3a. SQ-1 drill hole core.

Depth (m)	Magnetic Susceptibility (SI mass)	Standard Deviation (SI mass)	Fracture Density Complete (Cm^{-1})	Incomp. (Cm^{-1})
7.32	3.42E-04	6.51E-05	0.00	0.00
7.47	3.32E-04	1.18E-05	0.07	0.00
7.63	3.08E-04	4.74E-05	0.00	0.00
0.00	2.67E-04	5.86E-05	0.00	0.20
7.93	1.72E-04	1.57E-05	0.00	0.20
8.08	2.14E-04	1.60E-04	0.07	0.07
8.24	2.39E-04	1.70E-05	0.33	0.52
8.39	4.81E-04	5.93E-05	0.07	0.26
8.54	3.28E-04	3.28E-05	0.07	0.00
8.69	4.13E-04	6.90E-05	0.13	0.00
8.85	4.17E-04	1.34E-05	0.00	0.00
9.00	3.64E-04	1.65E-05	0.33	0.00
9.15	3.56E-04	3.94E-05	0.07	0.07
9.30	2.97E-04	1.16E-04	0.07	0.00
9.46	6.14E-04	3.25E-05	0.07	0.00
9.61	7.40E-04	6.55E-05	0.07	0.00
9.76	3.16E-04	4.75E-05	0.07	0.00
9.91	4.08E-04	2.63E-05	0.07	0.00
10.07	4.80E-04	4.49E-05	0.07	0.00
10.22	8.46E-04	1.28E-04	0.07	0.00
10.37	6.33E-04	3.77E-05	0.20	0.00
10.52	8.46E-04	2.80E-05	0.00	0.00
10.68	8.77E-04	6.20E-05	0.07	0.00
10.83	1.01E-03	1.30E-04	0.07	0.00
10.98	8.35E-04	4.86E-05	0.07	0.00
11.13	7.52E-04	7.12E-05	0.00	0.00
11.29	8.16E-04	4.58E-05	0.07	0.00
11.44	7.07E-04	8.11E-05	0.00	0.00
11.59	7.63E-04	8.16E-05	0.00	0.00
11.74	8.57E-04	1.26E-04	0.00	0.00
11.90	8.35E-04	7.13E-05	0.00	0.00
12.05	7.63E-04	3.71E-05	0.26	0.00
12.20	5.82E-04	5.82E-05	0.00	0.00
12.35	6.50E-04	5.32E-05	0.00	0.00
12.51	8.04E-04	3.76E-05	0.00	0.00
12.66	9.29E-04	3.80E-05	0.00	0.00
12.81	1.05E-03	1.32E-05	0.00	0.00
12.96	1.06E-03	9.52E-05	0.00	0.00
13.12	9.58E-04	1.06E-04	0.00	0.00
13.27	8.25E-04	8.63E-05	0.00	0.00
13.57	6.11E-04	3.19E-05	0.00	0.00
13.73	6.47E-04	1.20E-04	0.13	0.26
14.03	4.27E-04	8.16E-05	0.33	0.20
14.18	4.35E-04	8.77E-05	0.00	0.26
14.34	3.20E-04	4.77E-05	0.39	0.26
14.49	3.43E-04	6.25E-05	0.00	0.52

Appendix 3a. SQ-1 drill hole core.

Depth	Magnetic Susceptibility	Standard Deviation	Fracture Density	
			Complete	Incomp.
(m)	(SI mass)	(SI mass)	(Cm^{-1})	(Cm^{-1})
14.64	4.60E-04	2.54E-05	0.33	0.26
14.79	4.18E-04	2.14E-04	0.13	0.52
15.10	4.00E-04	4.63E-05	0.07	0.33
15.25	5.14E-04	8.93E-05	0.13	0.26
15.40	2.04E-04	1.13E-05	0.13	0.46
15.56	6.04E-04	1.22E-04	0.00	0.07
15.71	6.58E-04	1.06E-05	0.07	0.20
15.86	8.31E-04	3.35E-05	0.07	0.13
16.01	7.90E-04	7.53E-05	0.00	0.00
16.17	7.46E-04	3.35E-05	0.00	0.07
16.32	6.45E-04	3.52E-05	0.00	0.20
16.47	8.68E-04	9.22E-05	0.00	0.00
16.62	6.76E-04	2.99E-05	0.00	0.00
16.78	7.35E-04	4.45E-05	0.07	0.00
16.93	6.74E-04	5.57E-05	0.00	0.00
17.08	9.65E-04	2.77E-05	0.00	0.00
17.23	1.39E-03	5.57E-05	0.00	0.00
17.39	1.46E-03	7.60E-05	0.00	0.00
17.54	1.25E-03	4.02E-05	0.00	0.00
17.69	1.07E-03	4.82E-05	0.00	0.00
17.84	1.06E-03	4.12E-05	0.00	0.00
18.00	9.18E-04	3.33E-05	0.00	0.00
18.15	8.40E-04	2.56E-05	0.00	0.13
18.30	8.12E-04	7.40E-05	0.07	0.07
18.45	7.87E-04	5.85E-05	0.00	0.00
18.61	4.37E-04	7.32E-05	0.26	0.13
18.91	2.59E-04	9.63E-05	0.20	0.26
19.06	3.21E-04	4.28E-06	0.00	0.98
19.22	3.25E-04	3.08E-05	0.00	0.00
19.37	3.08E-04	1.61E-05	0.20	0.20
19.52	2.92E-04	4.47E-06	0.20	0.39
19.67	2.68E-04	1.59E-05	0.07	0.20
19.83	3.03E-04	1.84E-05	0.07	0.33
20.13	1.07E-03	3.10E-05	0.00	0.13
20.31	1.15E-03	5.42E-05	0.00	0.00
20.44	1.14E-03	5.98E-05	0.00	0.00
20.59	1.42E-03	1.37E-04	0.00	0.00
20.74	1.37E-03	7.76E-05	0.00	0.00
20.89	8.33E-04	2.46E-05	0.26	0.13
21.05	1.08E-03	1.34E-04	0.13	0.20
21.20	7.48E-04	7.20E-05	0.07	0.13
21.35	9.12E-04	2.19E-05	0.13	0.07
21.50	2.31E-03	7.67E-05	0.00	0.00
21.66	2.39E-03	5.27E-05	0.00	0.00
21.81	2.35E-03	8.81E-05	0.00	0.00
21.96	2.24E-03	1.49E-04	0.20	0.33

Appendix 3a. SQ-1 drill hole core.

Depth (m)	Magnetic Susceptibility (SI mass)	Standard Deviation (SI mass)	Fracture Density Complete (Cm^{-1})	Fracture Density Incomp. (Cm^{-1})
22.11	2.39E-03	3.19E-05	0.07	0.20
22.27	2.26E-03	9.75E-05	0.07	0.26
22.42	1.91E-03	7.36E-05	0.00	0.07
22.57	2.72E-03	9.46E-05	0.00	0.00
22.72	3.12E-03	1.77E-04	0.00	0.13
22.88	2.02E-03	1.10E-04	0.07	0.33
23.03	2.29E-03	1.61E-04	0.07	0.33
0.00	3.33E-03	1.20E-04	0.07	0.33
23.33	3.18E-03	1.19E-04	0.00	0.00
23.49	3.83E-03	3.25E-04	0.00	0.00
23.64	4.56E-03	5.08E-04	0.00	0.00
23.79	4.78E-03	5.56E-04	0.13	0.39
23.94	4.63E-03	5.76E-04	0.00	0.26
24.10	4.99E-03	2.16E-04	0.00	0.00
24.25	5.15E-03	1.07E-04	0.00	0.00
24.40	5.20E-03	1.91E-04	0.00	0.00
24.55	5.52E-03	2.54E-04	0.00	0.00
24.71	5.68E-03	2.94E-04	0.00	0.00
24.86	5.32E-03	1.15E-04	0.00	0.00
25.01	6.05E-03	1.84E-04	0.00	0.00
25.16	5.89E-03	7.64E-05	0.00	0.00
25.32	5.74E-03	7.64E-05	0.00	0.00
25.47	6.26E-03	2.14E-04	0.00	0.00
25.62	6.51E-03	1.93E-04	0.13	0.13
25.77	3.42E-03	7.77E-04	0.00	0.07
25.93	7.43E-03	1.48E-04	0.00	0.00
26.08	5.50E-03	3.91E-04	0.13	0.00
26.23	7.00E-03	2.57E-04	0.00	0.00
26.38	6.92E-03	2.49E-04	0.00	0.00
26.54	7.67E-03	4.42E-04	0.13	0.20
26.69	6.93E-03	1.73E-04	0.00	0.00
26.84	7.06E-03	3.68E-04	0.07	0.00
26.99	7.07E-03	2.44E-04	0.00	0.00
27.15	7.69E-03	2.35E-04	0.00	0.00
27.30	7.16E-03	2.20E-04	0.00	0.00
27.45	7.45E-03		0.00	0.00
27.60	7.41E-03	1.34E-04	0.00	0.00
27.76	6.84E-03	5.23E-04	0.00	0.00
27.91	7.17E-03	3.07E-04	0.00	0.00
28.21	7.47E-03	5.20E-04	0.00	0.00
28.37	7.76E-03	2.49E-04	0.00	0.00
28.52	8.16E-03	1.64E-04	0.00	0.00
28.67	8.02E-03	8.04E-05	0.00	0.00
28.82	7.38E-03	2.64E-04	0.00	0.00
28.98	7.51E-03	4.07E-04	0.00	0.00

Appendix 3a. SQ-1 drill hole core.

Depth (m)	Magnetic Susceptibility (SI mass)	Standard Deviation (SI mass)	Fracture Density	
			Complete (Cm^{-1})	Incomp. (Cm^{-1})
29.13	8.19E-03	3.43E-04	0.00	0.00
29.28	7.81E-03	2.46E-04	0.00	0.00
29.43	7.99E-03	2.23E-04	0.00	0.00
29.59	7.94E-03	2.49E-04	0.00	0.00
29.74	7.71E-03	2.20E-04	0.00	0.00
29.89	7.69E-03	1.52E-04	0.00	0.00
30.04	8.11E-03	1.38E-04	0.00	0.00
30.20	7.85E-03	1.10E-04	0.00	0.00
30.35	7.75E-03	2.42E-04	0.00	0.00
30.50	8.00E-03	0.00E+00	0.00	0.00
30.65	7.94E-03	2.49E-04	0.00	0.00
30.96	8.26E-03	4.29E-04	0.00	0.00
31.11	7.72E-03	1.65E-04	0.00	0.00
31.26	8.31E-03	1.69E-04	0.00	0.00
31.42	7.50E-03	1.10E-04	0.07	0.00
31.57	7.76E-03	2.20E-04	0.00	0.00
31.72	7.70E-03	3.97E-04	0.00	0.00
32.03	7.91E-03	1.69E-04	0.00	0.00
32.33	8.26E-03	1.18E-04	0.00	0.00
32.48	8.46E-03	2.26E-04	0.00	0.00
32.64	7.91E-03	8.14E-04	0.00	0.00
32.79	8.01E-03	1.18E-04	0.00	0.00
32.94	7.65E-03	1.59E-04	0.00	0.00
33.09	7.79E-03	2.72E-04	0.00	0.00
33.25	7.50E-03	2.71E-04	0.00	0.00
33.40	7.58E-03	3.06E-04	0.00	0.00
33.55	8.20E-03	2.26E-04	0.00	0.00
33.70	8.10E-03	3.60E-04	0.00	0.00
33.86	8.13E-03	3.70E-04	0.00	0.00
34.01	7.53E-03	2.77E-04	0.00	0.00
34.16	7.66E-03	2.62E-04	0.00	0.00
34.31	8.27E-03	4.46E-04	0.00	0.00
34.47	7.64E-03	2.20E-04	0.00	0.00
34.62	7.70E-03	3.67E-04	0.00	0.00
34.77	7.91E-03	4.10E-04	0.00	0.00
34.92	7.91E-03	2.05E-04	0.00	0.00
35.53	7.50E-03	6.52E-04	0.00	0.00
35.69	8.27E-03	3.34E-04	0.00	0.00
35.84	8.31E-03	1.94E-04	0.00	0.00
35.99	8.06E-03	2.61E-04	0.00	0.00
36.14	7.61E-03	2.62E-04	0.00	0.00
36.30	7.69E-03	2.54E-04	0.00	0.00

Appendix 3a. SQ-1 drill hole core.

Depth (m)	Magnetic Susceptibility (SI mass)	Standard Deviation (SI mass)	Fracture Density Complete (Cm^{-1})	Fracture Density Incomp. (Cm^{-1})
36.45	8.36E-03	1.73E-04	0.00	0.00
36.60	7.79E-03	3.06E-04	0.00	0.00
36.75	8.04E-03	3.49E-04	0.00	0.00
37.06	8.78E-03	2.14E-04	0.00	0.00
37.21	9.24E-03	4.59E-04	0.00	0.00
37.36	8.82E-03	2.59E-04	0.00	0.00
37.52	8.43E-03	2.84E-04	0.00	0.00
37.59	7.64E-03	8.23E-04	0.00	0.00
37.67	7.79E-03	3.77E-04	0.00	0.00
37.74	6.96E-03	9.85E-04	0.00	0.00
37.82	7.45E-03	6.92E-04	0.00	0.00
37.90	7.76E-03	1.10E-03	0.00	0.00
37.97	8.15E-03	1.01E-03	0.00	0.00
38.13	8.18E-03	4.77E-04	0.00	0.00
38.28	8.09E-03	3.00E-04	0.00	0.00
38.43	8.58E-03	1.48E-04	0.00	0.00
38.58	8.72E-03	3.11E-04	0.00	0.00
38.74	8.31E-03	3.29E-04	0.00	0.00
38.89	9.09E-03	2.57E-04	0.00	0.00
39.04	7.77E-03	3.97E-04	0.00	0.00
39.19	8.26E-03	4.75E-04	0.00	0.00
39.35	8.15E-03	1.83E-04	0.00	0.00
39.50	8.40E-03	8.16E-05	0.00	0.00
39.65	7.73E-03	3.73E-04	0.00	0.00
39.80	7.56E-03	4.22E-04	0.00	0.00
39.96	7.67E-03	4.23E-04	0.00	0.00
40.11	7.62E-03	6.60E-04	0.00	0.00
40.26	7.43E-03	4.02E-04	0.00	0.00
40.41	7.37E-03	6.54E-04	0.00	0.00
40.57	7.53E-03	5.32E-04	0.00	0.00
40.72	7.37E-03	2.44E-04	0.00	0.00
40.87	7.62E-03	3.51E-04	0.00	0.00
41.02	7.71E-03	2.86E-04	0.00	0.00
41.18	7.02E-03	1.09E-03	0.00	0.00
41.33	6.71E-03	1.20E-03	0.07	0.00
41.48	7.12E-03	9.47E-04	0.13	0.13
41.63	7.11E-03	1.45E-03	0.00	0.00
41.79	7.50E-03	6.20E-04	0.00	0.00
41.94	7.17E-03	1.67E-03	0.00	0.00
42.09	6.51E-03	1.35E-03	0.00	0.00
42.24	6.95E-03	1.62E-03	0.00	0.00
42.40	6.09E-03	2.05E-03	0.00	0.00

Appendix 3a. SQ-1 drill hole core.

Depth	Magnetic Susceptibility	Standard Deviation	Fracture Density	
			Complete	Incomp.
(m)	(SI mass)	(SI mass)	(Cm^{-1})	(Cm^{-1})
42.55	6.35E-03	1.63E-03	0.00	0.00
42.70	6.60E-03	1.57E-03	0.00	0.00
42.85	7.55E-03	4.64E-04	0.00	0.00
43.01	7.11E-03	1.53E-03	0.00	0.00
43.16	6.00E-03	2.17E-03	0.00	0.00
43.31	6.13E-03	1.90E-03	0.00	0.00
43.46	6.54E-03	9.59E-04	0.00	0.00
43.62	7.15E-03	1.47E-03	0.00	0.00
43.77	7.48E-03	7.91E-04	0.00	0.00
43.92	7.44E-03	8.43E-04	0.00	0.00
44.07	6.46E-03	1.18E-03	0.00	0.00
44.23	6.38E-03	1.40E-03	0.00	0.00
44.38	7.45E-03	7.30E-04	0.00	0.00
44.53	6.41E-03	9.49E-04	0.00	0.00
44.68	7.69E-03	9.18E-04	0.00	0.00
0.00	7.18E-03	3.85E-04	0.00	0.00
44.99	7.07E-03	6.33E-04	0.00	0.00
45.14	7.80E-03	6.01E-04	0.00	0.00
45.29	7.55E-03	3.81E-04	0.00	0.00
45.45	7.60E-03	3.48E-04	0.00	0.00
45.60	6.97E-03	5.56E-04	0.00	0.00
45.75	7.41E-03	3.99E-04	0.00	0.00
45.90	7.50E-03	7.39E-04	0.00	0.00
46.06	7.37E-03	5.37E-04	0.00	0.00
46.21	6.40E-03	1.30E-03	0.00	0.00
46.36	6.80E-03	9.24E-04	0.00	0.00
46.51	7.67E-03	9.13E-04	0.00	0.00
46.67	6.87E-03	9.46E-04	0.00	0.00
46.82	5.88E-03	1.18E-03	0.00	0.00
46.97	7.53E-03	6.99E-04	0.00	0.00
47.12	3.06E-03	3.75E-04	0.00	0.00
47.28	6.94E-03	5.93E-04	0.00	0.00
47.43	6.07E-03	1.38E-03	0.00	0.00
47.58	7.51E-03	6.33E-04	0.00	0.00
47.73	5.85E-03	1.38E-03	0.00	0.00
47.89	6.82E-03	8.13E-04	0.00	0.00
48.04	7.87E-03	8.36E-04	0.00	0.00
48.19	7.49E-03	9.43E-04	0.00	0.00
48.34	8.14E-03	4.18E-04	0.00	0.00
48.50	6.75E-03	1.09E-03	0.00	0.00
48.65	6.42E-03	1.19E-03	0.00	0.00
48.80	7.49E-03	8.95E-04	0.00	0.00

Appendix 3a. SQ-1 drill hole core.

Depth (m)	Magnetic Susceptibility (SI mass)	Standard Deviation (SI mass)	Fracture Density Complete (Cm^{-1})	Incomp. (Cm^{-1})
48.95	7.96E-03	2.04E-04	0.00	0.00
49.11	7.51E-03	7.98E-04	0.00	0.00
49.26	8.05E-03	4.27E-04	0.00	0.00
49.41	5.09E-03	3.68E-04	0.00	0.00
49.57	7.16E-03	6.24E-04	0.00	0.00
49.72	7.81E-03	6.71E-05	0.00	0.00
49.87	8.89E-03	2.14E-04	0.00	0.00
50.02	7.55E-03	5.29E-04	0.07	0.00
50.17	8.10E-03	2.94E-04	0.00	0.00
50.33	6.84E-03	1.59E-04	0.00	0.00
50.48	7.12E-03	6.84E-04	0.07	0.00
50.63	7.85E-03	4.50E-04	0.00	0.00
50.78	7.51E-03	2.93E-04	0.00	0.00
50.94	6.58E-03	1.13E-03	0.00	0.00
51.09	6.58E-03	8.72E-04	0.00	0.00
51.24	8.17E-03	3.29E-04	0.00	0.00
51.39	6.75E-03	7.05E-04	0.00	0.00
51.55	8.00E-03	5.94E-04	0.00	0.00
51.70	7.89E-03	2.08E-04	0.00	0.00
51.85	7.39E-03	2.49E-04	0.00	0.00
52.00	8.25E-03	1.75E-04	0.00	0.00
52.16	7.06E-03	4.62E-04	0.00	0.00
52.31	6.93E-03	5.83E-04	0.00	0 00
52.46	7.17E-03	4.65E-04	0.00	0.00
52.61	7.16E-03	5.36E-04	0.00	0.00
52.77	6.50E-03	6.00E-04	0.00	0.00
52.92	7.97E-03	2.27E-04	0.00	0.00
53.07	7.33E-03	3.35E-04	0.00	0.00
53.22	8.74E-03	2.20E-04	0.00	0.00
53.38	8.13E-03	2.21E-04	0.00	0.00
53.53	7.69E-03	3.49E-04	0.00	0.00
53.68	8.54E-03	2.97E-04	0.00	0.00
53.83	8.45E-03	2.85E-04	0.00	0.00
53.99	7.21E-03	4.75E-04	0.00	0.00
54.14	7.17E-03	7.58E-04	0.00	0.00
54.29	7.76E-03	4.02E-04	0.00	0.00
54.44	8.57E-03	4.40E-04	0.00	0.00
54.60	7.36E-03	6.05E-04	0.00	0.00
54.75	8.24E-03	3.43E-04	0.00	0.00
54.90	8.15E-03	7.31E-04	0.00	0.00

Appendix 3b. Magnetic susceptibility of the Sandy Creek Gabbro.

The Sandy Creek Gabbro at an estimated depth of 9 m in the SQ-2 hole. Retrieved core covers a ~continuous 167 cm interval.

Core SQ-2, Sandy Creek Gabbro

Depth (m)	Magnetic Susceptibility (SI mass)	Standard Deviation (SI mass)
9.04	1.50E-02	2.62E-05
9.12	1.19E-02	1.85E-04
9.16	1.11E-02	3.04E-05
9.25	1.70E-02	7.70E-06
9.29	1.78E-02	3.44E-06
9.33	1.77E-02	4.87E-06
9.37	1.82E-02	4.97E-06
9.41	1.66E-02	3.44E-06
9.68	1.78E-02	1.29E-05
10.09	1.29E-02	2.23E-05
10.13	1.20E-02	6.88E-06
10.38	1.52E-02	2.03E-05

NORTH SLOPE

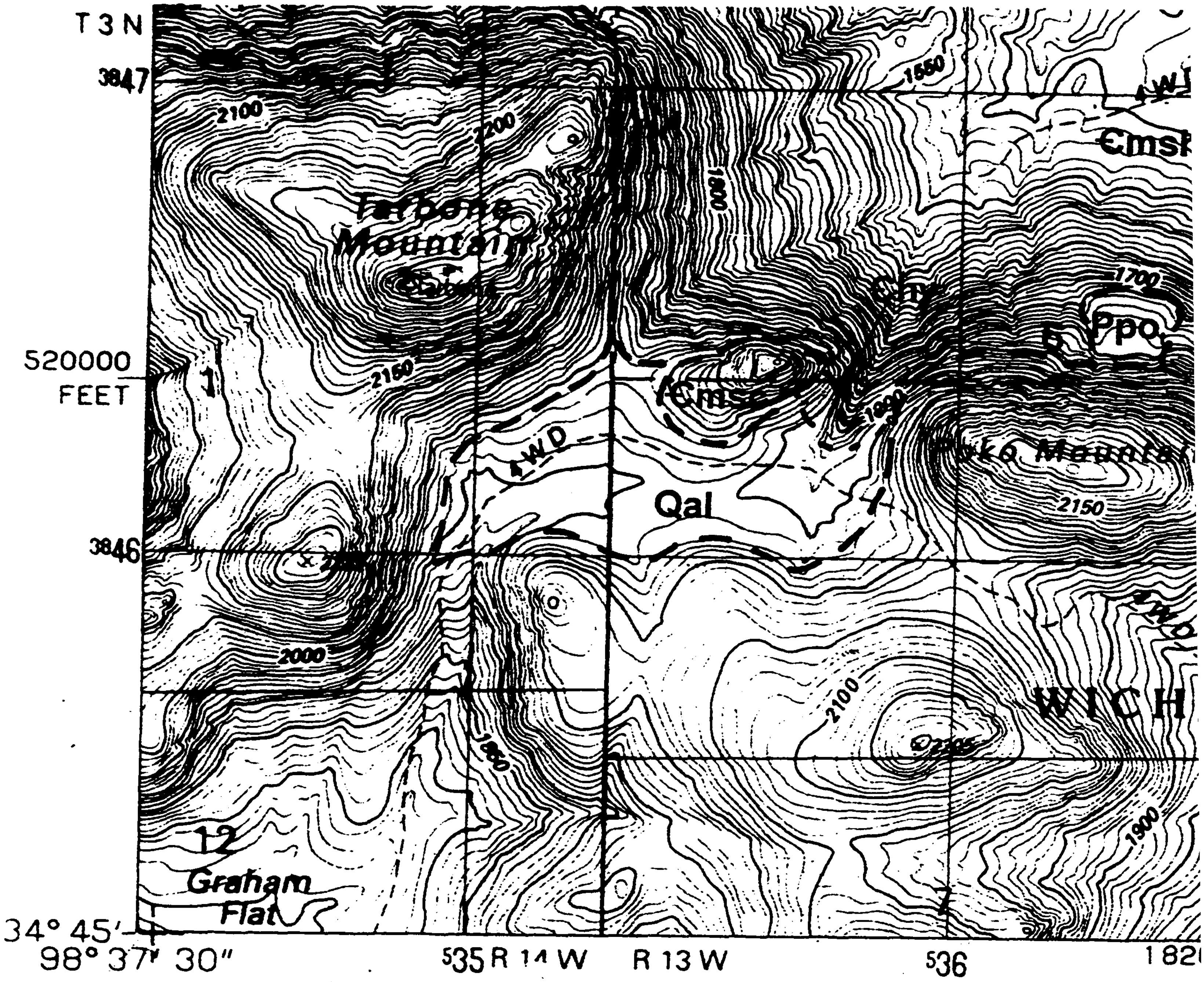
T 3 N
3847
3846
520000
FEET
34° 45′
98° 37′ 30″
535 R 14 W
R 13 W
536
182
2100
2200
1550
1800
Cms
Tarbone
Mountain
2150
1700
Ppo
Cms
4WD
Qal
1900
2150
2000
1800
2100
WICH
1900
12
Graham
Flat
1
6
7

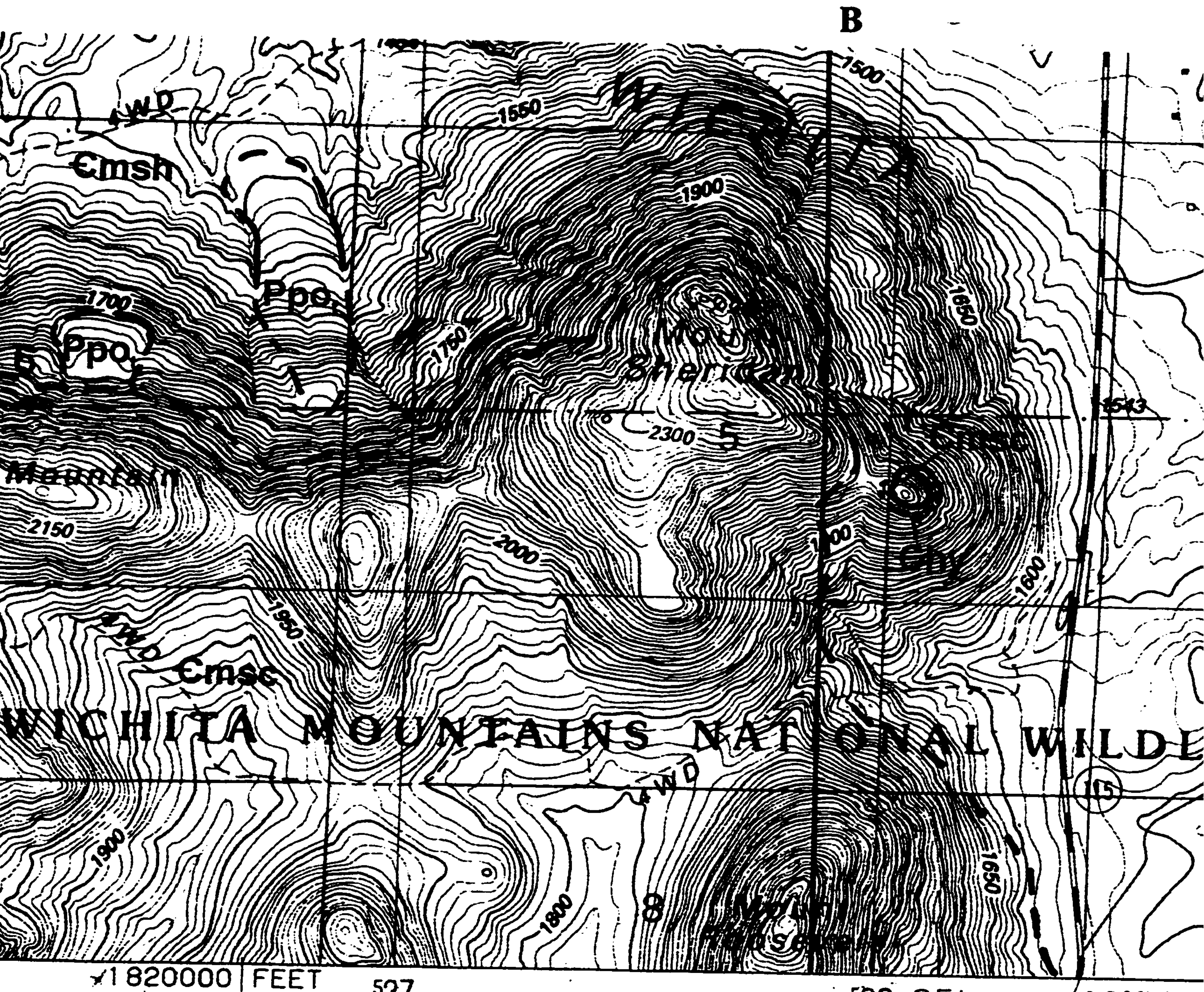

B
Єmsh
Ppo
Ppo
1700
1750
1550
1500
1900
1850
1543
2300
5
Єmsc
Mountain
2150
2000
1950
1600
Єmsc
WICHITA MOUNTAINS NATIONAL WILDE
115
1900
1800
8
1650
1820000 FEET
537
538 35′
1.3 MI. TO

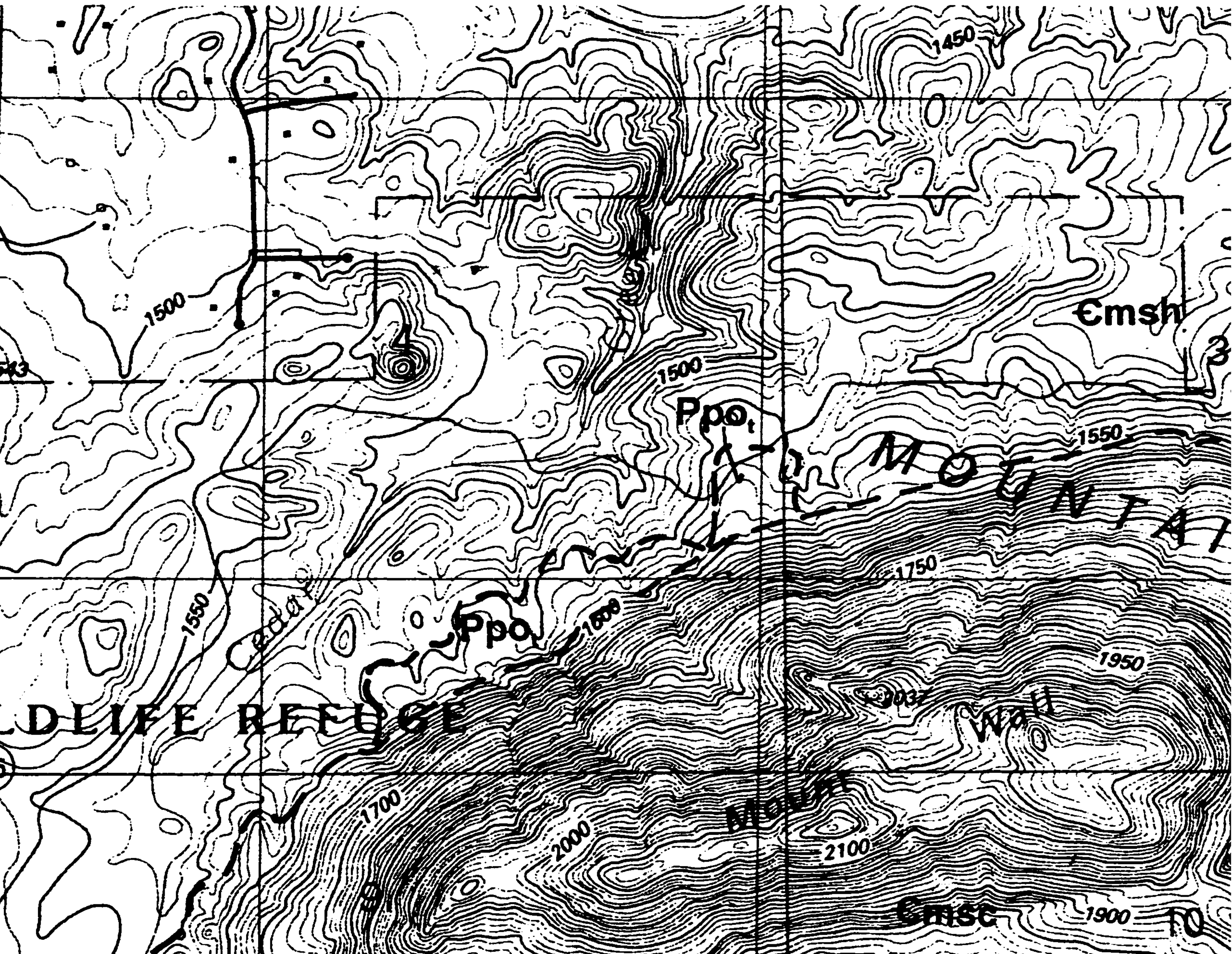

3 MI. TO OKLA 49 539

(MOUNT SCOTT)
6253 II NE

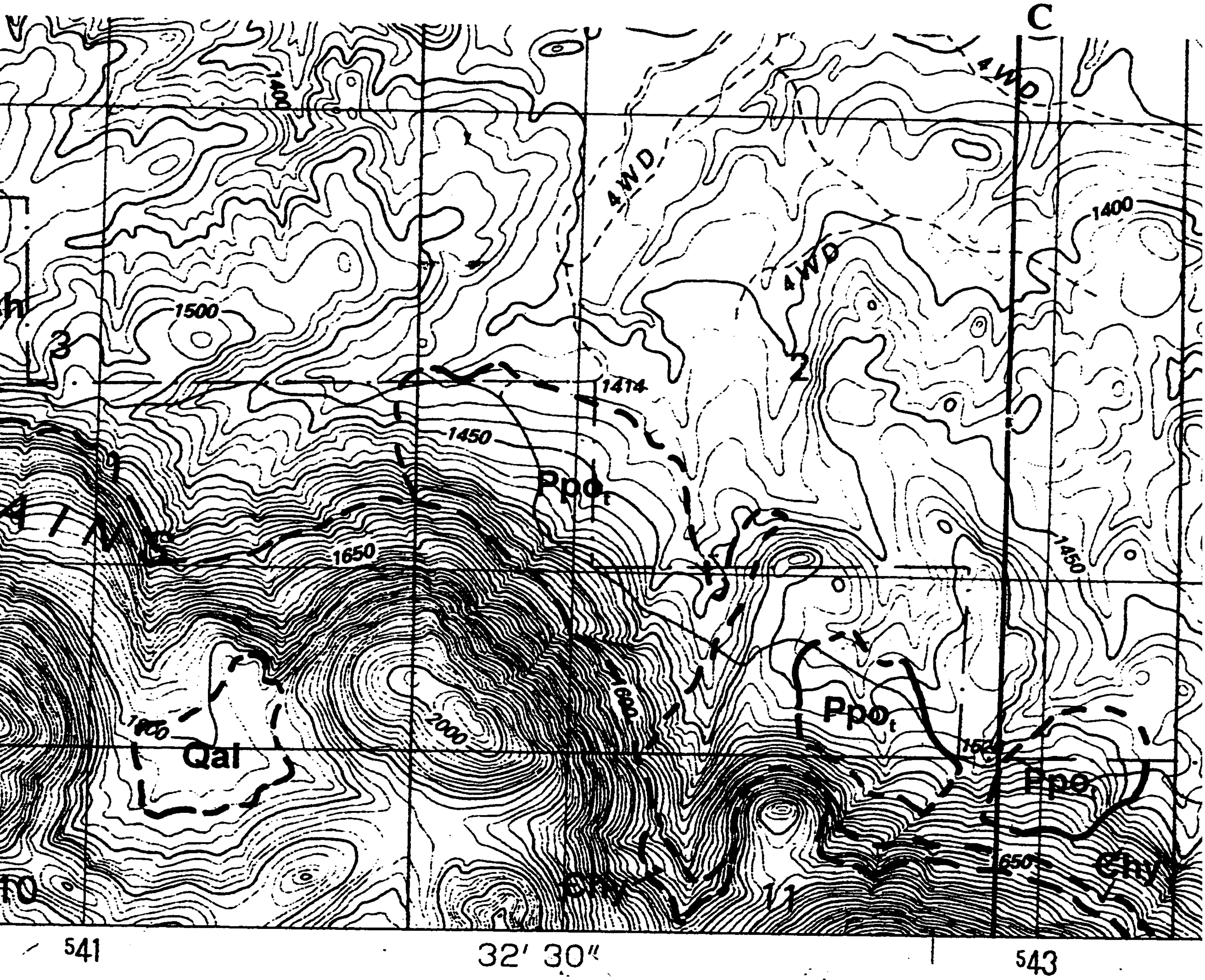
C
4WD
4WD
4WD
1400
1400
1450
1450
1500
1414
1650
2000
1600
1650
1800
Ppo$_t$
Ppo$_t$
Ppo$_t$
Qal
11
2
3
541
32′ 30″
543

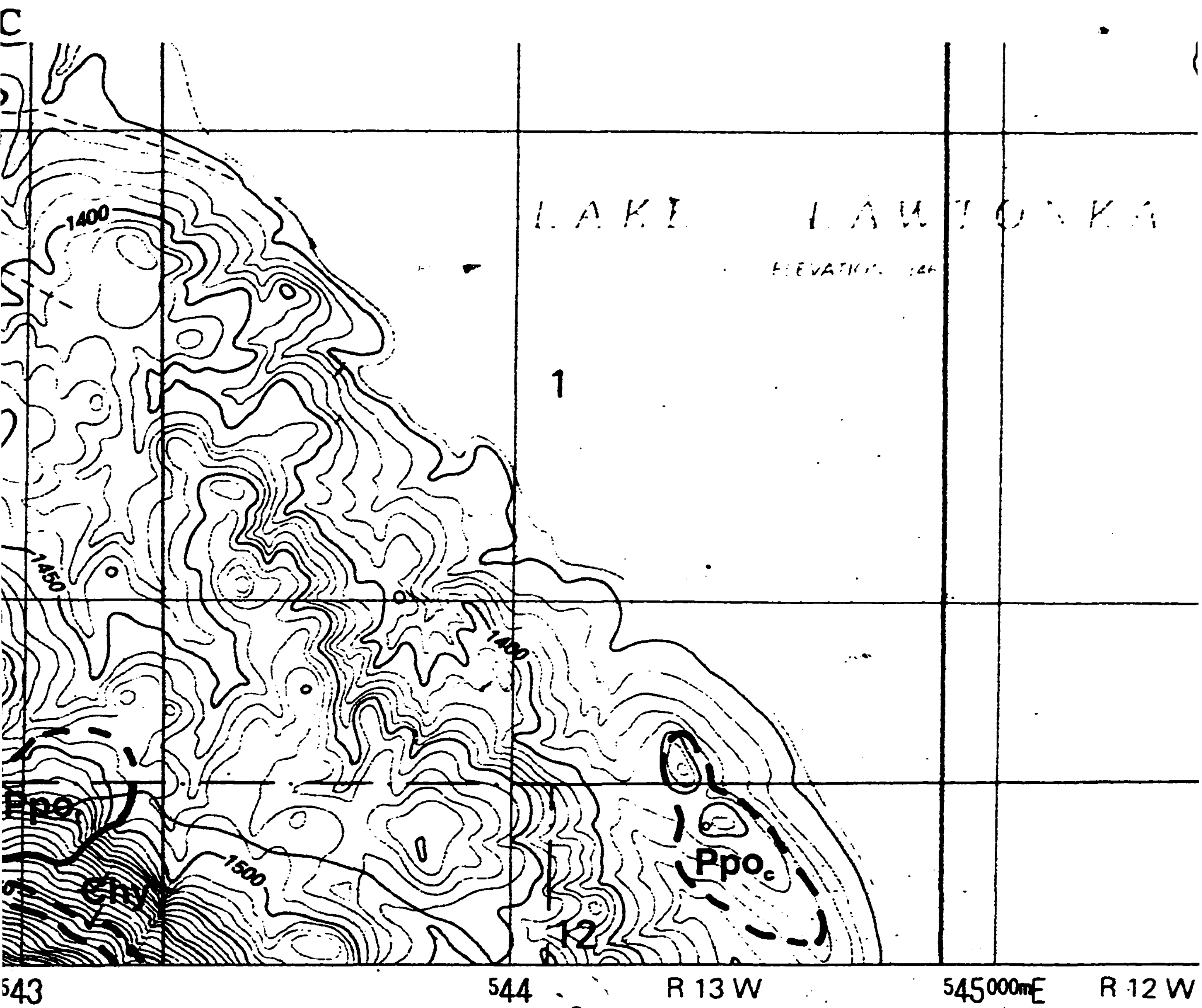

INTERIOR—GEOLOGICAL SURVEY, RESTON, VIRGINIA—19

Plate Ia

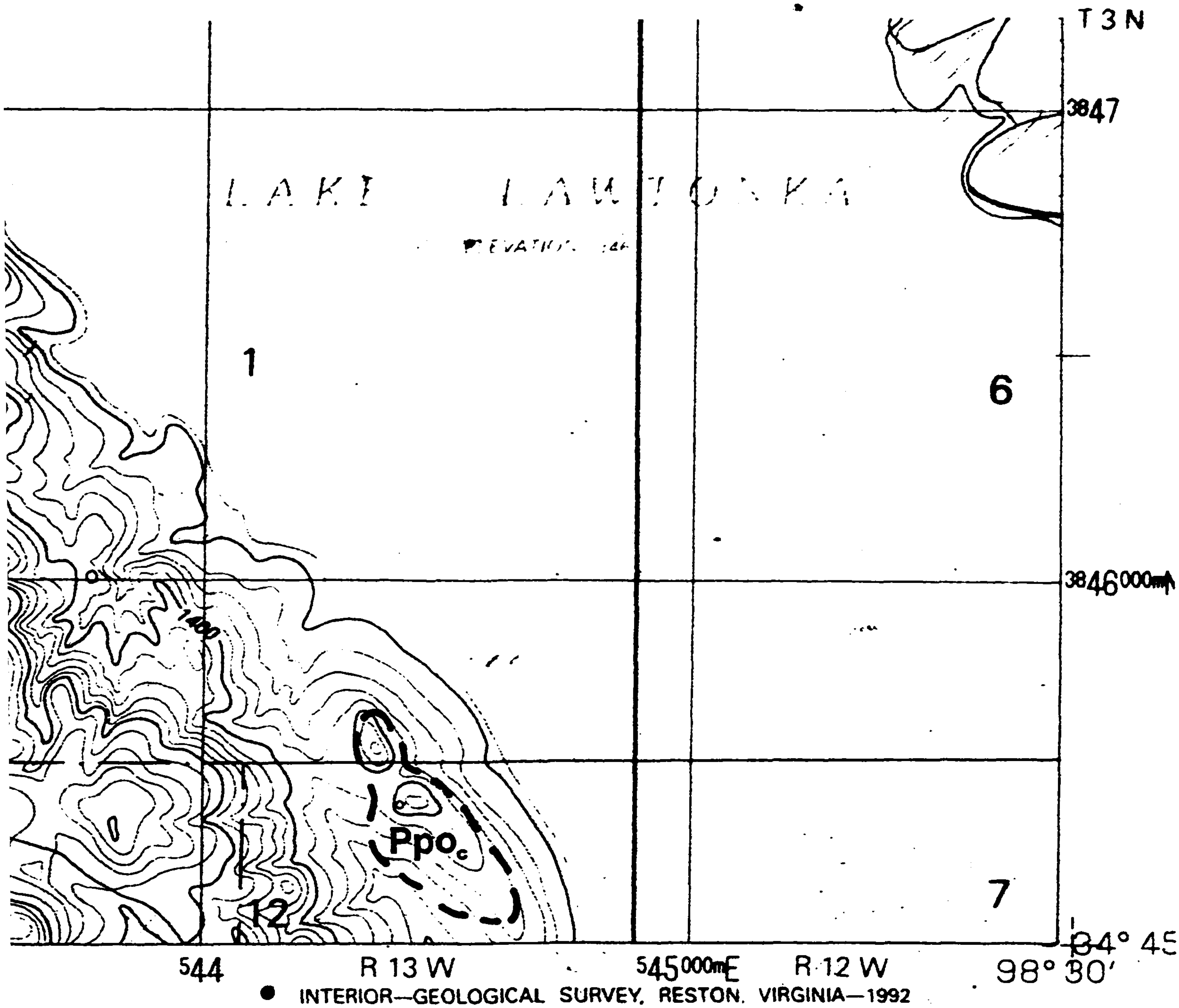
T 3 N
3847
1
6
3846000mN
1400
Ppoc
12
7
544
R 13 W
545000mE
R 12 W
98° 30′
34° 45
INTERIOR—GEOLOGICAL SURVEY, RESTON, VIRGINIA—1992

Graham
Flat
34° 45′
98° 37′ 30″
535
R 14 W
R 13 W
536
18

1620000 FEET 537

538 35′ 1.3 MI. TO OKLA

CENTRAL LOWLAND

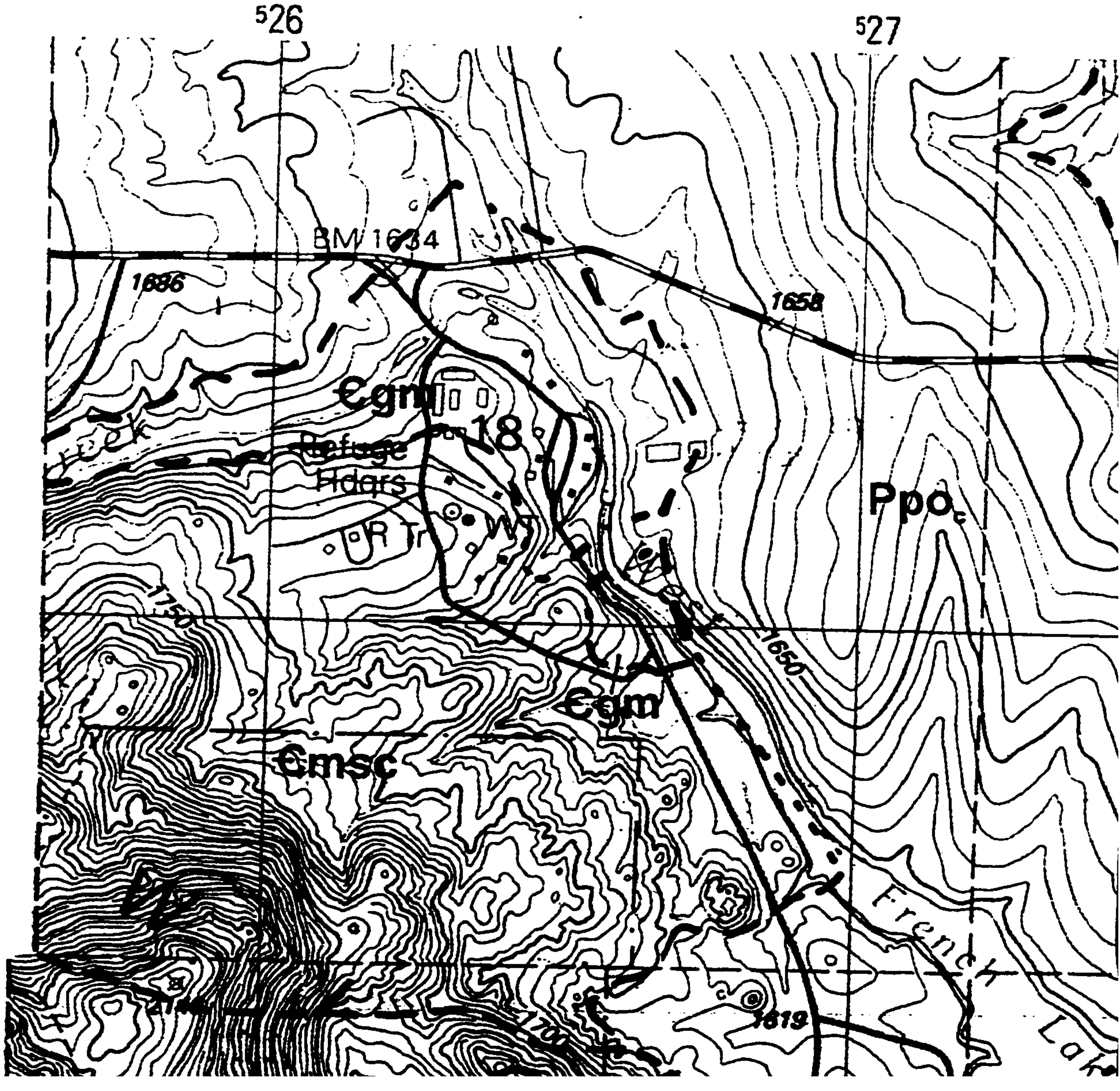


1.3 MI. TO OKLA 49
539
(MOUNT SCOTT)
6253 II NE

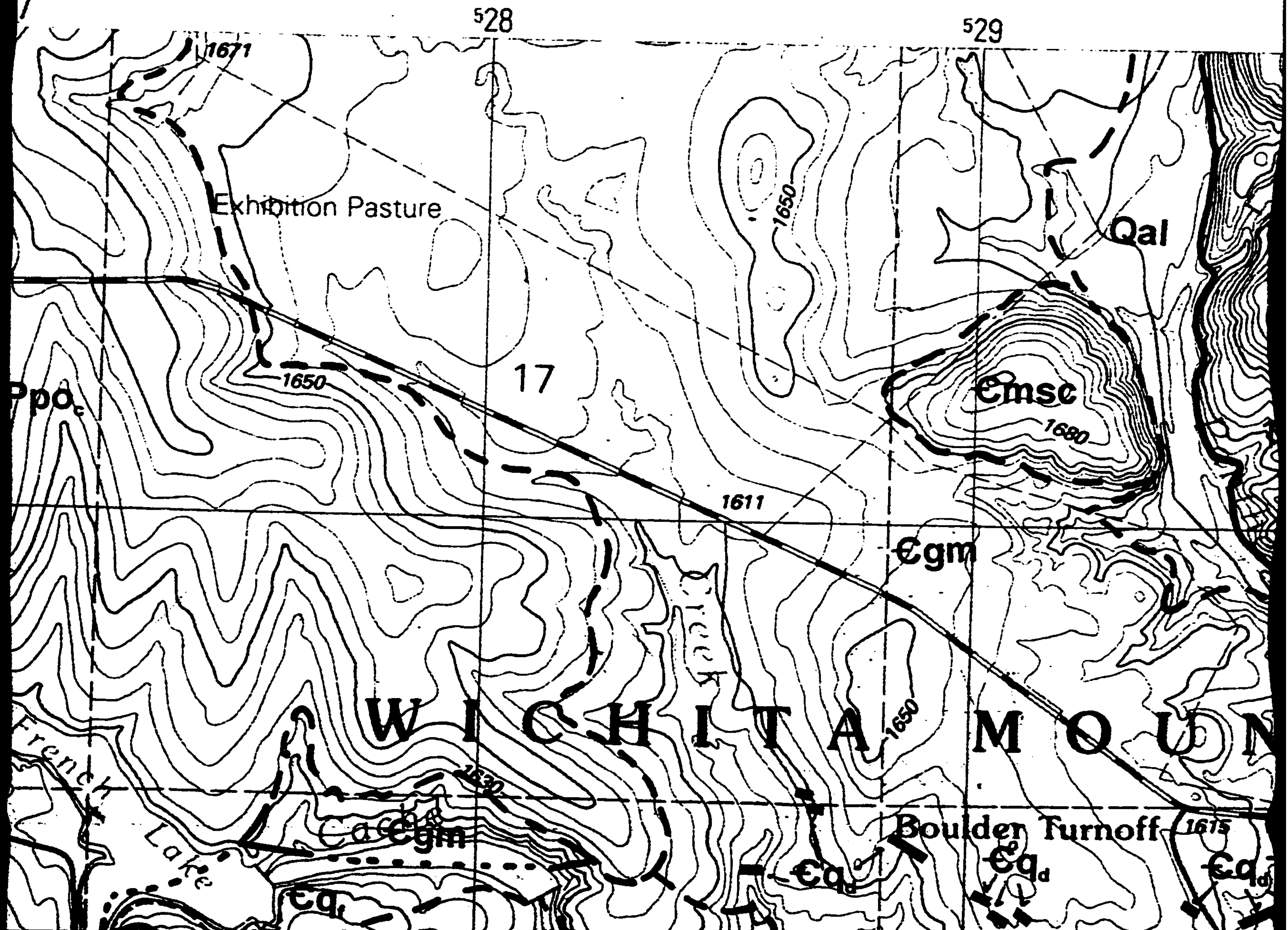
528
529
1671
Exhibition Pasture
1650
Qal
Ꞓmsc
1680
1650
17
Ppo
1611
Ꞓgm
Creek
WICHITA MOUN
1650
French Lake
1630
Cache
Ꞓgm
Boulder Turnoff
1615
Ꞓq
Ꞓq
Ꞓq
Ꞓq


1900
10
11
1650
541
32′ 30″
543

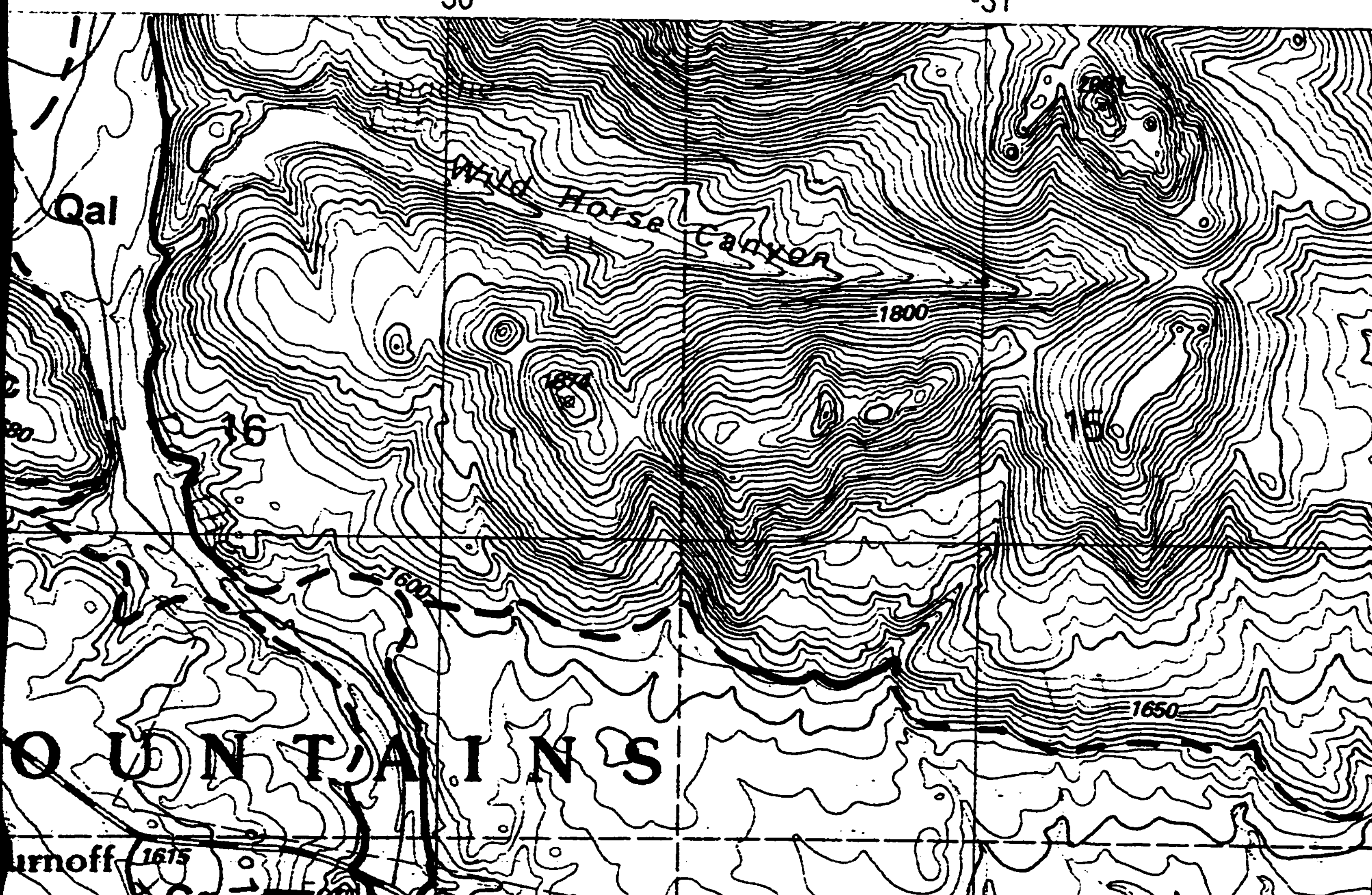
530
40′
531
Wild Horse Canyon
Qal
1800
16
15
1600
1650
OUNTAINS
urnoff
1615
Єgm

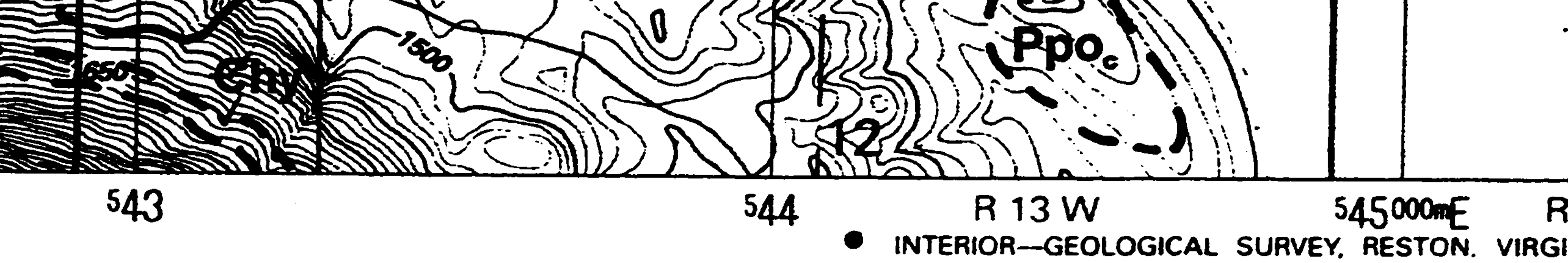
Ppo
12
1500
543
544
R 13 W
545000mE
R
INTERIOR--GEOLOGICAL SURVEY, RESTON, VIRGI

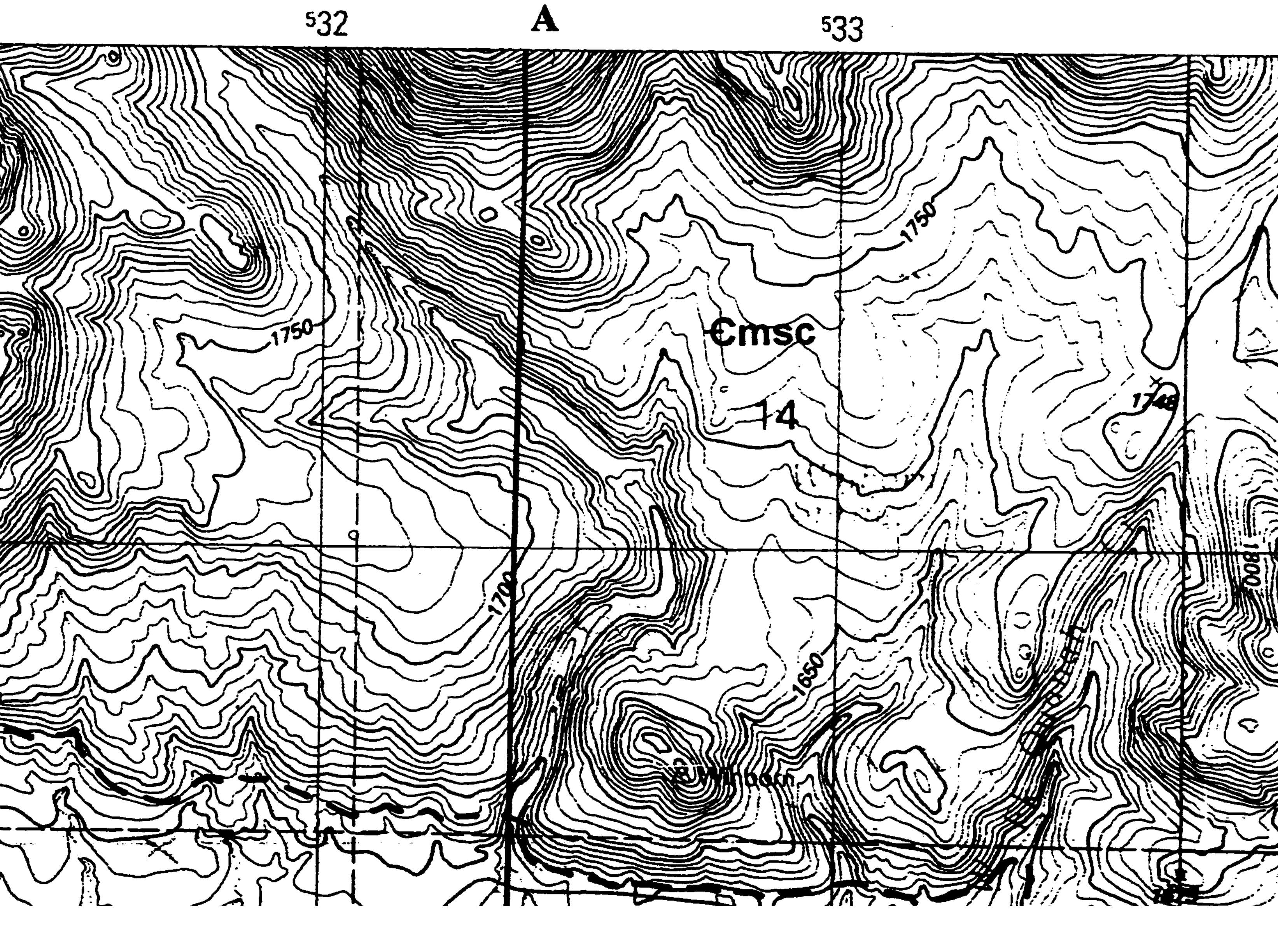
532
A
533
1750
1750
Cmsc
14
1700
1650
1800

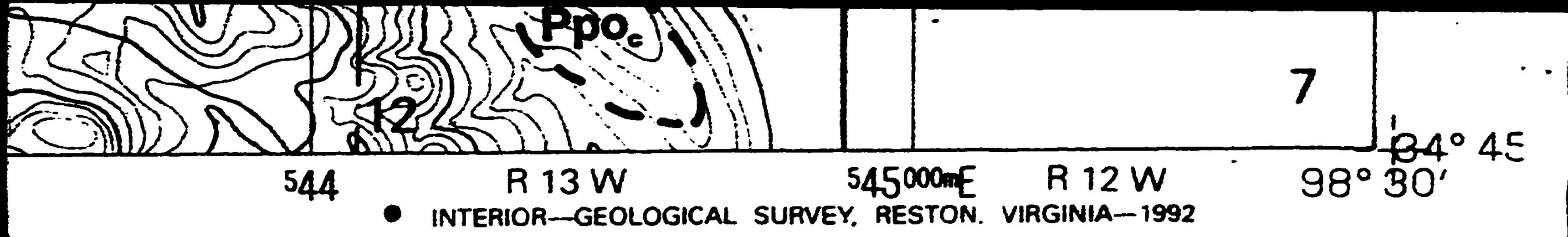
Ppo
12
7
34° 45
544
R 13 W
545000mE
R 12 W
98° 30′
INTERIOR—GEOLOGICAL SURVEY, RESTON, VIRGINIA—1992

Plate Ib

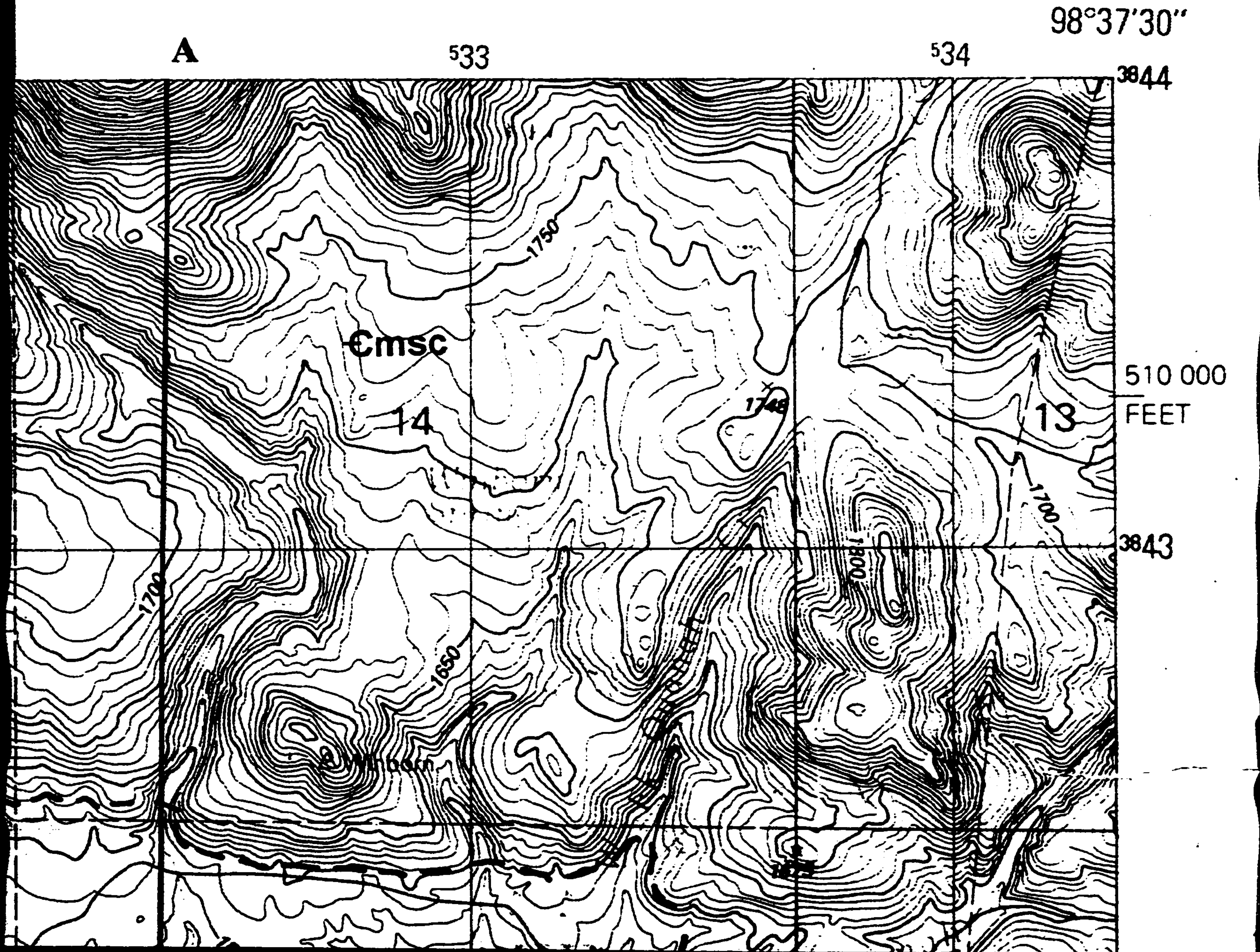
98°37′30″
A
533
534
3844
1750
Cmsc
14
1748
13
510 000
FEET
1700
3843
1800
1700
1650

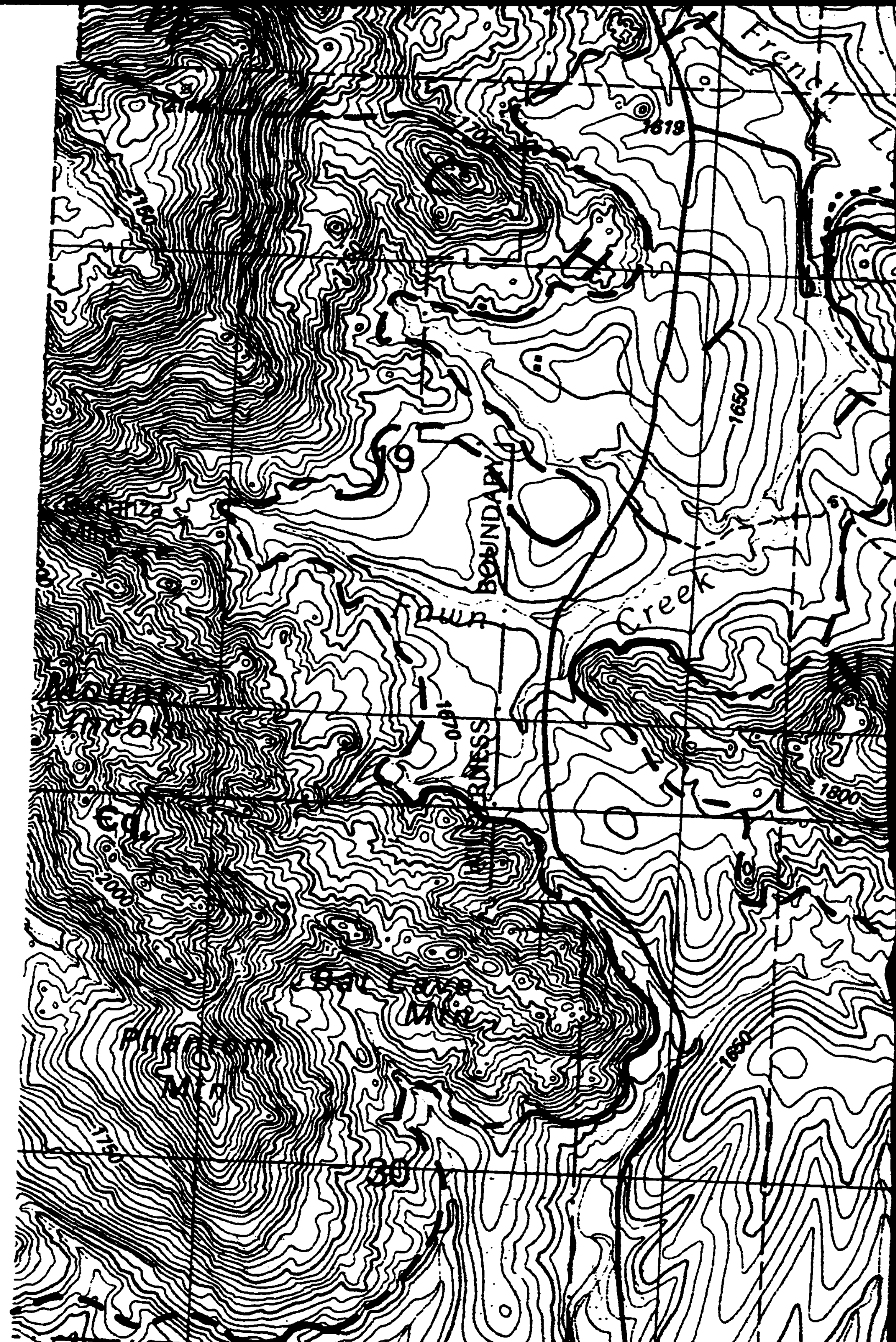
French
1619
1650
BOUNDARY
WILDERNESS
Creek
Mount
Lincoln
1800
2000
Bat Cave
Mtn
Phantom
Mtn
1650
30

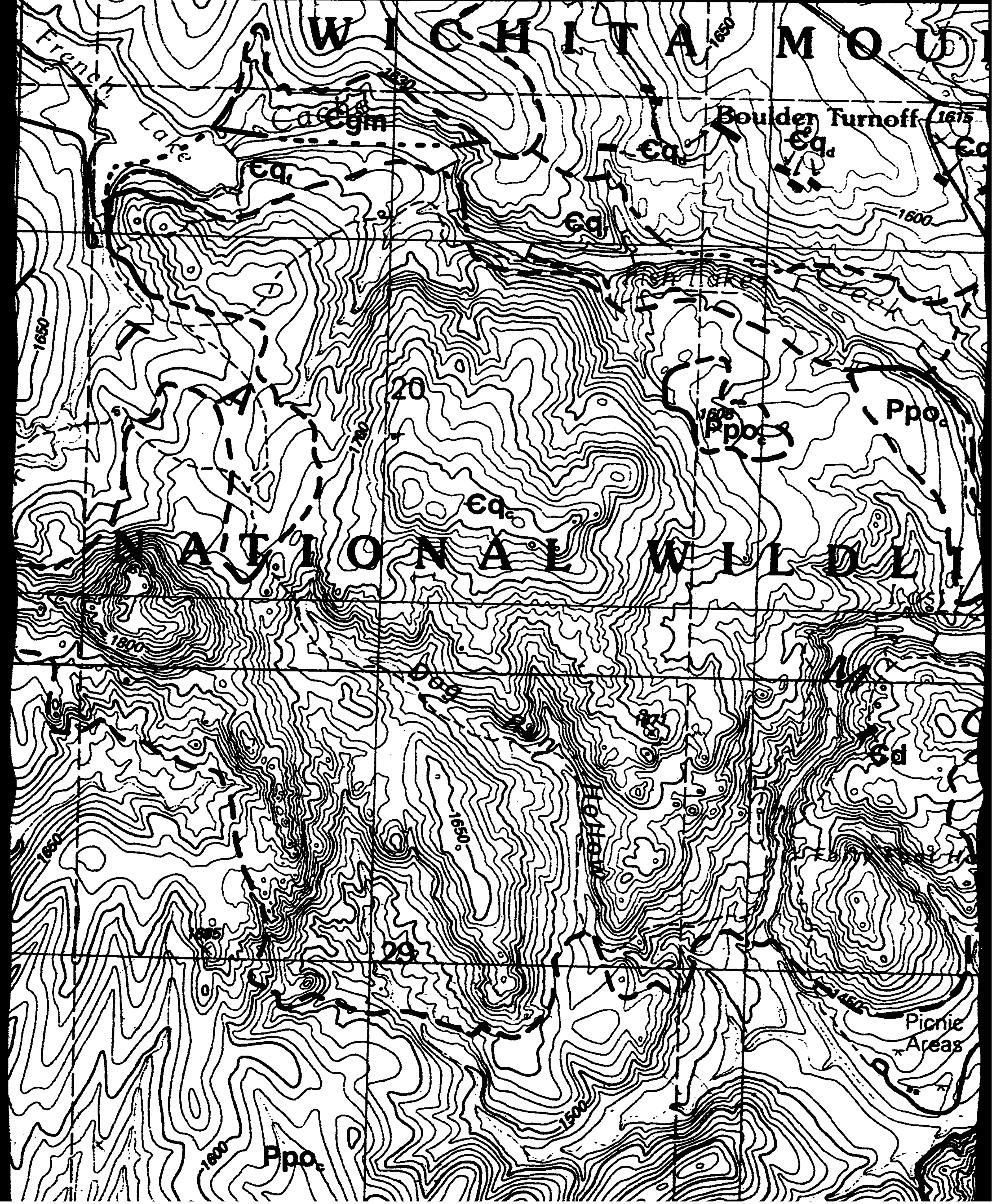

WICHITA MOU
Boulder Turnoff
1615
1650
1600
20
Ppo
NATIONAL WILDLI
1800
Dog
1650
29
1500
1600
Ppo
Picnic
Areas

off
1615
Єq
1600
Єq
1580
Єgm
Єq
Ppo
Timber
Hill
1621
Єgm
Ppo
22
1520
21
Ppo
1600
R E F U G E
1602
Єq
1500
1513
1530
N
Ppo
1500
T
A
1450
28
N
27
Picnic
Areas
Boulder
Camp

gm
1530
1520
1528
Campground
Qal
23
Visitor Ctr
1610
1550
Quanah Parker Lake
ELEV 1492
1490
Little Baldy
Cach
1550
1450
26
1750
Ca

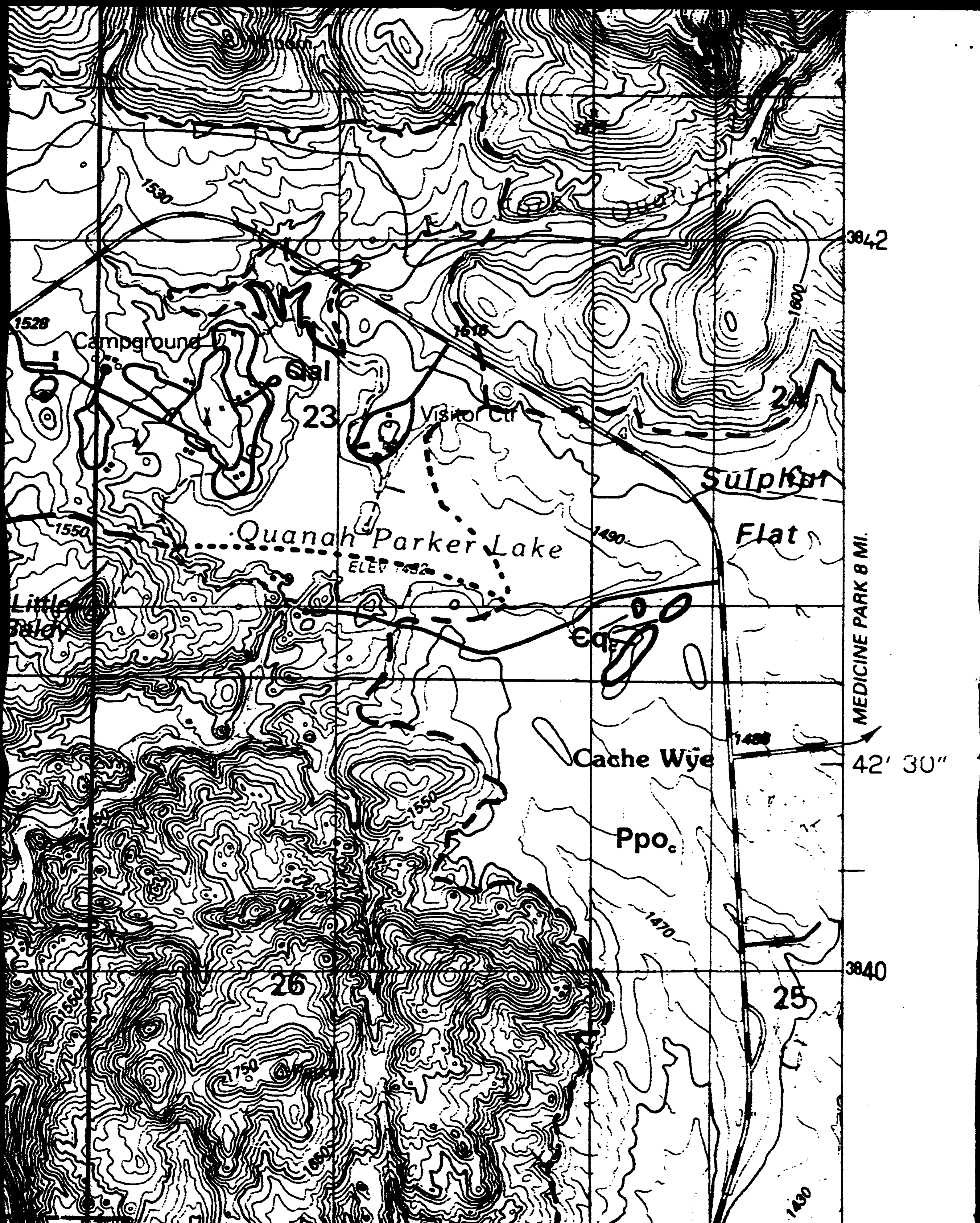
Campground
Gal
23
Visitor Ctr
Quanah Parker Lake
ELEV 1452
Little Baldy
Sulphur
Flat
24
Cache Wye
Ppo$_c$
26
25
1528
1530
1550
1610
1600
1490
1470
1430
1750
3842
3840
42′ 30″
MEDICINE PARK 8 MI.

GEOLOGIC
NORTH SLOPE
LOWLAND, EAS
MOUNTAINS

Jonathar

19

Produced in cooperation wi
National Cooperative Ge

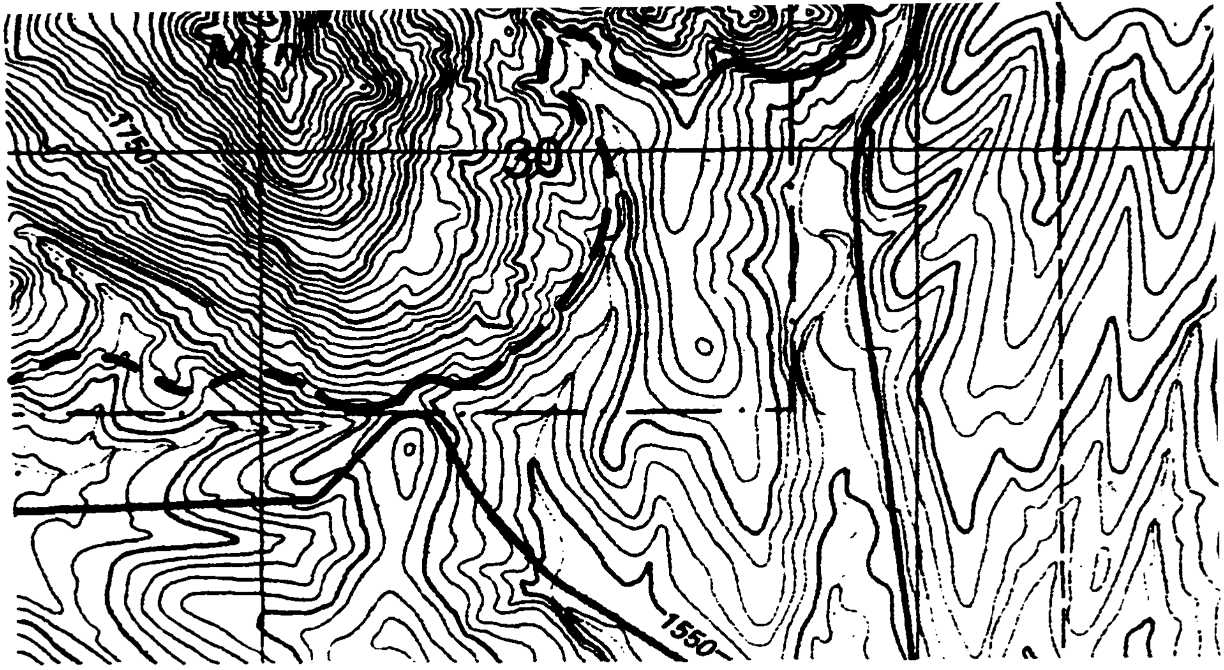

C MAPS OF THE PE AND CENTRAL :ASTERN WICHITA NS, OKLAHOMA

than D. Price

1998

ion with the U. S. Geological Survey,
/e Geological Mapping Program

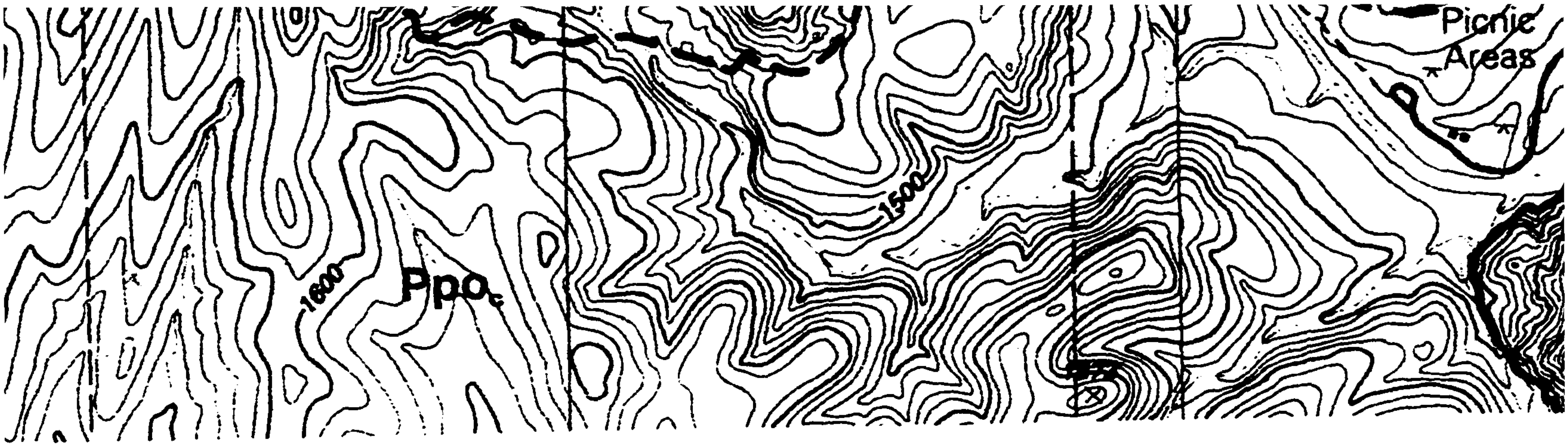

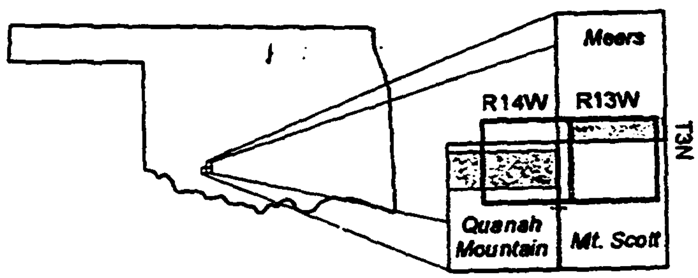

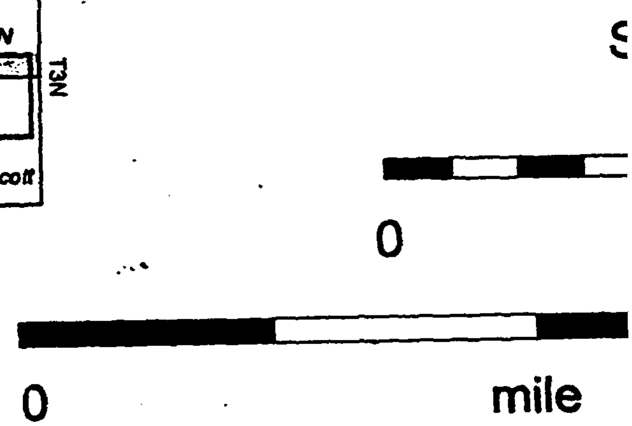

Topographic Base from
a. Meers and b. Quanah Mountain U.S.G.S.
7.5 minute quadrangles, 1991
N.A.D '27 projection
Universal Transverse Mercator Zone 14.

Scale 1:12 000

0 km 1

mile 1

Quaternary

Qal	**Alluvium** Sand and silt fill within modern and recent stream valleys.

Permian

Ppo_c	**Post Oak formation, conglomerate** Conglomerate with rounded boulders in a feldspar-rich matrix.
Ppo_t	**Post Oak formation, talus** Variably-sized boulders of Mount Scott Granite, some commonly infilled with sand, silt, and soil.

A'

fill within modern and recent
s.

formation, conglomerate
e with rounded boulders in a
matrix.

formation, talus
boulders of Mount Scott Granite,
ly infilled with sand, silt, and soil.

Cambrian

€d	**Diabase** Black, fine-grained aphyric dikes.
€q_d	**Quanah Granite, dikes** Pink to light pink coarse-grained pegmatitic granite dikes and apophyses.
€q_c	**Quanah Granite, coarse-grained** Pink to light pink coarse- to medium-grained equigranular granite.
€q_f	**Quanah Granite, fine-grained** Pink to light-pink fine- to medium-grained aplitic, seriate, and porphyritic granite.
€hy	**Hybrid rock** Pink and green, amphibole-rich granitoid rocks of intermediate composition.

€msh	**Mou** Dark comn
€msc	**Mou** Pink t grano
€rl	**Rusl** Pink t granit
€gm	**Glen** Dark- gabbr

A'

Diabase
Black, fine-grained aphyric dikes.

Quanah Granite, dikes
Pink to light pink coarse-grained pegmatitic granite dikes and apophyses.

Quanah Granite, coarse-grained
Pink to light pink coarse- to medium-grained equigranular granite.

Quanah Granite, fine-grained
Pink to light-pink fine- to medium-grained aplitic, seriate, and porphyritic granite.

Hybrid rock
Pink and green, amphibole-rich granitoid rocks of intermediate composition.

Ꞓmsh	**Mount Sheridan Gabbro** Dark-gray to dark-red-brown biotite gabbro with common white pegmatite dikes and pods.
Ꞓmsc	**Mount Scott Granite** Pink to brick red porphyritic, variably granophyric granite with gray ovoid feldspar.
Ꞓrl	**Rush Lake granite** Pink to brick-red, seriate, variably granophyric granite with connected quartz.
Ꞓgm	**Glen Mountains Layered Complex** Dark- to white-gray anorthosite, anorthositic gabbro, and olivine gabbro.

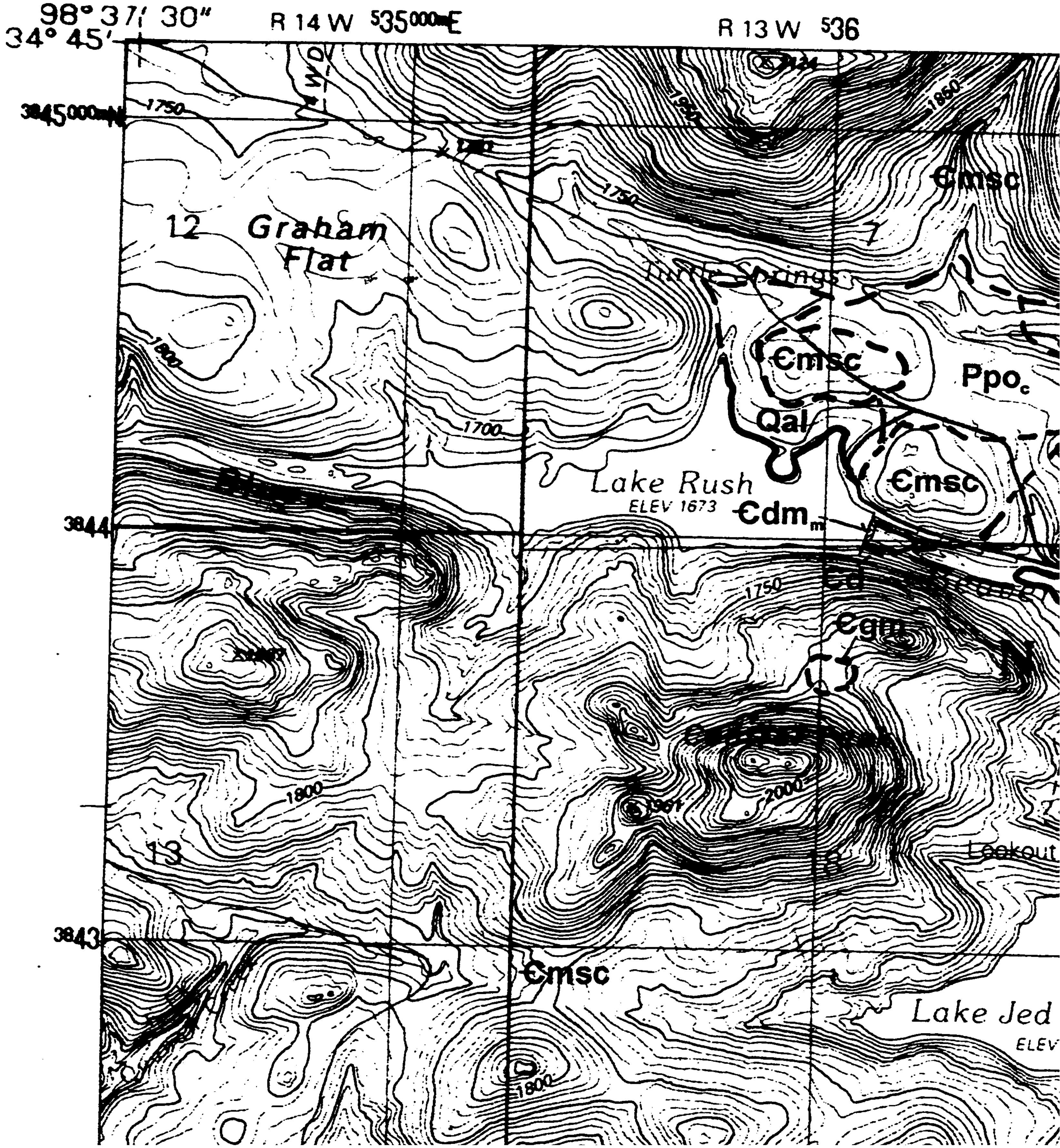
98° 37' 30"
34° 45'
R 14 W
535000mE
R 13 W
536
3845000mN
3844
3843
1750
1800
1700
2000
12
13
Graham Flat
Turtle Springs
Lake Rush
ELEV 1673
Lake Jed
Lookout
Ꞓmsc
Ppoc
Qal
Ꞓdm
Ꞓgm

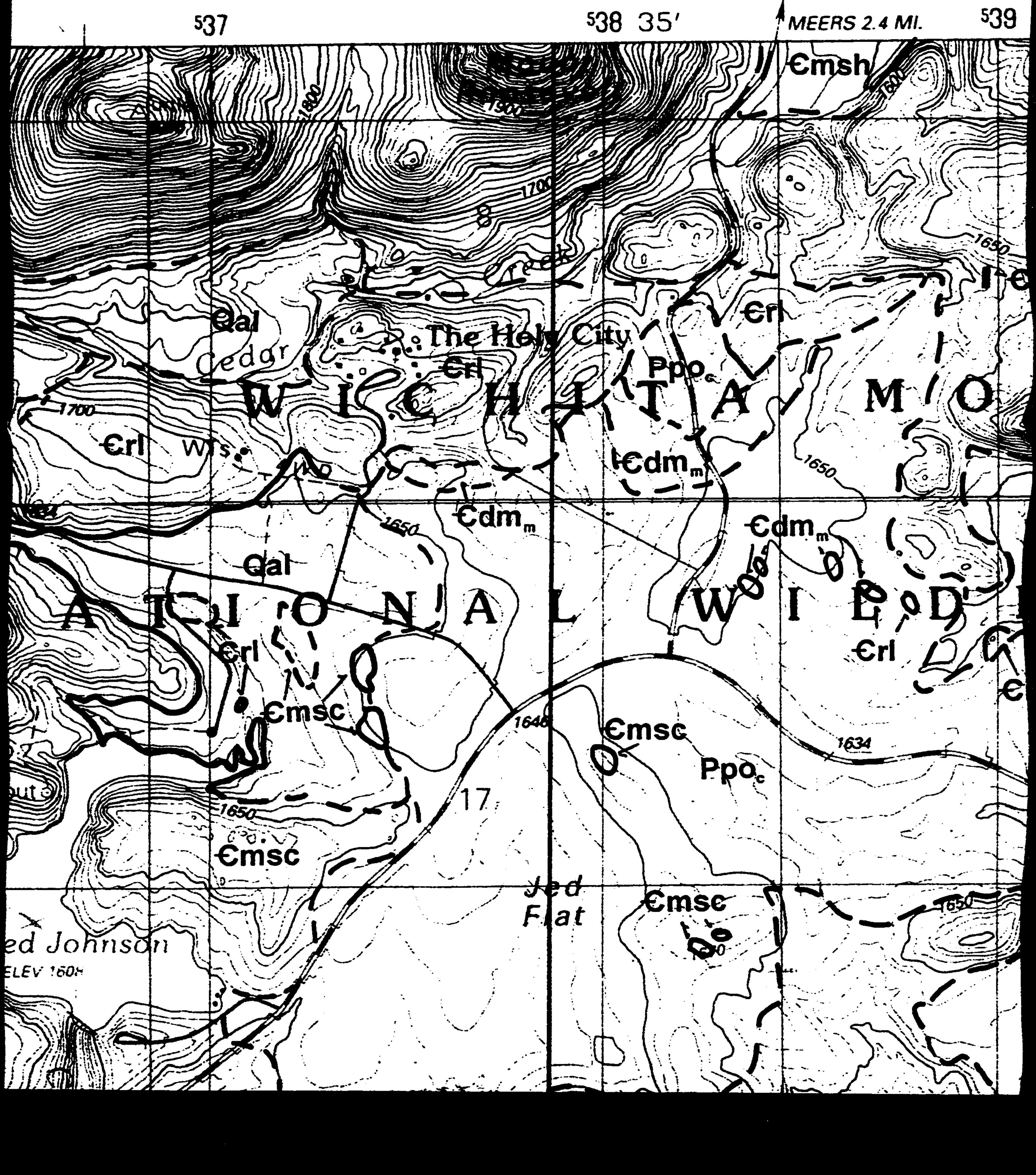
537
538 35′
MEERS 2.4 MI.
539
Ꞓmsh
1800
1900
1700
1650
Ꞓrl
Qal
Cedar
The Holy City
Ꞓrl
Ppo꜀
W I C H I T A M O
1700
Ꞓrl
Ꞓdm$_m$
1650
Ꞓdm$_m$
Ꞓdm$_m$
Qal
A T I O N A L W I L D
Ꞓrl
Ꞓrl
Ꞓmsc
1646
Ꞓmsc
1634
Ppo꜀
17
1650
Ꞓmsc
Jed
Flat
Ꞓmsc
1650
ed Johnson
ELEV 160

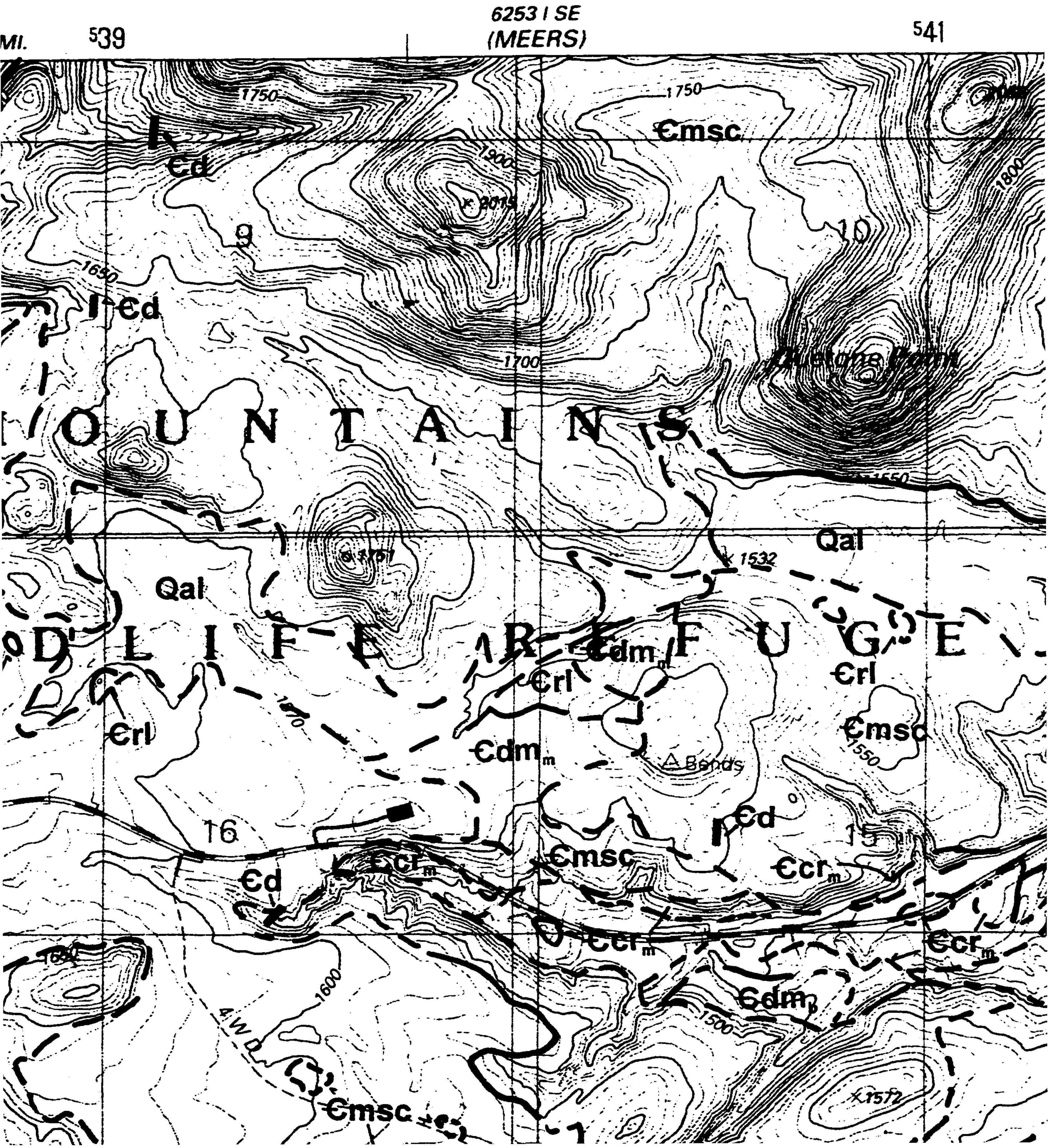

6253 I SE
(MEERS)
MI.
539
541
1750
Єmsc
Єd
1900
9
10
1800
1650
1700
OUNTAINS
1550
Qal
1532
DLIFE REFUGE
Єdm
Єrl
Єmsc
Bends
16
15
Єcr
1600
1500
4WD
1572

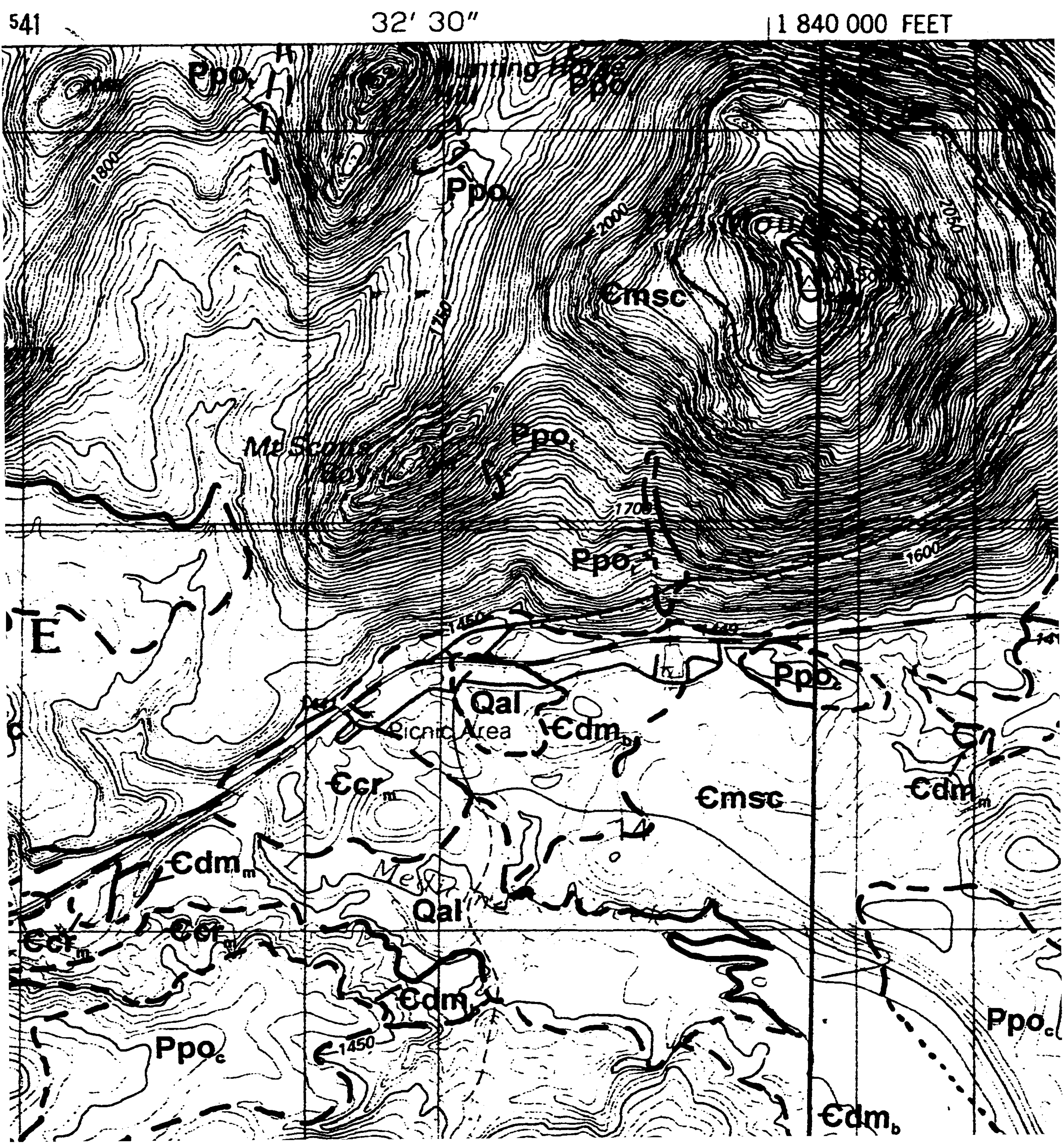
541
32′ 30″
1 840 000 FEET
Ppo
Ppo
Ppo
1800
2000
1750
Ɛmsc
Ppo
1700
Ppo
1600
1450
E
Qal
Picnic Area
Ɛdm
Ɛcr
Ɛmsc
Ɛdm
Ɛdm
Qal
Ɛcr
Ɛcr
Ɛdm
Ppo
Ppo
1450
Ɛdm
Ppo

Pl

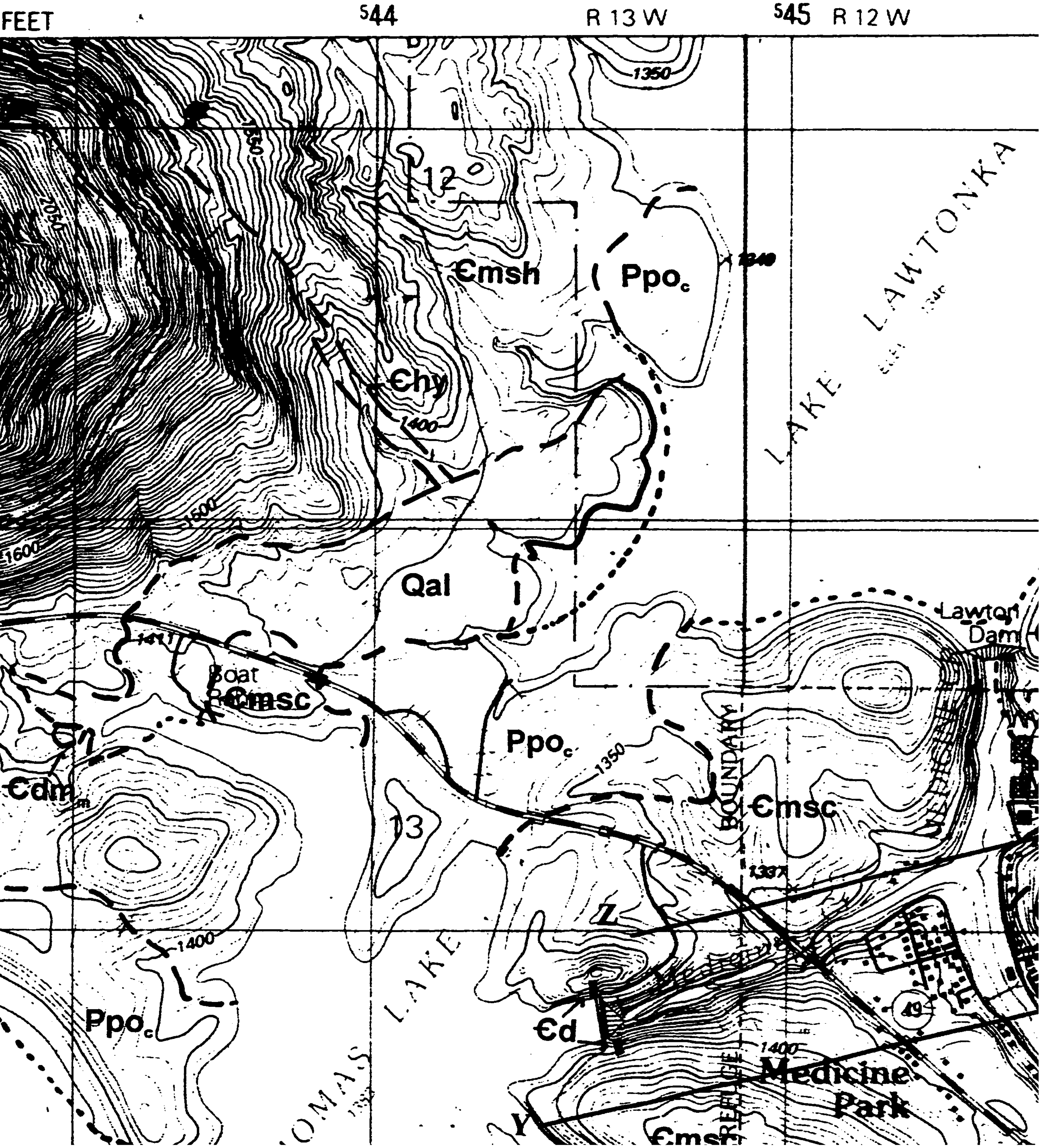

FEET
544
R 13 W
545
R 12 W
1350
12
Єmsh
Ppo$_c$
1340
LAKE LAWTONKA
Єhy
1400
1600
Qal
Boat
Єmsc
Lawton
Dam
Єdm$_m$
Ppo$_c$
1350
BOUNDARY
Єmsc
13
1337
Z
1400
LAKE
Ppo$_c$
Єd
1400
Medicine
Park
49
REFUGE
Y

Plate II

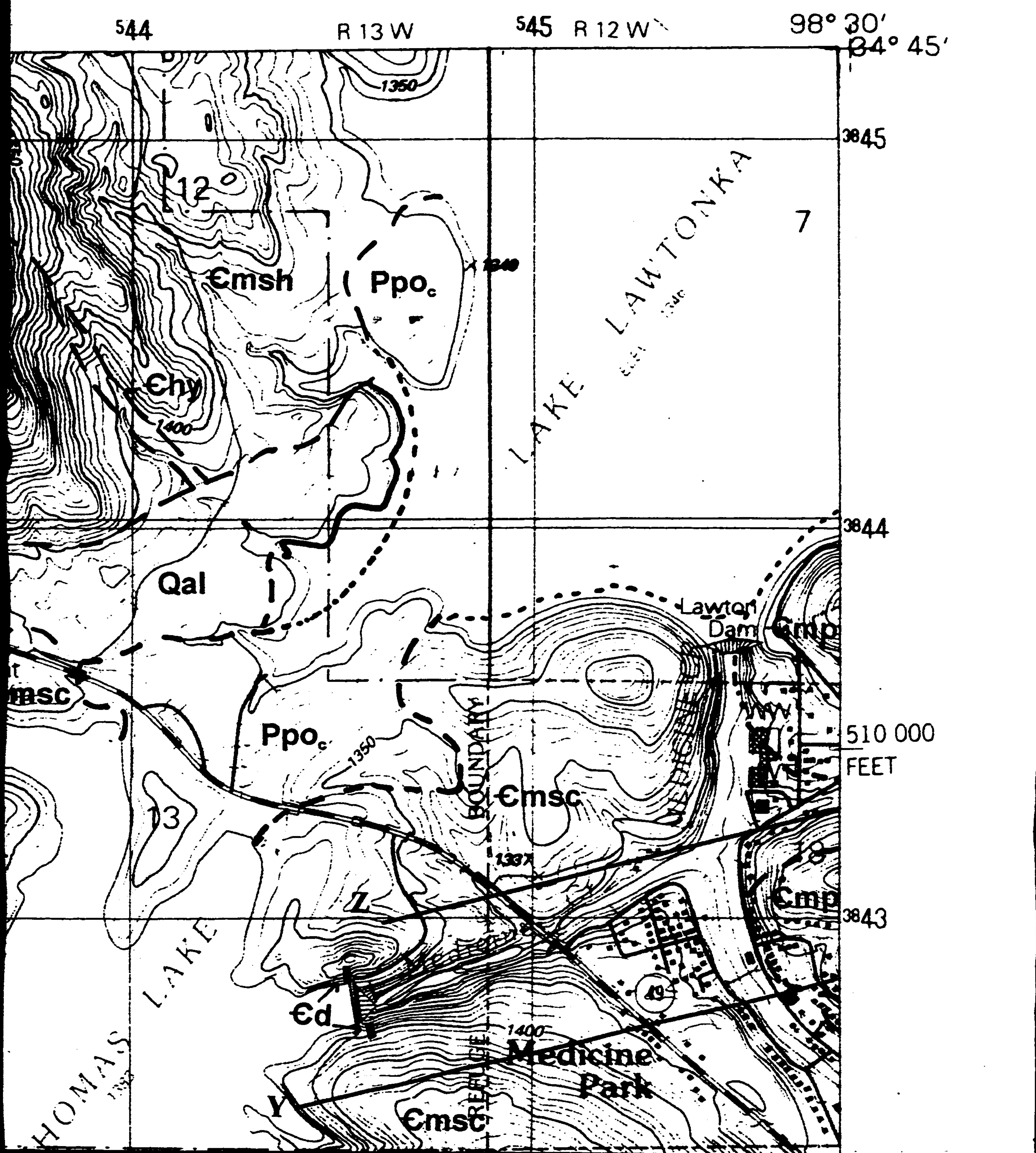

544
R 13 W
545
R 12 W
98° 30′
34° 45′
3845
3844
3843
510 000
FEET
1350
1400
12
7
13
8
LAKE LAWTONKA
THOMAS LAKE
Ꞓmsh
Ppo_c
Ꞓhy
Qal
Ꞓmsc
Ꞓmp
Ꞓd
Ꞓmsc
Lawton Dam
REFUGE BOUNDARY
Medicine Park
Z
Y
1337
49

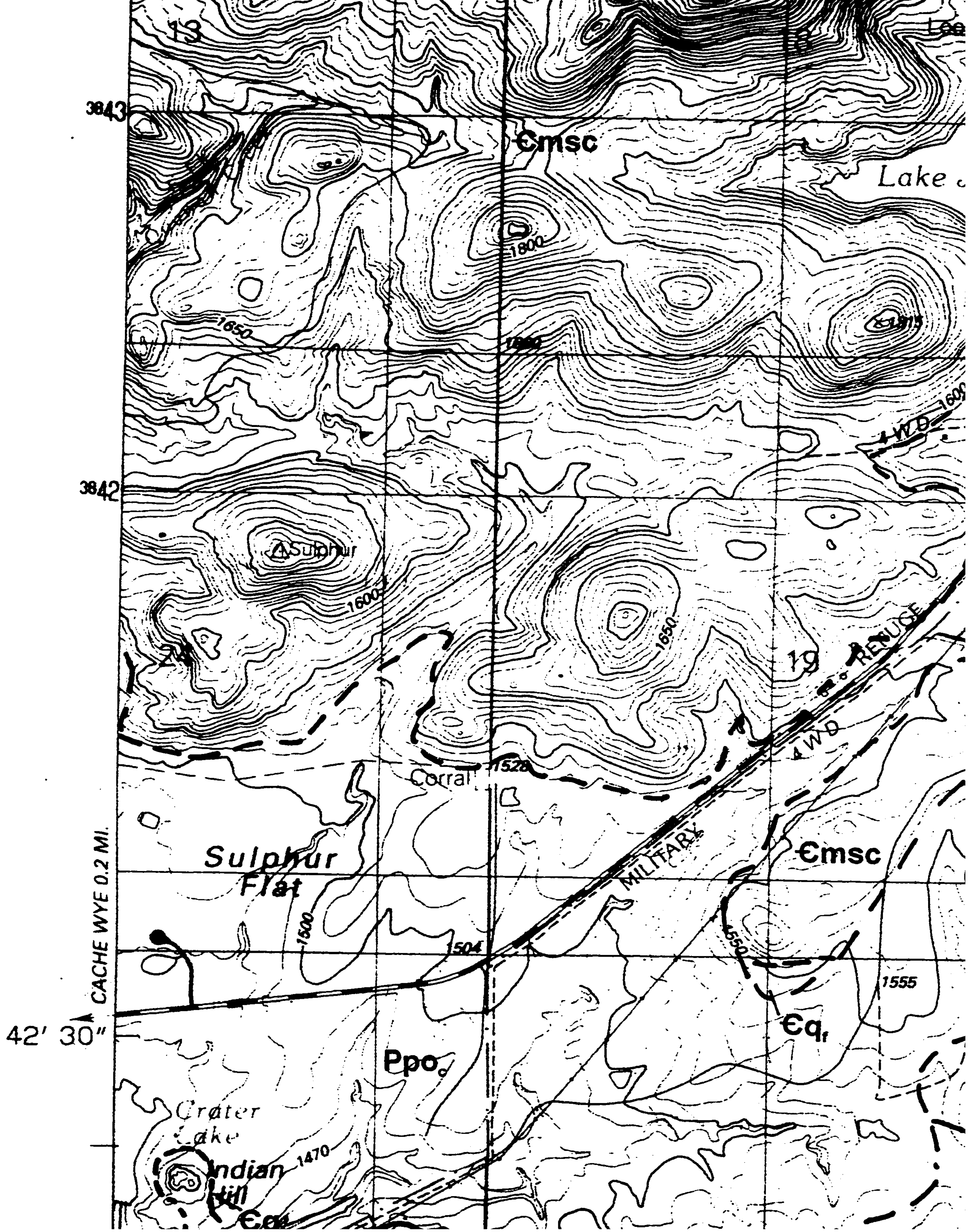
13
3843
Єmsc
1800
1650
3842
Sulphur
1600
1650
19
REFUGE
24
Corral
1528
4WD
Sulphur
Flat
MILITARY
Єmsc
1500
1504
1550
1555
Єq
Ppo
CACHE WYE 0.2 MI.
42' 30"
Crater
Lake
Indian
Hill
1470

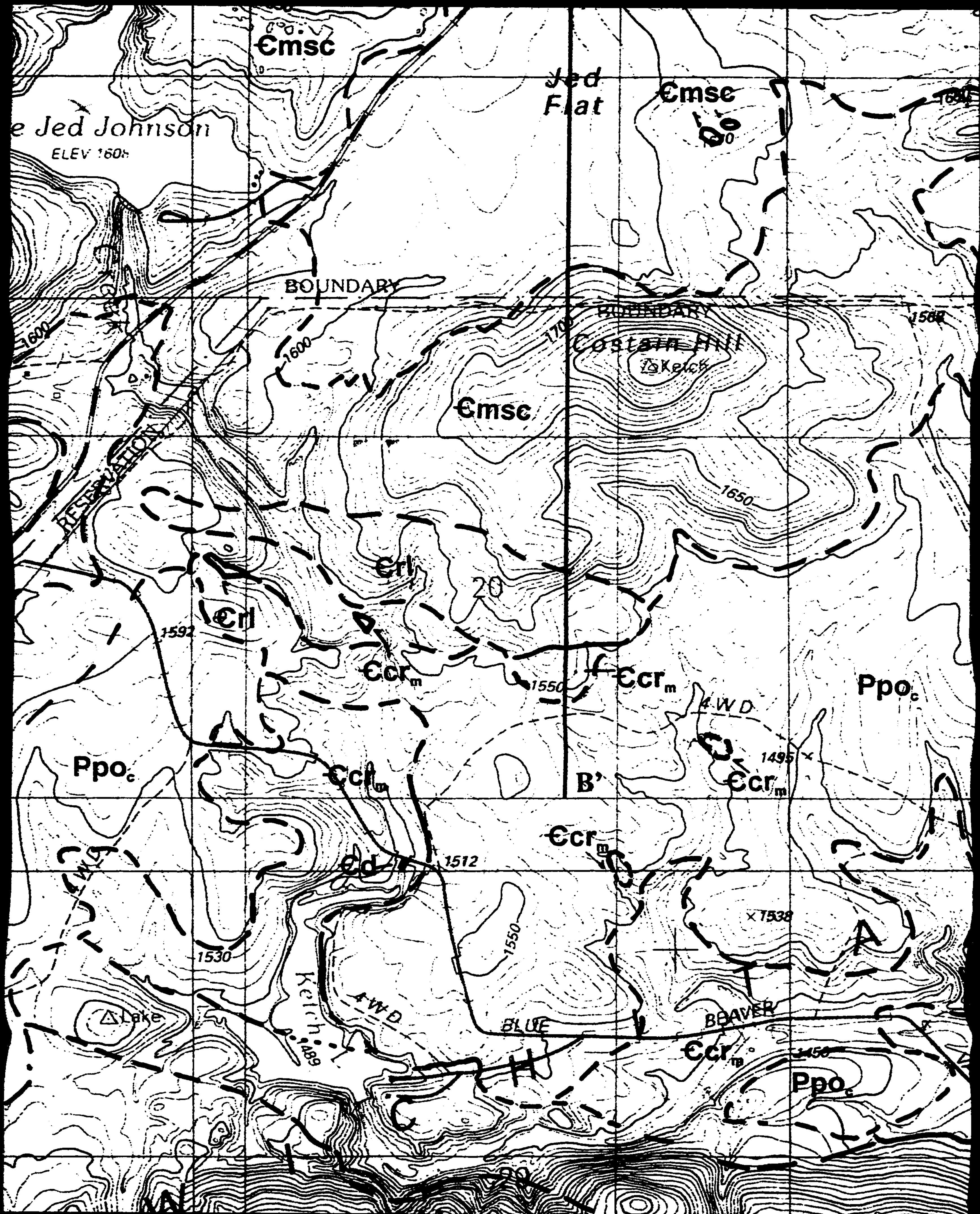

Ꞓmsc
Jed Flat
Ꞓmsc
e Jed Johnson
BOUNDARY
BOUNDARY
1600
1600
1700
Costain Hill
Ketch
Ꞓmsc
RESERVATION
1650
Ꞓrl
20
Ꞓrl
1592
Ꞓcrm
1550
Ꞓcrm
4WD
Pрoc
1495
Ppoc
Ꞓclm
B'
Ꞓcrm
Ꞓcrm
Ꞓd
1512
1550
1538
1530
Lake
4WD
BLUE
BEAVER
1489
1450
Ꞓcrm
Ppoc

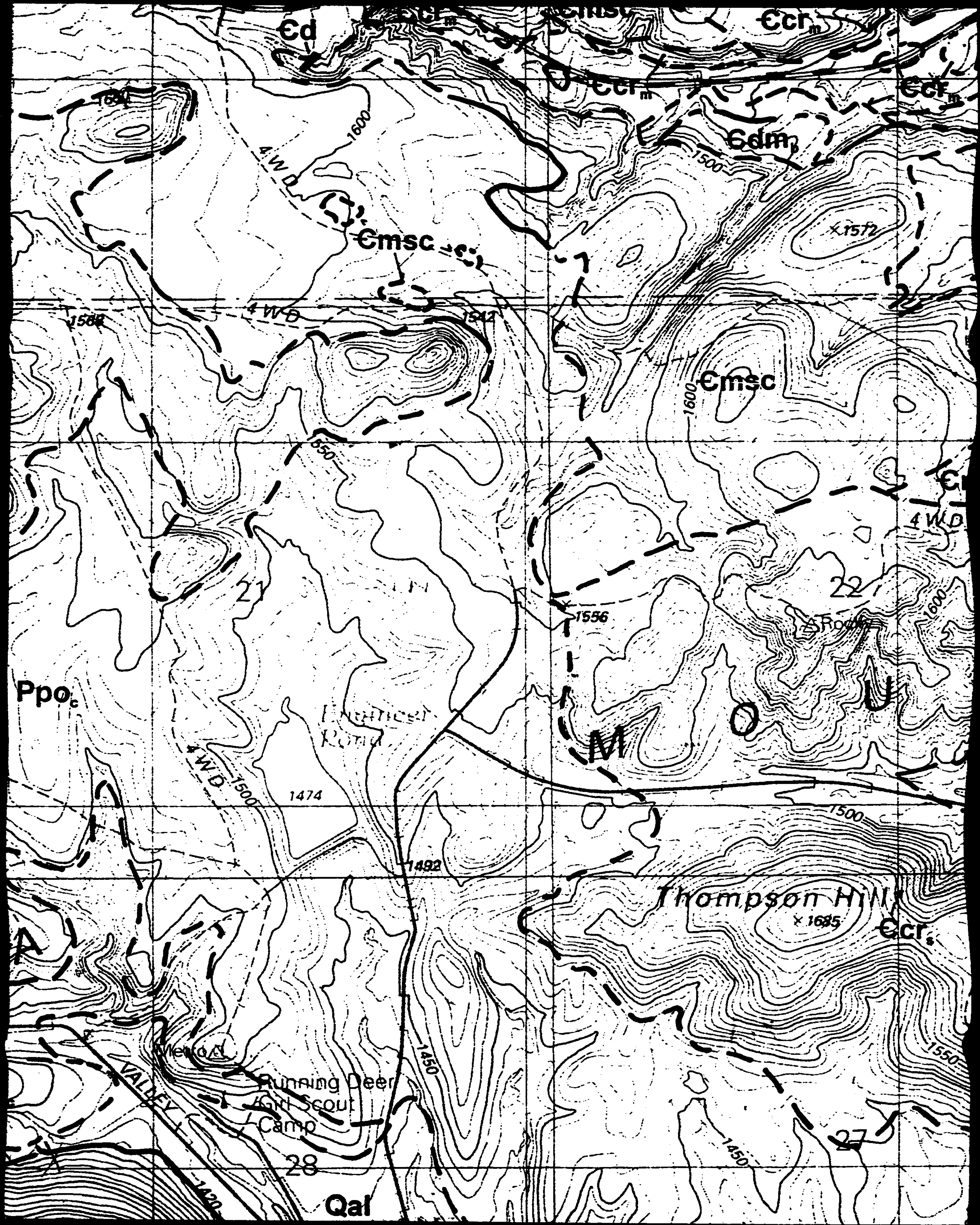
Ɛd
Ɛcr
Ɛcr
Ɛcr
Ɛdm
4 W D
1600
1500
Ɛmsc
x 1572
4 W D
1588
1542
Ɛmsc
1600
4 W D
21
22
1556
Ppo
M
O
U
4 W D
1500
1474
1482
Thompson Hill
× 1685
Ɛcr
1500
1450
1550
Running Deer
Girl Scout
Camp
VALLEY
28
27
1450
Qal

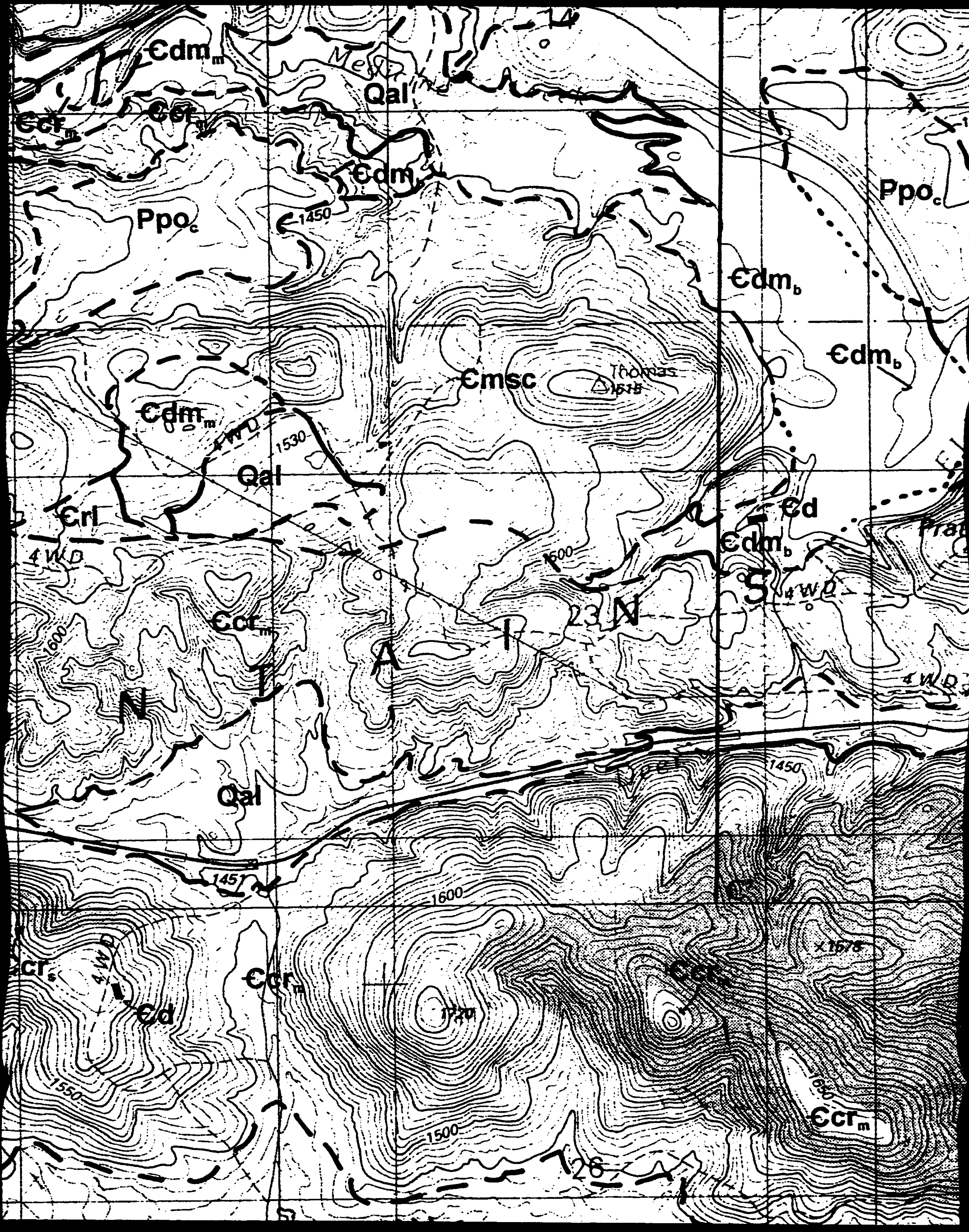

Ꞓdm$_{m}$
Ꞓcr$_{m}$
Ꞓcr$_{m}$
Qal
Ꞓdm$_{s}$
1450
Ppo$_{c}$
Ppo$_{c}$
Ꞓdm$_{b}$
Ꞓdm$_{b}$
Ꞓmsc
Thomas
Ꞓdm$_{m}$
4WD
1530
Qal
Ꞓrl
Ꞓd
Ꞓdm$_{b}$
4 W D
4 W D
1600
Ꞓcr$_{m}$
1600
23
N T A I N S
Qal
1450
1457
1600
Ꞓcr$_{s}$
Ꞓd
Ꞓcr$_{m}$
1720
Ꞓcr$_{m}$
1675
1550
1500
26
Ꞓcr$_{m}$

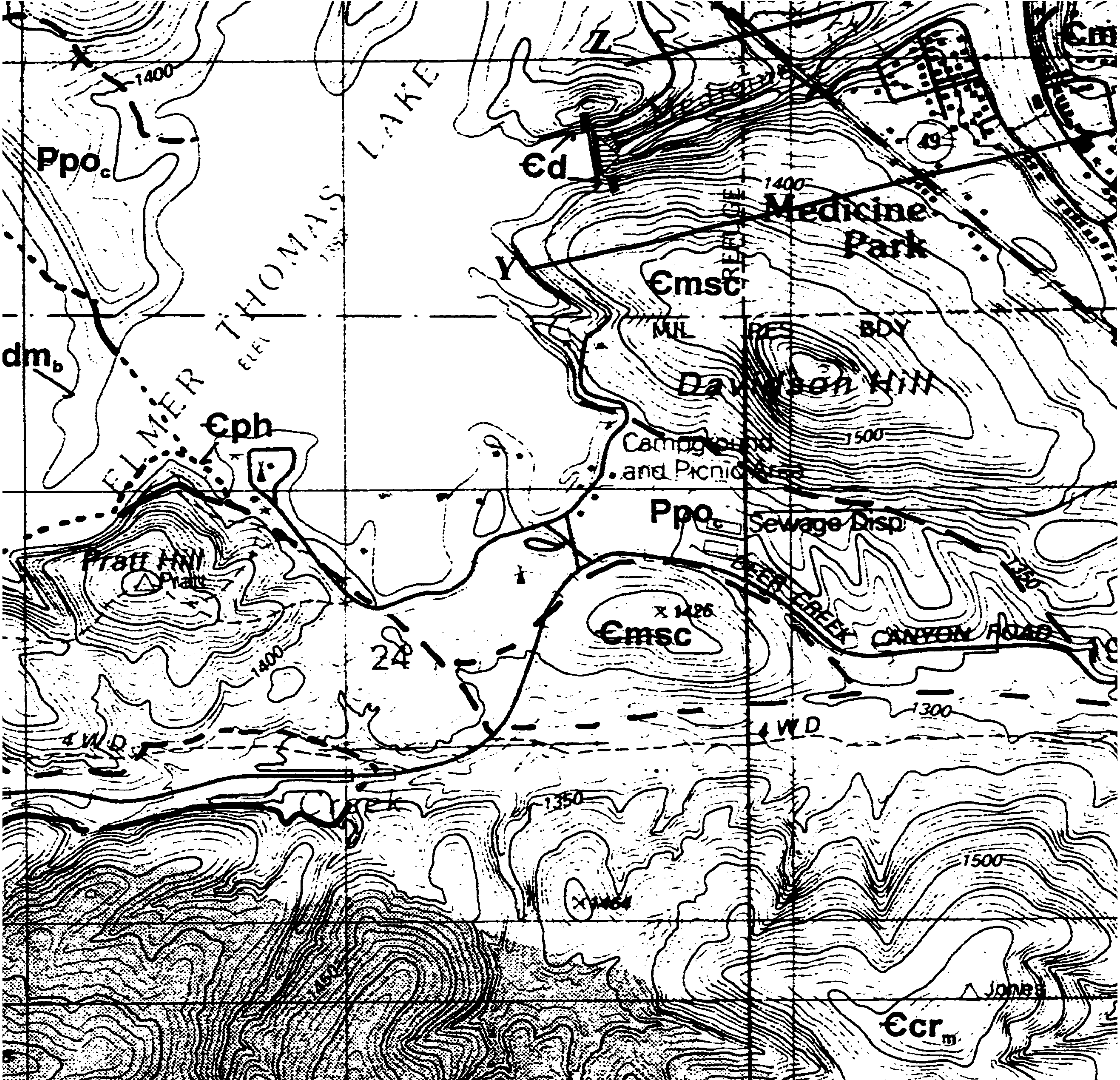
ELMER THOMAS LAKE
Ppo
c
dm
b
Єph
Pratt Hill
Pratt
1400
24
4 WD
1350
Єd
Y
Z
Medicine Park
49
Єmsc
MIL RES BDY
Campground and Picnic Area
Ppo
c
Sewage Disp
DEER CREEK CANYON ROAD
x 1426
1500
1300
Jones
Єcr
m

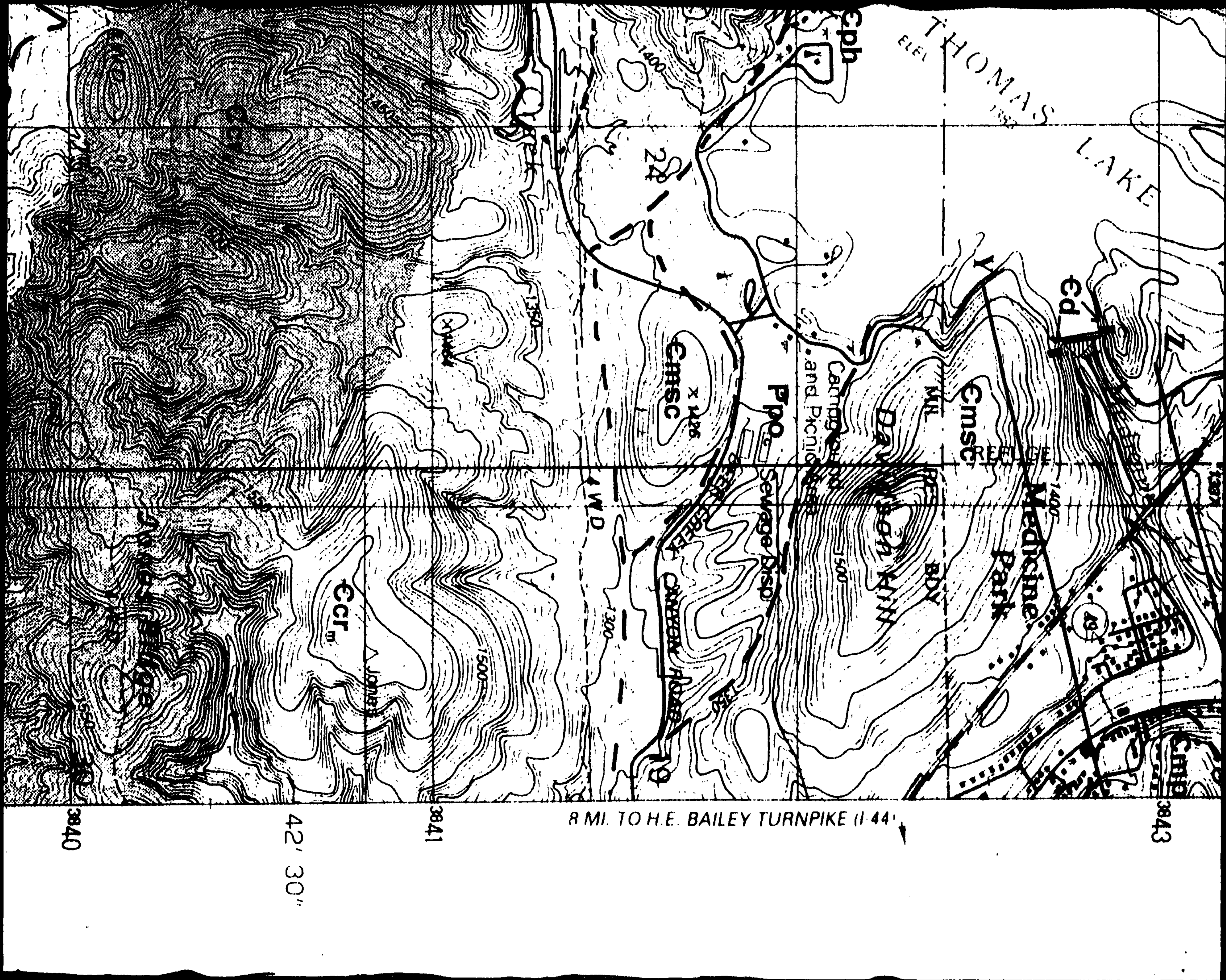

THOMAS
LAKE
Medicine
Park
REFUGE
BDY
Sewage Disp
8 MI. TO H.E. BAILEY TURNPIKE (I-44)
3840
3841
3843
42' 30"

GEOLOGIC MAP OF
MOUNT SCOT

T 3 N

6253 II NW
(QUANAH MOUNTAIN)

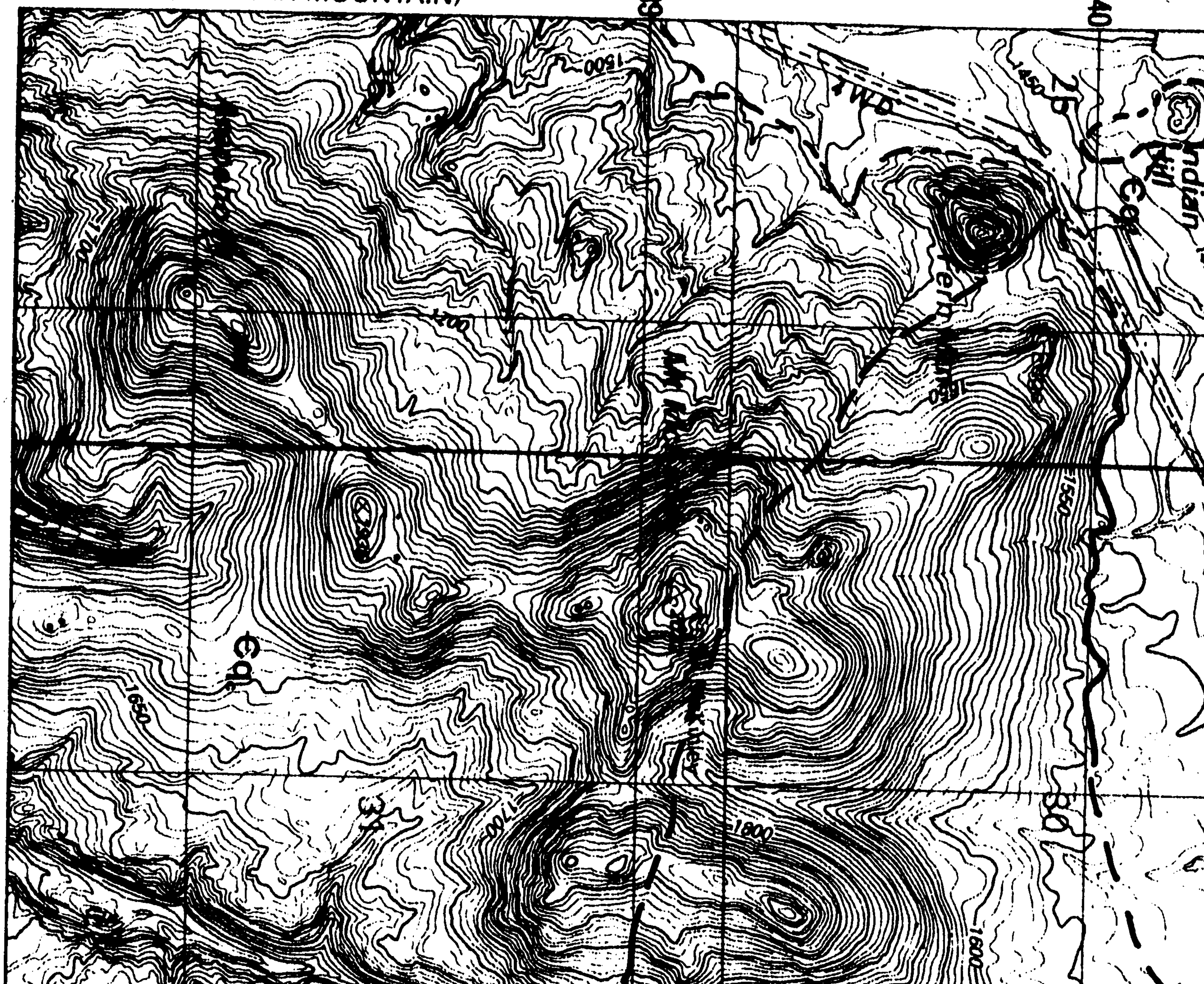

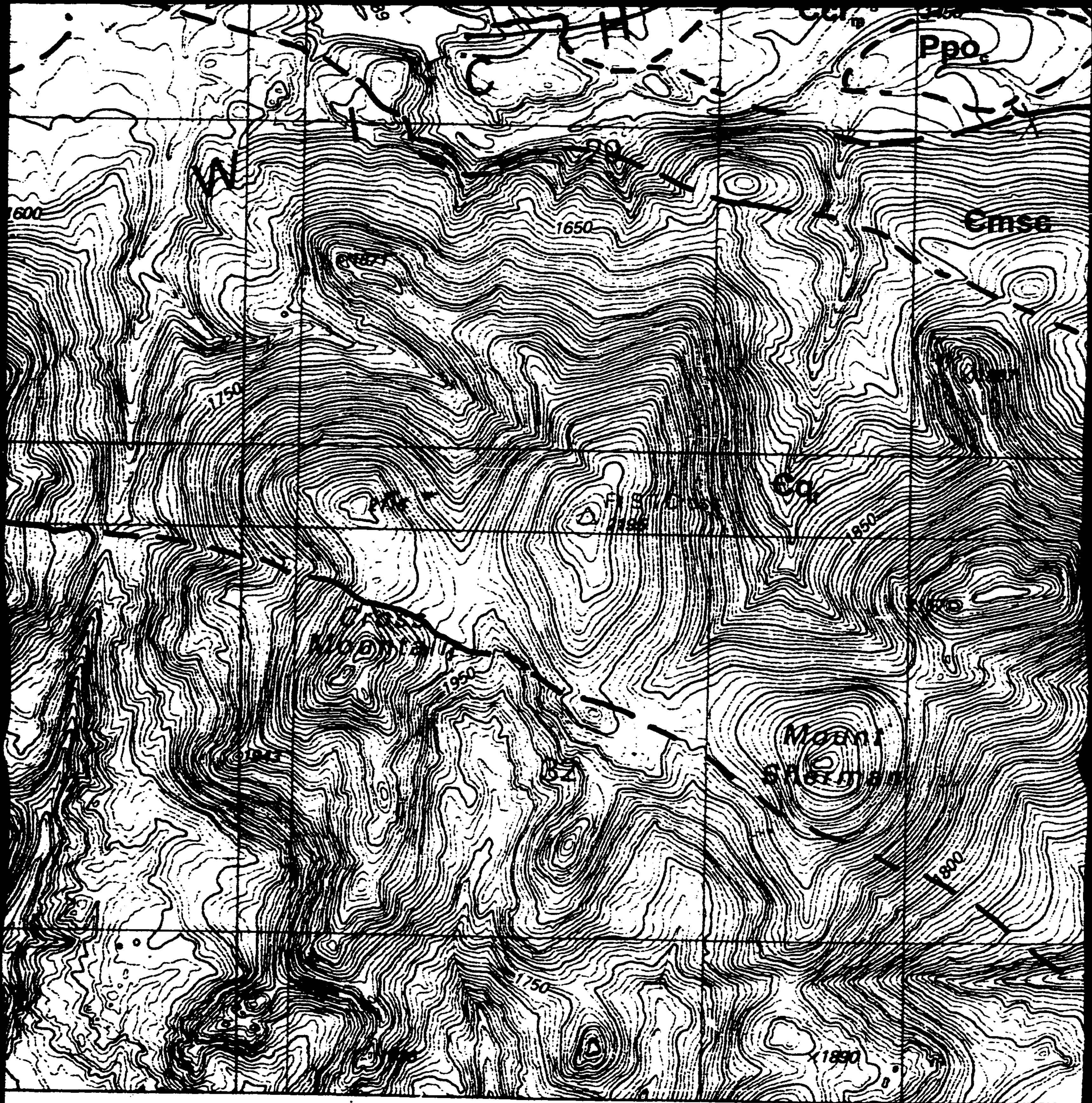

F THE NORTH
T 7.5′

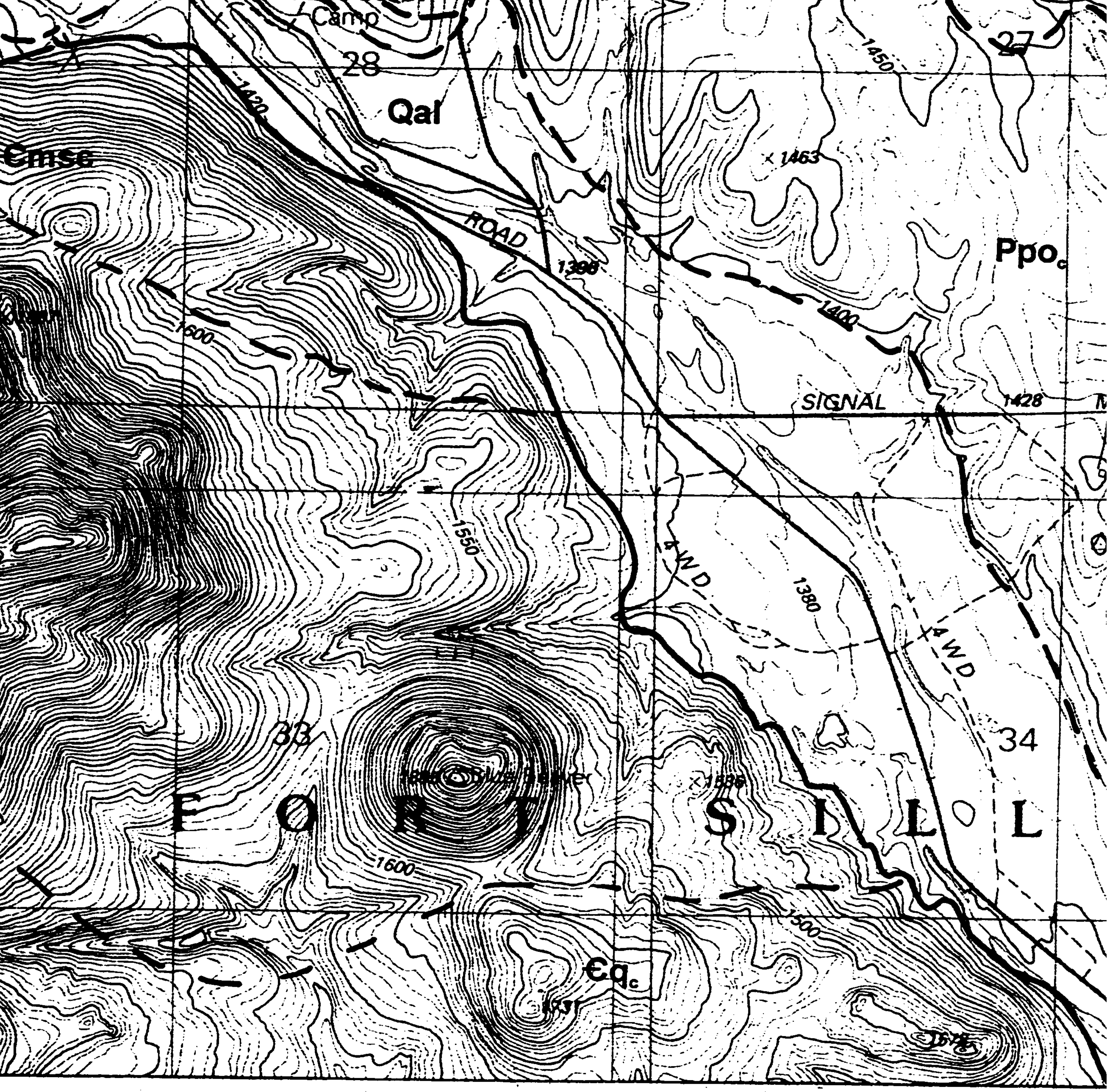

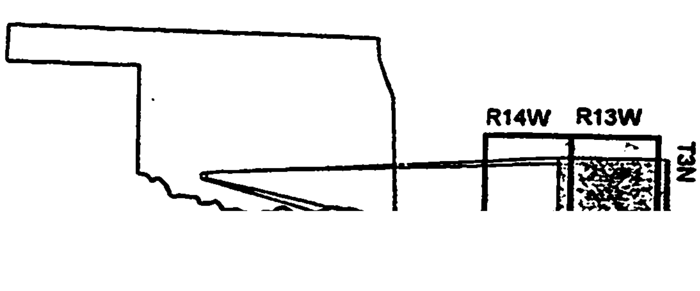

Scale 1:12 000

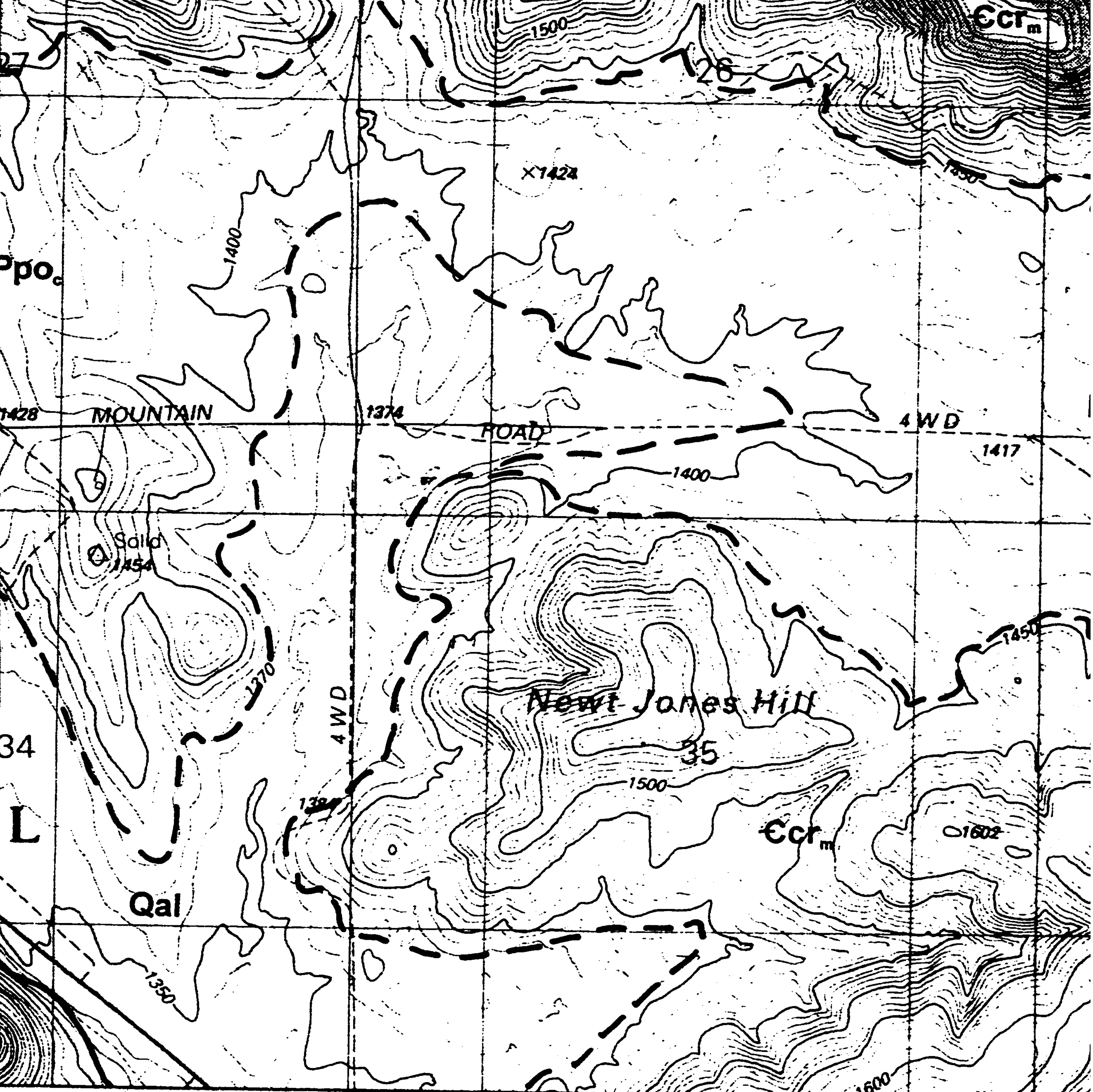

Quaternary

Qal — **Alluvium**
Sand and silt fill within modern and recent stream valleys.

Cambrian

€d

€q$_c$

:12 000

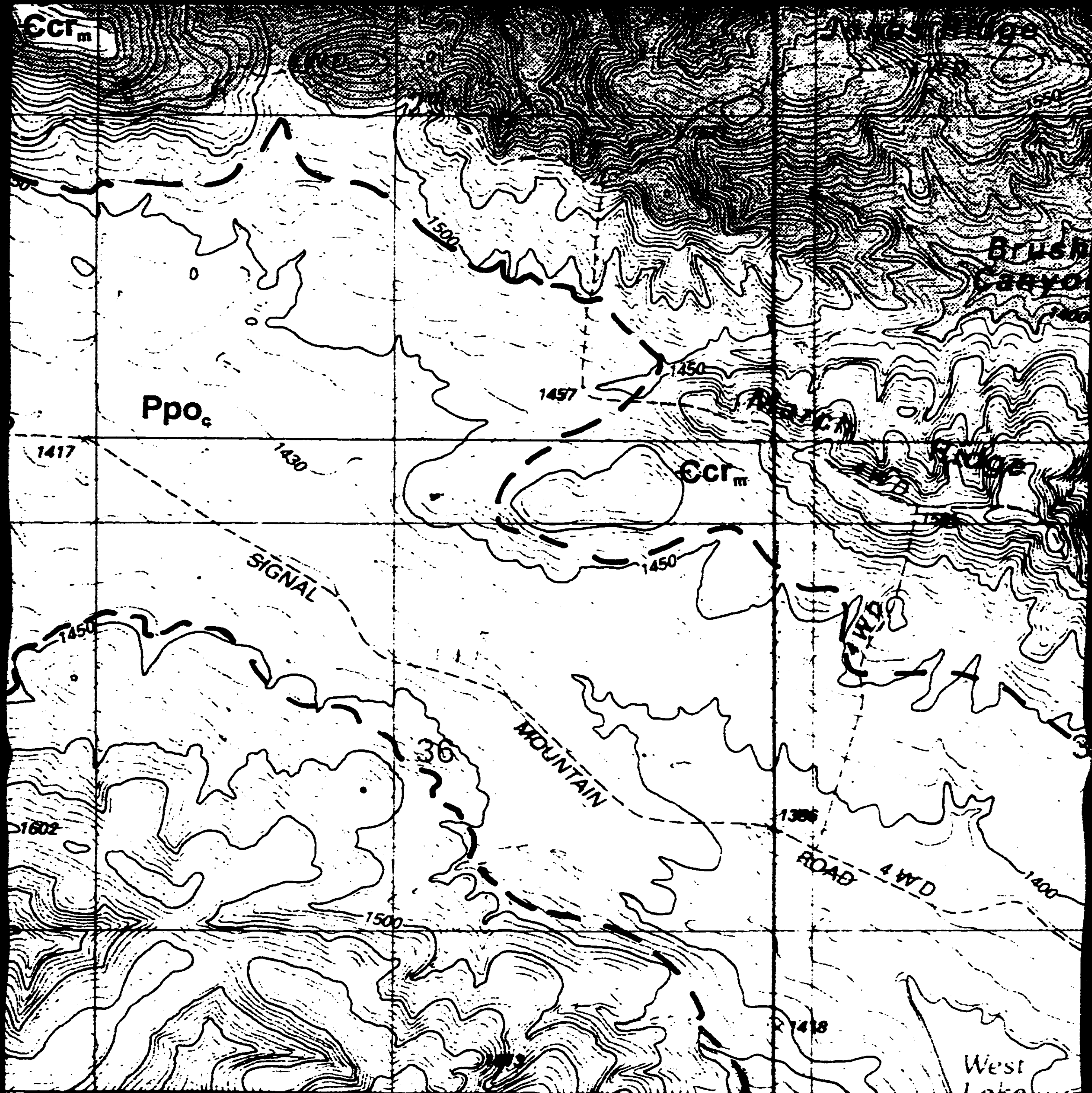

Cambrian

€d	**Diabase** Black, fine-grained aphyric dikes.
€q$_c$	**Quanah Granite, coarse-grained** Pink to light pink coarse- to medium-grained equigranular granite.
€mp	**Medicine Park Granite** Weakly porphyritic pink-purple fine-grained alkali-feldspar granite, with quartz veins.
€cr$_s$	**Carlton rhyolite, spherulitic** Porphyritic rhyolite with orange feldspar and gray quartz phenocrysts, and orange bands

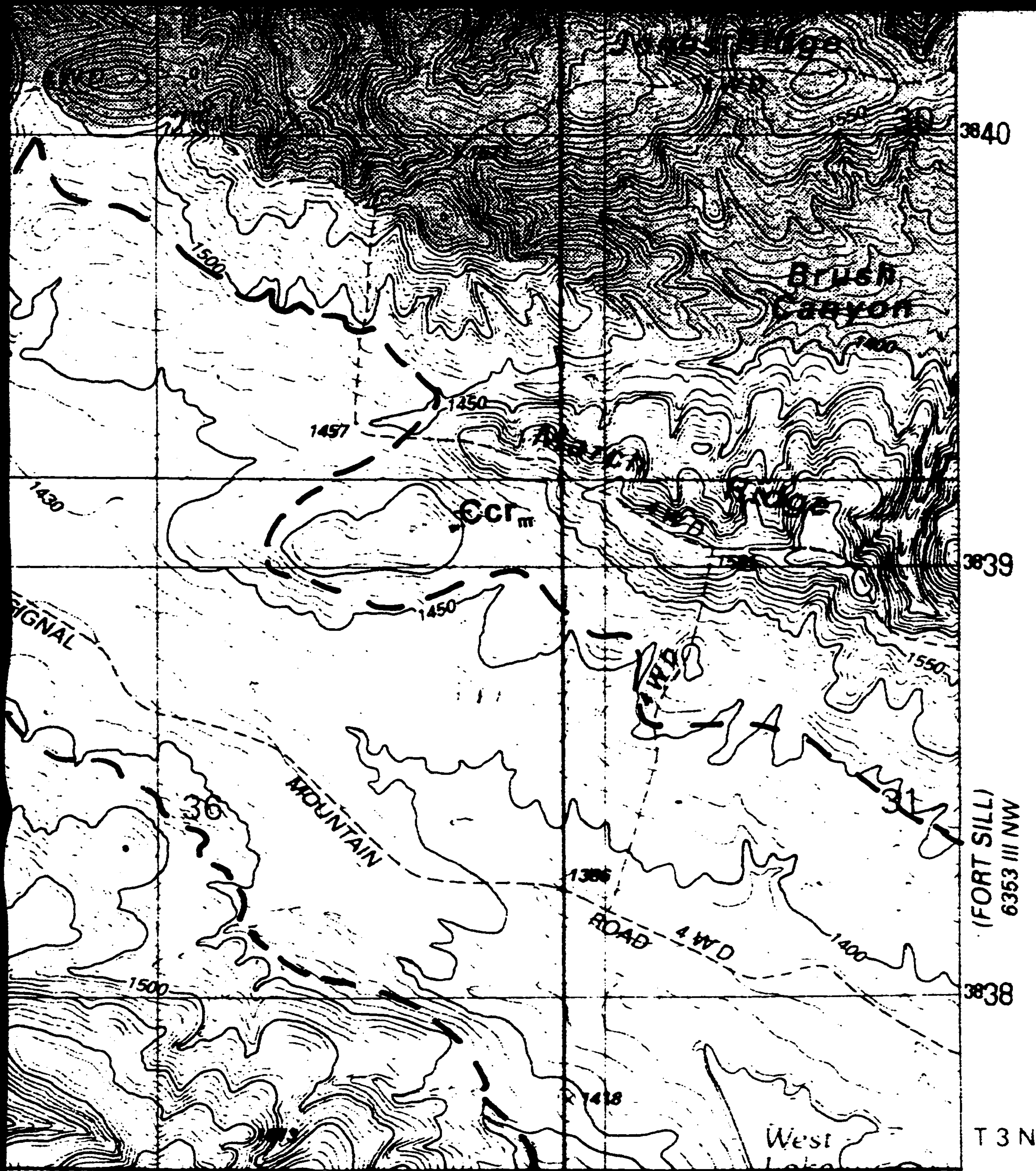

ained aphyric dikes.

Granite, coarse-grained
pink coarse- to medium-grained
granite

Ꞓmp	**Medicine Park Granite** Weakly porphyritic pink-purple fine-grained alkali-feldspar granite, with quartz veins.
Ꞓcr$_s$	**Carlton rhyolite, spherulitic** Porphyritic rhyolite with orange feldspar and gray quartz phenocrysts, and orange bands

GEOLOGIC MAP OF
MOUNT SCOTT
QUADRANGLE, OK

Jonathan D. Price

1998

Produced in cooperation with the U. S.
National Cooperative Geological M

)F THE NORTH
)TT 7.5'
OKLAHOMA
ce

U. S. Geological Survey,
al Mapping Program

Topographi
Mount Scot
quadrang
N.A.D '27 p
Universal Ti

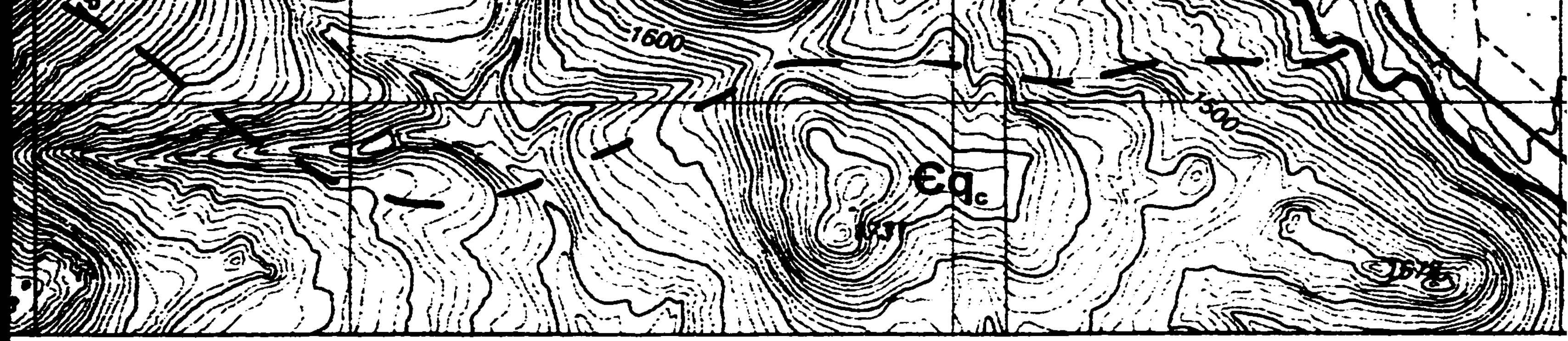

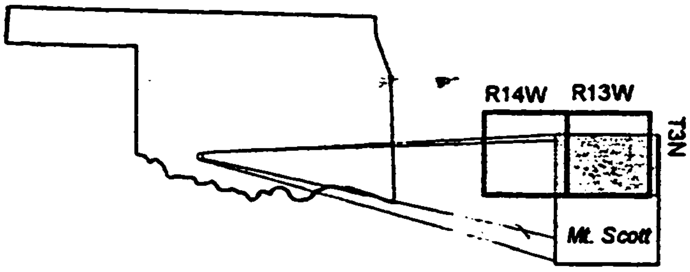

Scale 1:12

0 km

0 mile

Topographic Base from
Mount Scott U.S.G.S. 7.5 minute
quadrangle, 1991
N.A.D '27 projection
Universal Transverse Mercator Zone 14.

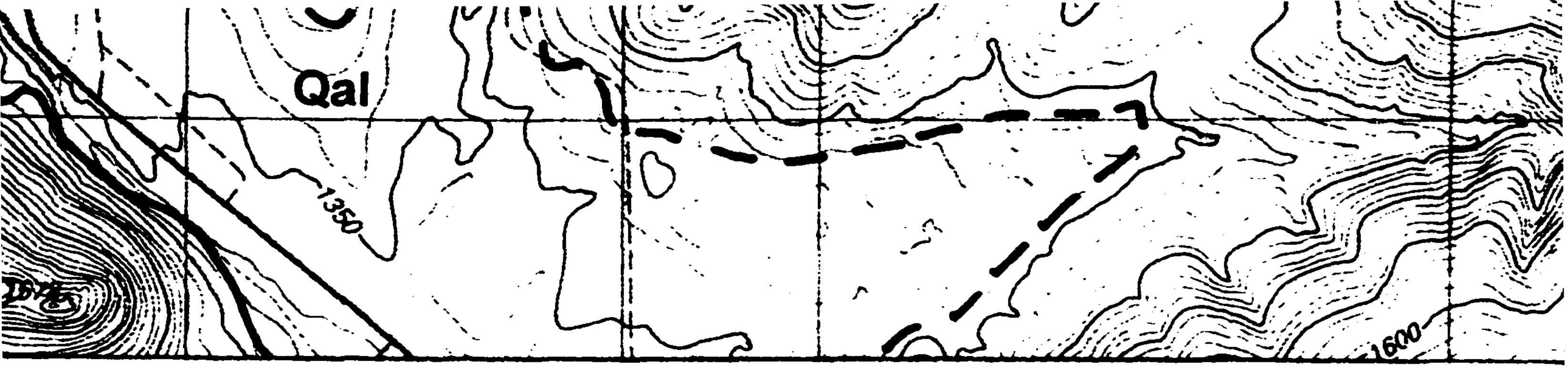

cale 1:12 000

km 1

1

Quaternary

Qal — **Alluvium**
Sand and silt fill within modern and recent stream valleys.

Permian

Ppo_c — **Post Oak conglomerate**
Conglomerate with rounded boulders in a feldspar-rich matrix.

Ppo_t — **Post Oak conglomerate, talus**
Variably-sized boulders of Mount Scott Granite, some commonly infilled with sand, silt, and soil.

Ca

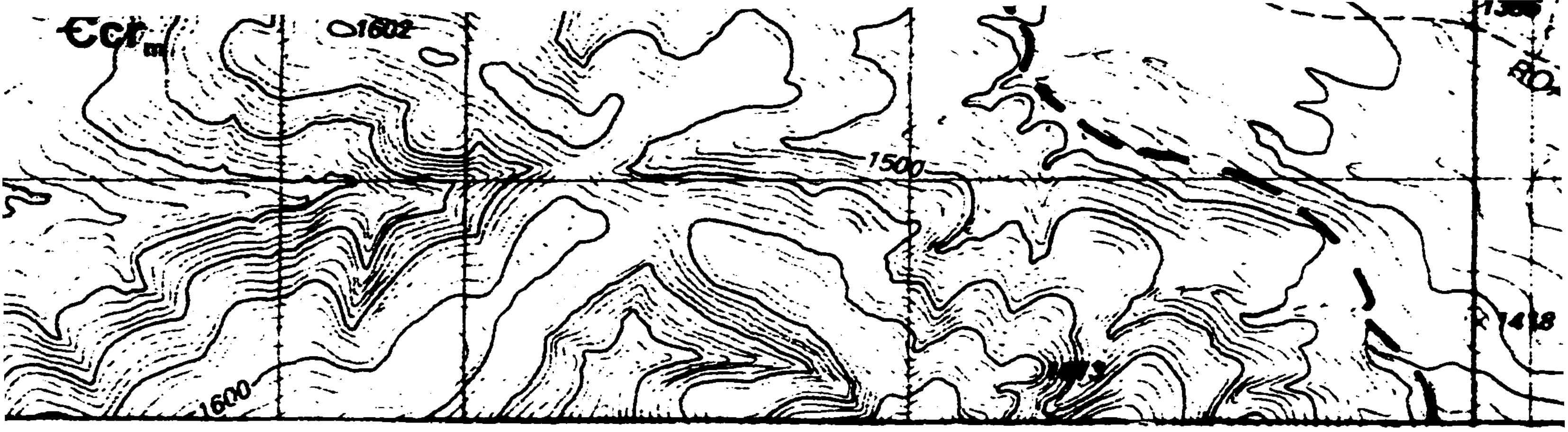

n and recent

te
ulders in a

e, talus
nt Scott Granite,
nd, silt, and soil.

Cambrian

Ꞓd — **Diabase**
Black, fine-grained aphyric dikes.

Ꞓq_c — **Quanah Granite, coarse-grained**
Pink to light pink coarse- to medium-grained equigranular granite.

Ꞓq_f — **Quanah Granite, fine-grained**
Pink to light-pink fine- to medium-grained aplitic, seriate, and porphyritic granite.

Ꞓhy — **Hybrid rock**
Pink and green, amphibole-rich granitoid rocks of intermediate composition.

Ꞓmsh — **Mount Sheridan Gabbro**
Dark-gray to dark-red-brown biotite gabbro with common white pegmatite dikes and pods.

Ꞓmsc — **Mount Scott Granite**
Pink to brick red porphyritic, variably granophyric granite with gray ovoid feldspar.

Ꞓrl — **Rush Lake granite**
Pink to brick-red, seriate, variably granophyric granite with connected quartz.

Ꞓmp — **Medicine**
Weakly porph
alkali-feldspa

Ꞓcr_s — **Carlton rh**
Porphyritic rh
gray quartz p

Ꞓcr_m — **Carlton rh**
Massive porph
and gray qua

Ꞓph — **Pratt Hill**
Green-gray, w
contact, white

Ꞓdm_m — **Davidson**
Pink to buff, h
feldspathic m

Ꞓdm_b — **Davidson**
Banded buff t
and white mic

Ꞓgm — **Glen Mou**
Dark- to white
gabbro, and o

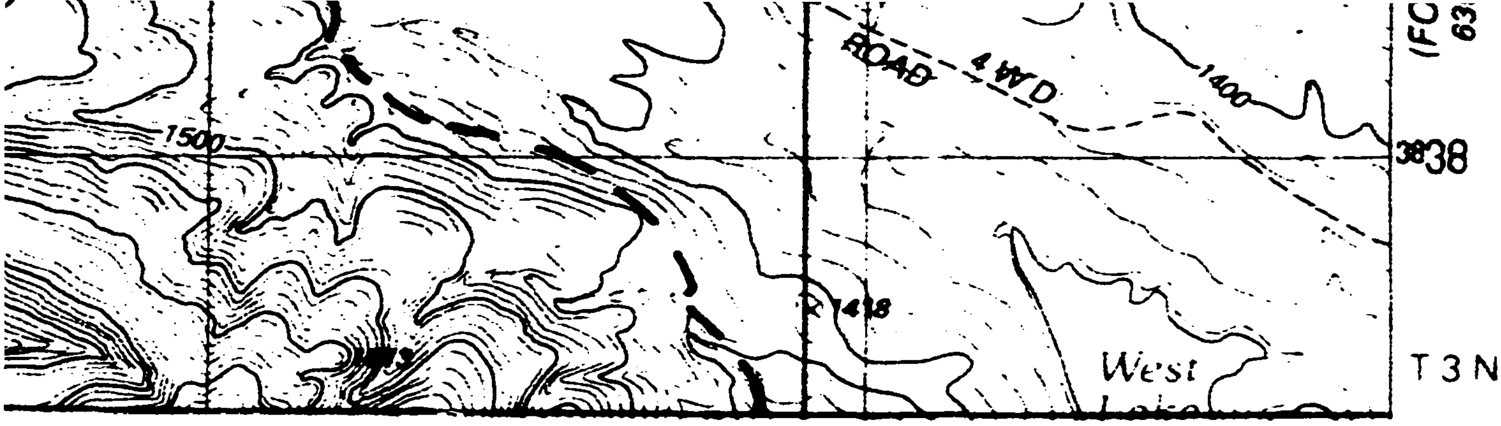

ed aphyric dikes.

anite, coarse-grained
k coarse- to medium-grained
anite.

anite, fine-grained
k fine- to medium-grained
nd porphyritic granite.

k
amphibole-rich granitoid rocks
composition.

idan Gabbro
rk-red-brown biotite gabbro with
pegmatite dikes and pods.

t Granite
l porphyritic, variably
nite with gray ovoid feldspar.

granite
l, seriate, variably granophyric
nected quartz.

€mp	**Medicine Park Granite** Weakly porphyritic pink-purple fine-grained alkali-feldspar granite, with quartz veins.
€cr_s	**Carlton rhyolite, spherulitic** Porphyritic rhyolite with orange feldspar and gray quartz phenocrysts, and orange bands
€cr_m	**Carlton rhyolite, massive** Massive porphyritic rhyolite with orange feldspar and gray quartz phenocrysts.
€ph	**Pratt Hill quartzite** Green-gray, with darker color near upper contact, white-mica bearing quartzite.
€dm_m	**Davidson metarhyolite, massive** Pink to buff, highly fractured, commonly veined feldspathic metarhyolite.
€dm_b	**Davidson metarhyolite, banded** Banded buff to brown colored quartz, feldspar and white mica metarhyolite.
€gm	**Glen Mountains Layered Complex** Dark- to white-gray anorthosite, anorthositic gabbro, and olivine gabbro.

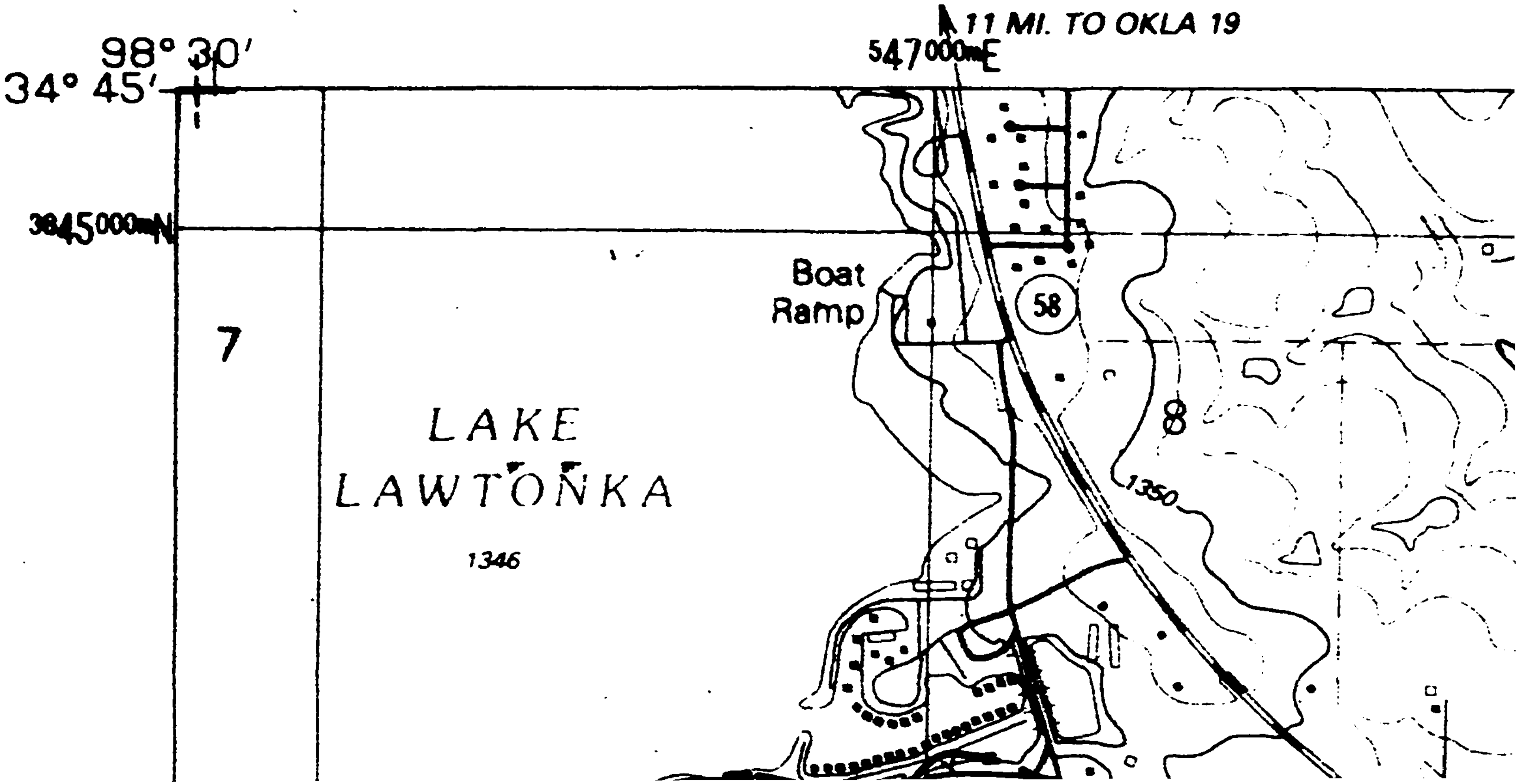

11 MI. TO OKLA 19
98° 30′
34° 45′
547000mE
3845000mN
Boat
Ramp
58
7
8
LAKE
LAWTOÑKA
1346
1350

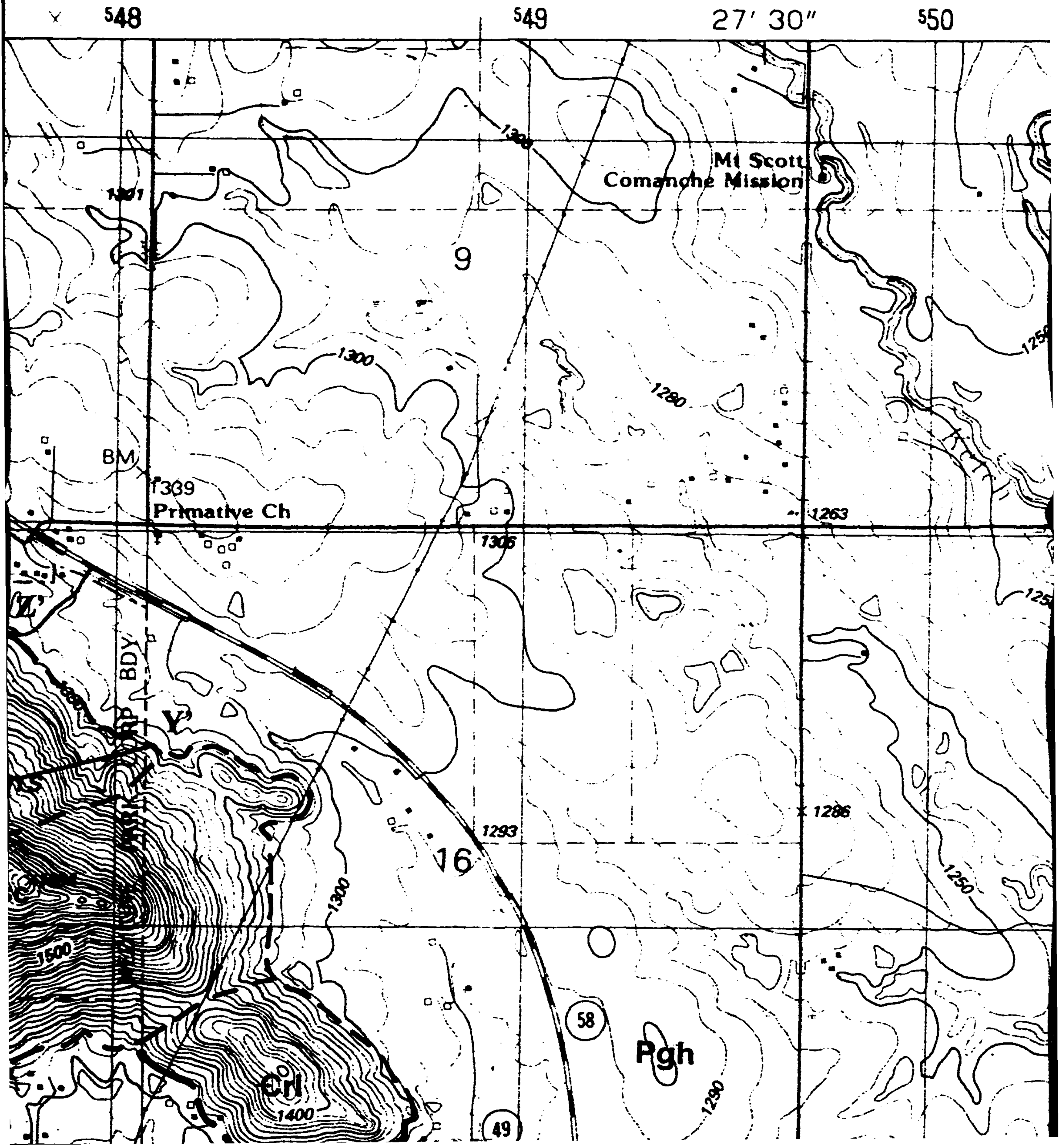

548
549
27′ 30″
550
Mt Scott
Comanche Mission
9
1301
1300
1280
BM
1339
Primative Ch
1263
1306
Y'
BDY
1293
16
1286
1250
1300
1500
58
Pgh
1290
Crl
1400
49

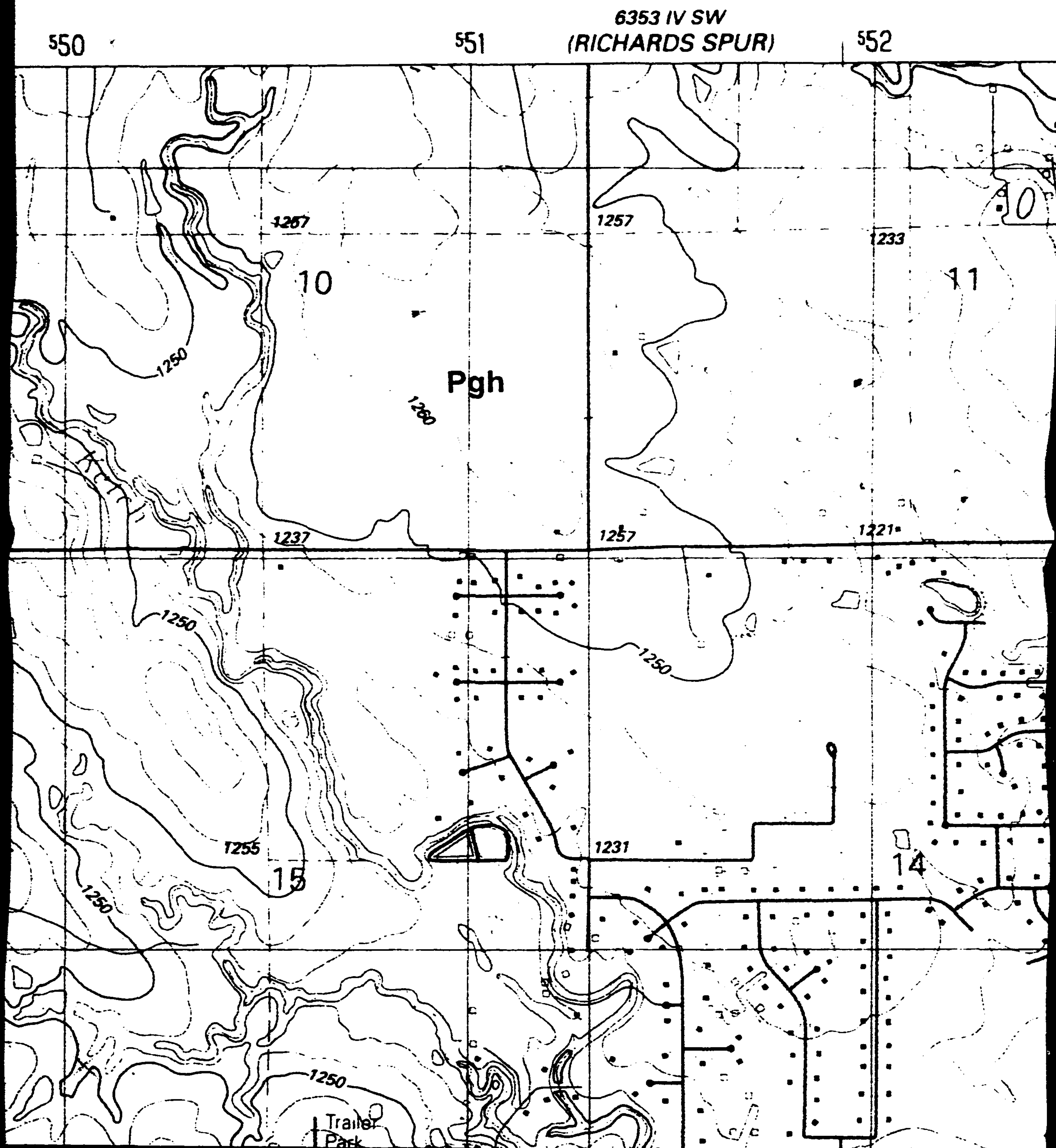
6353 IV SW
(RICHARDS SPUR)
550
551
552
10
11
14
15
Pgh
1257
1233
1250
1260
1237
1221
1255
1231
Trailer
Park

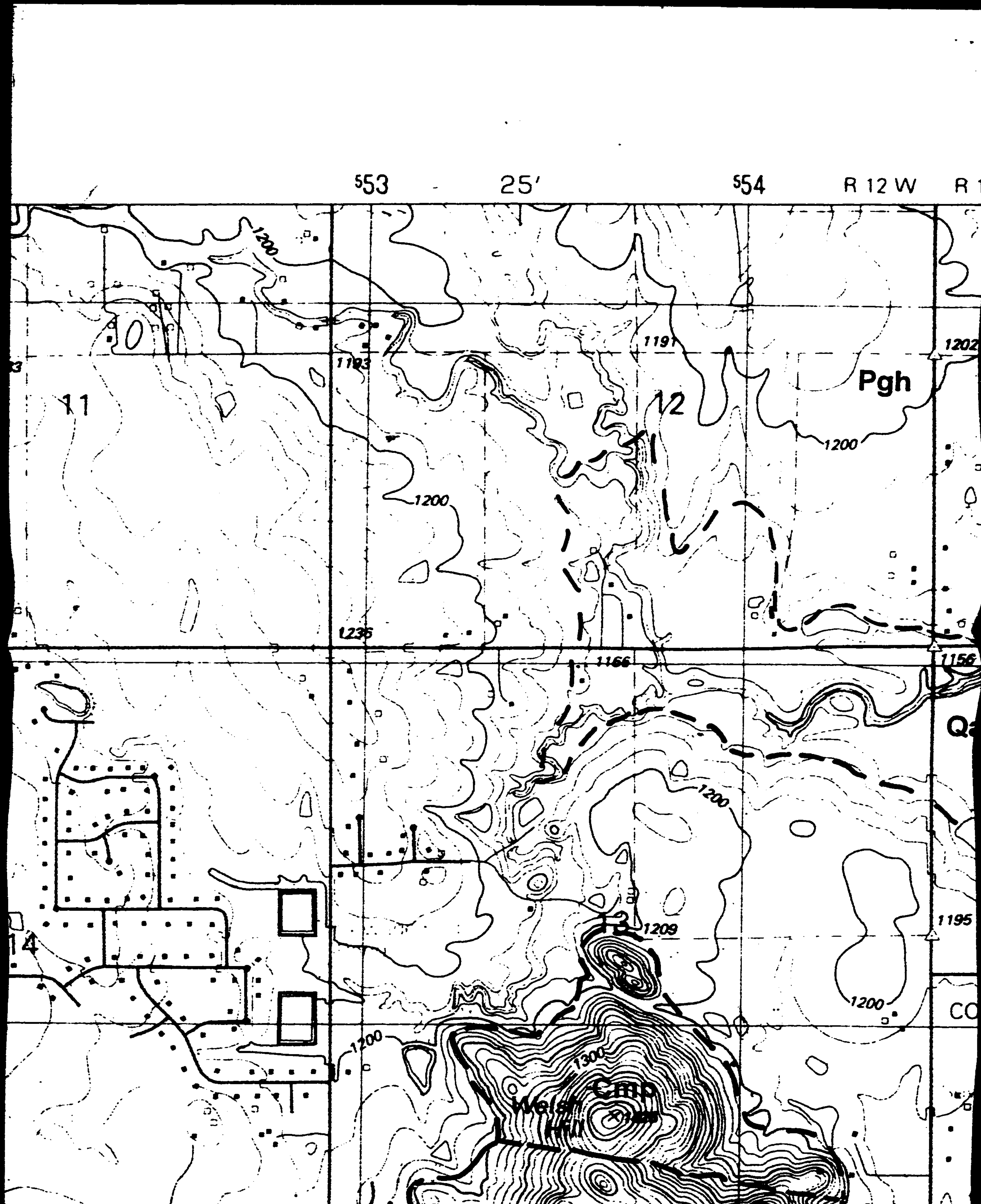

553
25′
554
R 12 W
R 1
1200
1193
1191
1202
Pgh
11
12
1200
1200
1235
1166
1156
Qa
1200
13
1209
1195
1200
CO
14
1200
1300
Cmp
Welsh
Hill

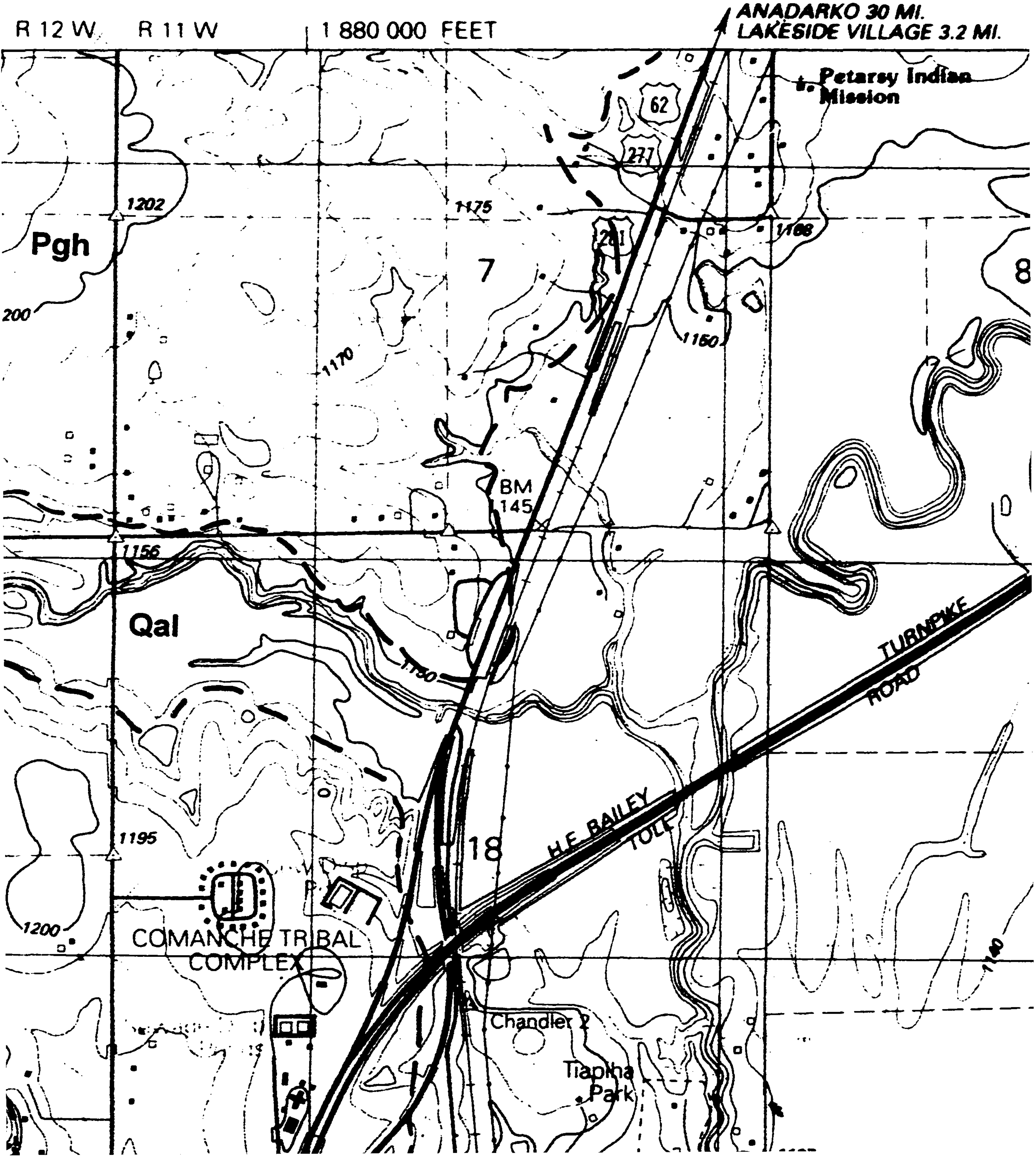
R 12 W.
R 11 W
1 880 000 FEET
ANADARKO 30 MI.
LAKESIDE VILLAGE 3.2 MI.
Petarsy Indian Mission
62
277
281
1202
1175
1168
Pgh
7
8
200
1170
1160
BM
145
1156
Qal
1150
TURNPIKE
ROAD
H.E. BAILEY
TOLL
1195
18
1200
COMANCHE TRIBAL
COMPLEX
1140
Chandler 2
Tiaptha
Park

Plate III

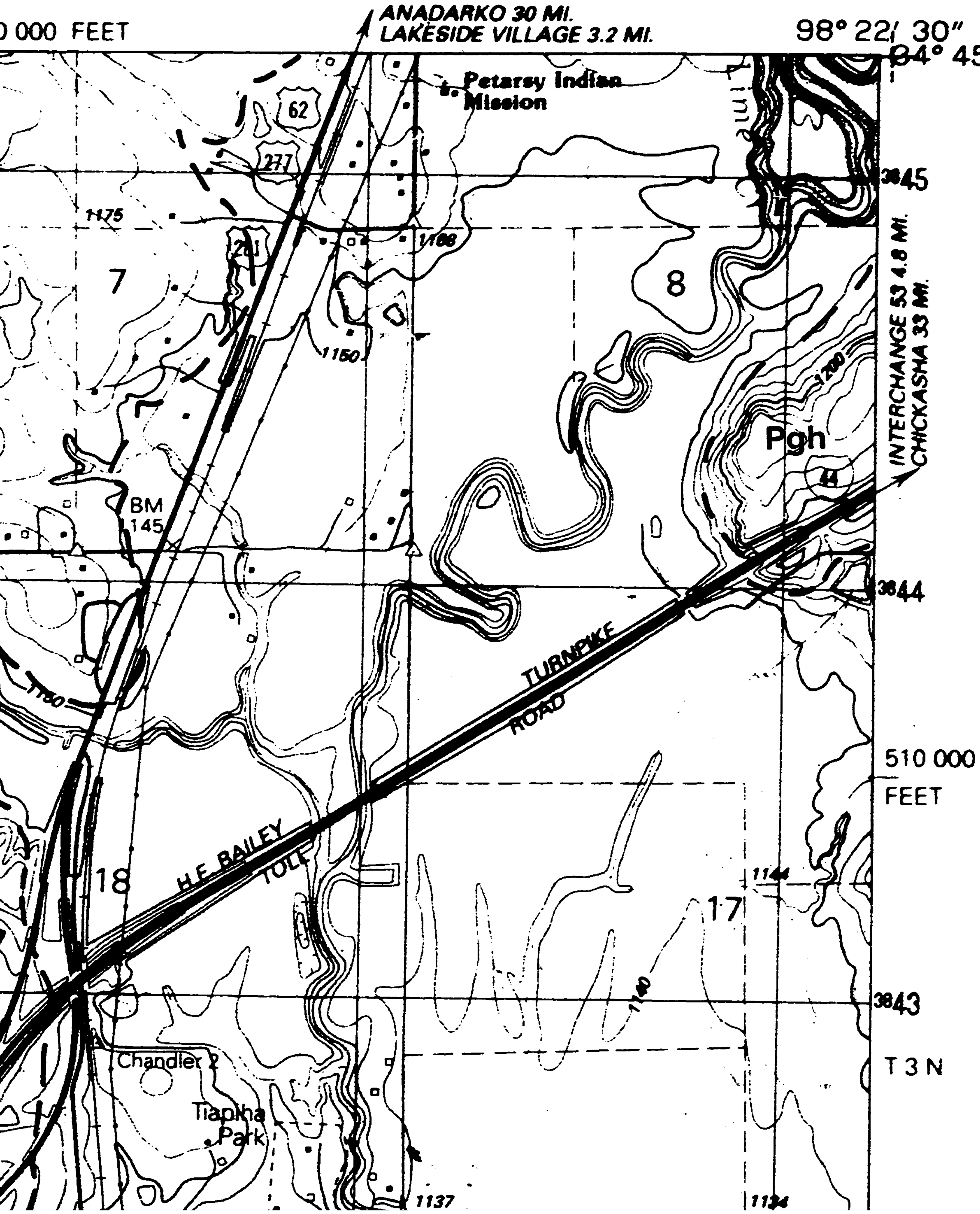

0 000 FEET
ANADARKO 30 MI.
LAKESIDE VILLAGE 3.2 MI.
98° 22' 30"
34° 45'
Petarsy Indian Mission
62
277
281
1175
1168
7
8
1150
3845
INTERCHANGE 53 4.8 MI.
CHICKASHA 33 MI.
Pgh
1200
44
BM
145
3844
TURNPIKE
ROAD
1150
510 000
FEET
H.E. BAILEY
TOLL
18
17
1144
1140
3843
T 3 N
Chandler 2
Tiapiha
Park
1137
1134

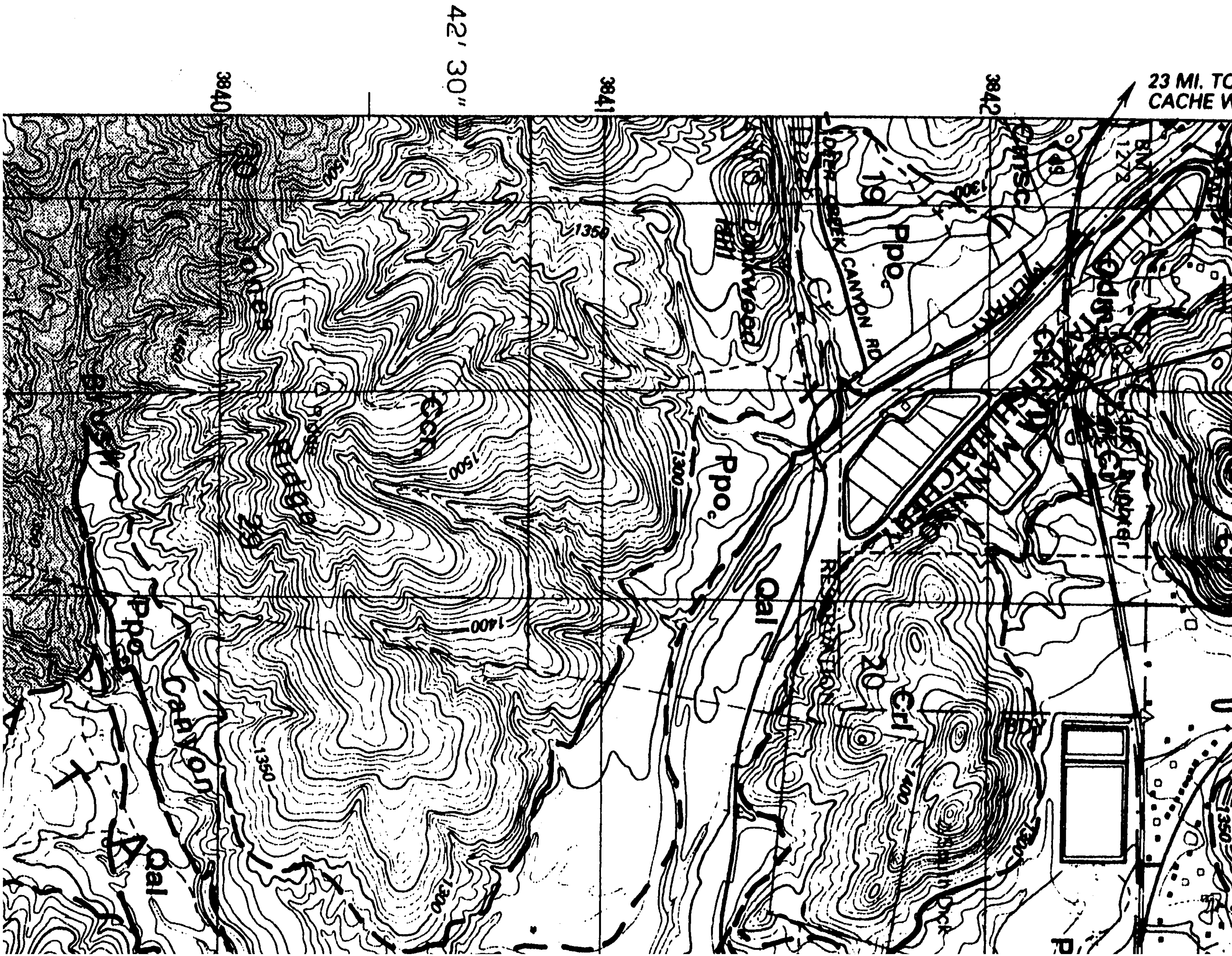
42' 30"
3840
3841
3842
23 MI. TO
CACHE W
1350
1500
1400
1300
Ppo
Qal
Canyon
DEER CREEK CANYON RD
RESERVATION
20
19
29

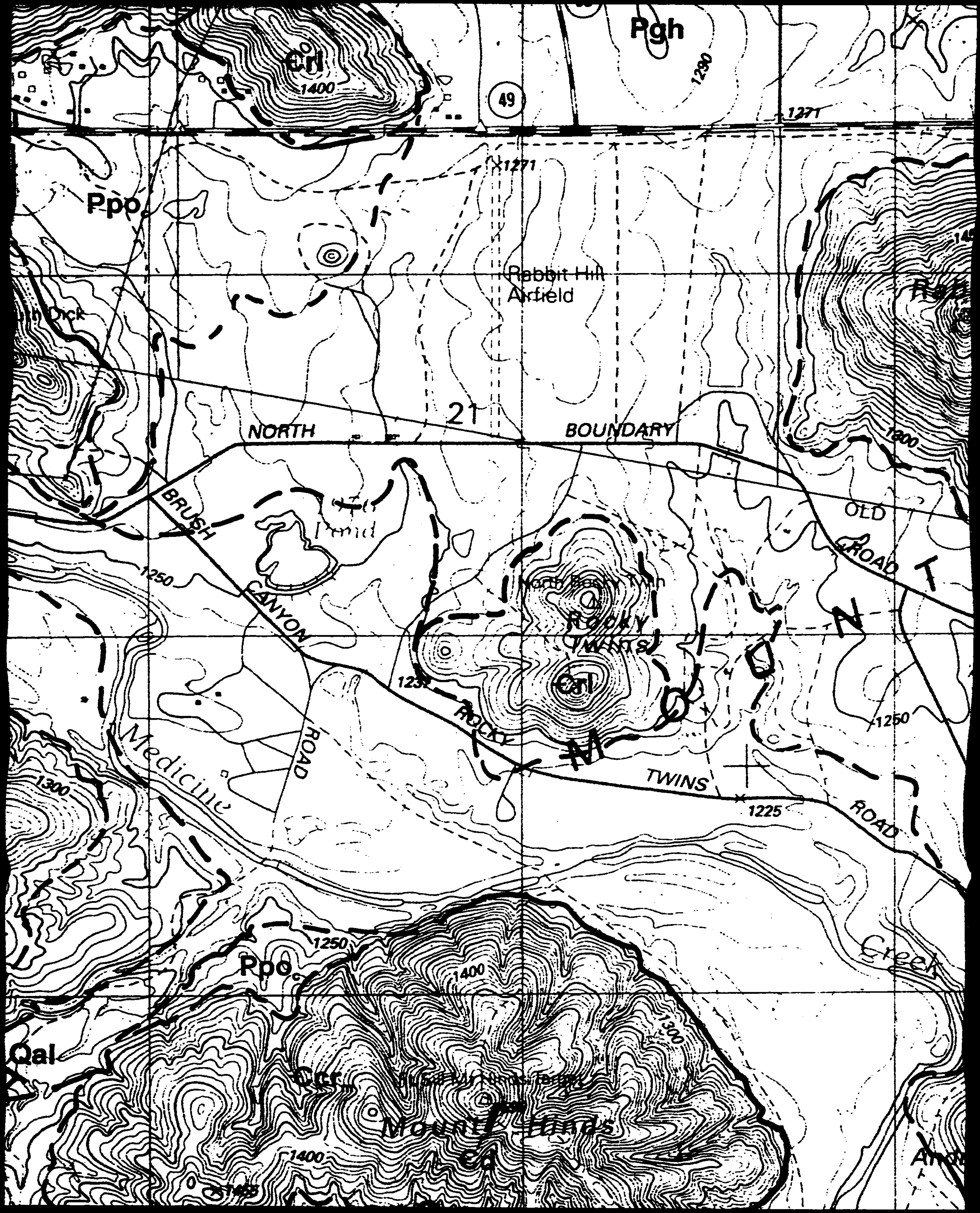

Pgh
Crl
1400
49
1290
1271
1271
Ppo
Rabbit Hill
Airfield
21
NORTH
BOUNDARY
OLD
ROAD
BRUSH
CANYON
ROAD
1250
Rocky
Twins
Crl
ROCKY
TWINS
ROAD
1250
1225
ROAD
1300
1300
Medicine
Creek
1250
Ppo
1400
1300
Qal
Ccr
Mount Hinds
Cd
1400

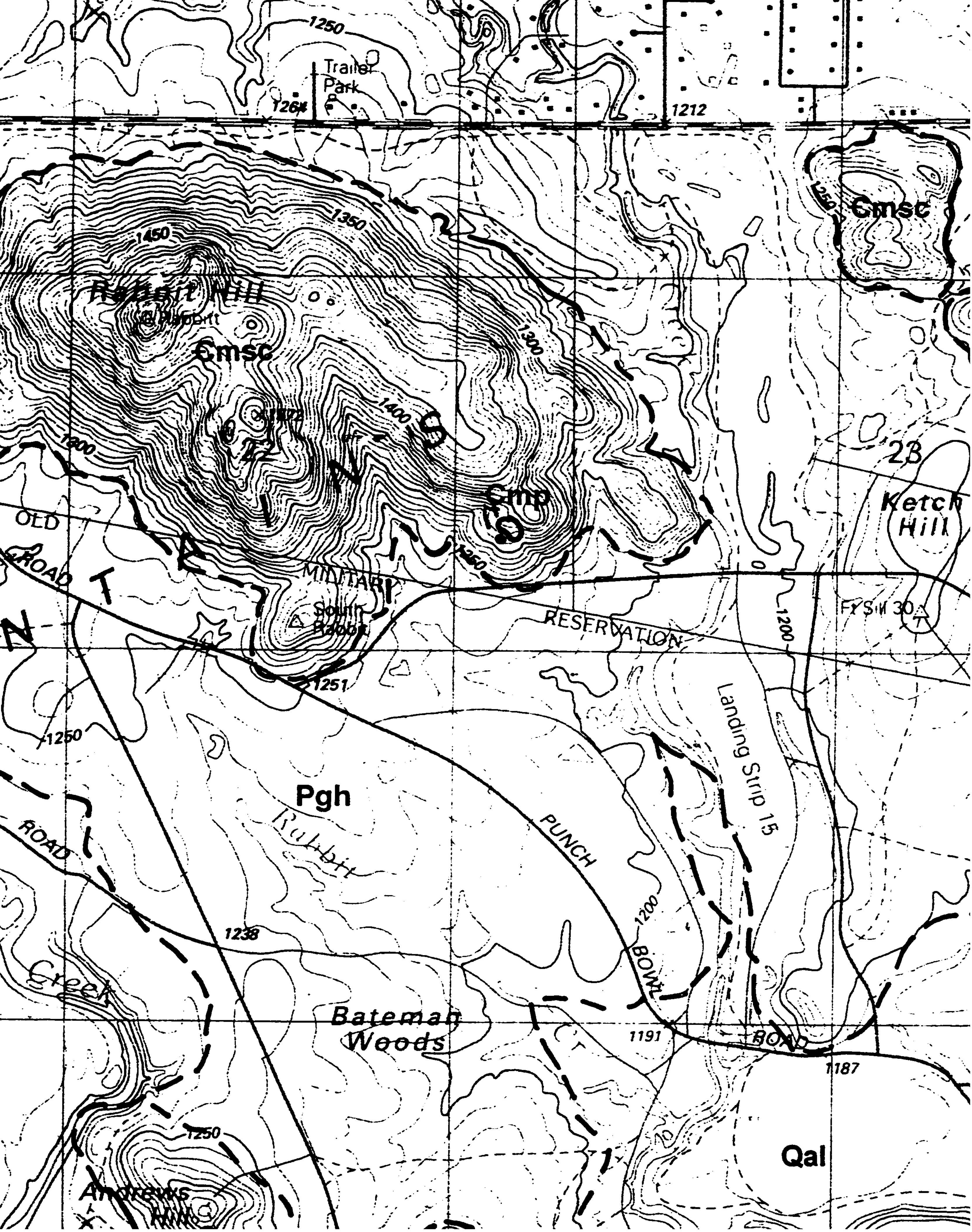

1250
Trailer Park
1264
1212
1350
1450
Rabbit Hill
Cmsc
1300
1400
Cmp
OLD
ROAD
MILITARY
RESERVATION
South Rabbit
1251
1250
23
Ketch Hill
1200
Landing Strip 15
Pgh
Rabbit
PUNCH
BOWL
ROAD
1238
1200
Creek
Bateman Woods
1191
ROAD
1187
1250
Qal
Andrews Hill

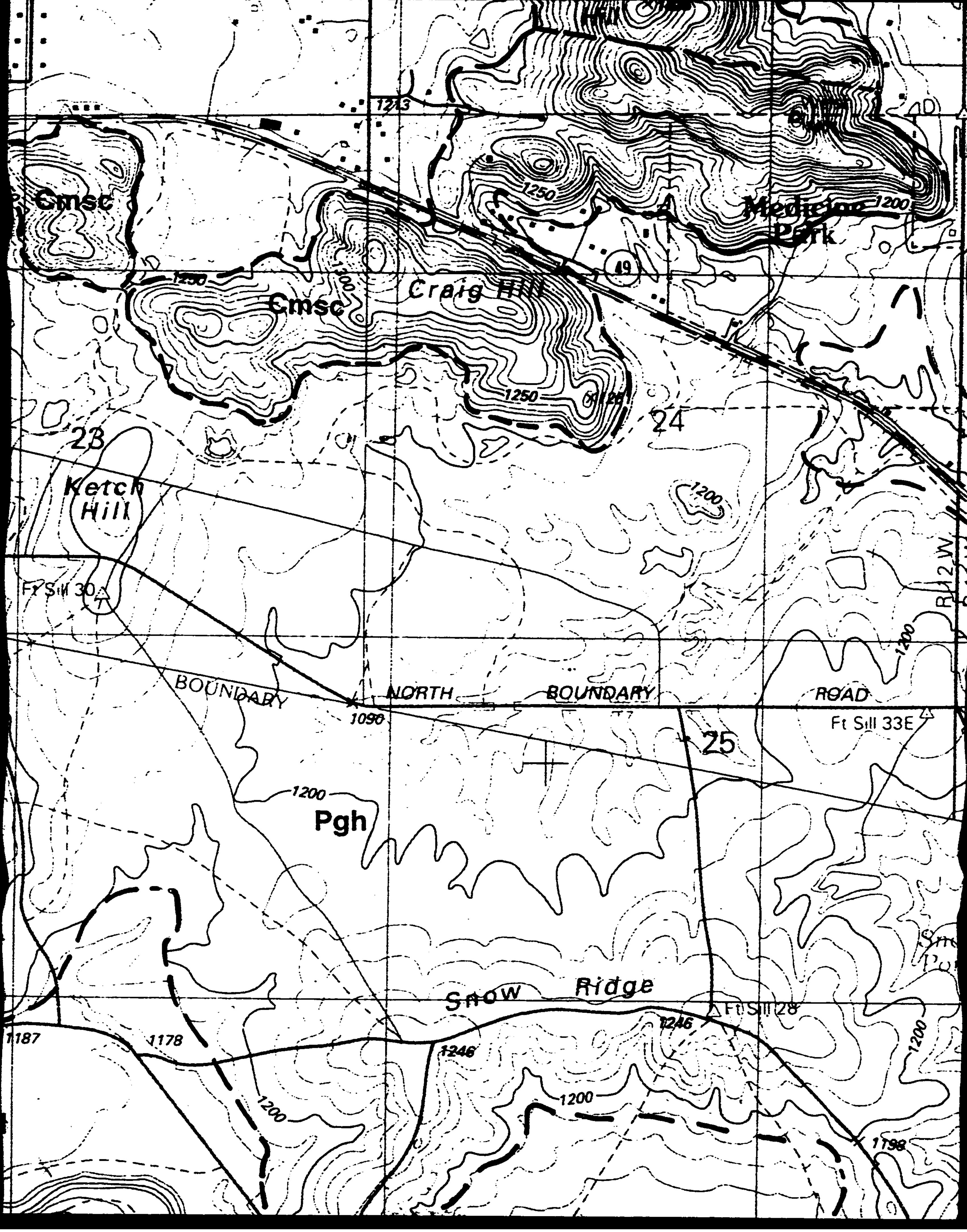

Cmsc
1213
1250
Medicine Park
1200
49
1250
Cmsc
Craig Hill
1250
24
23
Ketch Hill
1200
Ft Sill 30
BOUNDARY
NORTH BOUNDARY ROAD
1090
Ft Sill 33E
25
1200
1200
Pgh
Snow Ridge
Ft Sill 28
1246
1187
1178
1246
1200
1200
1198
1200

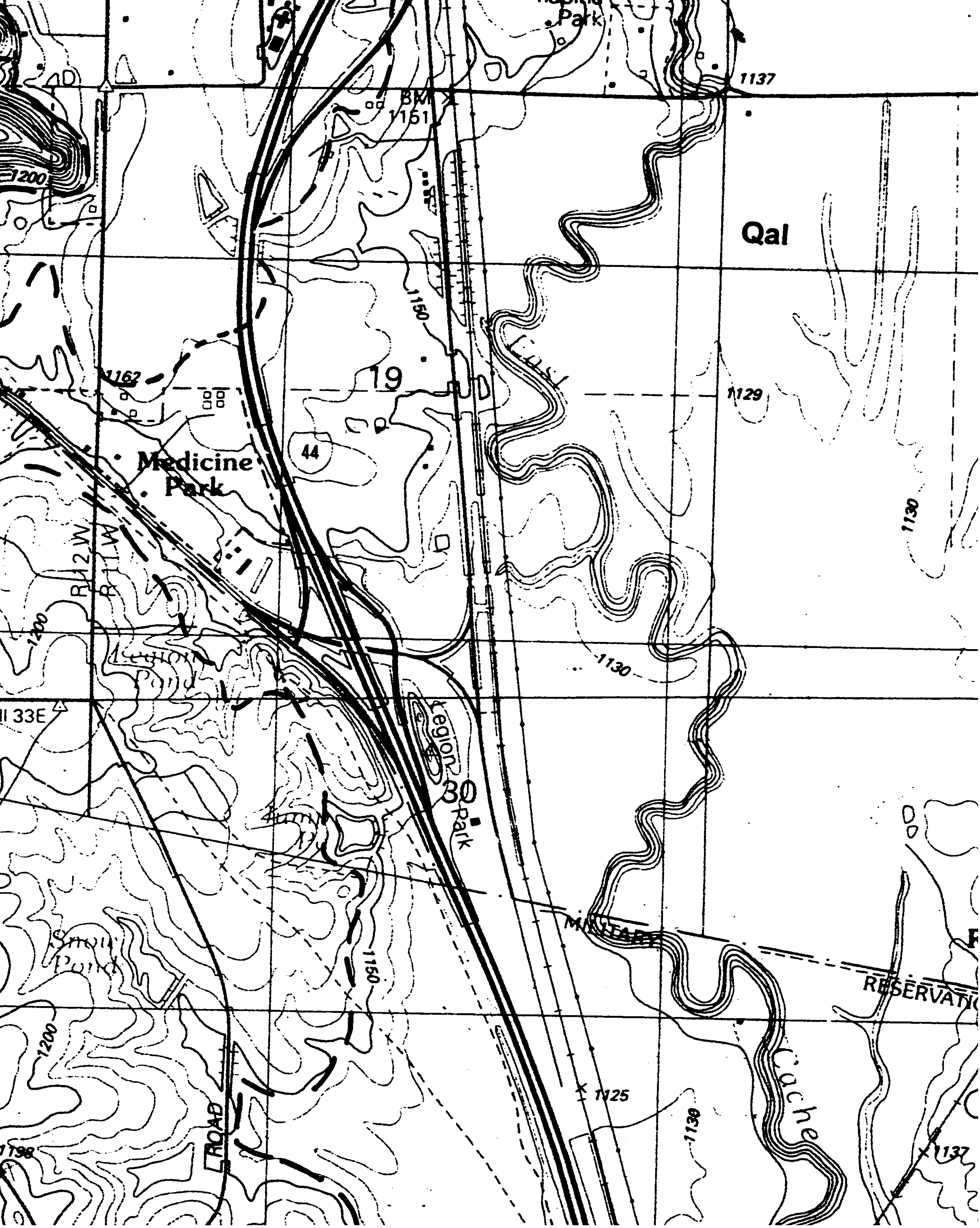
Park
BM
1151
1137
Qal
1200
1150
East
1162
19
1129
Medicine
Park
44
R 12 W
R 11 W
1130
1200
Legion
Pond
33E
Legion
Park
30
1150
MILITARY
RESERVATION
Snow
Pond
1200
Cache
1125
1130
1137
ROAD
1198

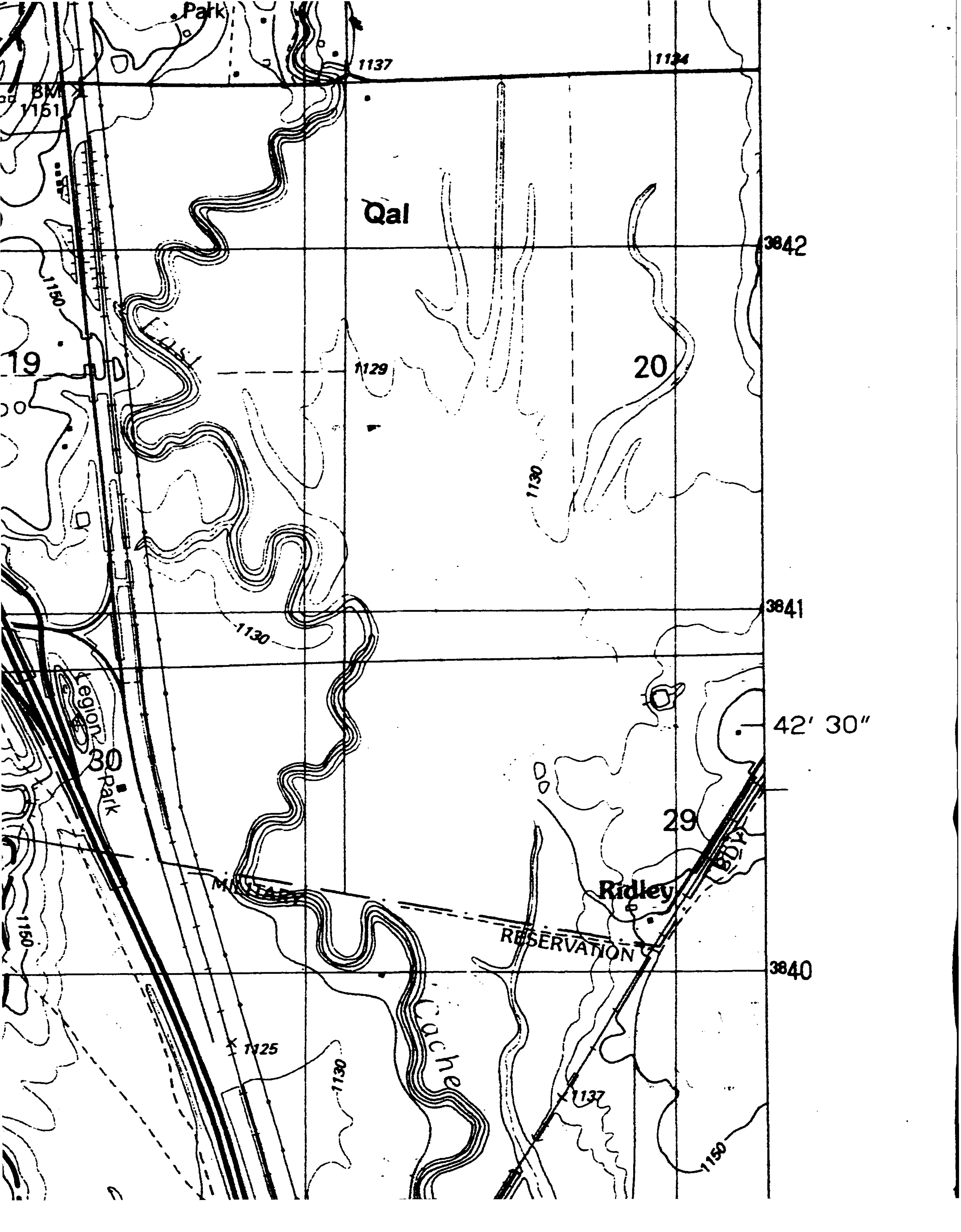

Park
1137
1134
BM
1151
Qal
3842
1150
19
1129
20
1130
3841
1130
Legion
Park
30
42′ 30″
29
BDY
MILITARY
Ridley
RESERVATION
3840
1150
Cache
1125
1130
1137
1150

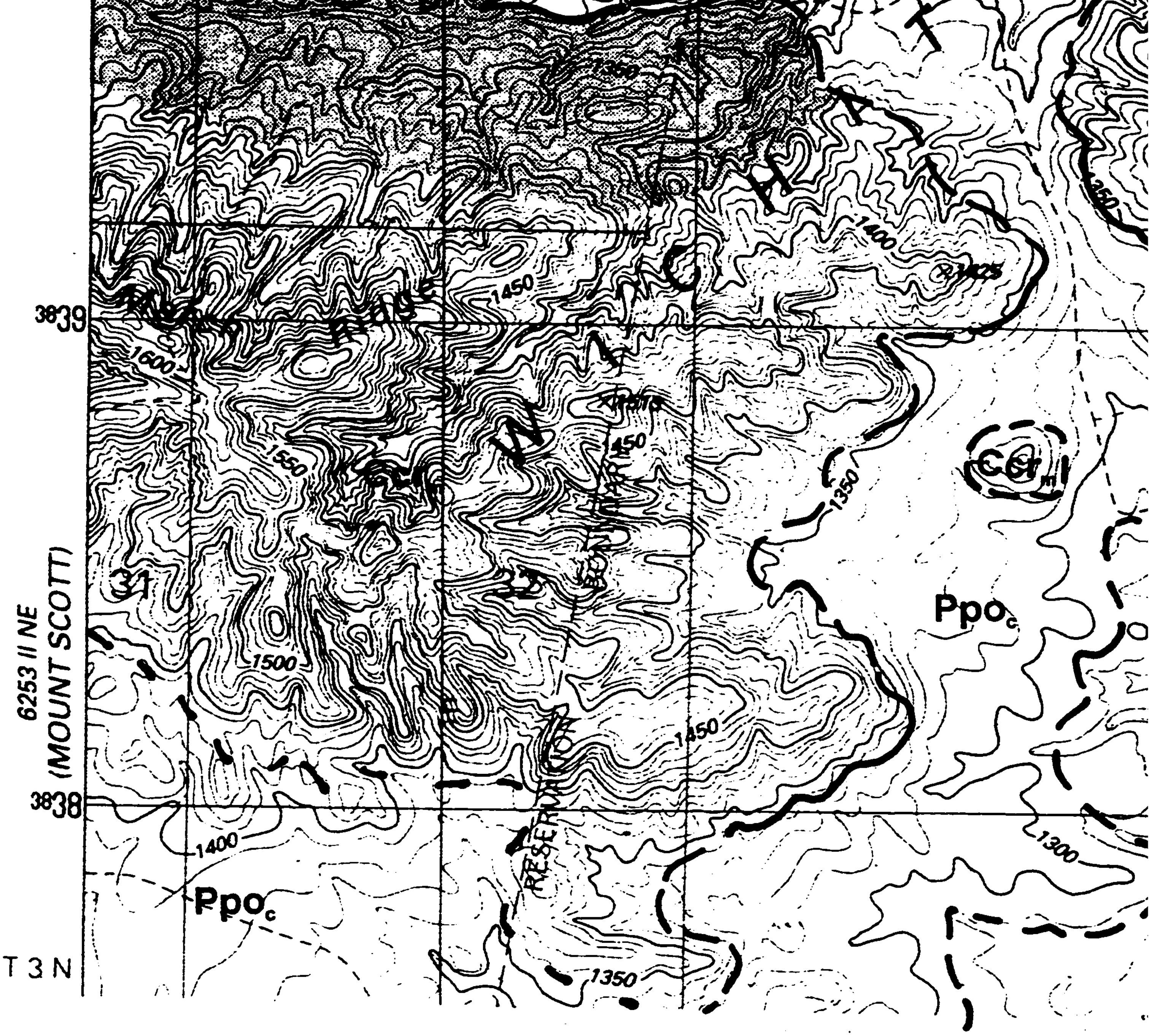

GEOLOGIC MAP OF
FORT SILL 7.5′ QUA
OKLAHOMA

Jonathan D. Price

1998

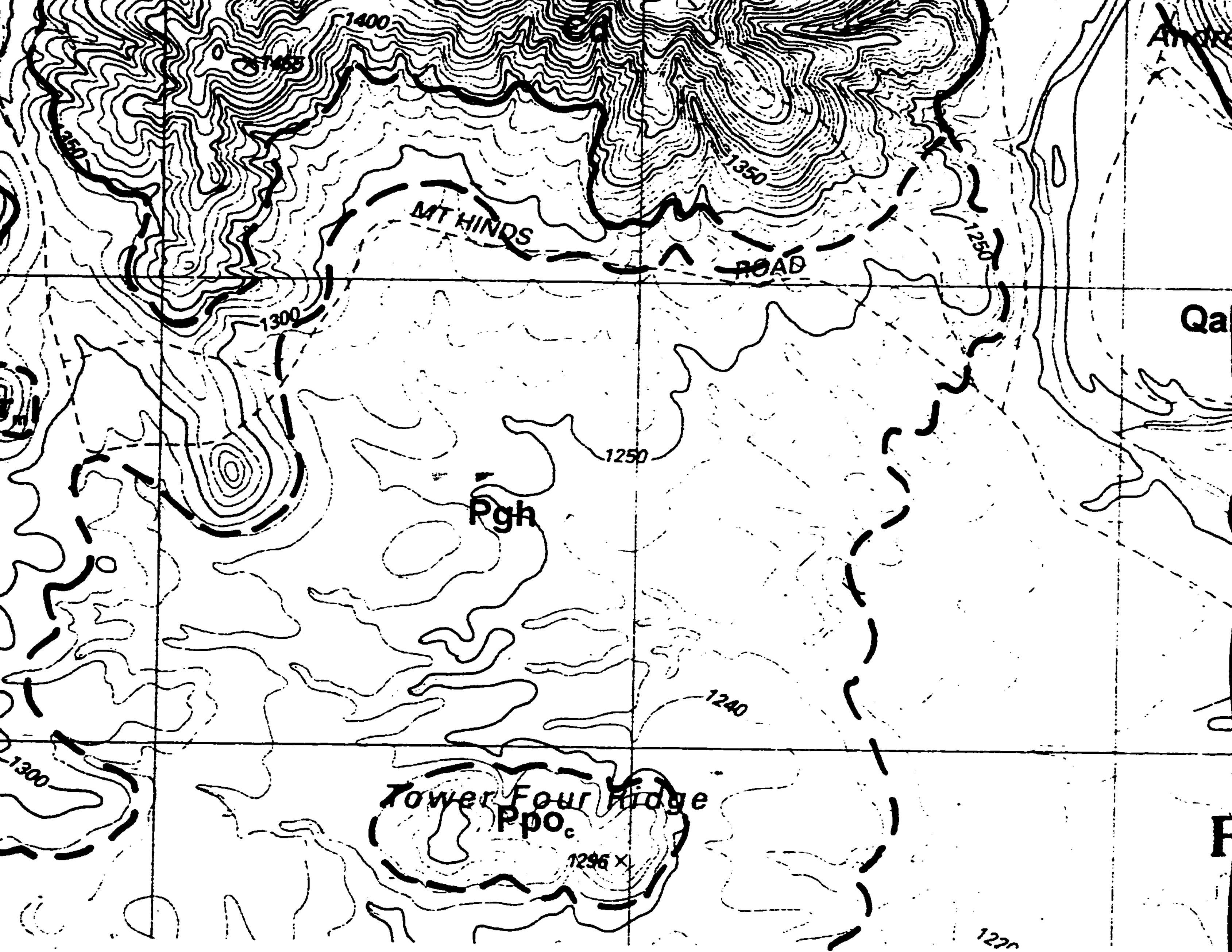

F THE NORTH
UADRANGLE,
MA

Price

Topographic Bas
Fort Sill U.S.G.S.
quadrangle, 19
N.A.D '27 proje

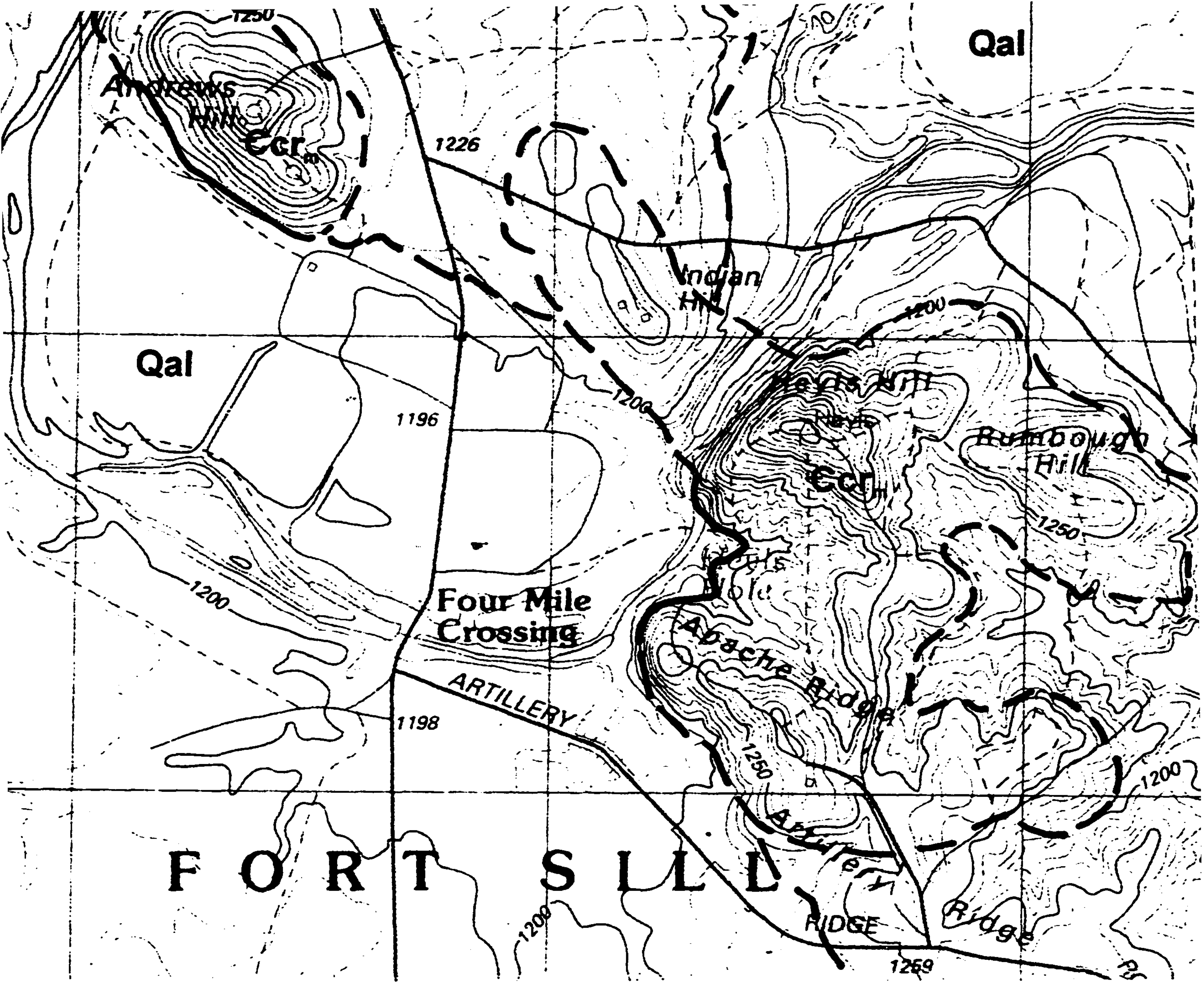

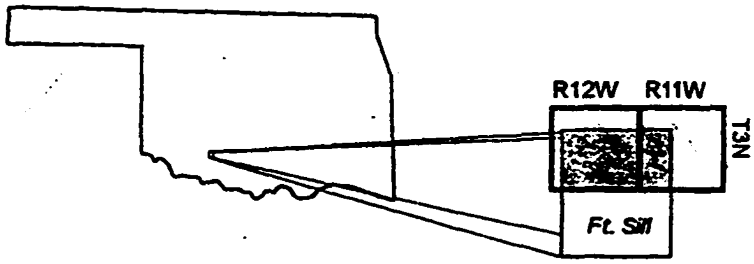

Scale 1:12 0

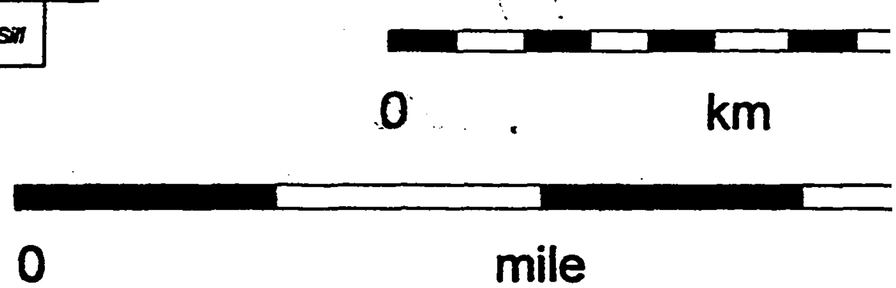

Topographic Base from
Fort Sill U.S.G.S. 7.5 minute
quadrangle, 1991.
N.A.D '27 projection
Universal Transverse Mercator Zone 14.

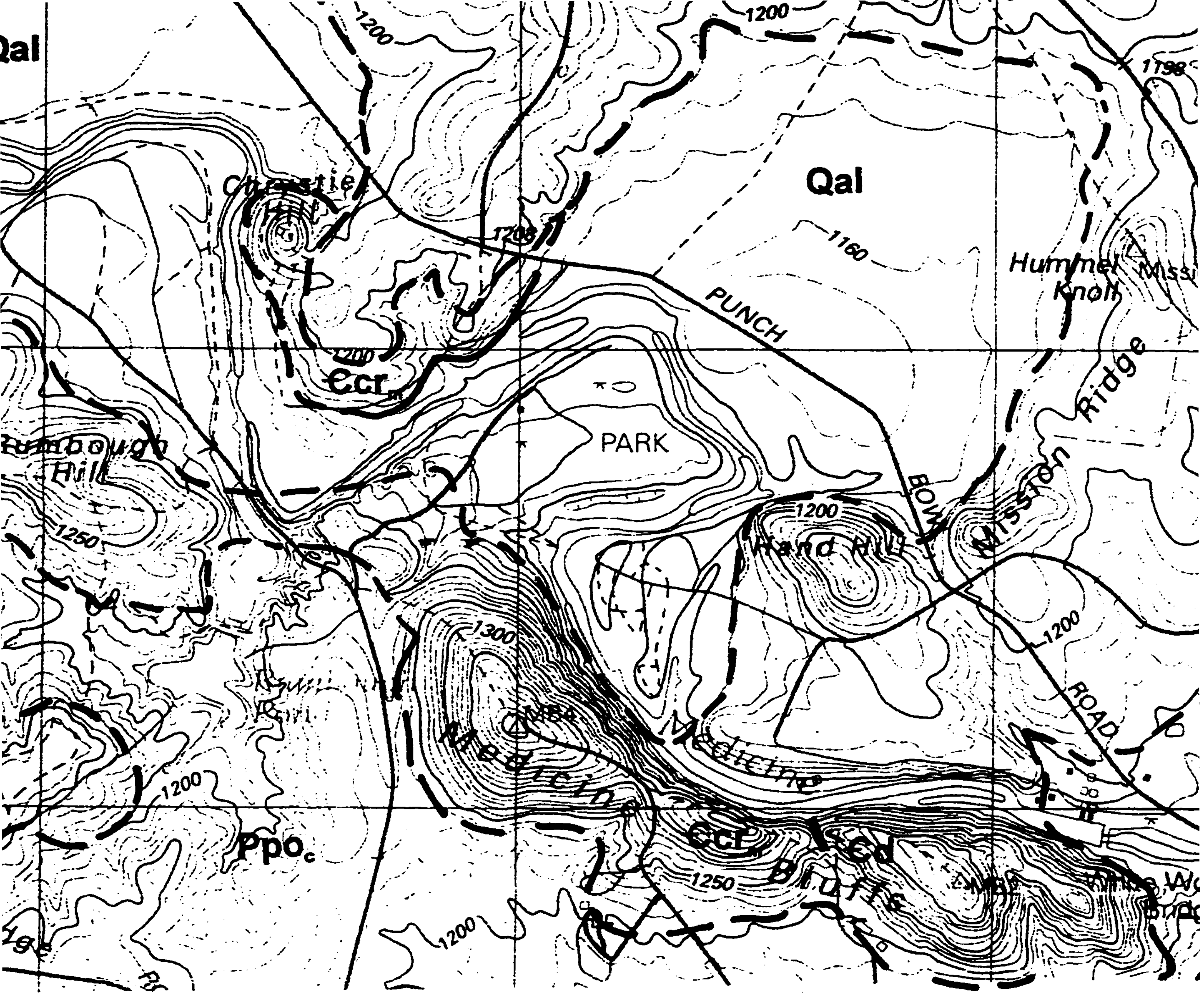

Scale 1:12 000

km 1

1

Quaternary

Qal	**Alluviu** Sand and s stream vall

Permian

Pgh	**Garber-** Interfingeri purple shal
Ppo	**Post Oal** Conglomer arkosic to li

Cambrian

	Rhyolite

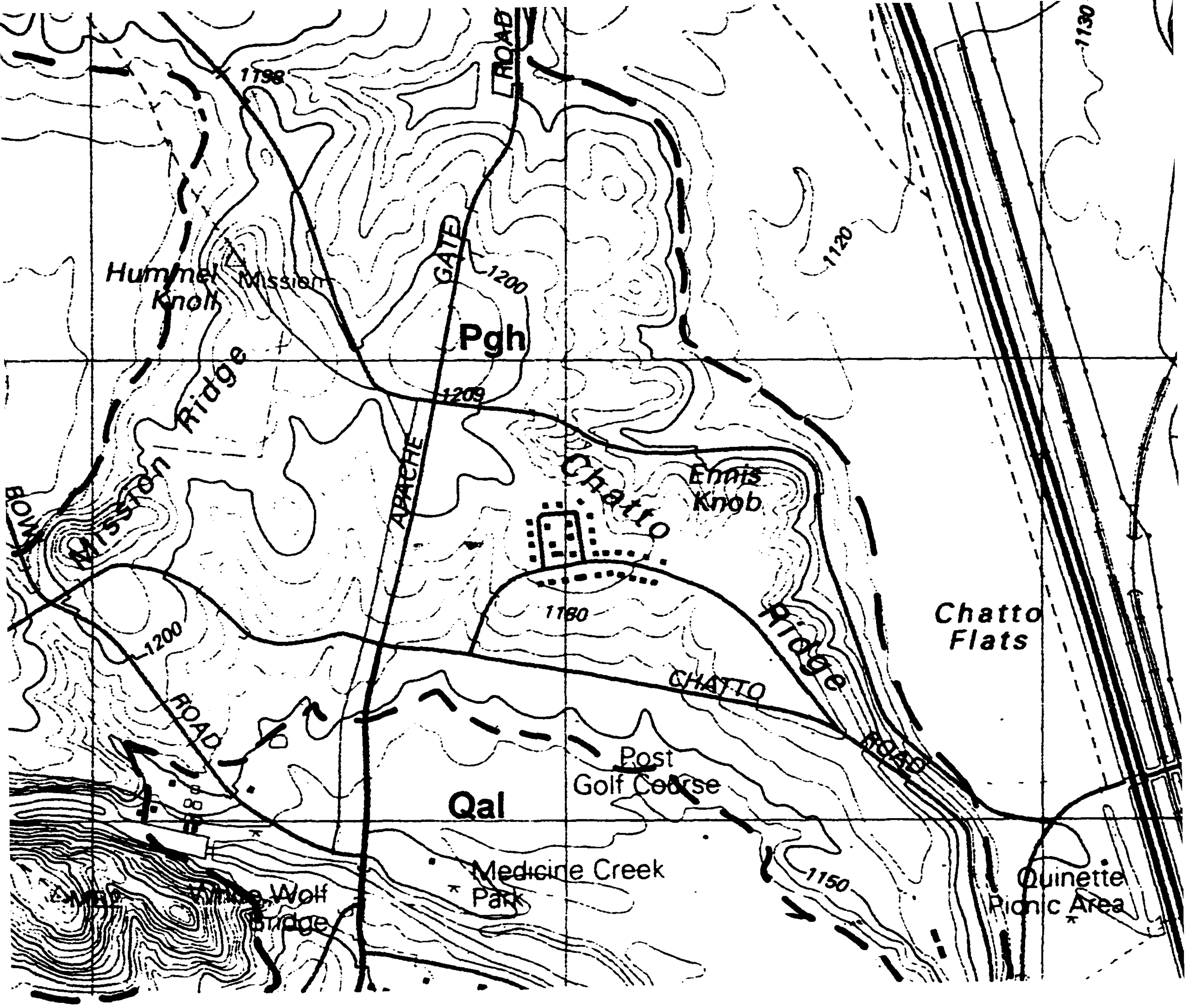

Quaternary

Qal — **Alluvium**
Sand and silt fill within modern and recent stream valleys.

Permian

Pgh — **Garber-Hennessey Formation**
Interfingering gray channel sandstone, red-purple shale, typically capped by buff sandstone.

Ppo — **Post Oak conglomerate**
Conglomerate with rounded boulders in a arkosic to lithic matrix.

Cambrian

€msc — **Mount Scott Granite**
Pink to brick red porphyritic, variably granophyric granite with gray ovoid feld

€rl — **Rush Lake granite**
Pink to brick-red, seriate, variably grano granite with connected quartz.

€mp — **Medicine Park Granite**
Weakly porphyritic, variably granophyri purple fine-grained alkali-feldspar granit

€cr — **Carlton rhyolite, spherulitic**
Porphyritic rhyolite with orange feldspar gray quartz, and orange-pink spherulitic

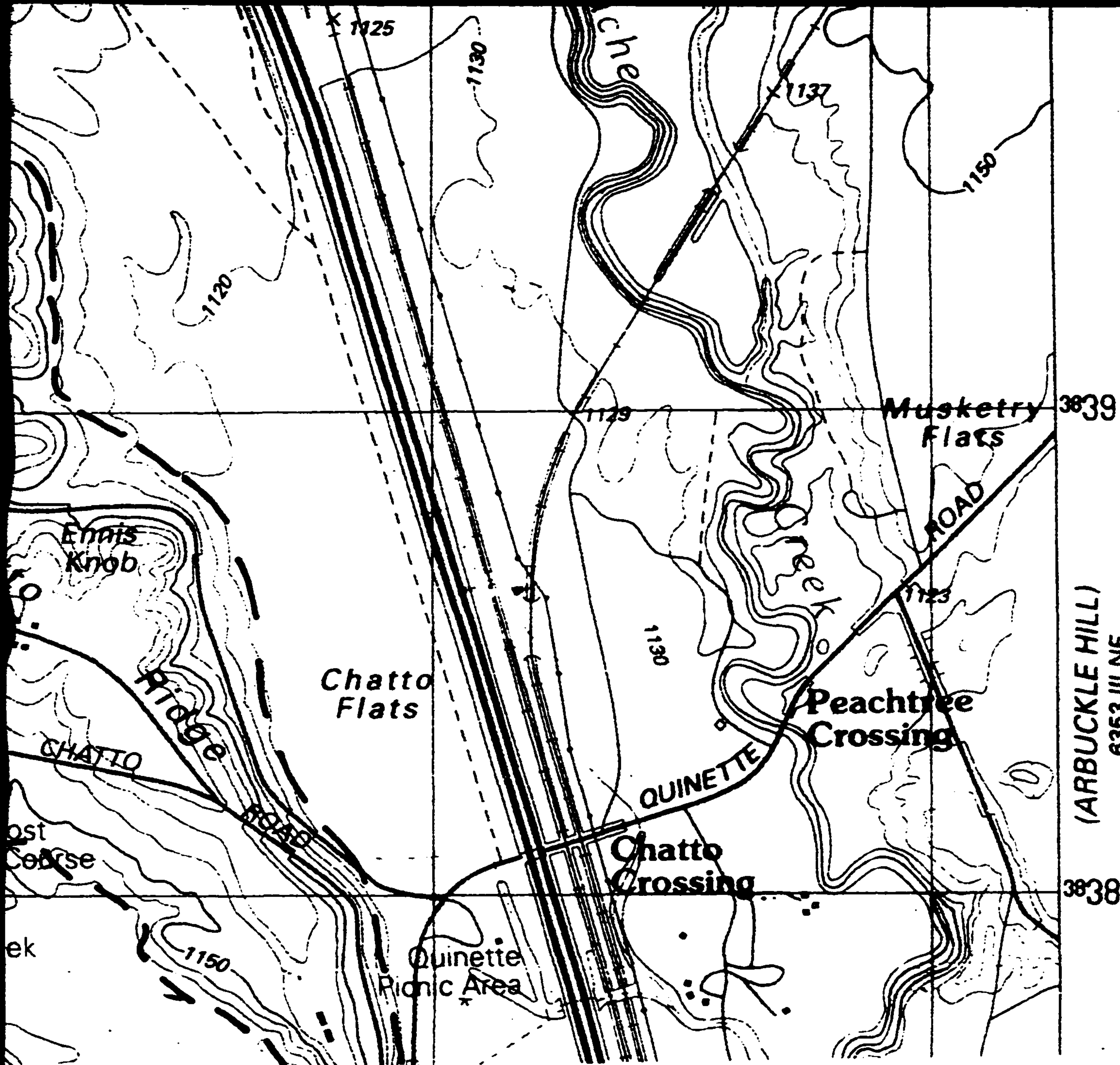

Ꞓmsc	**Mount Scott Granite** Pink to brick red porphyritic, variably granophyric granite with gray ovoid feldspar.
Ꞓrl	**Rush Lake granite** Pink to brick-red, seriate, variably granophyric granite with connected quartz.
Ꞓmp	**Medicine Park Granite** Weakly porphyritic, variably granophyric pink-purple fine-grained alkali-feldspar granite.
Ꞓcr	**Carlton rhyolite, spherulitic** Porphyritic rhyolite with orange feldspar and gray quartz, and orange-pink spherulitic bands.

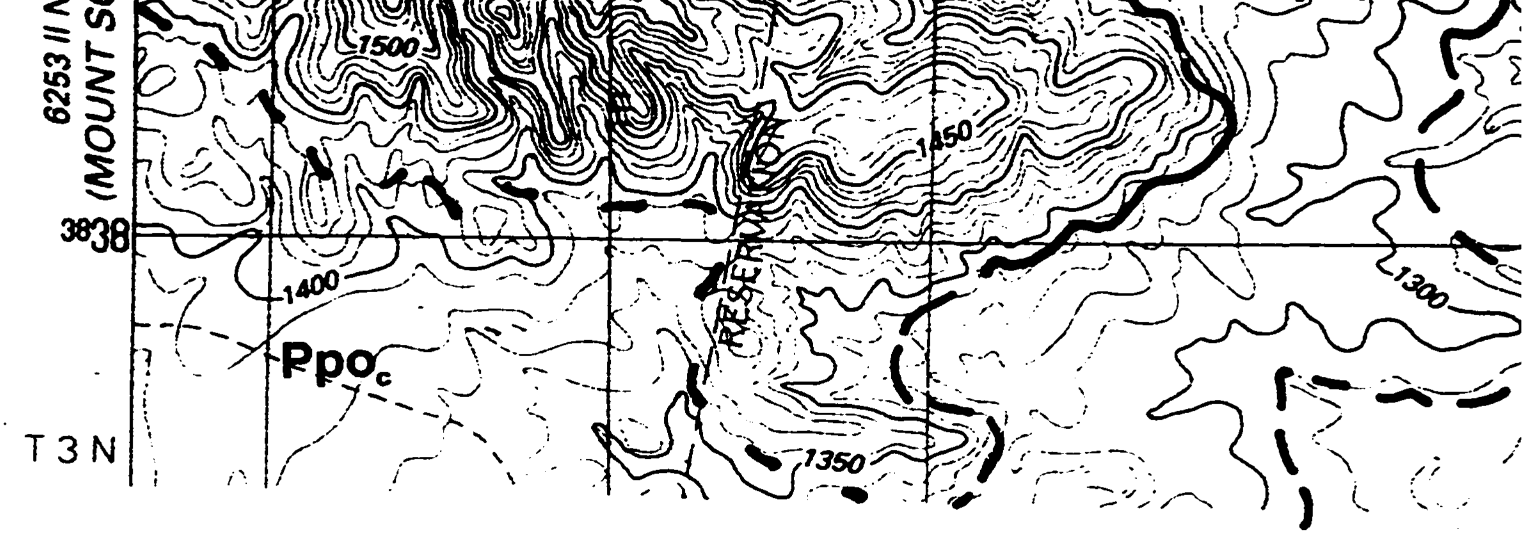

GEOLOGIC MAP OF
FORT SILL 7.5′ QUA
OKLAHOM

Jonathan D. Pric
1998

Produced in cooperation with the U. S
National Cooperative Geological M

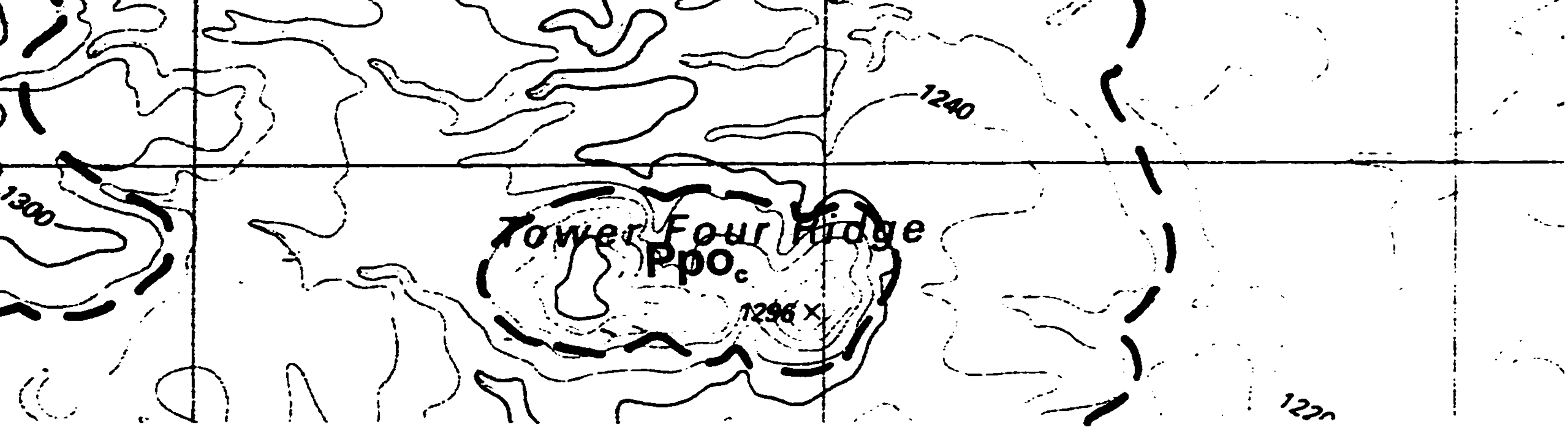

)F THE NORTH
UADRANGLE,
)MA

Price

e U. S. Geological Survey,
cal Mapping Program

Topographic
Fort Sill U.S.
quadrangle,
N.A.D '27 pr
Universal Tra

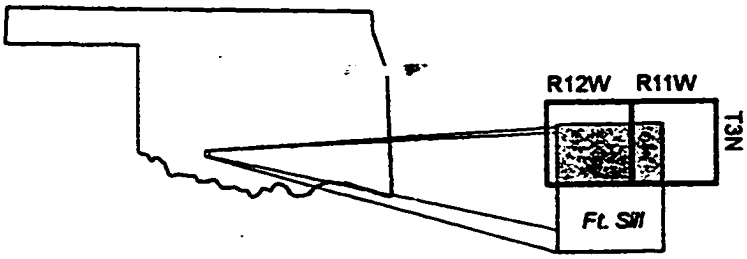

Scale 1:1

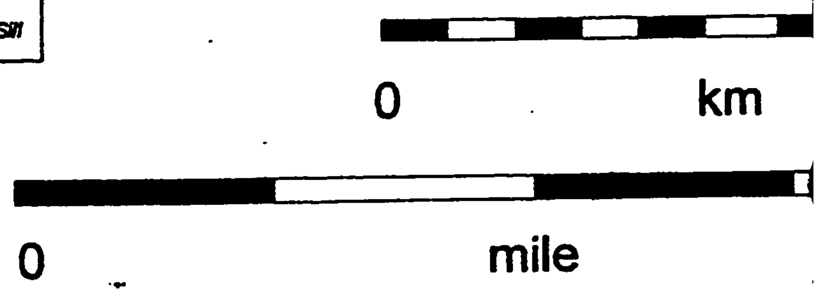

Topographic Base from
Fort Sill U.S.G.S. 7.5 minute
quadrangle, 1991.
N.A.D '27 projection
Universal Transverse Mercator Zone 14.

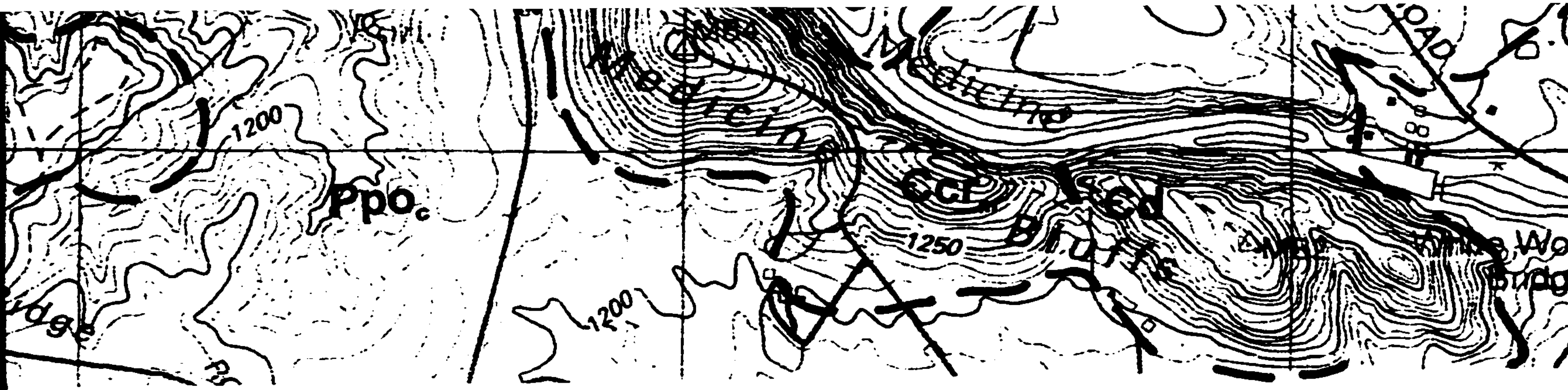

Scale 1:12 000

km 1

le 1

Quaternary

Qal	**Alluvium** Sand and si stream valle

Permian

Pgh	**Garber-** Interfingerin purple shale
Ppo	**Post Oa** Conglomer arkosic to li

Cambrian

€r	**Rhyolite** Brown-red p angular qua
€d	**Diabase** Black, fine g

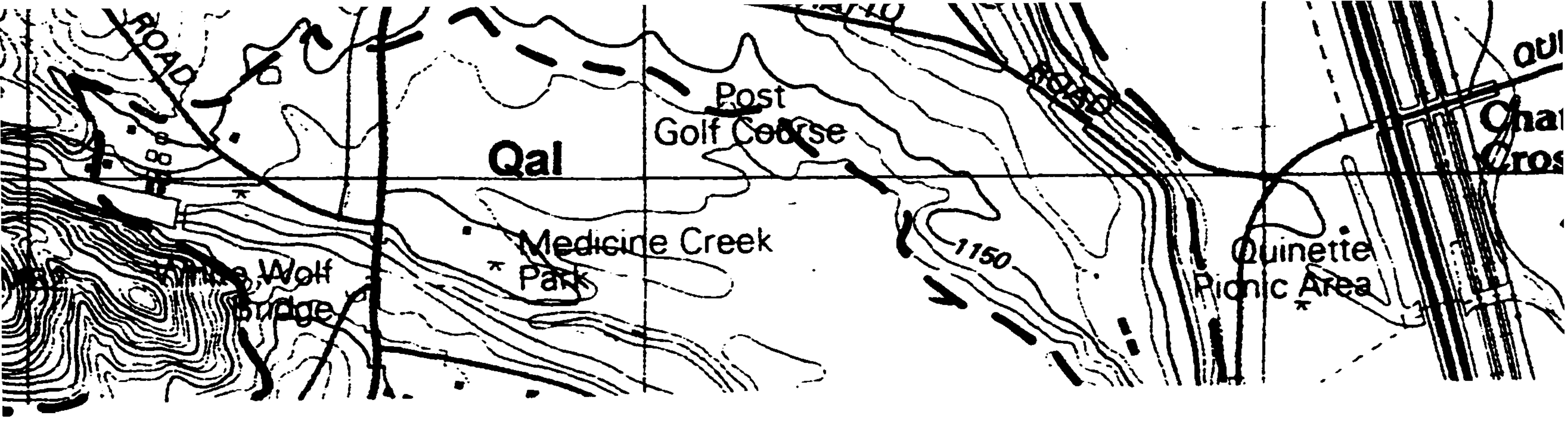

Quaternary

Qal — **Alluvium**
Sand and silt fill within modern and recent stream valleys.

Permian

Pgh — **Garber-Hennessey Formation**
Interfingering gray channel sandstone, red-purple shale, typically capped by buff sandstone.

Ppo — **Post Oak conglomerate**
Conglomerate with rounded boulders in a arkosic to lithic matrix.

Cambrian

€r — **Rhyolite dike**
Brown-red porphyritic with pink feldspars and angular quartz.

€d — **Diabase**
Black, fine grained aphyric dikes.

€msc — **Mount Scott Granite**
Pink to brick red porphyritic, variably granophyric granite with gray ovoid feldspar.

€rl — **Rush Lake granite**
Pink to brick-red, seriate, variably granophyric granite with connected quartz.

€mp — **Medicine Park Granite**
Weakly porphyritic, variably granophyric pink-purple fine-grained alkali-feldspar granite.

€cr$_s$ — **Carlton rhyolite, spherulitic**
Porphyritic rhyolite with orange feldspar and gray quartz, and orange-pink spherulitic bands.

€cr$_m$ — **Carlton rhyolite, massive**
Massive porphyritic rhyolite with orange feldspar and gray quartz phenocrysts.

€dm$_m$ — **Davidson metarhyolite, massive**
Pink to buff, highly fractured, commonly veined feldspathic metarhyolite.

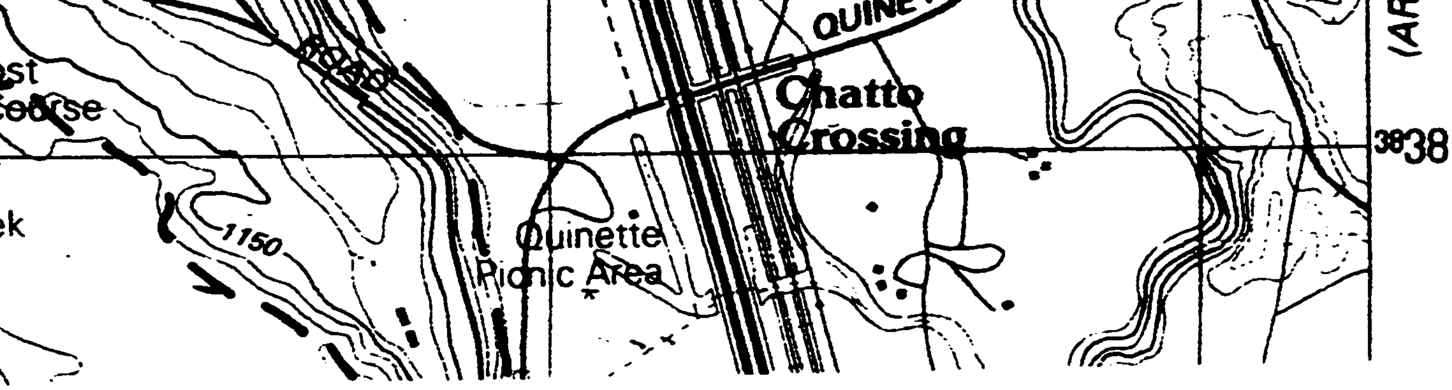

€msc	**Mount Scott Granite** Pink to brick red porphyritic, variably granophyric granite with gray ovoid feldspar.
€rl	**Rush Lake granite** Pink to brick-red, seriate, variably granophyric granite with connected quartz.
€mp	**Medicine Park Granite** Weakly porphyritic, variably granophyric pink-purple fine-grained alkali-feldspar granite.
€cr_s	**Carlton rhyolite, spherulitic** Porphyritic rhyolite with orange feldspar and gray quartz, and orange-pink spherulitic bands.
€cr_m	**Carlton rhyolite, massive** Massive porphyritic rhyolite with orange feldspar and gray quartz phenocrysts.
€dm_m	**Davidson metarhyolite, massive** Pink to buff, highly fractured, commonly veined feldspathic metarhyolite.

SECTI

All Sections from Plates I & II
A-A' from Plate Ib
B-B' and C-C' from Plates Ia & II

Cross Section B-B'

CTIONS THROUGH THE MC

Jonathan D. Price, 1

Produced in cooperation with the U. S. Geol
National Cooperative Geological Mappir

II

ı & II

Cross section A-

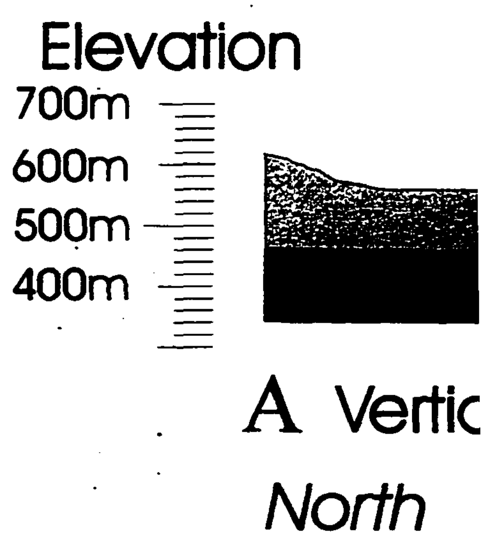

MOUNT SCOTT AREA

ce, 1998

S. Geological Survey,
l Mapping Program

tion A-A'

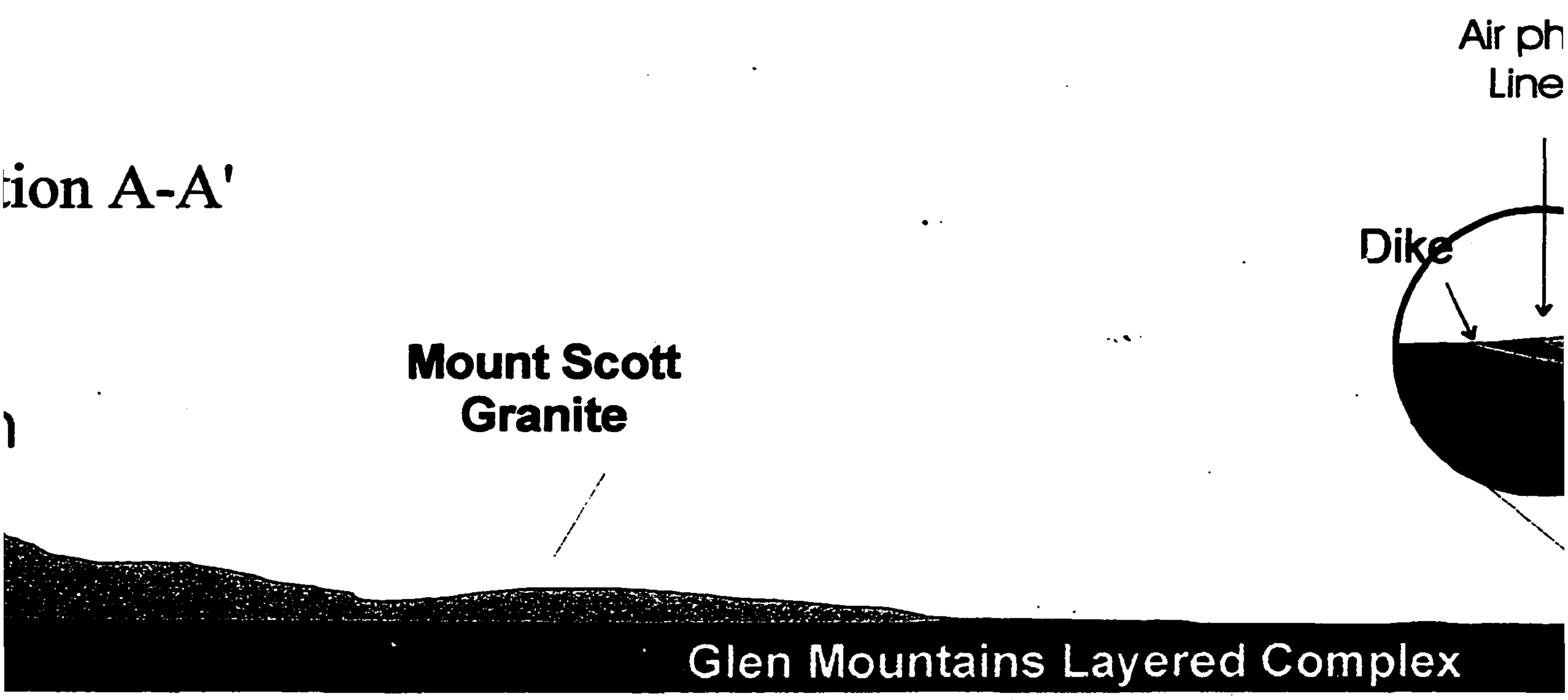

Vertical = Horizontal

North

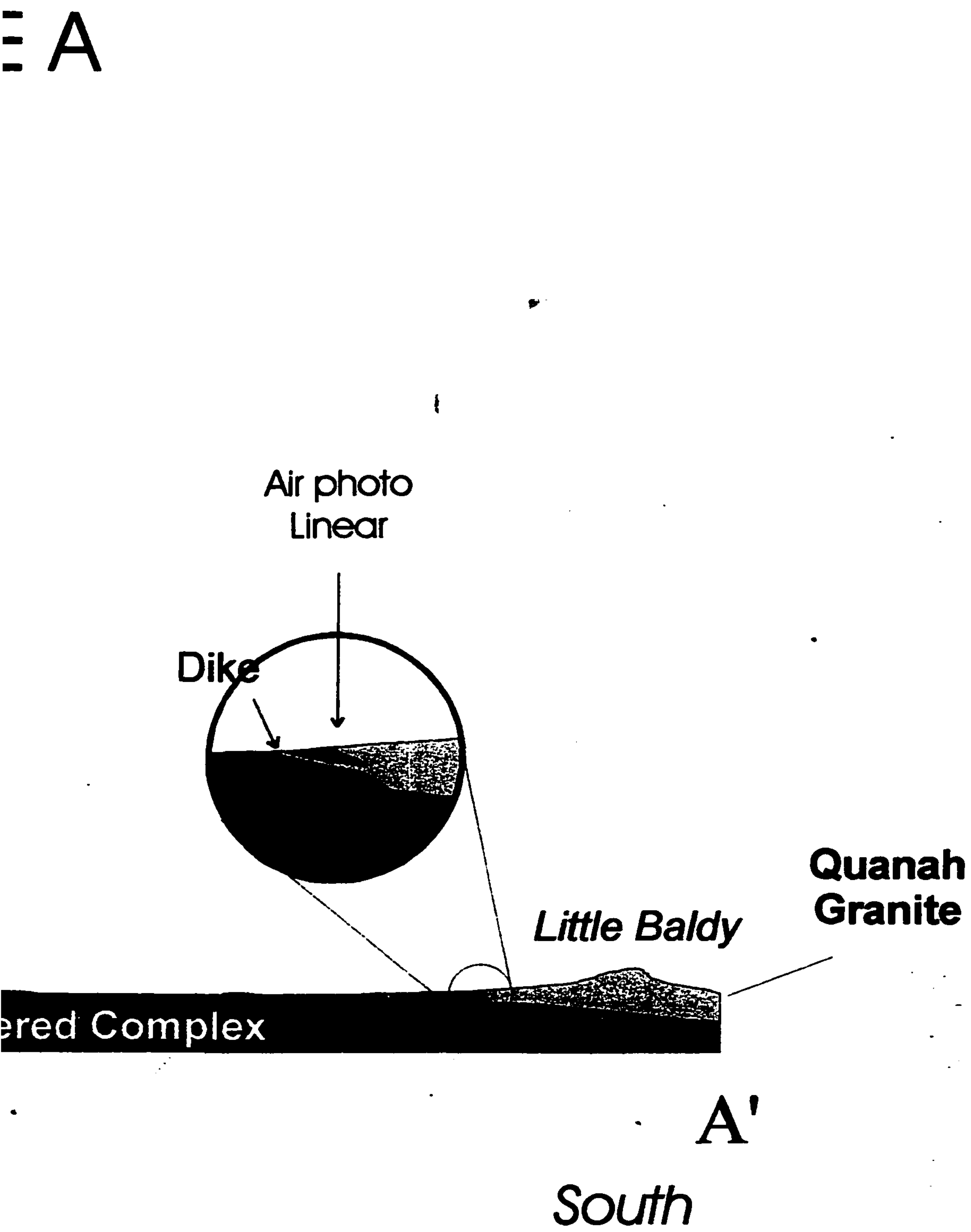
A
Air photo
Linear
Dike
Quanah
Granite
Little Baldy
ered Complex
A'
South

Cross Section B-B'

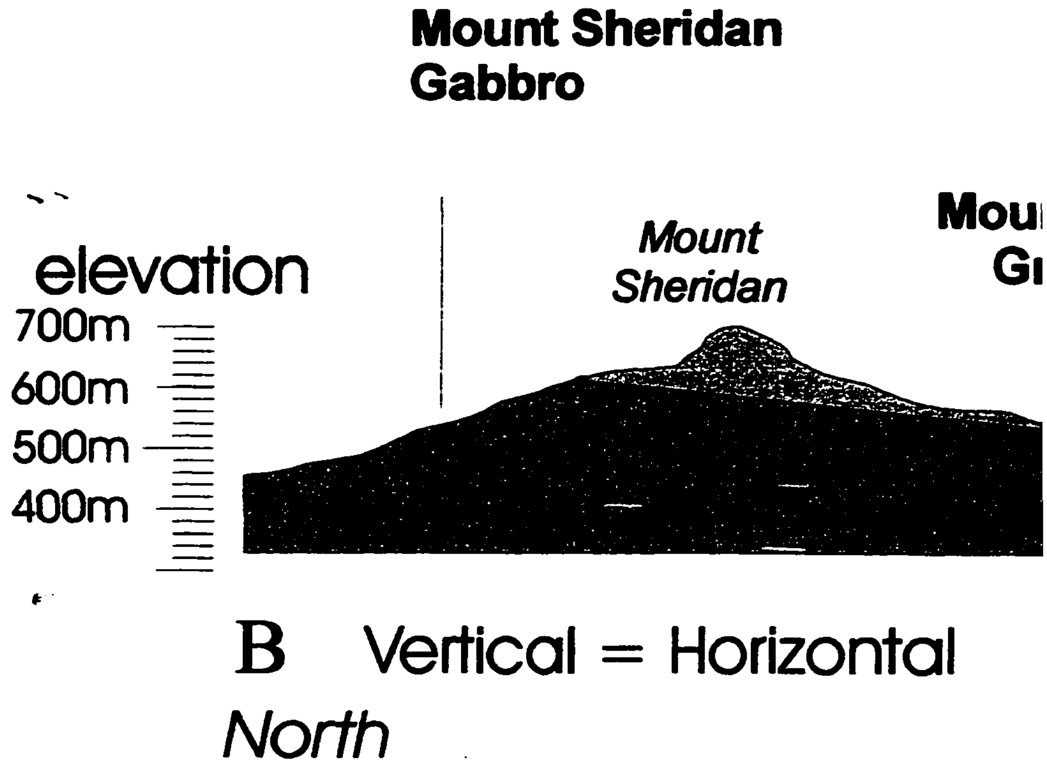

Cross Section C-C'

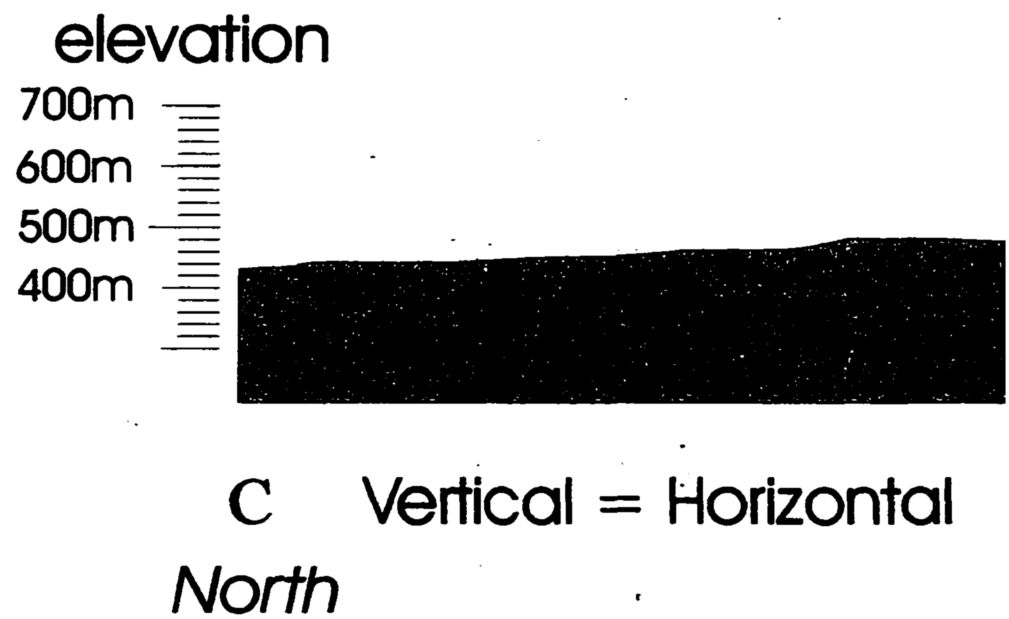

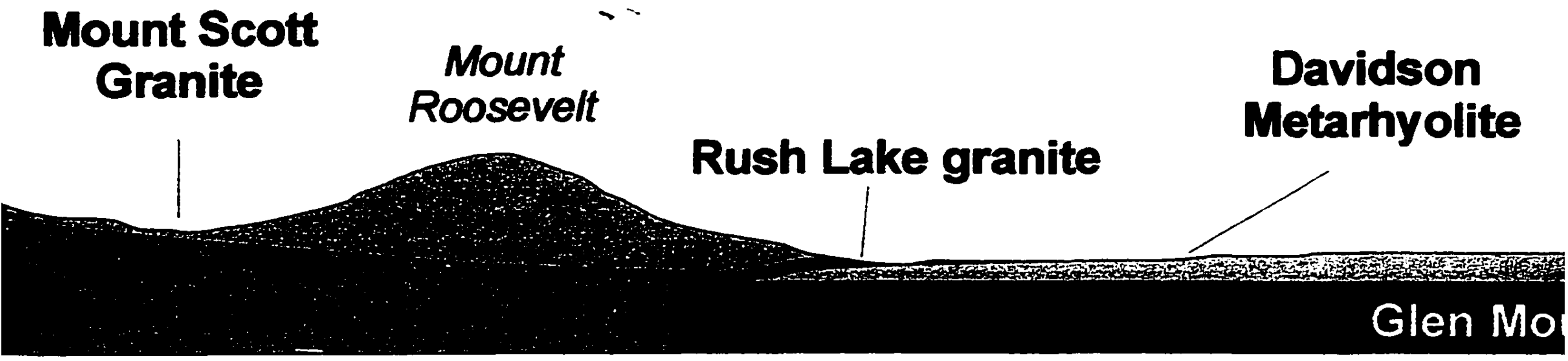
Mount Scott
Granite
Mount
Roosevelt
Rush Lake granite
Davidson
Metarhyolite
Glen Mo

tal

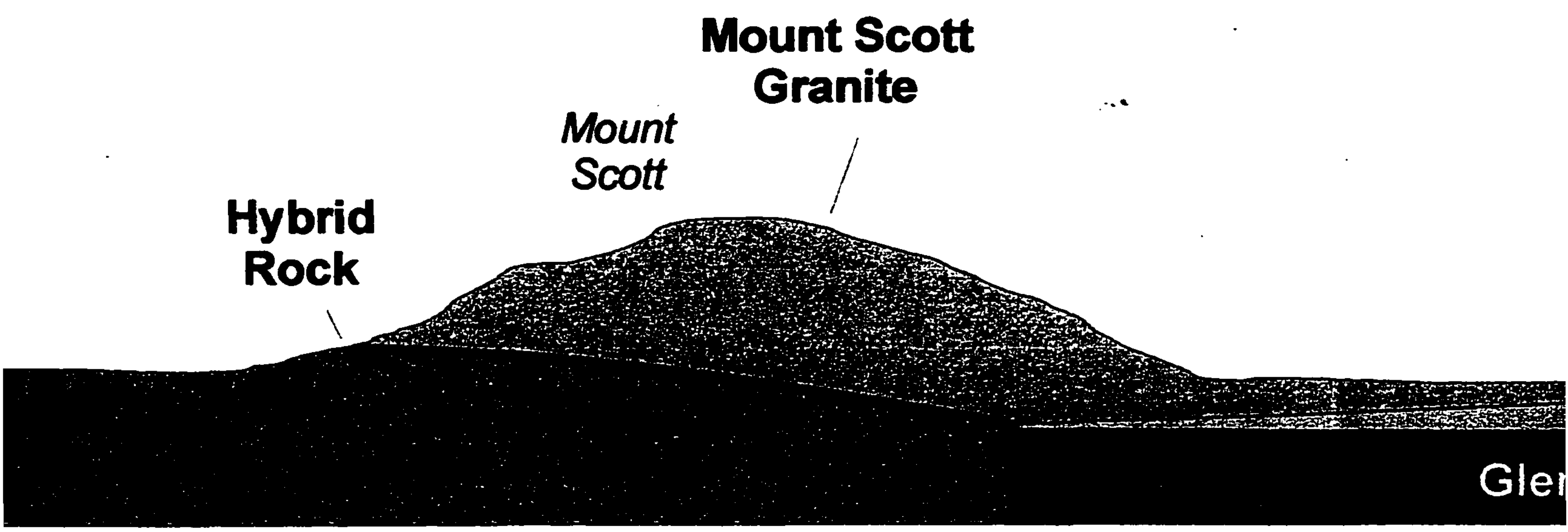
Mount Scott
Granite
Mount
Scott
Hybrid
Rock
Gle

ntal

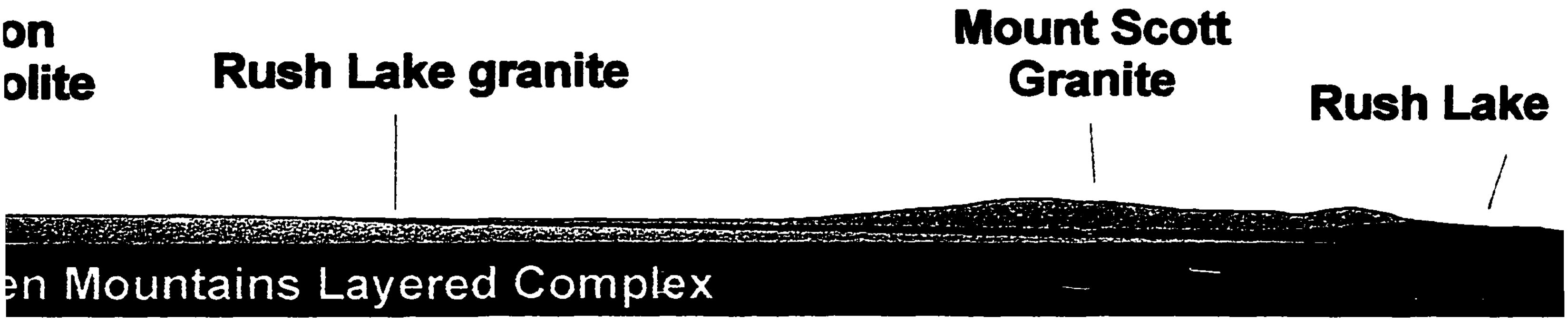
on
olite
Rush Lake granite
Mount Scott
Granite
Rush Lake
en Mountains Layered Complex

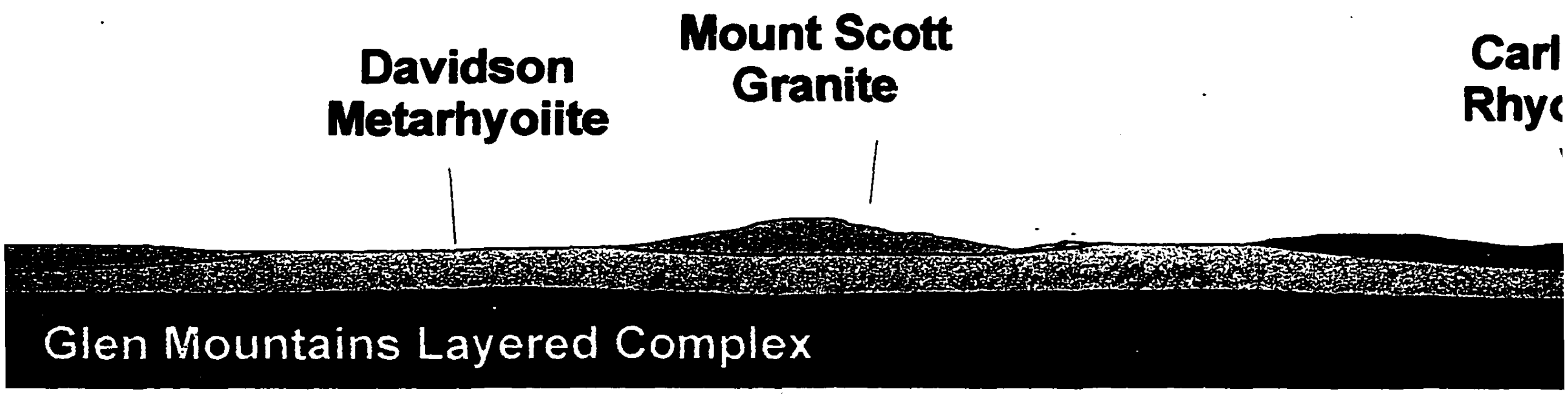
Davidson
Metarhyoiite
Mount Scott
Granite
Carl
Rhy
Glen Mountains Layered Complex

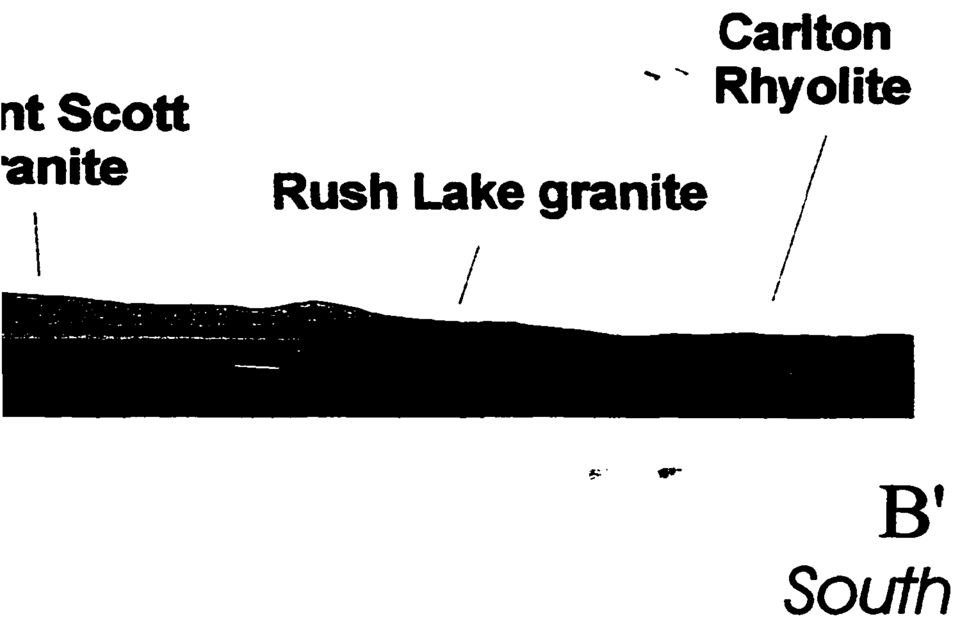
Carlton
Rhyolite
nt Scott
'anite
Rush Lake granite
B'
South

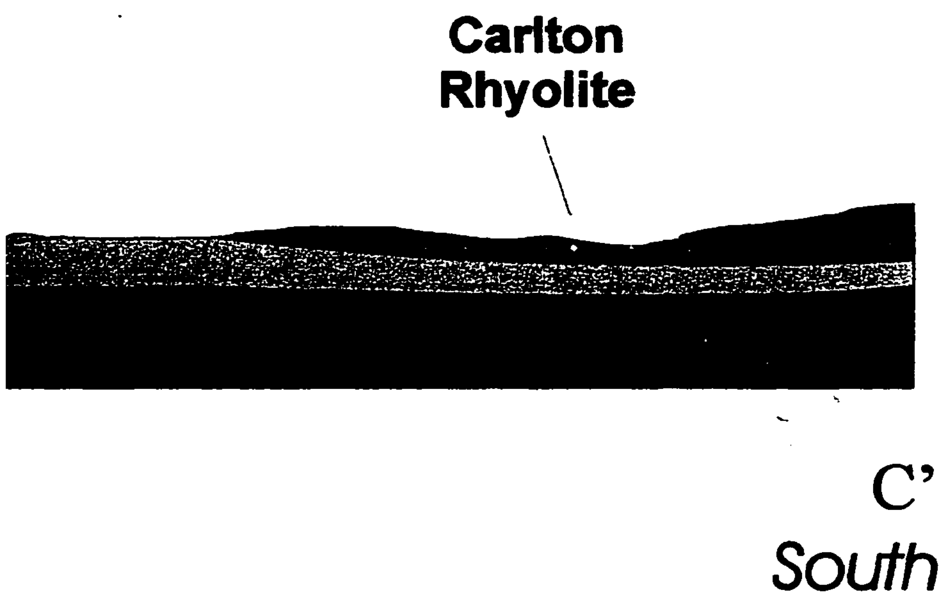
Carlton
Rhyolite
C'
South

MEDICINE PARK FEN

Jonathan D. Pric

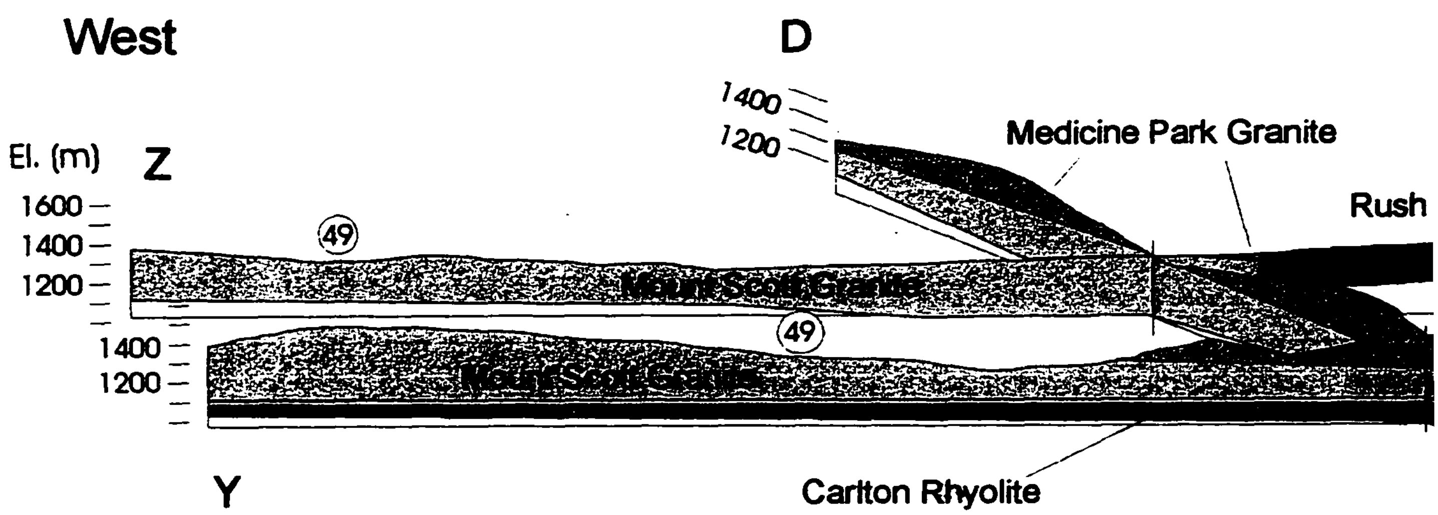

Section lines from plate II and III
Vertical = Horizontal in Y-Y' and Z-Z' section lines

FENCE DIAGRAM

D. Price, 1998

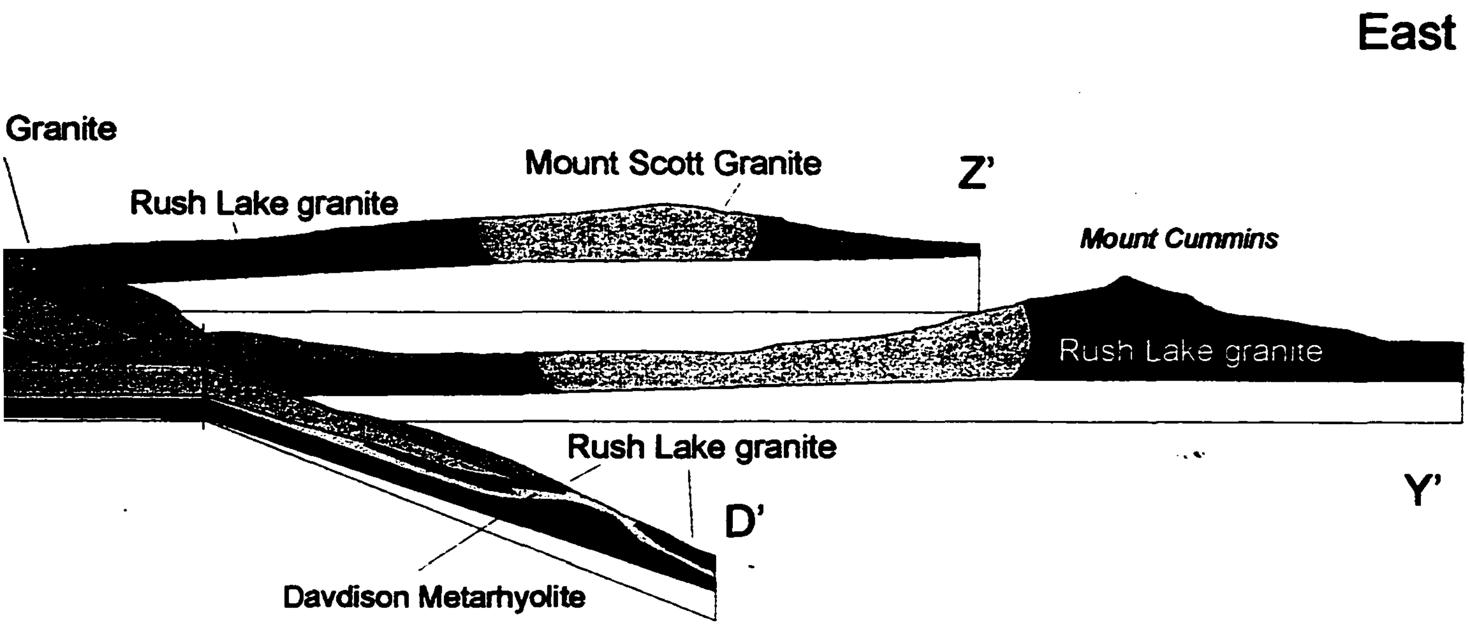

Produced in cooperation with the U. S. Geological Survey,
National Cooperative Geological Mapping Program

GEOLOGIC MAP
LAKE EL

Jon

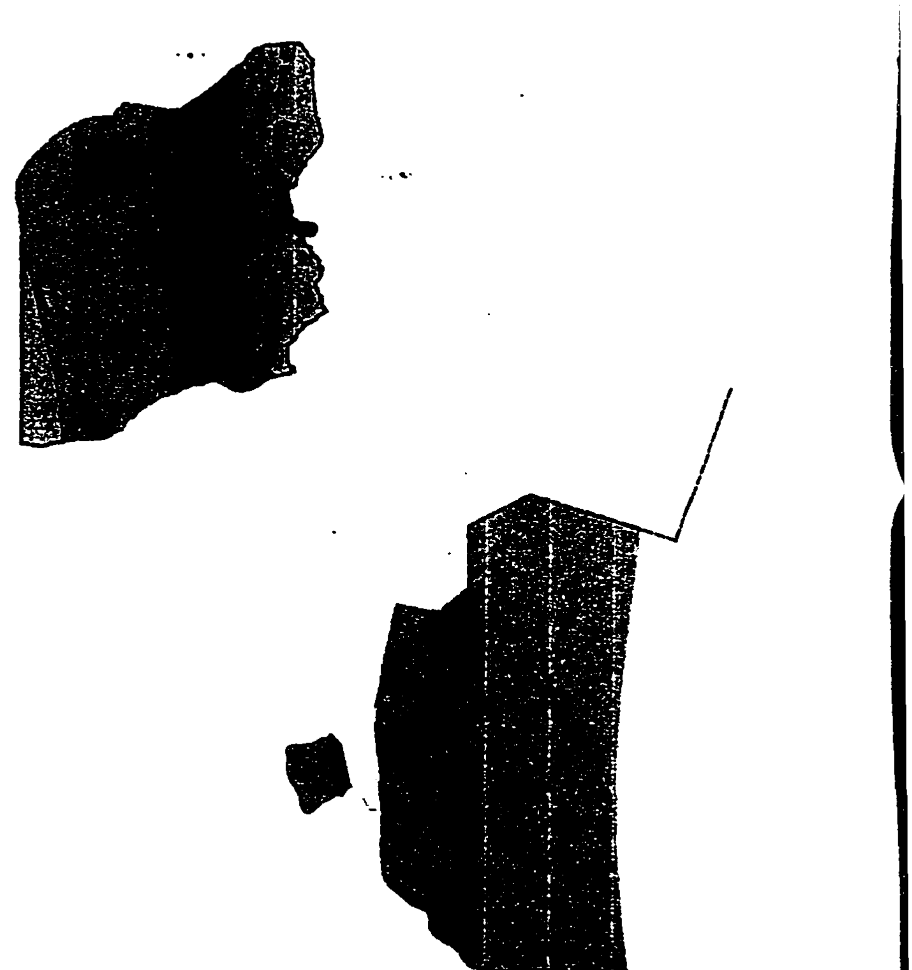

MAP OF THE EAST DIABASE
E ELMER THOMAS DAM

Jonathan D. Price, 1998

Covered

Late Diabase

T DIABASE DIKE
S DAM

98

ered

Diabase

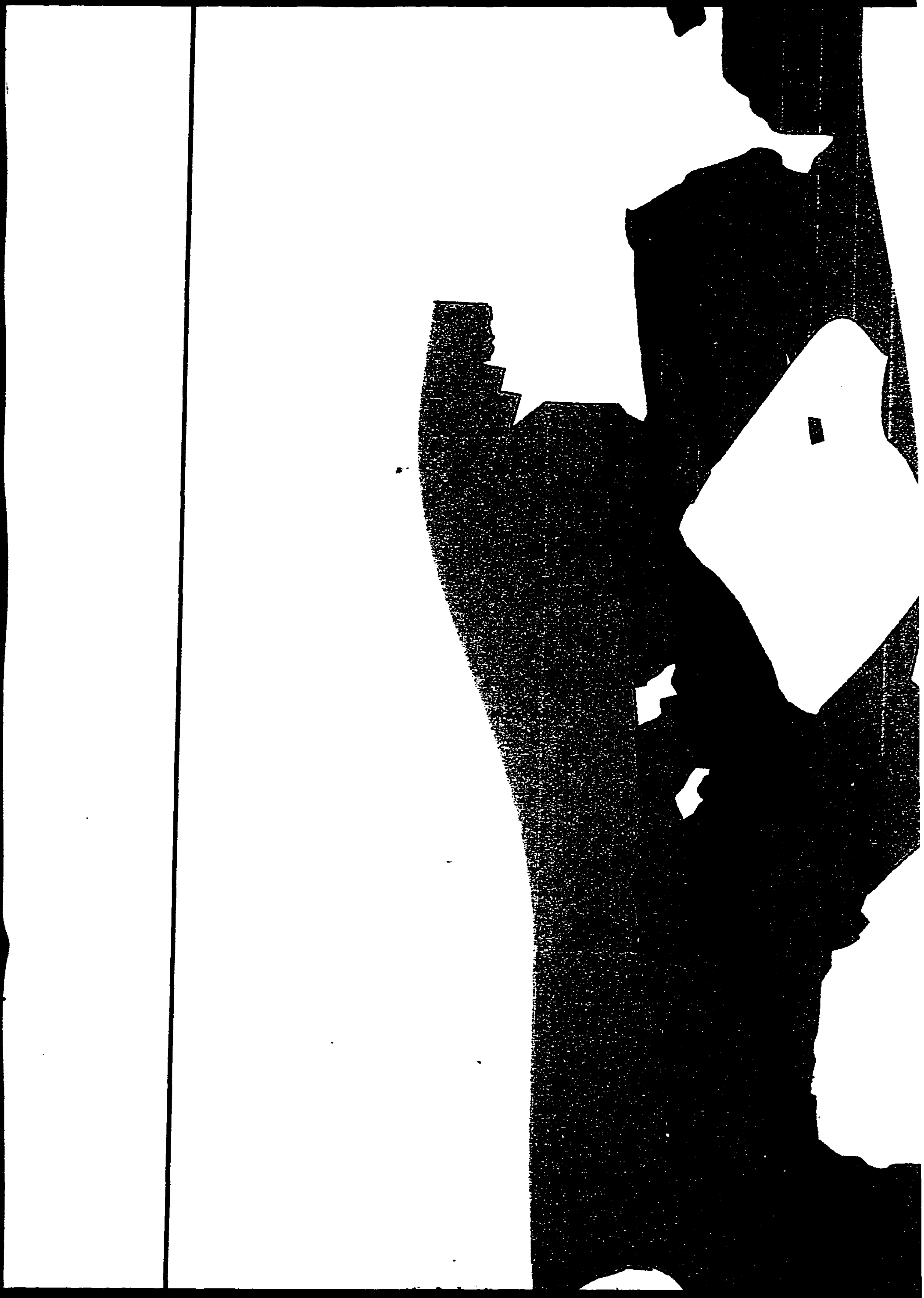

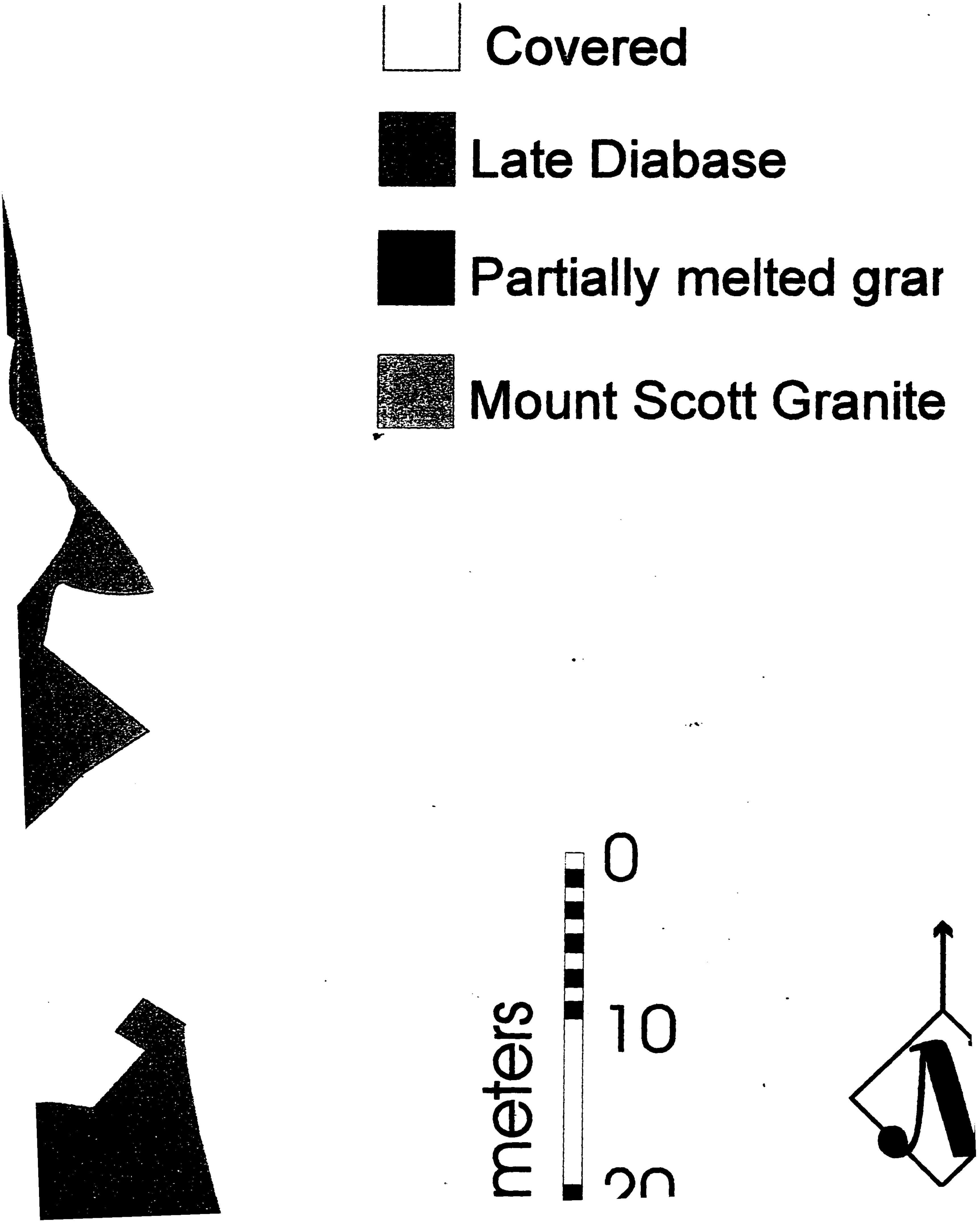
Covered
Late Diabase
Partially melted gra
Mount Scott Granite
0
10
20
meters

ered

Diabase

ally melted granite

nt Scott Granite

0

10

20

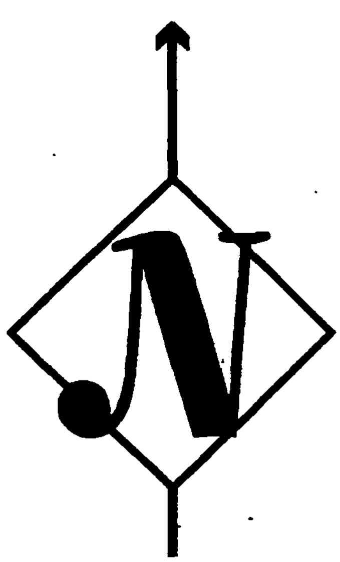

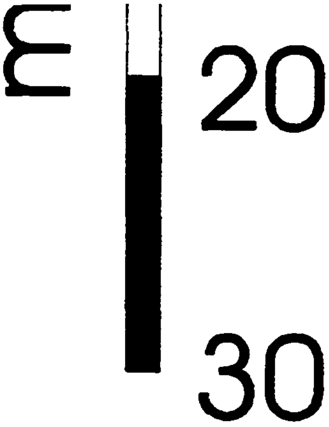

Produced in cooperation with the
National Cooperative Geologic

20

30

ed in cooperation with the U. S. Geological Survey,
nal Cooperative Geological Mapping Program

IMAGE EVALUATION TEST TARGET (QA-3)

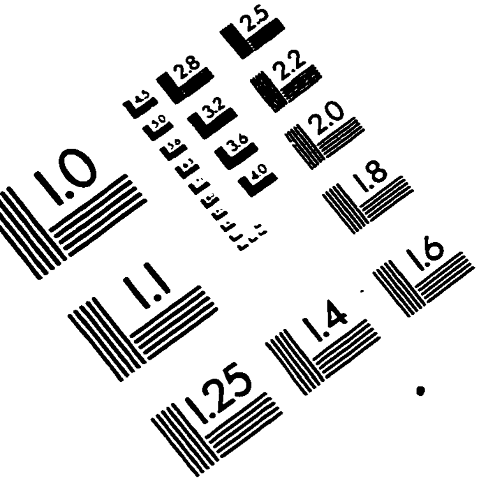

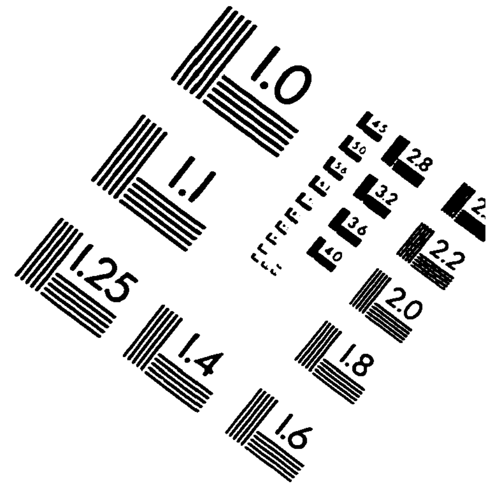

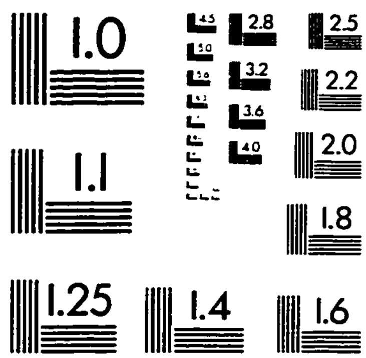

150mm

6"

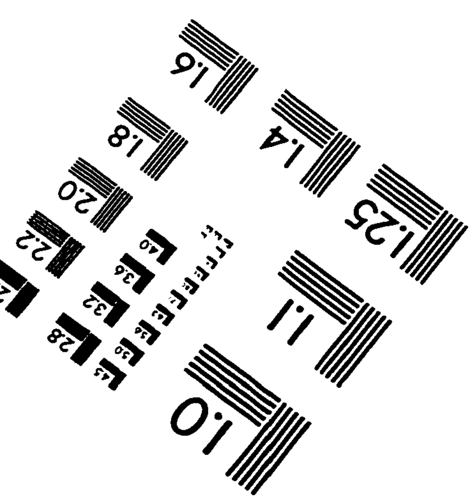

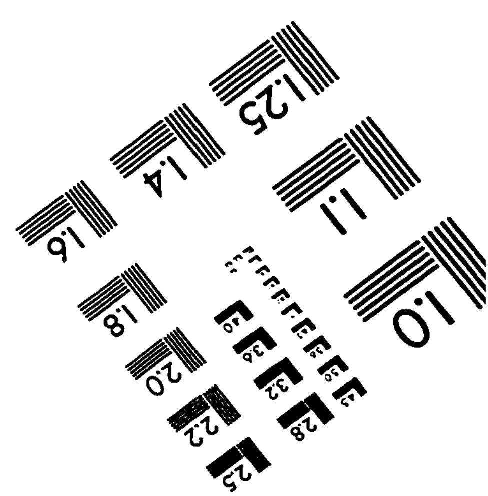

APPLIED IMAGE . Inc
1653 East Main Street
Rochester, NY 14609 USA
Phone: 716/482-0300
Fax: 716/288-5989